The Role of Framework Flexibility and Coordinatively Unsaturated Metal Sites on Gas Adsorption of Selected Metal Organic Frameworks

Thesis

Submitted in partial fulfillment of the
requirements for the degree of

DOCTOR OF PHILOSOPHY

by

Prashant Mishra

Department of Chemical Engineering

Indian Institute of Technology Guwahati

Guwahati 781039, INDIA

June, 2014

Department of Chemical Engineering
Indian Institute of Technology Guwahati
Guwahati 781039 (INDIA)

CERTIFICATE

It is certified that the work contained in the thesis entitled **"The Role of Framework Flexibility and Coordinatively Unsaturated Metal Sites on Gas Adsorption of Selected Metal Organic Frameworks"**, by *Prashant Mishra* has been carried out under our supervision and that this work has not been submitted elsewhere for a degree.

(Dr. Sasidhar Gumma)
Associate Professor
Department of Chemical Engineering
Indian Institute of Technology Guwahati
Guwahati 781039 (India)

(Dr. Bishnupada Mandal)
Professor
Department of Chemical Engineering
Indian Institute of Technology Guwahati
Guwahati 781039 (India)

Dedicated To

To My Parents

&

Beloved Sisters 'Swati' and 'Manjulika'

ACKNOWLEDGEMENTS

I would first like to acknowledge my supervisor **Dr. Sasidhar Gumma**. It is only with his patience and guidance that I have been able to complete this process, and I am grateful for all of the opportunities that he has provided me. It is his hortative nature that inspired me to stick on to my work. Through his actions he has shown me how research should be done, and it has been a privilege to study under his guidance. I believe his teachings will always remain with me in my entire life. During my stay at IIT Guwahati, he took care of me like parents and never let me realize that I am staying far away from my home.

I would like to express my sincere gratitude to my other supervisor **Prof. Bishnupada Mandal** for his invaluable support, undaunted encouragement, interesting discussions and crucial contribution during this research work. I appreciate very much his flexibility and openness in dealing with the specific and general needs of the project. Due to his kind and supportive nature, it was also very easy for me to take useful advice from him time to time. He has always assisted and helped me and it has really been a remarkable experience working with him.

I must also acknowledge my doctoral committee chairman **Prof. Aloke K. Ghoshal,** Department of Chemical Engineering, for his useful suggestion during the course of my research. His constant visits to the research lab and regular queries on my research have helped me to maintain a good momentum in my research. In spite of his busy schedule, he has always listened to my all questions and provided the suitable explanations. I would also like to profoundly acknowledge my other doctoral committee members **Prof. Gopal Das,** Department of Chemistry, and **Dr. Chandan Das,** Department of Chemical Engineering, and for their valuable suggestions during

my progress review seminars. Their suggestions have really helped me to make necessary improvements towards various stages of my research work.

I must also thank the faculty members of the Department of Chemical Engineering, for their consistent encouragements and supports to me. My sincere thanks also goes to **Prof. Vijay S. Moholkar,** (HOD, Department of Chemical Engineering) and **Dr. Nanda Kishore** (DPPC Chairman, Department of Chemical Engineering) for their assistance on administrative proceedings.

I would like to thank the Central Instruments Facility and Analytical Lab Facility, Department of Chemical Engineering of IIT Guwahati for providing the facilities to carry out BET, TGA and XRD analysis. I also express my gratitude to "Department of Science and Technology, New Delhi" for providing Powder X-Ray Diffraction analysis facility in our department through DST FIST 2010 Project # SR/FST/ETII-047/2010.

I am extremely thankful to the IIT Guwahati administration for providing a high quality accommodation facility and a home like environment to the students. In, particular, I am going to miss the rapid internet speed of IIT Guwahati a lot. I feel to be privileged for being a student of such a great institution.

I express my thanks to all the technical staffs of my department specially **Mr. Prasun Bhattacharjee, Mr. Kaustavmoni Deka, Mr. Debajit Borah, Mr. Harsaraj Biswanath and Ms. Ritumoni Kalita** for their assistance during my experimental work. I would also like to thank **Ms. Gitanjali Hazarika** (former Junior Assistant), **Mr. Kalyan Boro** (Junior Assistant) and **Mr. Bhagya Boro** (Attendant) for their support in various forms.

Coming to Lab mates, I must acknowledge **Dr. Pradip Chowdhury** (Assistant Professor, NIT, Rourkela) for his guidance at the beginning of my work. Even now also I used to get advice from him. I am thankful to **Mr. Debjyoti Sahu** and his family for taking care of me like a family member. I was fortunate enough to get excellent junior M. Tech. students whose cooperation and friendly behavior comforted me in many ways. It was a wonderful journey of knowledge and idea sharing while working with **Mr. Samuel Mekala, Mr. Hari Uppara** and **Mr. Satyannarayana Edubilli** (all M. Tech students)**.** I hope you guys have also enjoyed working with me. I am also thankful other lab mates such as **Mr. Vyas, Mr. Pruthavi, Mr. Nitun Das, Mr. Pradip Das, Mr. Mudit Baurai, Mr. Abhik** and **Mr. Ramesh** for maintaining a nice lab environment.

I am also thankful to all my friends for their enriching friendship and useful support during the course of my stay here.

Finally, but most of all, I would like to express my heartfelt thanks to my beloved parents for their love, affections, support and blessings. I would also like to acknowledge my sisters **Swati** and **Manjulika** for being my best friends. I will always be thankful to the GOD for having such a wonderful parents and Sisters.

Date:

Place: _____

(Prashant Mishra)

VITAE

Prashant Mishra

Date of Birth: August 30, 1986

Email: prashant.iitg09@gmail.com
m.prashant@iitg.ernet.in

Permanent address: S/O Ram Naresh Mishra
Purani Bazar
Badausa Banda
Uttar Pradesh
INDIA 210202
Call: +91-05191-288488

Education:

- Ph.D. (2014)
  Department of Chemical Engineering
  Indian Institute of Technology Guwahati
  Assam 781039, INDIA
  India

- B.Tech (2008)
  Chemical & Bio Engineering
  Harcourt Butler Technological Institute,
  Kanpur, INDIA

Publications

Journals

1. Prashant Mishra, Satyannarayana Edubilli, Bishnupada Mandal and Sasidhar Gumma, *Adsorption Characteristics of Metal Organic Frameworks Containing Coordinatively Unsaturated Metal Sites: Effect of Metal Cations and Adsorbate Properties*, **J. Phys. Chem. C** 118 (2014) 6847–6855.

2. Prashant Mishra, Satyannarayana Edubilli, Hari Prasad Uppara, Bishnupada Mandal and Sasidhar Gumma, *Effect of Adsorbent History on Adsorption Characteristics of MIL-53(Al) Metal Organic Framework*, **Langmuir** 29 (2013) 12162–12167.

3. Prashant Mishra, Hari Uppara, Bishnupada Mandal and Sasidhar Gumma, *Adsorption and Separation of Carbon dioxide using MIL-53(Al) Metal Organic Framework*, **Ind. Eng. Chem. Res. DOI: 10.1021/ie5006146**.

4. Prashant Mishra, Satyannarayana Edubilli, Bishnupada Mandal and Sasidhar Gumma, *Adsorption of CO_2, CO, CH_4 and N_2 on DABCO based Metal Organic Frameworks*, **Microporous Mesoporous Mater.** 169 (2013) 75–80.

5. Prashant Mishra, Hari Uppara, Bishnupada Mandal and Sasidhar Gumma, *Adsorption of Lower Alkanes on a Zinc Based Metal Organic Framework*, **J. Chem. Eng. Data** 57 (2012) 2610–2613.

6. Prashant Mishra, Samuel Mekala, Freider Dreisbach, Bishnupada Mandal and Sasidhar Gumma, *Adsorption of CO_2, CO, CH_4 and N_2 on a zinc based metal organic framework*, **Sep. Purf. Tech.** 94 (2012) 124–130.

7. Debjyoti Sahu, Prashant Mishra, Satyannarayana Edubilli, Anil Verma and Sasidhar Gumma, *Hydrogen Adsorption on Zn-BDC, Cr-BDC, Ni-DABCO and Mg-DOBDC Metal Organic Frameworks*, **J. Chem. Eng. Data** 58 (2013) 3096–3101.

8. Debjyoti Sahu, Prashant Mishra, Anil Verma and Sasidhar Gumma, *The Net Adsorption of Hydrogen on Palladium Nanoparticles*, **Surf. Rev. Lett.** 21 (2014) 1450022(1–6).

Conference Proceedings

1. Prashant Mishra, Satyannarayana Edubilli, Bishnupada Mandal and Sasidhar Gumma, "Capitalization of Breathing Phenomena of Flexible MIL-53 (Al) Solid to Enhance Its Carbon Dioxide Capacity and Selectivity" *Adsorption and Ion Exchange Plenary: Fundamentals and Applications,* **AIChE Annual Meeting 2013, San Francisco, CA USA**.

2. Prashant Mishra, Satyannarayana Edubilli, Bishnupada Mandal and Sasidhar Gumma, "Adsorption Characteristics of Coordinatively Unsaturated Metal Sites Containing Dhtp Series of Metal Organic Frameworks" *Adsorbent Materials: MOFs,* **AIChE Annual Meeting 2013, San Francisco, CA USA**.

3. Prashant Mishra, Hari Uppara, Bishnupada Mandal and Sasidhar Gumma, "Adsorption and separation of carbon dioxide using MIL-53(Al) Metal Organic Framework" **ESMOC 2013**.

4. Prashant Mishra, Hari Uppara, Satyannarayana Edubilli, Bishnupada Mandal and Sasidhar Gumma, "Gas adsorption properties of an Aluminium based metal organic framework-MIL 53(Al)" **CHEMCON 2011**.

5. Prashant Mishra, Bishnupada Mandal and Sasidhar Gumma, "Synthesis and Gas adsorption properties of a Copper based metal organic framework" **CHEMCON 2011**.

6. Prashant Mishra, Bishnupada Mandal and Sasidhar Gumma, "Structural Tuning of Flexible MIL 53 (Al) MOF to increase CO_2 Loading and Selectivity" **REFLUX 2012, IIT Guwahati**.

Workshops Attended

1. Industry-Academia Workshop on "Recent Trends in Oil and Gas Production Technology" at ONGC Sivsagar from 04/02/2013 to 08/02/2013 (organized by **ONGC, India**).

2. Workshop on "Effecient Fossil Energy Technology" at IIT Guwahati in 2011 (jointly organized by **The University of Nottingham UK and IIT Guwahati India**).

ABSTRACT

In this work, adsorption characteristics of various categories of metal organic frameworks (MOFs) *viz.* flexible MIL-53(Al) MOF, unsaturated metal sites containing M/DOBDC MOFs (M = Mg, Mn, Co and Ni) and saturated metal sites containing M/DABCO MOFs (M = Ni, Cu and Zn) are investigated. Equilibrium adsorption capacities of these materials for several adsorbates are measured over a wide range of temperature and pressure to understand the effect of adsorbate physical properties, framework flexibility, coordinatively unsaturated (*cus*) metal sites and metal constituents in the framework on their adsorption characteristics.

In the first part of work, the breathing phenomenon (or framework flexibility) of MIL-53(Al) is thoroughly studied by measuring the adsorption and desorption of CO_2, CH_4, N_2, CO and O_2 gases at 293 K on this sample. X-ray diffractograms of the sample were measured at different stages of adsorbent *history* to identify the structural phase of the corresponding sample. The role of adsorbent *history* on the structural transformation is capitalized to tune its adsorption characteristics. By choosing an appropriate *history*, the sample under vacuum is tuned into the narrow pore (**np**) form which exhibits more than fourfold increase in CO_2 capacity (at about 0.17 bar and 293 K) along with exceptional enhancement in its selectivity over N_2, CH_4, CO and O_2 at sub-atmospheric pressures.

Isotherms of CO_2, CO, CH_4, N_2, Ar, C_2H_6 and C_3H_8 are measured on M/DOBDC frameworks at 294, 315 and 352 K over a wide range of pressure. Similarly CO_2, CO, CH_4 and N_2 isotherms are measured on M/DABCO frameworks in the range of 0 – 25 bar at three different temperatures. Isotherms are modeled to obtain important parameters like Henry's constant and enthalpy of

adsorption. Ideal Adsorbed Solution Theory (IAST) is used to predict multi-component adsorption data.

M/DOBDC MOFs exhibit significantly higher Henry's constant and adsorption enthalpy at zero coverage for polar CO_2 and CO gases than that for non-polar gases with similar polarizability (like CH_4 and N_2) due to the presence of electrostatic interactions between the polar gas molecules and the *cus* metal centers of DOBDC frameworks. Amongst non-polar gases, these quantities vary linearly with polarizability. Adsorption characteristics of DOBDC frameworks in the Henry's region substantially change for polar gases by variation of the metal constituent in the framework. For example, Mg/DOBDC exhibits highest adsorption enthalpy (42 kJ mol^{-1} at zero coverage) and Mn/DOBDC exhibits lowest adsorption enthalpy (28 kJ mol^{-1} at zero coverage) for CO_2. On the other hand, adsorption enthalpy of non-polar CH_4 (~ 17 kJ mol^{-1} at zero coverage) is similar on all the frameworks. Saturation uptake of both polar as well as non-polar adsorbates almost linearly correlates with the pore volume of these frameworks. CO_2 selectivity on Mg/DOBDC is significantly higher than that on most of the adsorbents including other DOBDC MOFs with selectivity value of 251, 24 and 288 over CH_4, CO and N_2, respectively, at zero coverage and 294 K. In contrast, Ni/DOBDC and Co/DOBDC have preferential selectivity for CO over other gases and have shown CO selectivity value of ~ 7.5, 441 and 677 over CO_2, CH_4 and N_2, respectively, at zero coverage and 294 K. With increase of loading, selectivity and adsorption enthalpy of CO_2 and CO decrease because the reduction in the electrostatic interactions are more pronounced than the increase in lateral interactions for these gases. M/DOBDC MOFs are stable upon exposure to CO_2, CO, CH_4 N_2, Ar, C_2H_6 and C_3H_8. But, the samples lose their adsorption characteristics after exposure to O_2 at higher temperatures.

The M/DABCO frameworks show considerably lower loading and selectivity for polar CO_2 and CO gases at low pressures than the M/DOBDC frameworks due to absence of electrostatic interactions. In contrast to DOBDC samples, DABCO samples have negligible effect of metal cation on their adsorption characteristics and adsorption uptake in the Henry's region is same on all DABCO frameworks for each gas including that for polar gas such as CO_2 and CO. The small values of adsorption enthalpy at zero coverage (only ~ 19 kJ mol^{-1} for CO_2) should make the easier regeneration for DABCO frameworks. IAST predicts an increase in the selectivity of CO_2 over the other three gases, with increasing pressure and CO_2 mole-fraction. The DABCO frameworks are found to be selective for CH_4 over CO (which is not common in adsorption literature) with a selectivity value of ~ 2 at zero coverage and 294 K.

CONTENTS

LIST OF TABLES

LIST OF FIGURES

Nomenclature

a	Molar area of the adsorbent, $m^2\ mol^{-1}$
A	Specific area of the adsorbent, $m^2\ kg^{-1}$
b	Second virial coefficients for adsorption, $mol^{-1}\ kg$
$b^{(0)}$ and $b^{(1)}$	Temperature independent parameters of second virial coefficients, $mol^{-1}\ kg$ and $mol^{-1}\ kg\ K$, respecively
B^{gas}	Gas phase second virial coefficient, $m^3\ Kmol^{-1}$
B_1, B_2, B_3, B_4, B_5	Parameters used for describing temperature dependency of second virial coefficient of gas (see Eqns. 4.4 and 4.5)
c	Third virial coefficients for adsorption, $mol^{-2}\ kg^2$
$c^{(0)}$ and $c^{(1)}$	Temperature independent parameters of third virial coefficients, $mol^{-2}\ kg^2$ and $mol^{-2}\ kg^2\ K$, respecively
C	Number of chemical species
f	Fugacity, bar
F	Number of degrees of freedom
Δh_{ads}	Enthalpy of adsorption, $kJ\ mol^{-1}$
$\Delta h_{ads,0}$	Enthalpy of adsorption at zero coverage, $kJ\ mol^{-1}$
I_1, I_2	Isotherm models relating N_i^0 and P_i^0
I_3, I_4	Equations relating spreading pressure ψ, excess amount adsorbed N and fugacity P
M	Metal cation in an adsorbent
M_0	True adsorbent weight including bucket weight in vacuo, g
M_{eq}	Adsorbent plus bucket weight at equilibrium, g
M_f	Molecular weight of unit cell of adsorbent, $g\ mol^{-1}$

M_t	Gibbs' amount adsorbed, g
M_w	Molecular weight of the gas, g mol^{-1}
n	Number of metal atoms in one unit cell
N	Excess amount adsorbed, mol kg^{-1}
N^{max}	Saturation capacity, mol kg^{-1}
N_1^{max} and N_2^{max}	Saturation capacities of sites 1 and 2, respectively, in DSL model, mol kg^{-1}
Ni^0	Excess amount adsorbed of pure component '*i*' at fugacity f_i^0
N_m	Amount adsorbed per metal atom in the adsorbent, molecules metal $atom^{-1}$
N_u	Excess amount adsorbed on a unit cell basis, molecules $unit\ cell^{-1}$
N_v	Excess amount adsorbed on volumetric basis, mol L^{-1}
P	Pressure, bar
P_i^0	Standard state pressure of component '*i*'
R	Universal gas constant, J mol^{-1} K^{-1}
T	Temperature, K
V	Volume, m^3
V_{bucket}, V_s	Buoyancy volume of bucket and impenetrable solid volume, respectively, cm^3
V_p	Pore volume of adsorbent, cm^3 g^{-1}
$V_{buoyancy}$	Buoyancy volume of the sample, cm^3
x_i	Equilibrium mole fraction of the component '*i*' in adsorbed phases
y_i	Equilibrium mole fraction of the component '*i*' in bulk gas phases
z_1, z_2	Integers representing alumina and silica content, respectively in zeolites
z_3	Number of water molecules in each unit cell of zeolites

GREEK LETTERS

α_{ij}	Selectivity of the adsorbent for species ***i*** over species ***j***
β	Henry's constant, mol kg^{-1} bar^{-1}
$\beta^{(0)}$	Parameter related to entropy used for describing temperature dependency of Henry's constant, mol kg^{-1} bar^{-1}
$\beta^{(1)}$	Parameter related to enthalpy used for describing temperature dependency of Henry's constant, K
β_1 and β_2	Affinity parameters for sites 1 and 2, respectively, in Dual Site Langmuir model, bar^{-1}
$\beta_1^{(0)}$ and $\beta_2^{(0)}$	Parameters related to entropy for sites 1 and 2, respectively, in Dual Site Langmuir model, bar^{-1}
$\beta_1^{(1)}$ and $\beta_2^{(1)}$	Parameters related to adsorption enthalpy for sites 1 and 2, in Dual Site Langmuir model, respectively, K
γ_i	Activity coefficient in the adsorbed phase
π	Spreading pressure, N m^{-1}
ρ_c	Crystal density of the adsorbent, g cm^{-3}
ρ^{gas}	Bulk gas density, g cm^{-3}
$\hat{\phi}_i^{gas}$	Fugacity coefficient of bulk gas
χ	Number of phases
ψ	Reduced spreading pressure, mol kg^{-1}

ABBREVIATIONS

BDC	Benzene 1,4-dicarboxylic acid
BTC	Benzene 1,3,5-tricarboxylic acid
cus	Coordinatively unsaturated
DABCO	1,4-diaza bicycle [2,2,2] octane
DOBDC	2,5-dioxido, benzene 1,4-dicarboxylic acid
lp	Large pore
np	Narrow pore

CHAPTER 1

INTRODUCTION

*Porous materials have been extensively studied by chemists, physicists, and material scientists during last three decades. Many applications have been proposed for these materials in strategic domains such as adsorption, separation and purification, as well as catalysis [**1 – 3**]. Synthesis of novel porous materials and evaluation of their performance for the mentioned applications is still an important subject of scientific research. This chapter presents a discussion on adsorption, industrially relevant adsorbents and CO_2 emissions. It elaborates the background of the research work. Importance and objectives of the present work are highlighted accordingly in this chapter.*

1.1 Adsorption

Adsorption is a surface phenomenon where the density of a fluid increases near the vicinity of a solid surface. In this process the fluid near the vicinity is called "adsorbate" and the solid is called as "adsorbent". When a gas is exposed to a solid surface, the gas molecules interact with the surface through van der Waal's forces, electrostatic forces and/or other chemical bonds. [**4**].

The concept of adsorption was first recognized by Scheele and Fontana [**5**] in the eighteenth century; however the use of adsorption for large scale separation and purification is a relatively new advancement [**6**]. The most familiar known example of adsorption process is the removal of trace amount of moisture from either gas or liquid streams. Similarly, adsorption is also

employed in large scale applications of removal of H_2S from natural gas and organic pollutants from water. The application of adsorption as a means of separating mixtures into two or more streams is a more recent development. Recovery of aromatic hydrocarbons in Arosorb process in the early 1950s [**6**] and separation of linear paraffins from branched and cyclic isomers in the early 1960s are the earliest example of adsorptive separation processes [**6, 7**]. After 1970s, there has been a tremendous advancement in field of adsorption due to discovery of many porous materials such as carbon molecular sieves, zeolites etc.

1.2 Types of Adsorption

Based on difference in the mechanism, adsorption can be broadly divided in two categories

(i) Physisorption: When adhesion between adsorbate molecules and adsorbent surface takes place purely due to electrostatic and/or van der Waal's forces, the process is called physisorption. While, van der Waal contribution is always present, electrostatic contributions are significant only for adsorbents with ionic structure such as zeolites. Physisorption is a reversible process and the binding energy is typically low [**8**], however heat of adsorption for polar molecules like H_2O or NH_3 on zeolite type of adsorbents may be unusually high (100 – 130 kJ mol^{-1}). Multilayer adsorption is possible at appropriate conditions in case of physisorption.

(ii) Chemisorption: In this type of adsorption, the adsorbate molecules associate to adsorbent surface through chemical binding and the energy in case of chemisorption (100 – 1000 kJ mol^{-1}) is significantly higher than that of physisorption [**8**]. Since in chemisorption, the adsorbate molecules are attached to the surface by valence bonding, only monolayer adsorption is possible. Heterogeneous catalysis mostly involves this type of adsorption.

1.3 Adsorbents of Industrial Importance

The adsorbent is the heart of any adsorption process and the success of the process largely depends upon its selection. From a large number of adsorbents that are reported in the literature, only a few have survived the technological progress. Silica gel, activated carbon, carbon molecular sieve, activated alumina and zeolites are the most studied adsorbent materials. Based on the elemental composition, conventional adsorbents can be divided into two categories.

(i) Organic frameworks: Activated carbons are a typical example in this category. They are usually synthesized by the pyrolysis of carbon-rich materials and generally have higher pore volume which results into large saturation capacities [**6**]. However, these materials have disadvantages such as unordered structures and poor selectivities. To overcome the issue of poor selectivity, carbon adsorbents with narrow distribution of micropore sizes are prepared using special activation procedures and are known as carbon molecular sieves. Carbon sieves with pore diameter ranging from about 4 to 9 Å [**6**] are synthesized to obtain enhanced selectivities; however, porosity and hence saturation adsorption capacity for these materials is lower. Another disadvantage of carbon molecular sieves is the lack of reproducibility of properties between different batches [**9**].

(ii) Inorganic frameworks: In these frameworks, porous structure is formed entirely by inorganic elements. Silica gel, activated alumina and zeolites are the common examples of inorganic frameworks.

Silica Gel. Partial dehydrated form of polymeric colloidal silicic is known as silica gel ($SiO_2.nH_2O$) [**6**]. The presence of hydroxyl group in the structure yields polarity and it exhibits selectivity for polar adsorbates such as water, alcohol, amine etc. over non-polar adsorbates.

However, the pore size distribution is quite large for this material and thus its adsorption capacity is lower than that of carbon molecular sieves at low pressures.

Activated Alumina. Activated alumina is a porous high-area form of aluminium oxide. The surface of this material is more polar than that of silica gel and has both acidic and basic characters, indicating the amphoteric nature of aluminium [**6**]. This material has similar affinity for water at room temperature as that of silica gel; however, at higher temperature capacity of activated alumina is higher and therefore this material was earlier used as desiccant before its replacement by molecular sieves.

Zeolites. Zeolites are crystalline aluminosilicates of alkali or alkali earth elements, such as sodium, potassium and calcium. The chemical composition of zeolites can be represented by the following formula [**6**].

$$M_{z_1/n}[(AlO_2)_{z_1}(SiO_2)_{z_2}].z_3H_2O$$

Where z_1 and z_2 are the integers with z_2/z_1 equal to or greater than 1, n is the valancy of the metal cation M, and z_3 is the number of water molecules in each unit cell [**4**]. In these materials, silica and alumina tetrahedra are connected together in various arrangements through shared oxygen atoms to form an open crystal lattice [**6**]. Since the micropore structure in these materials is determined by crystal lattice, the pore size in these materials is fixed [**6**]. Change in Aluminium to Silicon ratio leads to a systematic shift in the adsorption properties of these materials. Aluminium rich zeolitic frameworks are hydrophilic and have very high affinities for polar molecules (such as water) whereas microporous silicas (that are *Si* rich) such as silicalite are hydrophobic. The transition from hydrophilic to hydrophobic character generally occurs at a *Si/Al* ratio ranging from 8 to10. Some zeolites (Zeolite 13X) have shown very promising CO_2 adsorption capacities [**10**] and selectivities at lower pressures, but they have limited high

pressure capacity compared to activated carbons due to low pore volume. In addition, due to strong affinity for CO_2 at low pressure, the regeneration energy requirement of Zeolite 13X is also high.

Some features of adsorbents have a strong effect on their adsorption characteristics and are worthy to be discussed.

(a) Surface Polarity: Some adsorbents exhibit surface polarity due to the presence of charged ions in the structure. Polar adsorbents such as silica gel, activated alumina and zeolites are generally hydrophilic in nature and show enormous affinity for polar adsorbates (such as H_2O). On the other hand, activated carbons have non-polar surface; however, a slight polarity may arise from surface oxidation. As a result these materials exhibit hydrophobic and organophilic nature [**6**]. The feature of hydrophilicity or hydrophobicity can be judicially exploited for many separation processes based on adsorption equilibrium.

(b) Porosity: Since adsorption is a surface phenomenon, porosity is one of the important characteristics for an adsorbent. Higher porosity indicates higher specific surface area and pore volume. Higher surface area and pore volume generally results into higher saturation adsorption capacity and thus can extremely be useful for adsorptive storage of gases (such as methane and hydrogen) at high pressures. However, extremely porous materials usually tend to have low/poor volumetric uptake capacities and hence the adsorbent bed sizes might be large. A reasonable balance should be obtained between these two contradicting necessities. In addition to porosity, pore size distribution also affects the adsorption characteristics of adsorbents. Based on International Union of Pure and Applied Chemistry (IUPAC) standards, porous materials can be divided into three different category: (i) microporous (pore size < 2 nm), (ii) mesoporous (pore size from 2 to 50 nm) and (iii) macroporous (pore size > 50 nm). It is of great interest to study

the adsorption characteristics of microporous materials due to their potential for adsorptive storage, separations, and catalysis applications. Wilmer et al. [**11**] reported that among best adsorbents for CH_4 storage, the most frequent pore sizes are between 4 and 8 Å, exactly big enough for one or two CH_4 molecules.

1.4 Important Factors to be Considered in Adsorbent Selection

The following factors are some of the important factors that should be considered in choosing a suitable adsorbent [**4, 6, 12 – 14**]:

(A) Uptake Capacity: A high loading capacity at the desired process conditions reduces the size of adsorber column and thus less operating and fixed costs can be achieved. The measurement of equilibrium isotherms of all the constituents of the gas mixture at different operating conditions of pressure and temperature is one of the prerequisites for effective evaluation of an adsorbent for a particular process. Another important parameter commonaly known as working capacity is obtained as the difference between uptake capacities at adsorption and desorption conditions. Working capacity is a preferred parameter over pure uptake capacity in evaluating the potential of any adsorbent in a real process as it directly corresponds to the actual amount of adsorbate quantity that can be captured during a full adsorption/desorption cycle.

(B) Selectivity: Selectivity is one of the important parameter for any adsorptive separation process.

The selectivity is defined as

$$\alpha_{ij} = \frac{x_i/y_i}{x_j/y_j} \qquad 1.1$$

where x_i and y_i are the equilibrium mole fractions of the component '***i***' in adsorbed and bulk gas phases respectively. A good adsorbent also should be selective to component(s) of interest for better separation. However, if selectivity of retained component(s) is very high then it's desorption would be difficult. Hence, the optimal selectivity value should be decided based on the process. For example in case of purifier where adsorbent bed is supposed to capture the trace amount of impurities, a higher value of selectivity would be desired because in this case bed saturates after a long time and costly regeneration can be afforded. On the other hand in a separation process where bed saturates shortly, the selectivity should be moderate to have easier regeneration of the bed.

(C) Adsorbent regeneration: An ideal adsorbent should be easily regenerable (*i.e.* desorption should be achieved by mild changes in either pressure or temperature). Regeneration at high temperatures or rigorous vacuum substantially increases the operational cost. Typically, low value of enthalpy of adsorption translates into easy regeneration, but lower enthalpy values also tend to decrease the adsorption uptake capacity of an adsorbent. Thus, a reasonable balance between low enthalpy values and uptake capacity needs to be achieved.

(D) Stability of the adsorbent under process conditions: Stability of the adsorbent material is also an important parameter in adsorbent selection. For example, adsorbents used for CO_2 capture from flue gas must be stable in the presence of at least some water vapor as flue gases generally contain some water.

1.5 Novel Adsorbents

Over the last three decades, the enormous amount of research has taken place on synthesis and characterization of porous adsorbent materials due to their potential for a large numbers of

practical applications such as storage, separation and purification, drug delivery, catalysis etc. [**3**] Conventional adsorbents such as activated carbons and zeolites were successfully commercialized and have been used for a variety of industrial applications. However, since adsorption is primarily a material driven technology, it is necessary to develop porous materials with better characteristics for development of efficient adsorptive processes.

In pursuit of developing novel adsorbent materials, the focus has shifted towards hybrid structures, with the word 'hybrid' used to indicate the involvement of both 'organic' and 'inorganic' components. The logic behind these attempts was to incorporate the properties of both metal coordination and organic functionalities in the same structure. The concept of reticular synthesis has been adopted to connect building blocks together to form a bigger network. The structural integrity and rigidity of molecular building blocks has to remain unaltered during construction process for the practical realization of this technique. Based on this concept, a large volume of novel porous structures have been synthesized during last decade. These novel materials were called by different names e.g. 'hybrid organic-inorganic materials', 'co-ordination polymers' or 'metal organic frameworks'. Even though each terminology has its own reason, 'Metal Organic Framework' or MOF is mow widely used. For this category of materials, variation in organic functionalities, metal clusters, and structural motifs can easily afford an infinite number of possible structures [**15**]. The numbers of possible structures can further be magnified by post-synthetic modifications [**16**]. In addition, by choosing an appropriate combination of inorganic cluster and organic ligand with appropriate functionality, a tailor made structure can be easily synthesized. The uniform and good porosity in MOFs coupled with heterogeneity has encouraged researchers to investigate these materials in the fields of CO_2 capture [**17 – 19**], catalysis [**20 – 21**], drug delivery [**22 – 23**], biomedical imaging [**24**], and Hydrogen storage [**25 – 28**].

1.6 Overview on CO_2 Emissions

The last century has witnessed humanity actively exploiting organic fossil fuels like coal, petroleum, and natural gas as energy sources. Approximately 80% of the total CO_2 emissions come from energy generation whereas industry contributes the remaining 20% emissions (cement - 7%, refinery - 6%, steel - 5%) [**29**]. The enhancement in these activities is further expected to increase in the future to meet the economic growth and the industrial development of developing countries. The burning of fossil fuels produces significant quantities of CO_2 (a ton of solid fuel releases 2.76 tons of CO_2 into atmosphere) [**30**]. Being a chemically stable molecule, CO_2 sustains in the Earth's atmosphere for about 120 years [**30**], resulting in gradual accumulation. This accumulation leads to the greenhouse effect which creates global warming. Scientists believe that present trend of CO_2 emission into atmosphere may increase its concentration to such a level which will increase earth atmospheric temperature sufficient to melt the polar ice caps and to increase sea level drastically in the near future. These types of climate changes will be a disaster for the humanity and cannot be afforded.

1.7 Different Pathways of CO_2 Separation

At present, a lot of research is devoted to develop technologies to reduce the anthropogenic emissions of CO_2 into the atmosphere. The three major pathways for carbon capture are listed below.

- **Post-Combustion:** The flue gas from burning of fossil fuel is in presence of air contains a mixture of gases such as CO_2, O_2, N_2, H_2O, SO_x and NO_x etc. CO_2 is then separated from this flue gas stream using a suitable processes such as absorption, adsorption etc. In majority of the

situations, this pathway is adopted because the existing plant can be retrofitted to include a suitable carbon capture section.

- **Pre-Combustion:** Hydrocarbon fuel is first burnt in a gasifier producing syn gas. CO is further converted to CO_2 by Water-Gas-Shift reaction to yield hydrogen. CO_2 is separated from the resulting mixture of CO_2 and H_2, while pure hydrogen is the product that is obtained as a carbon-free fuel.
- **Oxy-Combustion:** Fuel is burnt in a stream of pure oxygen instead of ordinary air. Thus, the flue gas stream contains no nitrogen and CO_2 can be captured more efficiently with lower cost by simple condensation process. Although this pathway looks very simple, the challenge lies in obtaining pure oxygen without adversely affecting the economics of the existing process.

Different pathways have different methods of CO_2 separation [**31**]. For post combustion technology, absorption of CO_2 in aqueous alkanolamine solutions is the most common technique of CO_2 capture. However, scientific community is actively involved in search for alternate technologies due to high energy requirement for the amine absorption process in addition to corrosive nature of the solvents used for absorption. Membranes, solid adsorbents, ionic liquids and biological processes are some of novel techniques that are being widely investigated for CO_2 separation. Amongst these processes, adsorption on porous materials has received considerable focus [**32 – 38**]; zeolites and activated carbons have been studied first in this category [**32 – 35**]. Difficult regeneration in case of zeolites and low selectivity in case of carbons make their usage economically unviable. In recent years, novel adsorbents known as Metal Organic Frameworks (MOFs) have received considerable attention [**36 – 38**]. These adsorbents have been widely investigated for CO_2 capture applications due to their tunable pore structure and ligand functionality.

1.8 Background of the Present Work

During the last decade MOFs received considerable attention worldwide. A large number of MOF compounds with varying surface properties were synthesized. Some MOFs are reported to have surface areas in range of 4000 - 6200 m^2 g^{-1} which is considerably higher than that of other porous materials [**38**]. While the initial research focus has been on synthesis of the materials, a considerable amount of research in the later years focused on the evaluation of their potential for various gas storage/separation applications. Some MOFs (like Mg/DOBDC and Ni/DOBDC) exhibited exceptional potential for industrial applications of CO_2 capture and CH_4 storage. The stability of MOFs still remains a challenge and a large number of MOFs are known to have poor stability under humid environment.

In general adsorption is primarily governed by the adsorption of high binding energy sites at low pressures and availability of large surface area at higher pressures. In addition, the adsorption characteristics also depend upon the structural configuration (*i.e* the phase) for the flexible adsorbents. The physical properties of adsorbate *viz.* polarity, polarizability and the kinetic diameter also play an important role on the adsorption. A systematic investigation (to understand the role of adsorbate properties, the adsorbent structure, its pore size and its pore volume, the availability of unsaturated metal sites in the framework, the organic linkers and metal cations in the framework, and the framework flexibility) is essential to design and develop MOFs with tailor made structures for targeted applications.

1.9 Research Objectives

The following is a brief of the research objectives of this work. In the first part, structural flexibility of MIL-53(Al) MOF is investigated to tune its structure and obtain enhanced CO_2

uptake capacity and selectivity. In the second part of this work, two categories of MOFs with rigid framework are selected to understand the effect of coordinatively unsaturated (*cus*) metal sites and constituent metal cations in the framework on the adsorption characteristics of MOFs.

Effect of Adsorbent History on the Framework Flexibility of MIL-53(Al)

In general, adsorbents have rigid framework and their adsorption characteristics remain unaltered at a given temperature and partial pressure of the adsorbate. However, some MOFs such as MIL-53 exhibit flexibility in their structure. MIL-53(Al) transforms its structure from large pore (**lp**) domain to narrow pore (**np**) domain and vice versa (so called breathing phenomena); each of these phases have different Henry's constant and adsorption enthalpy for a given gas. Factors such as adsorption of certain guest molecules (like CO_2, H_2O etc.), change in temperature or application of mechanical pressure are known to induce structural transformation in MIL-53(Al). But all the literature reports indicate poor capacity and selectivity of CO_2 on this material. In this work, a systematic investigation will be performed to understand the effect of the adsorption and desorption history of the sample on the adsorption characteristics of MIL-53(Al). By understanding the effect of adsorbent history, we plan to develop a protocol to tune the structure of MIL-53(Al) suitably to enhance its CO_2 uptake and selectivity. MIL-53(Al) has good stability comparable to that of other conventional adsorbents and is one of the reasons behind its choice for this work.

Role of cus Metal Sites, Metal Constituents and Adsorbate Physical Properties on the Adsorption Characteristics of MOFs

Isostructural MOFs with the same metal atom, but with varying organic ligands are fairly common (IRMOF series for example). A significant change in adsorption characteristics of these IRMOFs was observed when organic ligands are varied. On the other hand, studies on adsorption

characteristics for a wide range of gases on isostructural MOFs with same organic ligand but different metal atoms are limited. Substitution of metal centers in the structure has a significant effect on adsorption characteristics of many zeolites. In an effort to understand the role of coordinatively unsaturated (*cus*) metal sites and the constituent metal in the framework on the adsorption characteristics, two different series of isostructural MOFs (*i.e.* M/DOBDC MOFs with coordinatively unsaturated metal sites and M/DABCO MOFs with coordinatively saturated metal sites) with different metal cations were chosen for this study. In the DOBDC series Mg/DOBDC, Mn/DOBDC, Co/DOBDC and Ni/DOBDC MOFs will be synthesized, whereas for DABCO series Ni/DABCO, Cu/DABCO and Zn/DABCO samples will be synthesized. The effect of the metal cations on the adsorption characteristics of a given gas within each of the two isostructural series will be examined.

Several industrially important gases covering a wide degree of polarity and polarizability (*viz.* CO_2, CO, CH_4, N_2, Ar, C_2H_6, and C_3H_8) will be chosen as adsorbates in this study. The adsorption characteristics will be evaluated by measuring adsorption isotherms over a wide range of temperature and pressure in a gravimetric unit. The isotherm modeling will be performed to obtain insights of adsorbate–adsorbent interactions. The model parameters will be utilized to calculate important thermodynamic parameters such as enthalpy of adsorption and Henry's constant. Variation of the enthalpy of adsorption with loading helps in understanding of adsorbate–adsorbent interactions and is also essential to understand the ease of regeneration. Selectivities for various industrially important binary mixtures will also be calculated using Ideal Adsorbed Solution Theory (IAST). The effect of physical properties (kinetic diameter, polarity and polarizability) of adsorbate on their adsorption characteristics on a given MOF will be examined.

The arrangement of this thesis is done as follows.

Chapter 1 discusses the definition of adsorption along with an overview on various types of adsorbents, their importance and limitations. It also includes background and objectives of the present research work. **Chapter 2** presents literature review on history and progress of metal organic frameworks. Adsorption uptake and adsorption enthalpy of several gases of our interest on MOFs as well as on some conventional adsorbents has also been presented. **Chapter 3** includes relevant theory related to adsorption and isotherm modeling. The valuation of important parameters such as Henry's constant, adsorption enthalpy and selectivity predictions using Ideal Adsorbed Solution Theory (IAST) are presented. **Chapter 4** provides the details and protocol for various experiments performed in this work. Details on the calculation methodology for converting raw experimental data into appropriate domain are also presented. **Chapter 5** discusses a tuning method developed in this work to enhance CO_2 uptake and selecitivty of flexible MIL-53(Al) framework. **Chapter 6** contains an adsorption analysis of M/DOBDC MOFs that contain coordinatively unsaturated *(cus)* metal sites. An attempt is made to understand the effect of adsorbate polarity, polarizability, *cus* metal sites and different metal constituent in the framework on the adsorption characteristics of these MOFs. **Chapter 7** discusses adsorption characteristics of various industrially important gases on coordinatively saturated metal site containing M/DABCO series of MOFs. The effect and importance of *cus* metal sites is also highlighted. **Chapter 8** outlines conclusions and future scope.

CHAPTER 2

LITERATURE SURVEY

This chapter presents literature review on history and progress of metal organic frameworks. Some major achievements on MOFs in the field of gas adsorption and gas storage are highlighted. Adsorption uptake and adsorption enthalpy of several gases of our interest on MOFs as well as on some conventional adsorbents have also been listed.

2.1 Metal Organic Frameworks (MOFs)

Metal organic frameworks (MOFs) are the relatively novel porous materials [**36 – 43**] in which metal cations are connected by multitopic organic linkers to form extended crystalline structures [**44**]. Due to lack of a specific definition for these materials during their early stage, other designation such as porous coordination polymer (PCP) [**45**], porous coordination network (PCN) [**46**], zeolite-like metal organic framework (ZMOF) [**47**], metal azolate framework (MAF) [**48**], ZIF (zeolitic imidazolate framework) **[49**], etc. have also been widely used for them. MOFs have unparalleled advantage over other porous materials due to their structural tunability and diversity; a large variety of MOF structures can be realized by varying organic linkers, metal ions, and structural motifs. Due to these reasons, the number of reported MOFs has been increased exponentially over the last few years. Wilmer et al. [**11**] have generated 137,953 hypothetical MOFs from the library of 102 building blocks. The variation in adsorption characteristics have been further magnified by post-synthesis modifications of existing MOFs.

In addition to the structural tunability, MOFs also have large internal surface areas and porosity. In fact, the highest known specific surface area is possessed by MOF-210 (6200 m^2 g^{-1}) [**38**].

2.1.1 Background on MOFs

It is widely accepted that the idea of 3D networks synthesis was first introduced by Hoskins and Robson [**50**] in 1990, using organic molecular building blocks (linkers) and metal ions. This idea proved to be historic after 10 years when two milestone MOFs *viz.* MOF-5 (Figure 2.1) [**36**] and Cu-BTC [**51**] with robust porosity were synthesized. However, the stability of these MOFs was not as good as that of conventional adsorbents such as zeolites and activated carbons. But after that, MIL series of MOFs were synthesized [**39, 41, 52**], with good stability. MIL-53 MOFs also have another especially of exhibiting structural flexibility [**39, 41**]. In 2002, a series of Zn dicarboxylates MOFs have been synthesized based on the concept of isoreticular chemistry [**53**]. Development in MOF synthesis continued further and. in another advancement, $M_2(BDC)_2DABCO$ (M = Cu, Zn) MOFs [**39, 41, 54, 55**] containing mixed organic linkers were reported. Thereafter, large variations in metal ions and organic linkers have been utilized by various research groups to synthesize several MOFs during the last 10 years.

Several developments in the MOF research have occurred over the last few years. A large number of MOFs with varying properties have been synthesized and are reported by several research groups [**36, 38 – 42, 52, 53, 56 – 82**]. O'Keeffe and Yaghi [**36, 38, 40, 53, 56 – 63**] worked extensively on synthesis of several new MOFs. Simultaneous to the development of new structures, focus was also on applications of these materials. It is desirable to have an adsorbent with large specific surface areas to enhance its adsorption characteristics. Due to their large specific surface areas, pore volumes and high porosity, MOFs have been evaluated widely for their adsorption based applications such as gas storage [**25 – 28, 38**], gas separations [**17 – 19**],

catalysis [**20 – 21**] and drug delivery [**22 – 23**]. In gas storage area, MOFs are extensively investigated for methane and hydrogen storage. A major focus of adsorptive separations using MOFs was on evaluation of their performance for carbon dioxide capture applications [**67 – 69**]. In addition, researchers have also explored MOFs as potential candidates for separation of O_2/N_2 and hydrocarbon mixtures. In most of the studies, the separation performance of MOFs is hypothesized from the single component adsorption data of constituent gases.

2.1.2 Design and Synthesis of MOFs

MOFs are self-assembled crystals obtained from metal-containing nodes and organic ligands, connected together through coordination bonds. Thus, the structure of formed material depends on linkage geometries and shape of both components [**72**]. The idea of "node and spacer" was used by many researchers to form "coordination polymers" [**27, 72**]. Based on this concept, synthesis of MOFs with simple structure can be tuned and controlled up to at least certain level; however, it is difficult to implement the "on-paper" design for more complicated cases [**3**]. In many instances, it is impossible to control formation of inorganic clusters during synthesis of MOFs [**73**].

Yaghi and co-workers locked metal ions into rigid metal-oxygen-carbon clusters (by using carboxylate functionality) with the points of extension to obtain entities known as secondary building units (SBUs) [**40**]. MOF-2 [**83**] and MOF-5 [**36**] are the first synthesized MOFs based on this concept of SBUs. In MOF-5 (Figure 2.1), octahedral $Zn_4O(CO)_6$ SBUs are connected to each other through benzene links. This yields a cubic network in which octahedral SBUs act as "nodes' and benzene links as "strut". Since SBUs as well as links are large, the resultant structure has shown exceptional porosity. The concept of SBUs has been used extensively to develop different topologies for MOFs structures [**40, 84**]. Variations in geometry of SBUs and

organic linkers have resulted in the synthesis of a large number of MOFs. To date, more than 11,000 MOF compounds are documented in the Cambridge Structure Database (CSD). Some of the representative organic linkers and MOFs synthesized using them are tabulated in Table 2.1.

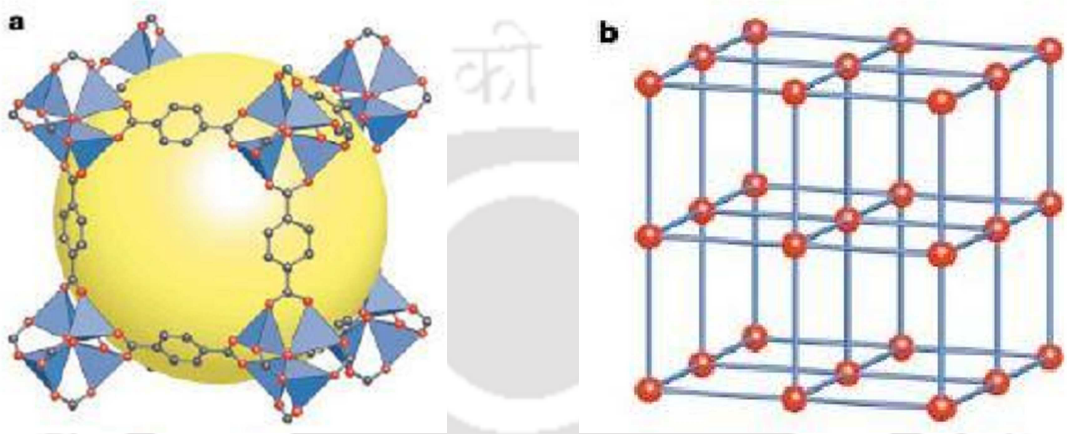

Figure 2.1: MOF-5 structure with topology. (**a**) ZnO_4 tetrahedra (blue polyhedra) are connected by benzene dicarboxylate linkers (O, red and C, black) to form MOF-5 structure; (**b**) The topology of the structure shown as a ball-and-stick model [**40**].

Table 2.1: Some commonly used organic linkers in MOF synthesis.

Organic Linker		MOF	Surface Area ($m^2 g^{-1}$)	Ref.
Name	**Structure**			
benzene 1,4-dicarboxylic acid	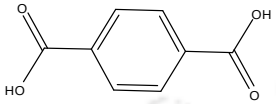	MOF-5	2900	[**59**]
		MIL-53	1140	[**41**]
		MIL-101	2674	[**74**]
2-amino, benzene 1,4-dicarboxylic acid	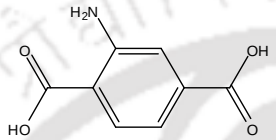	NH_2-MIL-53	960	[**75**]
		IRMOF-3	2160	[**62**]
benzene 1,3,5-tricarboxylic acid	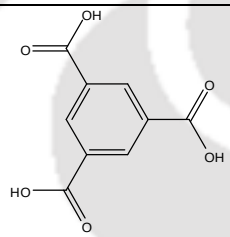	Cu-BTC or HKUST	1482	[**76**]
		MIL-100	1810	[**77**]
2,5-dihydroxy, benzene 1,4-dicarboxylic acid	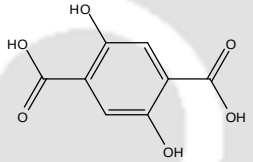	MOF-74 or M/DOBDC (M = Mg, Zn etc.)	885 – 1800	[**67, 78**]
benzene 1,4-dicarboxylic acid and 1,4-diaza bicycle [2,2,2] octane	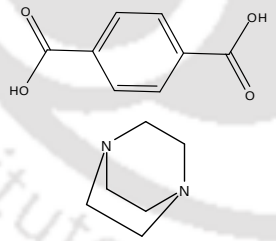	$M_2(BDC)_2DABCO$ or M/DABCO	1400 – 1925	[**79, 80**]
4,4',4''-benzene-1,3,5-triyl-tribenzoic acid	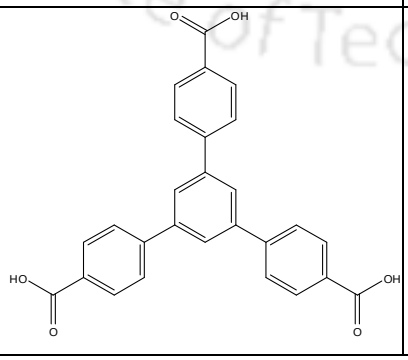	MOF-177	4508	[**62**]

MOFs are generally synthesized through one-pot self-assembly reaction between a metal salt and the organic ligand. The temperature of the reaction is an important parameter in MOF synthesis. Two types of temperature profiles solvothermal and non-solvothermal, are defined in the literature [**85**]. Reaction that takes place in a closed container under autogenous pressure and above the solvent boiling point is known as solvothermal reaction [**86**]. On the other hand, non-solvothermal reactions occur below or at boiling temperature of solvent under ambient pressure [**85**]. In conventional synthesis procedures of MOF, the energy necessary for the reaction is given by heating the reactor typically in an "autoclave" type setup. Energy can also be supplied by more sophisticated means such as electromagnetic radiation, mechanical waves, electric potential or by microwaves [**87**]. These differences in the synthesis routes yield different particle size distributions as well as morphologies, which affect the properties of the product.

2.1.3 Structural Transformation in MOFs

In general, the structure of MOFs is rigid as in case of most Zeolites. However, for some MOFs, significant structural changes take place under certain conditions. When material exhibits two successive structural changes *i.e.* first from a phase with large pore (**lp**) volume to a phase of narrow pore (**np**) volume and then a second one from the **np** to the **lp**, the behavior is known as breathing phenomena [**88**].

MIL-53 series of MOFs are the classic examples of MOFs with flexible structure. These MOFs are made up of interconnecting metal (Cr or Al) clusters which share the corners with benzene dicarboxylate (BDC) organic ligands [**41, 42, 88**]. The structure of these materials changes from large pore (**lp**) domain to narrow pore (**np**) domain and vice versa (Figure 2.2) upon suitable change in its external environment (partial pressure of adsorbate, for example). The cell volume of MIL-53(Al) decreases approximately 35% from 1412 $Å^3$ to 947 $Å^3$ [**41**] during its

transformation from **lp** to **np** domain. MIL-88 is another example of a flexible MOF which changes its structure from one phase to another upon adsorption of various guest molecules. The change in cell volume of this MOF is almost three times from ~2480 $Å^3$ to 8240 $Å^3$ [**89**].

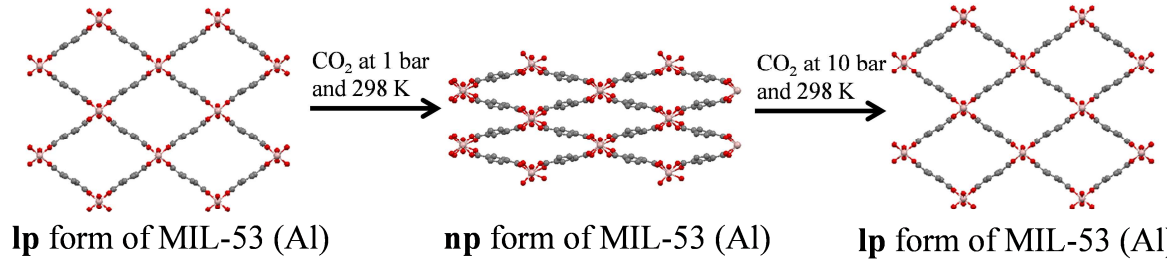

Figure 2.2: Structural transformation of MIL-53(Al) from large pore (**lp)** to narrow pore (**np)** domain followed by reverse transformation to large pore (**lp)** [**90**].

Several factors affect the structural transformation in MOFs. As an example, factors affecting the structural transformation in MIL-53 MOF are discussed next.

(a) Adsorption of certain guest molecules

Férey et al. [**39, 41, 42**] reported the structural transformation of MIL-53 materials upon adsorption of CO_2 and H_2O at room temperature. They propose an initial pore filling stage during CO_2 adsorption where the molecules of CO_2 or H_2O adsorb onto the opposite hydroxyl groups and result in a structural shrinking of pores in the framework; the isotherm shows saturation at about 2 molecules of CO_2 per unit cell. Upon further increase in the pressure, the pores reopen and additional CO_2 adsorption takes place [**42, 91**].

(b) Temperature

Liu et al. [**88**] proposed that structural transformation for MIL-53 occurs even due to change in the temperature. They have reported the following relationship between MIL-53(Al or Cr)

structure and temperature under vacuum. (i) Below 125 K: narrow phase (**np**); (ii) Above 375 K: large phase (**lp**); (iii) 350 – 375 K: **np** to **lp** during heating; (iv) 125 – 150 K: **lp** to **np** during cooling.

(c) Mechanical Pressure

Beurroies et al. [**92**] reported that the structure of MIL-53 can also be transformed from **lp** to **np** phase under vacuum by applying 55 MPa of external mechanical pressure. They also reported that this transformation is reversible.

2.2 Adsorption of Different Gases

One of the important parameter to screen an adsorbent for gas storage and separation applications is its pure component equilibrium adsorption capacities. These investigations also help in understanding the material's adsorption properties. Single-component adsorptions of various gases have so far been reported over a large number of MOFs [**43**]. An overview of literature data on representative adsorption uptakes of several adsorbates used in this study on a variety of MOFs is presented in Tables 2.2 – 2.9. For the sake of comparison, adsorption data on some conventional adsorbents is also included.

Table 2.2: Representative literature for CO_2 adsorption.

Adsorbent	BET Surface Area (m^2 g^{-1})	At 1 bar		At 40 bar		Enthalpy of adsorption at zero coverage (kJ mol^{-1})	Ref.
		Excess amount adsorbed (mol kg^{-1})	Temperature (K)	Excess amount adsorbed (mol kg^{-1})	Temperature (K)		
MOF-2	345	0.6	298	3.2	298	–	[**62**]
MOF-5 (IRMOF-1)	2833	1.0	298	22	298	–	[**62**]
	–	–	–	–	–	14.5	[**93**]
MIL-101	4230	–	–	37	304	44	[**94**]
	2674	2.8	295	–	–	32	[**74**]
Cu-BTC	1663	5.8	295	15.4	295	23	[**95**]
MIL-100	1900	–	–	17.5	303	62	[**94**]
IRMOF-3	2160	1.1	298	18.8	198	–	[**62**]
IRMOF-6	2516	1.05	298	19.7	298	–	[**62**]
IRMOF-11	2096	1.5	298	14.8	298	–	[**62**]
MOF-505 (NOTT-100)	1547	3.2	298	10.4	298	–	[**62**]

Table 2.2 contd.

Adsorbent	BET Surface Area ($m^2 g^{-1}$)	At 1 bar		At 40 bar		Enthalpy of adsorption at zero coverage ($kJ\ mol^{-1}$)	Ref.
		Excess amount adsorbed ($mol\ kg^{-1}$)	Temperature (K)	Excess amount adsorbed ($mol\ kg^{-1}$)	Temperature (K)		
MOF-177	4508	0.8	298	33.9	298	–	[**62**]
	–	–	–	–	–	14	[**68**]
MOF-74 (Zn/DOBDC)	816	4.6	298	10.4	298	–	[**62**]
Mg/DOBDC	1800	8.0	293	15	313	–	[**67**]
Ni/DOBDC	1218	6.9	298	12	298	36	[**96**]
Co/DOBDC	1080	6.7	296	–	–	–	[**97**]
Cu-BTTri	1750	1.9	313	15.6	313	–	[**67**]
MIL-53(Al)	1500^{L}	2.3	304	10.4 (25 bar)	304	35 – 17	[**42**]
MIL-47	1500^{L}	2.5	304	11.4 (25 bar)	304	25-20	[**42**]
Zn/DABCO	1725	2.0	298	14 (15 bar)	298	21.6	[**79**]
Ni/DABCO	1705	2.0	298	12 (15 bar)	298	20.4	[**79**]
MOF-200	4530	–	–	55	298	–	[**38**]
MOF-205	4460	–	–	33	298	–	[**38**]
MOF-210	6240	–	–	53	298	–	[**38**]
Zeolite 13X	616	4.7	298	6.9	298	49	[**35**]

Table 2.2 contd.

Adsorbent	BET Surface Area (m^2 g^{-1})	At 1 bar		At 40 bar		Enthalpy of adsorption at zero coverage (kJ mol^{-1})	Ref.
		Excess amount adsorbed (mol kg^{-1})	Temperature (K)	Excess amount adsorbed (mol kg^{-1})	Temperature (K)		
Norit R1	1450	2.5	298	10	298	22	[**34**]
Maxsorb	3250	2.1	298	27	298	16.2	[**34**]
Silicalite	440	–	–	–	–	–	[**98**]
	–	1.4	308	2.9	304	28	[**99**]

L: Langmuir surface area

Table 2.3: Representative literature for CH_4 adsorption.

Adsorbent	BET Surface Area ($m^2\ g^{-1}$)	Pore volume ($cc\ g^{-1}$)	Crystal density ($g\ cc^{-1}$)	Excess amount adsorbed ($mol\ kg^{-1}$)	Total amount adsorbed		Pressure (bar)	Temperature (K)	Ref.
					($mol\ kg^{-1}$)	($mol\ L^{-1}$)			
Ni/DOBDC	1593[L]	0.56	1.20	7.77	8.62	10.27	35	298	[**100**]
Cu-BTC	2203[L]	0.77	0.88	10.23	11.38	10.04	35	298	[**100**]
Co/DOBDC	1433[L]	0.51	1.17	7.63	8.39	9.87	35	298	[**100**]
PCN-14	2360[L]	0.83	0.83	9.64	10.89	9.02	35	298	[**100**]
Mg/DOBDC	1957[L]	0.69	0.91	8.78	9.82	8.93	35	298	[**100**]
NJU-Bai10	2883	1.11	0.67	11.49	13.21	8.79	35	290	[**101**]
NOTT-109	2110	0.85	0.79	9.89	11.16	8.79	35	300	[**102**]
UTSA-20	1156	0.63	0.61	8.75	9.69	8.79	35	300	[**103**]
NOTT-101	2805	1.08	0.68	11.16	12.77	8.75	35	300	[**102**]
PCN-11	1931	0.91	0.75	10.20	11.56	8.66	35	298	[**104**]
NOTT-100	1661	0.68	0.93	8.32	9.33	8.66	35	300	[**102**]
NOTT-103	2958	1.16	0.64	11.71	13.44	8.66	35	300	[**102**]
PCN-16	2273	1.06	0.72	10.25	11.83	8.57	35	300	[**105**]
NOTT-107	1770	0.77	0.76	10.10	11.25	8.53	35	298	[**106**]
Zn/DOBDC	885	0.41	1.23	6.21	6.83	8.39	35	298	[**78**]

Table 2.3 contd.

Adsorbent	BET Surface Area (m^2 g^{-1})	Pore volume (cc g^{-1})	Crystal density (g cc^{-1})	Excess amount adsorbed (mol kg^{-1})	Total amount adsorbed		Pressure (bar)	Temperature (K)	Ref.
					(mol kg^{-1})	(mol L^{-1})			
MIL-53(Al)	1235	0.54	0.98	7.69	8.48	8.30	35	303	[**107**]
NOTT-102	3342	1.27	0.59	11.86	13.75	8.08	35	300	[**102**]
NU-125	3120	1.29	0.58	11.90	13.84	7.99	35	298	[**108**]
IRMOF-6	2630^{L}	0.92	0.65	10.70	12.14	7.90	36.5	298	[**53**]
Mn/DOBDC	1102	0.50	1.08	11.39	12.14	7.90	35	298	[**78**]
UIO-66-NH_2	1080	0.40	1.36	4.90	5.49	7.46	35	303	[**109**]
IRMOF-1	3995^{L}	1.40	0.62	8.65	10.76	6.70	35	298	[**100**]
UIO-66	970	0.36	1.32	4.38	4.91	6.52	35	303	[**109**]
IRMOF-3	2160	1.07	0.63	8.57	10.18	6.43	36.5	298	[**62, 110**]
MIL-125	1820	0.67	0.81	6.78	7.77	6.29	35	303	[**109**]
UTSA-62	2190	0.91	0.59	9.17	10.54	6.21	35	298	[**111**]
NU-111	4930	2.09	0.41	11.72	14.87	6.07	35	298	[**112**]
PCN-66	4000	1.63	0.44	11.12	13.57	5.98	35	298	[**113**]
DUT-23 (Co)	4850	2.03	0.40	11.72	14.78	5.94	35	298	[**114**]
SNU-71	1770	0.71	0.84	5.85	6.92	5.80	35	298	[**115**]

Table 2.3 contd.

Adsorbent	BET Surface Area (m^2 g^{-1})	Pore volume (cc g^{-1})	Crystal density (g cc^{-1})	Excess amount adsorbed (mol kg^{-1})	Total amount adsorbed		Pressure (bar)	Temperature (K)	Ref.
					(mol kg^{-1})	(mol L^{-1})			
PCN-68	5109	2.13	0.38	11.62	14.82	5.63	35	298	[**113**]
MOF-177	4500	1.89	0.43	10.24	13.08	5.63	35	298	[**38**]
ZIF-8	1445	0.59	1.14	4.00	4.87	5.54	35	303	[**116**]
MIL-125	1820	0.67	0.81	6.78	7.77	6.29	35	303	[**109**]
UTSA-62	2190	0.91	0.59	9.17	10.54	6.21	35	298	[**111**]
NU-111	4930	2.09	0.41	11.72	14.87	6.07	35	298	[**112**]
PCN-66	4000	1.63	0.44	11.12	13.57	5.98	35	298	[**113**]
DUT-23 (Co)	4850	2.03	0.40	11.72	14.78	5.94	35	298	[**114**]
SNU-71	1770	0.71	0.84	5.85	6.92	5.80	35	298	[**115**]
PCN-68	5109	2.13	0.38	11.62	14.82	5.63	35	298	[**113**]
MOF-177	4500	1.89	0.43	10.24	13.08	5.63	35	298	[**38**]
ZIF-8	1445	0.59	1.14	4.00	4.87	5.54	35	303	[**116**]
MIL-100	1900	1.10	0.70	6.01	7.63	5.36	35	303	[**94**]
MOF-205	4460	2.16	0.38	10.77	14.02	5.31	35	298	[**38**]
IRMOF-8	4326	1.83	0.45	8.59	11.34	5.09	35	298	[**117**]
NOTT-119	4118	2.35	0.36	9.59	13.13	4.73	35	298	[**118**]
MIL-101	4230	2.15	0.44	7.10	10.27	4.51	35	303	[**94**]

Table 2.3 contd.

Adsorbent	**BET Surface Area (m^2 g^{-1})**	**Pore volume (cc g^{-1})**	**Crystal density (g cc^{-1})**	**Excess amount adsorbed (mol kg^{-1})**	**Total amount adsorbed**		**Pressure (bar)**	**Temperature (K)**	**Ref.**
					(mol kg^{-1})	**(mol L^{-1})**			
MOF-210	6240	3.60	0.25	9.36	14.78	3.71	35	298	[**38**]
MOF-200	4530	3.59	0.22	8.17	13.57	2.99	35	298	[**38**]
AX-21 activated carbons	4880^{L}	1.64	0.49	11.59	14.06	6.88	35	298	[**100**]
Zeolite 13X	616	0.27	1.43	2.89	3.30	4.73	35.5	298	[**119, 120**]

L: Langmuir surface area

Table 2.4: Representative literature for CO adsorption.

Adsorbent	**Low pressure**			**High pressure**			**Enthalpy of adsorption at zero coverage (kJ mol^{-1})**	**Ref.**
	Excess amount adsorbed (mol kg^{-1})	**Pressure (bar)**	**Temperature (K)**	**Excess amount adsorbed (mol kg^{-1})**	**Pressure (bar)**	**Temperature (K)**		
IRMOF-1	0.58	1	298	7.2[g]	40	298	9.3	[**121**]
IRMOF-3	0.6[g]	1	298	7.2[g]	40	298	10.1	[**121**]
Zn/DABCO	–	–	–	7.8[g]	40	298	12	[**121**]
Cu-BTC	1.4	1	295	9.1	43	295	24	[**95**]
MIL-101	0.89	1	295	6.6	68	295	44	[**95**]
Ni/DOBDC	5.6	0.8	303	–	–	–	58	[**122**]
MIL-53(Al)	0.30	1	303	–	–	–	16.4	[**107**]
Zeolite 13X	1.17	1.1	303	3.12	10.2	303	20	[**123**]
Silicalite	0.27	1.2	305	1.0	7.3	305	16.7	[**124**]

g: data obtained from GCMC simulation

Table 2.5: Representative literature for N_2 adsorption.

Adsorbent	**Low pressure**			**High pressure**			**Enthalpy of adsorption at zero coverage (kJ mol^{-1})**	**Ref.**
	Excess amount adsorbed (mol kg^{-1})	**Pressure (bar)**	**Temperature (K)**	**Excess amount adsorbed (mol kg^{-1})**	**Pressure (bar)**	**Temperature (K)**		
IRMOF-1	–	–	–	4.8[g]	40	298	8.4	[**121**]
IRMOF-3	–	–	–	4.85[g]	40	298	9	[**121**]
Zn/DABCO	–	–	–	5.2[g]	40	298	11	[**121**]
	–	–	–	1.48	15	298	–	[**79**]
Ni/DABCO	–	–	–	1.46	15	298	–	[**79**]
MIL-53(Al)	0.20	1	303	–	–	–	15.9	[**107**]
Cu-BTC	0.31	1	295	2.32	10	298	–	[**125, 126**]
MOF-177	0.2	1	293	–	–	–	10	[**68**]
Mg/DOBDC	1.1	1	293	–	–	–	18	[**68**]
Ni/DOBDC	1.02	1	298	6.45	100	298	–	[**96**]
Zeolite 13X	0.8	2	298	–	–	–	–	[**35**]
	–	–	–	2.5	100	288	14 – 9.1	[**127**]
Silicalite	0.27	1.2	305	1.0	7.3	305	16.7	[**124**]
Norit R1	0.39	1.1	298	4.1	59.8	298	–	[**128**]

g: data obtained from GCMC simulation

Table 2.6: Representative literature for Ar adsorption.

Adsorbent	**Low pressure**			**High pressure**			**Enthalpy of adsorption at zero coverage (kJ mol^{-1})**	**Ref.**
	Excess amount adsorbed (mol kg^{-1})	**Pressure (bar)**	**Temperature (K)**	**Excess amount adsorbed (mol kg^{-1})**	**Pressure (bar)**	**Temperature (K)**		
Cu-BTC	1.25	5	298	2.13	10	298	–	[**125**]
	0.44	1.6	295	1.91	9.2	295	–	[**76**]
MIL-53(Al)	0.17	1	303	–	–	–	15.1	[**107**]
MIL-101	0.12	0.9	283	2.0	10	283	15	[**74**]
Zeolite 13X	0.9	12.5	288	2.5	100	288	11 – 8	[**127**]
Silicalite	0.19	1.2	305	0.9	7.3	305	–	[**124**]
AC (BPL)	0.39	1.4	303	3.6	37.4	303	–	[**129**]

Table 2.7: Representative literature for C_2H_6 adsorption.

Adsorbent	**Low pressure**			**High pressure**			**Enthalpy of adsorption at zero coverage (kJ mol^{-1})**	**Ref.**
	Excess amount adsorbed (mol kg^{-1})	**Pressure (bar)**	**Temperature (K)**	**Excess amount adsorbed (mol kg^{-1})**	**Pressure (bar)**	**Temperature (K)**		
Cu-BTC	1.0	0.1	295	4.8	1	295	–	[**126**]
MOF-5	–	–	–	1.9	1	297	15.1	[**130**]
MIL-101	3.0	1	298	15.5	8.5	298	45-30	[**131**]
Mg/DOBDC	1.5	0.1	298	6.3	1	298	27	[**132**]
Fe/DOBDC	1.03	0.1	318	6.6	1	318	25	[**133**]
Zeolite 13X	0.4	0.1	323	1.6	1	323	29.22	[**134**]
Silicalite	1.9	1	308	2.4	20	308	29	[**99**]
Zeolite 5A	1.4	1	293	2.22	13.9	293	10	[**135**]

Table 2.8: Representative literature for C_3H_8 adsorption.

Adsorbent	**Low pressure**			**High pressure**			**Enthalpy of adsorption at zero coverage (kJ mol^{-1})**	**Ref.**
	Excess amount adsorbed (mol kg^{-1})	**Pressure (bar)**	**Temperature (K)**	**Excess amount adsorbed (mol kg^{-1})**	**Pressure (bar)**	**Temperature (K)**		
Cu-BTC	5.2	0.1	318	7.2	1	303	44	[**136**]
MOF-5	17.5	0.1	300	19	1	300	20.17	[**137**]
MIL-53(Cr)	2.4	0.1	303	4.0	1	303	–	[**138**]
MIL-53(Fe)	0.0	0.1	303	2.4	1	303	–	[**138**]
Mg/DOBDC	7.1	0.1	298	8.2	1	298	33	[**132**]
Fe/DOBDC	4.6	0.1	318	5.3	1	318	33	[**133**]
NaX	3	0.1	293	3.2	1	293	34.4	[**139**]
Silicalite	1.66	0.1	308	1.94	1	308	41	[**99**]
activated carbon ASA	5.0	0.1	273	8.3	1	273	40.7	[**140**]

Table 2.9: Representative literature for O_2 adsorption.

Adsorbent	**Low pressure**			**High pressure**			**Enthalpy of adsorption at zero coverage (kJ mol^{-1})**	**Ref.**
	Excess amount adsorbed (mol kg^{-1})	**Pressure (bar)**	**Temperature (K)**	**Excess amount adsorbed (mol kg^{-1})**	**Pressure (bar)**	**Temperature (K)**		
Cu-BTC	0.3	1	295	–	–	–	13.88	[**126**]
MIL-53(Al)	0.13	1	303	–	–	–	14.5	[**107**]
Zn/DABCO	0.4	2.5	298	–	–	–	–	[**79**]
Fe/DOBDC	3.75	0.1	226	5.4	1	226	41	[**141**]
Zeolite 13X	0.2	1	306	–	–	–	15	[**32**]
Silicalite	0.15	1	305	–	–	–	16.3	[**142**]
Zeolite 5A	0.18	0.96	296	1.8	17.7	296	10	[**143**]
AC (BPL)	0.42	1.6	303	3.4	37.4	303	–	[**129**]

The data in tables 2.2 – 2.9 clearly indicates that considerable variation in the adsorption uptake is observed for MOFs than in case of conventional adsorbents such as zeolites or activated carbons. While significant studies are done on CO_2 and CH_4 adsorption on MOFs, the research work reported on adsorption of other industrially important gases (like CO, for example) on MOFs is limited. Some MOFs with moderate surface area (M/DOBDC, Cu-BTC etc.) exhibit high CO_2 uptake at ambient conditions. In addition, these MOFs have also shown exceptionally high saturation volumetric loading for CH_4 at ambient temperature, however saturation gravimetric uptakes of CH_4 at ambient temperature on these MOFs would not be as high as that on MOFs with high surface area such as MOF-177, MOF-200, MOF-205, MOF-210 etc. It should be emphasized that adsorption uptake on volumetric scale is also important, since the size (volume) of adsorptive vessel is governed by the volumetric uptakes.

2.3 Potential Applications of MOFs

The porosity in MOFs coupled with the heterogeneity in the surface characteristics has encouraged researchers to study them for potential applications in the fields of separation, gas storage, catalysis, biomedicine, sensors, microelectronics etc. This section presents the highlights of some important developments on MOFs for gas (H_2, CH_4) storage and separation applications.

2.3.1 Gas Storage

Methane is considered to be a cleaner fuel. However, its energy density at ambient temperature and pressure is only 0.04 MJ L^{-1}, compared to 32.4 MJ L^{-1} for gasoline [**144**]. The volumetric energy density of methane can be increased by compression or liquefaction, but these techniques are economicaly expensive [**100**]. In order to overcome these limitations, the energy density of methane at ambient temperature and moderate pressure (~ 35 bar) can be alternatively increased

by adsorbing it onto porous materials. US Department of Energy (DOE) has set volumetric methane storage target as 263 cc/cc. Considering a 25% volumetric loss due to packing of adsorbent [**100**], methane uptake of 350 cc(STP)/$cc_{adsorbent}$ is needed to meet the above target. Over the last decade, MOFs are widely evaluated for methane adsorption as illustrated in Table 2.3. In a major contribution, Yaghi and coworkers have synthesized a series of very high surface area / pore volume possessing MOFs such as MOF-177, MOF-200, MOF-205 and MOF-210 [**38**]. These MOFs exhibit very good gravimetric methane uptake (293-331 cc/g) at 35 bar and ambient temperature [**38**]. However, their volumetric uptake for the same conditions is considerably lower (only 67-126 cc(STP)/ $cc_{adsorbent}$) due to the poor crystal densities [**38, 100**]. In fact, these uptake values are lower than that on activated carbons such as AX-21 [**100**]. Ma et al. [**145**] reported Cu_2(adip) ($adip^{4-}$ = 5,5`-(9,10-anthracene-diyl)di-isophthalate) or PCN-14 MOF as the best adsorbent for methane storage with a volumetric uptake of about 230 cc(STP)/cc at 35 bar and 290 K. Later, Peng et al. [**146**] reported the highest total volumetric uptake (267 cc(STP)/cc) on Cu-BTC at 65 bar and 298 K meeting the DOE target of 263 cc/cc methane storage. Recently, uptake at 35 bar and 298 K on Ni/DOBDC (228 cc(STP)/cc) was found to be slightly higher than that on Cu-BTC (227 cc(STP)/cc) and PCN-14 (195 cc(STP)/cc) [**146**]. Mason et al. [**100**] performed the methane adsorption on six representative MOFs *viz.* Cu-BTC, Ni/DOBDC, Mg/DOBDC, Co/DOBDC, PCN-14, MOF-5 and one AX-21 activated carbon over 0 – 100 bar range at 298 K; similar to Peng et al. [**146**] work, volumetric uptake was highest on Ni/DOBDC up to ~35 bar and later at higher pressures, Cu-BTC exhibits a better capacity due to its high pore volume.

Hydrogen is also considered as a promising fuel to meet the energy requirements of future [**147**]. On a gravimetric basis, hydrogen has almost three times higher energy value than gasoline; lower heating value of hydrogen and gasoline are 123 MJ kg^{-1} and 47.2 MJ kg^{-1}, respectively

[**148**]. However, on a volumetric basis, liquid hydrogen has only 8 MJ L^{-1} energy density compared to 32 MJ L^{-1} for gasoline [**148**]. For a car using hydrogen as fuel, about 5 – 13 kg of hydrogen would be needed per 300 miles drive [**148**]. In order to reduce the size and pressure of on-board hydrogen feed tank, the energy density of hydrogen needs to be improved. DOE targets for 2017 of hydrogen storage are 5.5 wt% in gravimetric scale and 40 g L^{-1} in volumetric scale at an operating temperature of – 40 to 60 ^{o}C under a maximum delivery pressure of 100 bar [**148**]. Hydrogen storage on a variety of materials such as chemical hydrides [**149**], carbohydrate [**150**], inorganic nanotubes [**151**], porous adsorbents [**152**] etc. was reported in the literature. MOFs are one of the extensively studied adsorbent materials for hydrogen storage and are considered to be the promising candidates. Hydrogen uptake on MOF (4.5 wt% at 77K and 1 bar on MOF-5) was reported in 2003 for the first time [**57**]. Thereafter, a large number of research articles reporting hydrogen adsorption on several MOFs are published in the literature. The highest known excess hydrogen uptake at 77 K is 9.95 wt% on NU-100 MOF at 56 bar [**65**]. This material also has total uptake of 16.4 wt% at 77 K and 70 bar. On the other hand, the highest reported total uptake is 17.6 wt% (excess 8.6 wt%) on MOF-210 at 77 K and 80 bar [**38**]. Zhou et al. [**147**] have measured the hydrogen uptake on M/DOBDC (M = Mg, Mn, Co, Ni, Zn) MOFs at 150, 100 and 77 K up to 30 bar. While their excess uptake (2.3 – 2.8 wt%, 77 K) below 5 bar pressure is promising, the same is not true for higher pressures. At ambient temperature, hydrogen uptake on MOFs are very low (typically ~0.5 wt%). Till date no MOF is known which meet the DOE target. However, in order to achieve DOE target, several attempts are being made by improving the surface functionalities of MOFs [**153 – 157**].

2.3.2 Separation of Gases

Mason et al. [**68**] evaluated the performance of MOF-177 and Mg/DOBDC for temperature swing adsorption process of CO_2 capture from flue gas by measuring the single component

adsorption isotherms of CO_2 and N_2 across the entire temperature range (293 – 473 K). They calculated the working capacity as the difference between CO_2 loading at adsorption condition (0.15 bar and 313 K) and desorption condition (1 bar and considered desorption temperature). Maximum working capacity of 17.6 wt% was obtained for 473 K desorption temperature. As expected, with increase of desorption temperature working capacity increased, but at the same time regeneration at higher temperature is also more expensive. On the other hand, negative working capacities were obtained for MOF-177. Authors also compared the working capacities of Mg/DOBDC with that of benchmark NaX. NaX exhibits higher working capacity than Mg/DOBDC for desorption temperature less than 353 K, but for higher desorption temperatures, working capacity of NaX was lower. CO_2 selectivity over N_2 at 313 K for a mixture of 0.15 bar CO_2 and 0.75 bar N_2 was also significantly higher on Mg/DOBDC (175) than that on MOF-177 (5) and NaX (115).

Krishna [**158**] examined Cu-BTC, MIL-101, Zn/DABCO and Zeolite NaX for separation of CO_2 from mixture of CH_4 and CO for pressure swing adsorption process. NaX appeared to have highest selectivity for CO_2 over both CO and CH_4. For lower pressures (up to 10 bar), NaX exhibits best performance due to its highest working capacity; however, at higher pressures *ca.* 60 bar, Cu-BTC was found to perform better. Among all adsorbents studied, MIL-101 exhibits lowest working performance even though it has highest surface area.

Herm et al. [**67**] tested MOF-177, Co(BDP), Cu-BTTri and Mg/DOBDC for hydrogen purification and precombustion CO_2 capture. They measured single component adsorption data of both CO_2 and H_2 at 313 K up to 40 bar. They compared the performance of these materials with that of NaX and Carbon JX101. IAST predictions indicate exceptional CO_2 selectivity over H_2 (826) on Mg/DOBDC for a binary mixture containing 80% hydrogen at 313 K. Interestingly, both gravimetric as well as volumetric working capacities on Cu-BTTri were higher than those

on other adsorbents including Mg/DOBDC. In another work, Herm et al. [**69**] analyzed Mg/DOBDC MOF for high pressure $CO_2/CH_4/H_2$ separation. They concluded that significant enhancement in separation can be obtained by using Mg/DOBDC over NaX.

Xiang et al. [**159**] compared the performance of UTSA-16 with that of Mg/DOBDC and many more adsorbents for CO_2/CH_4 and CO_2/N_2 separation. Initially, Mg/DOBDC performed better than UTSA-16. However, after exposing both the adsorbents towards moisture, the performance of Mg/DOBDC decreases upon. On the other hand, CO_2 sorption was repeatable and reversible for UTSA-16 even after further exposing the adsorbent sample to air for three days.

Separation of O_2/N_2 is a useful industrial separation. Bloch et al. [**141**] synthesized a new MOF (Fe/DOBDC) with open iron-(II) coordination sites. This MOF exhibits selective binding for O_2 over N_2 *via.* electron transfer interactions. They reported the highest known O_2 over N_2 selectivity (7.5) for equimolar mixture at 1 bar and 298 K. However, high temperature (473 K) was needed for desorption of O_2, which resulted into the decomposition of the structure. So they identified 226 K to be more suitable for separation of O_2/N_2 using Fe/DOBDC.

MOFs have also shown extraordinary performance for lower olefin/paraffin separations. Bae et al. [**160**] calculated the propene/propane selectivity by using IAST for Mg/DOBDC, Mn/DOBDC and Co/DOBDC samples. They obtained a selectivity of 46 on Co/DOBDC at 1 bar and 298 K for equimolar mixture. They also performed the breakthrough experiments to confirm this result. Later, Bloch et al. [**133**] measured equilibrium adsorption isotherms of methane, ethane, ethylene, acetylene, propane, and propylene on Fe/DOBDC MOF at 318, 333, and 353 K to investigate its ability for $C_1 - C_3$ separation. This material exhibits very strong affinity for unsaturated acetylene, ethylene, and propylene hydrocarbons. For an equimolar mixture and 318 K, ethylene selectivity over ethane on Fe/DOBDC ranges from 13 to 18, which is higher than

that on NaX (9 to 14) and Mg/DOBDC (4 to 7). Similarly, selectivity of propylene over propane on Fe/DOBDC (13 to 15) was also higher than that on other adsorbents.

2.4 Modification of MOF Structure

In order to improve the performance of MOFs for gas storage, separation, and catalysis related applications, their structure can be modified by a variety of techniques as some of them discussed in this section.

2.4.1 Functionalization of MOFs

Functionalization of organic ligand (1,4-benzene dicarboxylic acid) of IRMOF-1 with $-NH_2$, resulted in a formation of a IRMOF-3 with different adsorption properties [**62**]. CO_2 uptake at ambient condition on IRMOF-3 was found to be higher that on IRMOF-1 [**62**]. IRMOF-3 was further acetylated with acetic anhydride to produce IRMOF-3-AM1 with a yield of >90% [**161, 162**]. Biswas et al. [**163**] observed the different breathing phenomena in MIL-53(Al) when they incorporated various functional groups (like -Cl, -Br, $-CH_3$, $-NO_2$, $-(OH)_2$) in the structure. In an attempt of metal functionalization, Himsl et al. [**164**] exchanged 15% of the acidic protons of the MIL-53(Al) MOF with lithium by using lithium diisopropylamide (LDA). As a result, the BET surface area reduced from 1564 $m^2\ g^{-1}$ to 1384 $m^2\ g^{-1}$. But hydrogen uptake at 1 bar and 77 K increased from 0.5 wt% to 1.7 wt%. Xiang et al. [**165**] doped lithium inside Cu-BTC and MIL-101 structure to improve hydrogen uptake at 1 bar and 77 K; however doping resulted in a decrease of the surface area of the resultant materials.

2.4.2 Generation of Coordinatively Unsaturated Metal Sites in MOFs

Metal centers in a MOF system possess fixed number of coordination vacancies through which they connect to the organic ligands. If some of these positions can be 'opened', the material will have coordinatively unsaturated (*cus*) metal sites. These *cus* metal sites induce additional electrostatic interactions for polar gases. MIL-101 is the one of the first synthesized MOF known to have *cus* metal sites [**52**]. This material exhibits a large Henry's constant and selectivity for polar gases such as CO_2 and CO compared to other MOFs without *cus* metal centers (MOF-5 for example) [**74, 94**]. However, due to bigger pore diameter and only a small number of *cus* metal sites in MIL-101, the effect is not pronounced and Cu-BTC with smaller pore size seems to be better for CO_2/CH_4 separation [**158**]. M/DOBDC series frameworks are one of the most interesting series of metal organic framework and are extensively studied for CO_2 capture. These materials are known to have a large number of *cus* metal sites. In these MOFs, 2,5-dihydroxyterepthalic organic linker exists in its tetraanionic form *i.e.* 2,5-dioxido-1,4-benzene-dicarboxylate (DOBDC), in which both the aryloxide and carboxylate moieties act as ligands to the metal. This coordination results occupation of five coordination positions by oxygen atoms. The sixth position is occupied by water (solvent) molecule which can be removed by thermal treatment (at higher temperature) under vacuum, making the metal sites in the framework unsaturated [**166 – 169**]. These metal sites exhibit exceptional affinity for polar CO_2 adsorbate. Substitution of suitable metal ions such as Mg in place of Zn increases the CO_2 uptake by more than 2 times at 0.1 bar and ambient temperature for M/DOBDC MOFs [**97**].

2.4.3 Structural Flexibility

MIL-53 series of MOFs are known to have flexible structure [**39, 41**]. In addition to being extensively investigated to understand the breathing phenomenon, these MOFs have also been

evaluated for selective adsorption of gases [**17, 42, 170**], vapor [**171**], and liquid compounds [**172, 173**]. Hydrated form of MIL-53(Cr) has showed near zero adsorption uptake for CH_4, but adsorbs CO_2 due to the gating effect [**170**]. A similar gating phenomenon has been observed in some others MOFs like SNU-M10 [**170**] and ELM-11 [**174**]. It has been demonstrated that these materials can be used for selective adsorption of different gases at different gate-opening pressures, which depends on the physical properties of gas molecules. $Cu(dhbc)_2(bipy)$ MOF[**175**] presents the typical example of gate-opening phenomena. On this MOF, initially CO_2, CH_4, N_2 and O_2 isotherms are flat (near zero uptakes in the low pressures), followed by a sudden increase in uptake of each gas at corresponding gate-opening pressure. Cd(bpndc)(bipy) has also shown different gate opening pressures during adsorption of Ar, O_2 and N_2 at low temperature. In addition, selective adsorption of O_2 and NO over N_2, as well as benzene over cyclohexane at room temperature has been obtained on Zn(TCNQ-TCNQ)(bipy). Attempts have also been made to develop the flexible motif into a rigid lattice of MOFs to obtain a highly selective sorption of CO_2 over N_2 and CH_4 [**176**]. In another work, mesh-adjustable molecular sieves (MAMSs) MOFs exhibit temperature-dependent selective adsorption of gases [**177, 178**].

2.5 Structural Properties of MOFs

An outstanding challenge in the prediction of a 'suitable MOF structure' for a target application is to understand the role of various parameters such as pore size, surface area, *cus* metal sites, different metal constituents, organic linker etc. on the adsorption characteristics of MOFs. Eddaoudi et al. [**53**] replaced organic linker (1,4-benzene dicarboxylic acid) of IRMOF-1 (or MOF-5) with other organic linkers and synthesized a series of MOFs (IRMOF-1 to IRMOF-16). With increasing the size of organic linker (from one benzene ring to two or more benzene rings),

the specific surface area of the resultant MOF increases; this indicates a better gravimetric saturation adsorption uptake on MOFs formed from a bulky organic linker. However, with increasing size of the organic linker, crystal density and hence the volumetric adsorption uptake of the MOF decreases.

Karra et al. [**71**] performed the numerical simulations to obtain the adsorption isotherms of CO, CH_4, N_2 and H_2 on Cu-BTC. They reported the presence of electrostatic interactions between CO and Cu-BTC framework and insignificant CO-CO interactions. However, Cu-BTC was not found to be selective for CO over CH_4 because lateral interactions between CH_4 molecules were large enough to counter balance both the electrostatic interactions and the lateral interactions of CO molecules as CO has smaller polarizability. They also further compared the adsorption characteristics of Cu-BTC, Zn/DABCO, IRMOF-1 and IRMOF-3 [**121**] to investigate effect of small pore size and *cus* metal sites. They observed slightly higher CO_2 adsorption uptake on Cu-BTC (MOF with moderate pore size and *cus* metal sites) than that on Zn/DABCO (MOF with smaller pore size and no *cus* metal sites) at low pressure and ambient temperature. However, the pore size has a much smaller impact than the *cus* metal sites and higher CO uptake was found on Cu-BTC. Recently, Chowdhury et al. [**95**] compared the adsorption characteristics of Cu-BTC (moderate pore size and less exposed *cus* metal sites) and MIL-101 (bigger pore size and exposed *cus* metal sites). They observed higher Henry's constants for CO_2 and CO and lower Henry's constant for CH_4 on MIL-101 at ambient temperature. This confirms the more pronounced impact of *cus* metal sites than that of pore size for polar adsorbates. However, for non-polar adsorbate, the effect of pore size has more impact. Similar to the observations of Karra et al. [**121**], the difference between the Henry's constant of MIL-101 and Cu-BTC was more for CO than CO_2 in the work by Chowdhary et al. [**95**].

2.6 Simulation Studies on MOFs

Due to possibility of synthesis of a large number of MOF structures, it is infeasible to design the optimal MOF structure for a targeted application only by experimentation. Molecular level information responsible for the experimentally observed macroscopic properties cannot be obtained by experimental methods and simulations can provide molecular level insights into the underlying mechanism involved [**179, 180**]. Simulations can help in screening the large number of MOFs for a particular application and it can also provide the ability to hypothesize the structure of best performing MOF. In most of the simulation studies, adsorption isotherms of MOFs are calculated using the grand canonical Monte Carlo (GCMC) method [**81, 82**]. Excellent review articles that summarize the development in simulation works on MOFs are available in literature [**70, 181 – 184**]. Duren et al. [**183**] have demonstrated that the information obtained from molecular simulations can help in developing the design principles for a specific adsorption application on MOFs. Krishna [**184**] presented a review on diffusion characteristics of a single gas as well as mixture in a wide spectrum of porous materials including MOFs. Jhon et al. [**185**] presented a simulation study highlighting the effect of alkoxy-functionalization on IRMOFs, as they found the highest CH_4 uptake at low and moderate pressure on IRMOF-6 due to the stronger potential overlap of smaller pores. Binding energies of CH_4 for its adsorption on M/DOBDC MOFs were calculated using first-principles calculations based on density-functional theory [**78**]. The results indicate that CH_4 affinity to the *cus* metal sites of these MOFs is higher than that to the typical adsorption sites in most of the other MOFs. Liu and Smit [**186**] have done simulations to compare the performance of zeolites (MFI, DDR and LTA) and MOFs (Cu-BTC, MIL-47, IRMOF-1, IRMOF-11, IRMOF-12, IRMOF-13, IRMOF-14). They reported that though MOFs exhibit better characteristics compared to zeolites for gas storage, their performance in separation is similar to that of zeolites. They reported that difference in the polarity of constituent

adsorbates in the mixture should be an important factor for selecting a suitable material for separation.

2.7 Stability of MOFs

Stability of an adsorbent is an important factor to understand the feasibility of its usage for practical applications. The stability of MOFs can be divided as framework stability, thermal stability and chemical stability. The structural stability upon removal of guest molecules from the as-synthesized product refers to the framework stability of the material. MOFs with smaller pore size or volume have better framework stability and those with higher pore size or volume generally have poor framework stability. Use of metal clusters as the nodes is one of the highly used techniques to synthesize stable MOFs. Thermal stability is a major issue for many MOFs because they are not stable at temperature above 473 K. However, few numbers of MOFs can be used up to 500 K or more without losing their framework stability. In contrast, conventional adsorbents are stable at even more than 1000 K temperature. When the bonds between metal nodes and organic ligands break upon its exposure to the adsorbate molecules, then the material is called chemically unstable. For practical applications such as CO_2 separation from flue gas, stability of MOFs in humid condition is essential. Recently, water stability of several MOFs such as Cu-BTC, MOF-5, MOF-177, UMCM-150, MOF-505, MIL-101 and ZIF-8 have been examined by Cychosz and Matzger [**187**]. They reported the best stability for MIL-101 followed by Cu-BTC and ZIF-8; MOF-5 and MOF-177 were found to be highly unstable. Kizzie et al. [**188**] explored the effect of humidity on performance of M/DOBDC MOFs, while all the M/DOBDC MOFs were found to be unstable upon exposure to moisture; Co/DOBDC was relatively less unstable compared to others in the series. Liang et al. [**79**] evaluated the stability

of $M_2(BDC)_2(Dabco)$ (M=Zn,Ni) MOFs in humid environment. They observed these frameworks were stable upon 30% relative humidity water vapor at 25 ^oC, but they collapsed at a 60% relative humidity water vapor sorption. Later, Walton and coworkers [**189**] have improved the stability of $Zn_2(BDC)_2(Dabco)$ for water exposure of up to 90% relative humidity by proper functionalization of the BDC ligand. Placing of non-polar shielding groups (e.g., methyl) on the BDC linker enhanced the stability whereas placing polar groups (e.g., −OH) on the BDC linker destabilized the structure at lower humidity.

MOFs look to be more versatile than conventional adsorbents. In most of the studies, the performance of MOFs are evaluated and compared with other adsorbents. However, to move from lab scale to pilot plant and eventually to industrial scale, a lot of "tuning" in terms of stability, selectivity, uptake capacity etc. is still necessary before MOFs make an appearance as practical alternatives to existing adsorbents. Limited amount of work is done on the investigation of the adsorption characteristics of these materials systematically and link it to the physical characteristics of the adsorbate / adsorbent pair. In this work, an attempt will be made to correlate the adsorption uptake with various parameters such as *cus* metal sites, the constituent metal in the MOF structure, polarity and polarizability of adsorbate. In addition, the structure of flexible MIL-53(Al) MOF will be judicially tuned to enhance its uptake and selectivity for CO_2.

CHAPTER 3

THEORY

This chapter includes some theory related to adsorption and isotherm modeling. The valuation of important parameters such as Henry's constant, adsorption enthalpy and selectivity predictions using Ideal Adsorbed Solution Theory (IAST) are presented.

3.1 Phase Rule for Adsorption

In general, phase equilibrium indicates equality of thermal, mechanical and chemical potentials. Adsorption is a surface phenomenon, and due to additional intensive variable, adsorption has one extra degree of freedom compared to that of bulk phase equilibria. The phase rule for adsorption is thus [**190**],

$$F = C - \chi + 3 \qquad 3.1$$

Where- F = number of degrees of freedom

C = number of chemical species and

χ = number of phases

3.2 Equilibrium Adsorption Isotherm

Due to additional degree of freedom, the equilibrium amount adsorbed for a pure gas on an adsorbent is a function of two variables (pressure and temperature).

$$N = I\{P,T\} \tag{3.2}$$

where, N is the amount adsorbed, P is the pressure and T is the temperature.

At constant temperature, the adsorbed amount is

$$N = I\{P\} \tag{3.3}$$

and this relationship is commonly called as an adsorption isotherm. Fugacity (f) is used instead of pressure to account for non-ideality in the gas phase at high pressures [**191**] and then isotherm relationship becomes.

$$N = I\{f\} \tag{3.4}$$

IUPAC has classified the adsorption isotherms into different types (Figure 3.1) [**192**]. Type I represent the adsorption characteristics of microporous adsorbent in which the molecular diameter of the adsorbate matches exactly with the pore diameter of the adsorbent. This type of isotherms have definite saturation limit corresponding to the complete filling of the micropores. Non-porous or macroporous adsorbents show types II, III and VI isotherms whereas mesoporous adsorbents exhibit types IV and V isotherms. Shape of isotherms itself indicate that there is stronger gas-solid interactions for type II and IV and weaker one for type III and V. Shape of type VI suggests the multilayer formation either on a plane surface or on the walls of pores which are much larger than the molecular diameter of the adsorbate molecule.

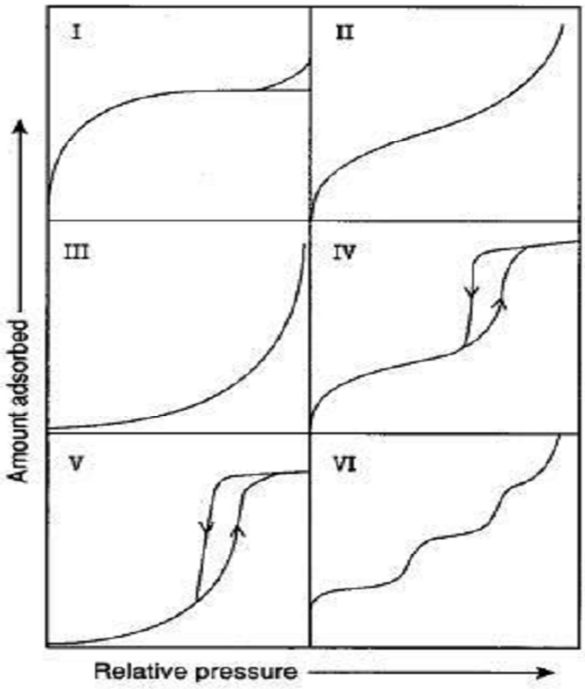

Figure 3.1: IUPAC classifications of adsorption isotherms [**192**].

3.3 Henry's Constant

The linear relationship between fluid phase and adsorbed concentrations is known as Henry's law and Henry's constant is defined as the slope of the isotherm at the limit of zero pressure.

Mathematically, Henry's constant, β, is written as Eq. 3.5.

$$\beta = \left(\frac{N}{P}\right)_{P \to 0} \qquad 3.5$$

The Henry's constant (β) is a measure of vertical interactions between adsorbate and adsorbent.

3.4 Models for Pure Gas Isotherms

In the following section, various adsorption isotherm models used in this work are presented. All of the discussion presented here is related to excess adsorption.

3.4.1 Langmuir Isotherm

The Langmuir model is based on the following assumptions:

(i) Fixed number of adsorption sites

(ii) Each site can hold only one molecule

(iii) All sites are equally energetic

(iv) No lateral interactions between adsorbate–adsorbate molecules

Based on the above assumption Langmuir equation is formulated as

$$N = \frac{N^{\max} \beta f}{N^{\max} + \beta f} \tag{3.6}$$

where, N (mol kg^{-1}) is the excess amount adsorbed, f (bar) is the fugacity, N^{max} (mol kg^{-1}) is the saturation capacity, β (mol kg^{-1} bar^{-1}) is Henry's constant. Saturation capacity is considered to be independent of temperature; and the temperature dependency for Henry's constant is expressed by

$$\beta = \beta^{(0)} \exp\left(\beta^{(1)}/T\right) \tag{3.7}$$

where, T is temperature in K. The two parameters $\beta^{(0)}$ and $\beta^{(1)}$ are related to entropy and enthalpy of adsorption at zero loading, respectively.

3.4.2 Dual Site Langmuir (DSL) Isotherm

The Dual Site Langmuir (DSL) model demonstrates the existence of two types of adsorption sites of different energetic. Each site follows a Langmuir adsorption behavior. A DSL isotherm model is given by [**193**]

$$N = \frac{N_1^{\max} \beta_1 f}{1+\beta_1 f} + \frac{N_2^{\max} \beta_2 f}{1+\beta_2 f} \qquad 3.8$$

where, N_1^{max} and N_2^{max} (mol kg^{-1}) are the saturation capacities of sites 1 and 2, respectively; β_1 and β_2 (bar^{-1}) are the affinity parameters for sites 1 and 2, respectively. Saturation capacities (N_1^{max} and N_2^{max}) are considered to be independent of temperature and the usual temperature dependency was considered for the affinity parameters (Eq. 3.9).

$$\beta_1 = \beta_1^{(0)} \exp\left(\beta_1^{(1)}/T\right) \quad ; \qquad \beta_2 = \beta_2^{(0)} \exp\left(\beta_2^{(1)}/T\right) \qquad 3.9$$

The Henry's constant (β) in this model can be calculated as

$$\beta = N_1^{\max} \beta_1 + N_2^{\max} \beta_2 \qquad 3.10$$

3.4.3 Virial Isotherm

A virial isotherm is versatile as it can accommodate the heterogeneity in adsorption. Simple virial isotherm with three parameters is expressed as follows [**193**]:

$$\ln\left(\frac{f}{N}\right) = bN + cN^2 - \ln(\beta) \qquad 3.11$$

where, b and c are second and third virial coefficients for adsorption. The temperature dependency for these parameters is

$$b = b^{(0)} + b^{(1)}/T \; ; \qquad c = c^{(0)} + c^{(1)}/T \qquad 3.12$$

The temperature dependency for β is same as that in Eq. 3.7.

Due to the nature of Eq. 3.11, the isotherm does not exhibit saturation at high pressures. Thus extrapolation of virial equation beyond the experimental measurements is not suggested. However, within the experimental range of temperature and pressure data, virial equation is flexible and is also thermodynamically consistent.

In general, an adsorption isotherm is plotted in *N* vs *f* domain. However, for an experimental data analysis perspective, isotherm in a virial domain [*ln(P/N)* vs *N*] can be extremely useful. The intercept [*-ln(β)*]of virial domain plot can directly be used to obtain the Henry's constant (β). In addition, the slope of the virial domain plot reflects the energetics of adsorption. Any step or inflection in the virial domain plot indicates the heterogeneity in the adsorbent. This type of information is not easily recognizable from isotherm plotted in conventional domain.

3.4.4 Langmuir-virial Isotherm

The Langmuir equation is derived for only energetic homogeneous surface which is generally not possible in a realistic situation. On the other hand, flexible virial equation is versatile and can describe adsorption on a variety of surfaces. However, this equation does not account for the saturation at high pressure, a phenomena usually observed for most of the cases. Thus, Langmuir and virial models are combined in a Langmuir-virial model [**193**] (Eq. 3.13) to overcome the limitations in either case.

$$\ln\left(\frac{f}{N}\right) = bN + cN^2 + \ln\left(\frac{N^{\max}}{\beta(N^{\max} - N)}\right) \qquad 3.13$$

This model correctly captures a saturation uptake of N^{max} at high pressure. The temperature dependency for the Henry's constant and virial parameters *b, c* are given by Eq. 3.7 and Eq. 3.12.

3.5 Enthalpy of Adsorption

Enthalpy of adsorption indirectly gives the strength of adsorbate and adsorbent binding and thus can be used to characterize the adsorption properties of any adsorbent. Enthalpy of adsorption at zero loading dictates the regeneration condition, for example lower adsorption enthalpy at zero coverage will result in easier regeneration of the adsorbent. The enthalpy of adsorption, Δh_{ads} can be readily calculated from the model parameters of adsorption isotherms using the following equation [**139**]

$$\Delta h_{ads} = -R\frac{\partial(\ln f)}{\partial(1/T)}\bigg|_N \qquad 3.14$$

where, R is universal gas constant. The enthalpy of adsorption for each model obtained *via.* Eq. 3.14 are given in Table 3.1.

Table 3.1: Enthalpy of Adsorption relevant isotherm models.

Model	**Enthalpy of Adsorption (Δh_{ads})**	**Eq. No.**	**Ref.**
Langmuir	$-R(\beta^{(1)})$	3.15	[**193**]
Dual-Site Langmuir	$-R\left(\frac{\beta_1^{(0)} N_1^{\max}\beta_1(1+\beta_2 f)^2 + \beta_2^{(0)} N_2^{\max}\beta_2(1+\beta_1 f)^2}{N_1^{\max}\beta_1(1+\beta_2 f)^2 + N_2^{\max}\beta_2(1+\beta_1 f)^2}\right)$	3.16	[**193**]
Virial	$-R\left(\beta^{(1)} - b^{(1)}N - c^{(1)}N^2\right)$	3.17	[**193**]
Langmuir-virial	$-R\left(\beta^{(1)} - b^{(1)}N - c^{(1)}N^2\right)$	3.17	[**193**]

3.6 Spreading Pressure

Since adsorbed phase is thermodynamically two-dimensional, pressure cannot be considered as an intensive variable. Therefore, pressure and its corresponding extensive variable volume are not appropriate variables for work term in two-dimensional adsorbed phase [**194**]. A different intensive variable known as spreading pressure π is defined for the adsorbed phase to fix its state [**195**]. It has units of N m^{-1} which is same as that of surface tension. The corresponding extensive variable is the molar area (area of the solid per mole of adsorbed gas), a. Thus mechanical work term for the adsorbed phase per mole of solid can be calculated as πa; this is analogous to PV in the bulk phase. Since the amount adsorbed N is generally expressed for a unit mass of the adsorbent, the area is also represented on the same basis as specific area A and has the units of m^2 kg^{-1}. For a single component system, the Gibbs' adsorption isotherm is given by [**196 – 197**].

$$-A.d\pi + RT.N.d\ln P = 0 \qquad \text{(at constant } T\text{)} \qquad 3.18$$

From the above equation, the reduced spreading pressure, ψ, is given by

$$\psi = \frac{\pi.A}{RT} = \int_0^P \frac{N}{P}.dP \qquad 3.19$$

The quantity ψ has the unit of moles per unit mass of adsorbent. It is also often used synonymously with π. At $P = 0$, the spreading pressure is zero due to no adsorption. Since the spreading pressure cannot be measured experimentally, Eq. 3.19 is used to calculate its value for a pure gas adsorption either by numerical integration or from isotherm model. The expression for ψ using various isotherm models is given below in Table 3.2. These expressions are essential for IAST calculation discussed in the next section.

Table 3.2: Spreading pressure for relevant isotherm models.

Model	Expression for ψ	Eq. No.	Ref.
Langmuir	$N^{\max}\ln(N^{\max}+\beta f)$	3.20	[**193**]
Dual-Site Langmuir	$N_1^{\max}\ln(1+\beta_1 f)+N_2^{\max}\ln(1+\beta_2 f)$	3.21	[**193**]
Virial	$N+\frac{1}{2}bN^2+\frac{2}{3}cN^3$	3.22	[**193**]
Langmuir-virial	$\frac{1}{2}bN^2+\frac{2}{3}cN^3-N^{\max}\ln\left(\frac{N^{\max}-N}{N^{\max}}\right)$	3.23	[**193**]

3.7 Ideal Adsorbed Solution Theory (IAST)

A solution thermodynamic approach yields the following phase equilibrium relation for equality of fugacities in the bulk and the adsorbed phases.

$$y_i P \hat{\phi}_i^{gas} = x_i \gamma_i P_i^0 \qquad 3.24$$

where, y_i is bulk gas mole fraction, P is the pressure, $\hat{\phi}_i^{gas}$ is fugacity coefficient of bulk gas to account for non-ideality, x_i is adsorbed phase mole fraction, γ_i is activity coefficient in adsorbed phase (to account for non-ideal adsorbate mixture) and P_i^0 is pressure at the standard state. A convenient standard state is pure gas at the same temperature and spreading pressure as that of the mixture. If the adsorbate mixture is ideal Eq. 3.24 simplifies to

$$y_i P = x_i P_i^0 \qquad 3.25$$

With this phase equilibrium relations along with an equation for total amount adsorbed (N), one can predict binary gas adsorption equilibria (*i.e.* finding partial amount adsorbed N_i for a given gas mixture of mole fraction y_i at T and P) [**198**]. For example in case of binary equilibrium, the following eight equations need to be solved.

$$y_1 P = x_1 P_1^0 \quad (3.26)$$

$$y_2 P = x_2 P_2^0 \quad (3.27)$$

$$I_1\{N_1^0, P_1^0\} = 0 \quad (3.28)$$

$$I_2\{N_2^0, P_2^0\} = 0 \quad (3.29)$$

$$I_3\{N_1^0, P_1^0, \psi\} = 0 \quad (3.30)$$

$$I_4\{N_2^0, P_2^0, \psi\} = 0 \quad (3.31)$$

$$x_1 + x_2 = 1 \quad (3.32)$$

$$\frac{1}{N} = \frac{x_1}{N^0{}_1} + \frac{x_2}{N^0{}_2} \quad (3.33)$$

where, I_1 and I_2 are isotherm models relating N_1^0 to P_1^0 and N_2^0 to P_2^0 for pure gas 1 and pure gas 2, respectively [Eqns. 3.6, 3.8, 3.11 or 3.13]. I_3 and I_4 are relations for spreading pressure ψ *via.* Eq. 3.19 as given in Table 3.2 for the respective model [Eqns. 3.20 – 3.23].

CHAPTER 4

EXPERIMENTAL

This chapter presents the details and protocols for various experiments performed in this work. The synthesis procedures followed for the synthesis of different MOFs are included. Details on the calculation methodology for converting raw experimental data into appropriate domain are also presented. Physical properties and purities of gases considered for this work are provided.

4.1 Synthesis of MOFs Studied

4.1.1 Synthesis of MIL-53(Al)

The synthesis of MIL-53(Al) was carried out under hydrothermal conditions using aluminium nitrate nonahydrate ($Al(NO_3)_2.9H_2O$, aldrich), benzene 1,4-dicarboxylic acid (BDC, Merck), dimethylformamide (DMF, Merck) and deionized water as per the procedure suggested by Loiseau et al. [**41**]. The molar composition of starting materials was 1 ($Al(NO_3)_3.9H_2O$) : 0.5 (BDC) : 80 (H_2O). The solution was placed in a Teflon lined steel autoclave at 493 K for 3 days and allowed to react hydrothermally. The product was filtered and washed with deionized water. The resultant product consists of mixture of MIL-53(Al) and unreacted BDC. For removal of unreacted BDC [**199**], typically 1 g of MIL-53(Al) as-synthesized was dispersed in 25 ml of DMF and introduced in teflon lined steel autoclave for 15 h at 423 K. The product was cooled, filtered and calcined overnight at 553 K.

4.1.2 Synthesis of Mg/DOBDC

The synthesis of Mg/DOBDC was carried out according to the procedure suggested by Caskey et al. [**97**]. A solid mixture of 2,5-dihydroxy terephthalic acid (0.888 g, 4.472 mmol, Sigma aldrich) and $Mg(NO_3)_2 \cdot 6H_2O$ (3.795 g, 14.8 mmol, Merck) was added into a 15:1:1 (v/v/v) mixture of DMF/ethanol/water (400 mL). The suspension was sonicated for about 5 minutes to make it homogeneous. Then the suspension was then equally distributed in twenty seven 30-mL polypropylene vials. These vials were capped tightly and kept in an oven at 398 K for 20 hours. Samples were then cooled to room temperature followed by decantation of mother liquid from the yellowish crystals. Methanol of similar quantity as that of the mother liquid (~15 mL per vials) was added. Then suspension was collected in a 500-mL polypropylene vial. After every 12 hours, methanol was decanted and replaced with fresh methanol for the next two days to get as-synthesized Mg/DOBDC crystals. These crystals were dried and stored in vacuum.

4.1.3 Synthesis of Mn/DOBDC

Synthesis procedure of Mn/DOBDC was slightly modified from that reported in literature [**147**]. A solid mixture of 2,5-dihydroxy terephthalic acid (0.888 g, 4.472 mmol, Sigma aldrich) and $Mn(NO_3)_2 \cdot 4H_2O$ (3.715 g, 14.8 mmol, Merck) was added into a 15:1:1 (v/v/v) mixture of DMF/ethanol/water (400 mL). The suspension was sonicated for about 5 minutes to make it homogeneous. Then the suspension was equally distributed in twenty seven 30-mL polypropylene vials. These vials were capped tightly and kept in an oven at 404 K for 24 hours. Samples were then cooled to room temperature followed by decantation of the mother liquid from the brownish crystals. Methanol of similar quantity as that of the mother liquid (~15 mL per vials) was added. Then suspension was collected in a 500-mL polypropylene vial. After

every 12 hours, methanol was decanted and replaced with fresh methanol for the next two days to get as-synthesized Mn/DOBDC crystals. These crystals were dried and stored in vacuum.

4.1.4 Synthesis of Co/DOBDC

As per procedure suggested elsewhere [**97**], 2,5-dihydroxy terephthalic acid (0.482 g, 2.43 mmol, Sigma aldrich), $Co(NO_3)_2 \cdot 6H_2O$ (2.377 g, 8.67 mmol, Merck) and a 1:1:1 (v/v/v) mixture of DMF–ethanol–water (200 mL) were mixed in a 500 ml polypropylene vial. Sonication of the suspension was done for about 5 minutes to make it homogeneous. Then vial was capped tightly and kept in an oven at 373 K for 24 hours. Sample was then cooled to room temperature followed by decantation of the mother liquid from the violet crystals. Methanol of similar quantity as that of the mother liquid (~200 mL) was added. After every 12 hours, methanol was decanted and replaced with fresh methanol for the next two days to get as-synthesized Co/DOBDC crystals. These crystals were dried and stored in vacuum.

4.1.5 Synthesis of Ni/DOBDC

The synthesis of Ni/DOBDC was carried out as per procedure suggested by Caskey et al. [**97**]. A solid mixture of 2,5-dihydroxy terephthalic acid (0.478 g, 2.41 mmol, Sigma aldrich) and $Ni(NO_3)_2 \cdot 6H_2O$ (2.378 g, 8.178 mmol, Merck) were added to a 1:1:1 (v/v/v) mixture of DMF–ethanol–water (200 mL) in a 500 ml polypropylene vial. Sonication of the suspension was done for about 5 minutes to make it homogeneous. Then vial was capped tightly and kept in an oven at 373 K for 24 hours. Sample was then cooled to room temperature followed by decantation of mother liquid from the light greenish crystals. Methanol of similar quantity as that of the mother liquid (~200 mL) was added. After every 12 hours, methanol was decanted and replaced with fresh methanol for two days to get as-synthesized Ni/DOBDC crystals. These crystals were dried and stored in vacuum.

4.1.6 Synthesis of Ni/DABCO

Ni/DABCO was synthesized as per procedure suggested by Arstad et al. [**75**]. A mixture of $Ni(NO_3)_2.6H_2O$ (3 mmol, Merck), benzene-1,4-dicarboxylic acid (3 mmol, Merck), 1,4-diazabicyclo (2,2,2) octane (2.49 mmol, Alfa Aesar) and DMF (60 cm^3, Merck) was taken in a conical flask at room temperature and stirred rigorously until it is well dissolved for about 20 minutes. This mixture was then transferred into a teflon lined autoclave. The autoclave was heated to 383 K and held for 24 hours. Then it was cooled to room temperature; the solid product was filtered and washed thoroughly with DMF followed by drying at ambient temperature (290 – 303 K) under vacuum. The dried material was transferred into a vacuum desiccator for storage.

4.1.7 Synthesis of Cu/DABCO

The synthesis procedure for Cu/DABCO was similar to that of Ni/DABCO but with minor changes. A mixture of $Cu(NO_3)_2.3H_2O$ (3 mmol, Merck), benzene-1,4-dicarboxylic acid (3 mmol, Merck), 1,4-diazabicyclo (2,2,2) octane (2.49 mmol, Alfa Aesar) and DMF (60 cm^3, Merck) was taken in a conical flask at room temperature and stirred rigorously until it is well dissolved for about 20 minutes. This mixture was then transferred into a teflon lined autoclave. The autoclave was heated to 393 K and held for 48 hours. Then it was cooled to room temperature; the solid product was filtered and washed thoroughly with DMF followed by drying at ambient temperature (290–303 K) under vacuum. The dried material was transferred into a vacuum desiccator for storage.

4.1.8 Synthesis of Zn/DABCO

The procedure suggested by Dybtsev et al. [**55**] was followed for the synthesis of Zn/DABCO compound. A mixture of $Zn(NO_3)_2.6H_2O$ (1.61 g, Merck), benzene-1,4-dicarboxylic acid (0.81 g, Merck), 1,4-diazabicyclo (2,2,2) octane (0.28 g, Acros) and DMF (60 cm^3, Merck) was taken

in a conical flask at room temperature and stirred rigorously until it is well dissolved for about 20 minutes. This mixture was then transferred into a teflon lined autoclave. The autoclave was heated to 393 K and this temperature was maintained for 48 hours. The product recovery and storage steps were similar to those of Ni/DABCO and Cu/DABCO.

4.2 Characterization of MOFs Synthesized

The following instruments were used to characterize the MOFs synthesized in this work.

In this work, Mettler TOLEDO, thermogravimetric analyzer (model no. TGA/SDTA 851^e) was used to perform Thermogravimetric analysis (TGA) of the synthesized samples. An alumina crucible was used as sample holder during all experiments. About 10 mg of the adsorbent sample was used for the analysis. All experiments were done under an inert atmosphere (N_2 flow of about 40 cm^3 min^{-1}) with a heating rate range of 5 – 10 K min^{-1}. Based on the TGA profile of sample, its out-gassing temperature was determined during subsequent surface area / pore volume analysis and isotherm measurement.

Surface area and pore volume were measured in Beckman-Coulter SA 3100 analyzer by performing N_2 physisorption study at 77 K. The samples were out-gassed under vacuum at high temperature prior to N_2 adsorption. The specific surface area was calculated by using the BET (Brunauer−Emmett−Teller) model and relative pressure (P/P_0) range of 0.05–0.2 was used in its calculation. The pore volume was calculated at a pre-determined relative pressure (P/P_0) of 0.98.

Powder X-ray diffraction (XRD) patterns of all samples synthesized in this work were measured on a Bruker A8 advance instrument operating at 40 kV and 40 mA using Cu Kα (λ =1.5406 Å) radiation.

4.3 Experimental System Used for Adsorption Measurements

The experimental setup used for gas adsorption measurement consists of a Rubotherm™ Magnetic Suspension balance. The balance was connected to the gas cylinders through the networks of stainless tubes as shown in Figure 4.1. Mass flow controllers, temperature transducers and pressure transducers were incorporated at appropriate locations. Pneumatic valves were used for the ease of experimentation.

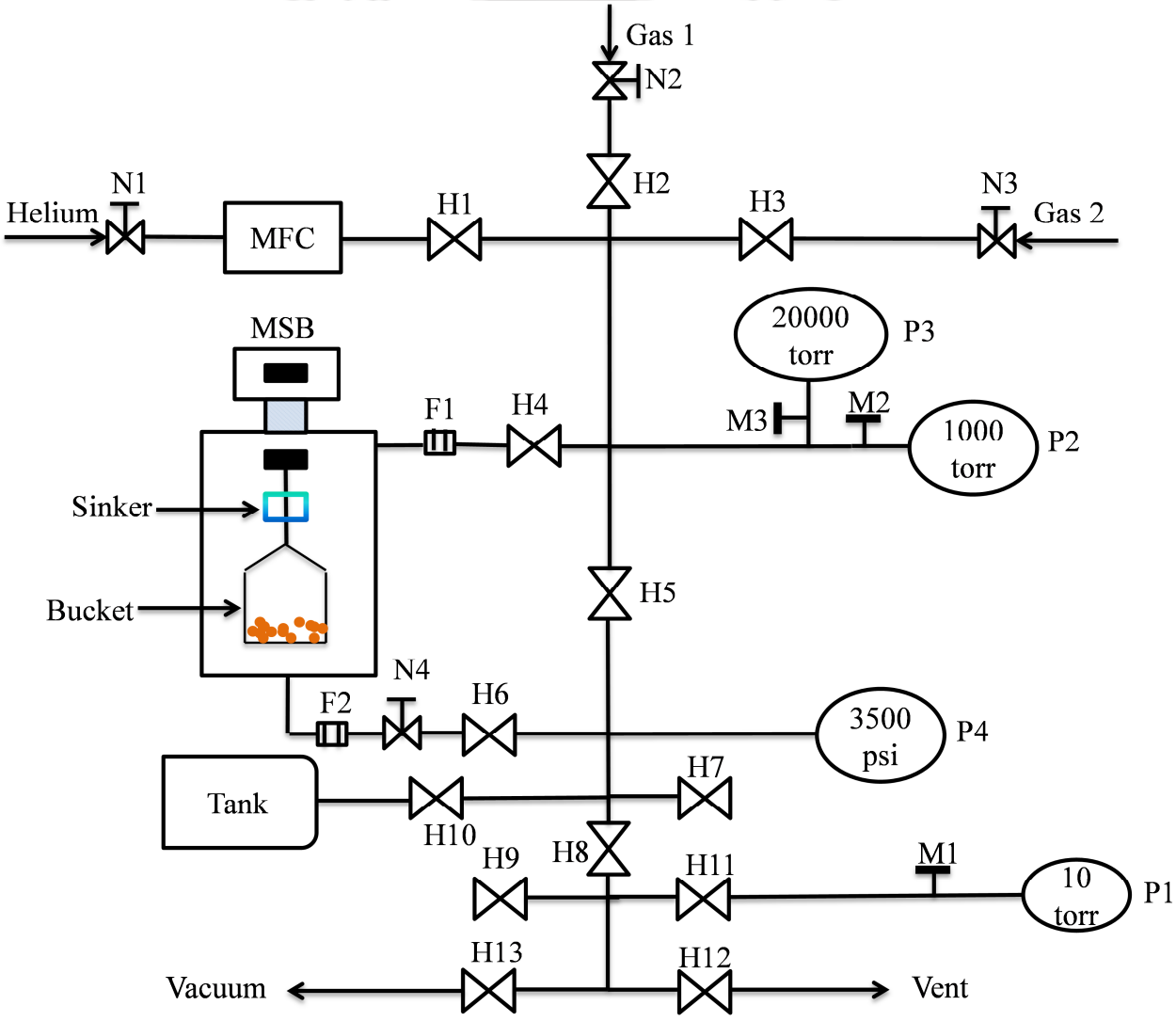

Figure 4.1: Schematic of gravimetric adsorption measurement unit used in this work.

Nomenclature

MSB # Magnetic Suspension Balance

MFC # Mass Flow Controller

H1 – H13 # Pneumatic Valves

N1, N2, N3, N4 # Needle Valves

M1, M2, M3 # Manual Swagelok Valves

P1, P2, P3, P4 # Pressure Transducers

F1 & F2 # Filters

More details on major hardware components used in this setup are given in Table 4.1.

Table 4.1: List of instruments used in the gravimetric experimental System.

Component	Model	Manufacturer	Range	Accuracy	Resolution
Gravimetric Balance	3-position Magnetic suspension balance	Rubotherm	0–25 g	±20 μg	10 μg
Mass flow controller	GFC-17	Diegler Aalborg	0–200 cc min^{-1}	2% of full scale	1 cc min^{-1}
Pressure transducers	627B11TDCAB	MKS Instruments	0–10 torr	±0.12% of full scale	0.001 torr
	627D18TBC1B		0–100 torr		0.1 torr
	627B24TBC1B		0–20000 torr		1 torr
	PX41C0-3500PSIA	Omegadyne	0–3500 psi	±0.5% of full scale	1psi
Thermocouples	JK Type		0–1200 ^{o}C	±2% of full scale	1 ^{o}C
Temperature indicators		Masibus			
Heated and refrigerated circulator	RW-2025 G	Jeio Tech	–25 to 150 ^{o}C	±0.05 ^{o}C	0.1 ^{o}C
Vacuum pump	DUO 2.5	Pfeiffer Vacuum	<6×10^{-3} torr	N/A	N/A
Compressor	HS-WP-1	High speed appliances	0–100 psi	N/A	N/A

In addition to the above mentioned instruments, Swagelok fittings and stainless steel tubings (of 1/4″ and 1/8″) were used for connecting various sections in the experimental assembly.

4.4 Equilibrium Adsorption Measurement

At first, the adsorbent was loaded into the bucket in the balance system and then the system is hermetically sealed. Adsorbent sample of about 1 g or more was used to avoid errors in measurement. Thereafter, activation of the sample was done by heating it at higher temperature (Table A1 in the Appendix A for more details) under vacuum (and about 30 cm^3 min^{-1} purge flow of helium). Activation of the sample was ensured when no significant reduction in its weight occurs with time. Activated sample was cooled to the experimental temperature under vacuum. The first measurement point on the isotherm was obtained by charging the desired adsorbate to the target pressure inside the adsorption cell; sufficient time was allowed to reach equilibrium. Usually, first few measurements were done at very low pressures (below 0.05 bar) in order to obtain accurate Henry's constant. Subsequent measurements for the isotherm were obtained by increasing the pressure in the incremental doses. Equilibrium adsorption was measured at approximately 15 – 20 points within entire pressure range to get more reliable isotherm model parameters. After completion of the experiment for an isotherm, the sample was again activated at higher temperature under vacuum as described earlier. The excess amount adsorbed was calculated from raw measurements using buoyancy corrections (as described in the next section). Relations between net, excess and absolute amount adsorbed have also been presented. However, only excess adsorption quantities are used/presented in whole thesis. The impenetrable solid volume of adsorbent for buoyancy correction was obtained from helium measurements at 293 K in the pressure range of 0 − 26 bar, using non-adsorbing helium assumption. Steps involved in the experimentation are elaborated in Appendix A in more detail.

4.4.1 Calculation of Amount Adsorbed

When activated sample is equilibrated with a gas at a particular temperature and pressure, Gibbs' amount adsorbed (M_t) is calculated as

$$M_t = M_{eq} - M_0 + V_{\text{buoyancy}}\rho^{\text{gas}} \qquad 4.1$$

where, M_0 is true adsorbent weight including bucket weight in vacuo, M_{eq} is adsorbent plus bucket weight at equilibrium. M_0 and M_{eq} can directly be obtained from the balence reading taken during the experiments *via.*

$$M_{eq} = MP1 - ZP \qquad (at\ equilibrium) \qquad 4.2$$

$$M_0 = MP1 - ZP \qquad (in\ vacuo) \qquad 4.3$$

where, *ZP* is the weight measurement at zero point position, *MP1* is the weight measurement when only bucket was lifted, and *MP2* is the weight measurement when both bucket and sinker were lifted.

The last term on RHS of Eq. 4.1 accounts for the buoyancy correction necessary to convert "raw" experimental measurements into appropriate amount adsorbed as discussed in the Section 4.5.

Bulk Gas Properties

The bulk density was obtained from the virial equation of state

$$\rho^{gas} = \left(\frac{-1 + \sqrt{1 + 4B^{gas}\frac{P}{RT}}}{2B^{gas}} \right) M_w \qquad 4.4$$

where, M_w is the molar mass of the gas, P is the pressure, T is the temperature, R is the gas constant and B^{gas} is the gas phase second virial coefficient. The usual temperature dependency for B^{gas} is taken as

$$B^{gas} = B_1 + \frac{B_2}{T} + \frac{B_3}{T^3} + \frac{B_4}{T^8} + \frac{B_5}{T^9} \qquad 4.5$$

The values of B_i for the gases used in this study are tabulated in Table 4.2.

Table 4.2: Second virial coefficients for different gases [**200**].

Gas	$B_1 \times 10^2$	$B_2 \times 10^{-1}$	$B_3 \times 10^{-5}$	$B_4 \times 10^{-15}$	$B_5 \times 10^{-17}$
	$m^3\ kmol^{-1}$	$m^3\ kmol^{-1}\ K$	$m^3\ kmol^{-1}\ K^3$	$m^3\ kmol^{-1}\ K^8$	$m^3\ kmol^{-1}\ K^9$
He	1.400	-3.540	-5.950E-06	3.610E-13	-7.940E-15
CO_2	5.440	-3.635	-14.960	85.900	-139.700
CH_4	5.438	-2.714	-2.135	0.920	-0.785
CO	5.122	-1.709	-0.742	0.046	-0.029
N_2	4.670	-1.495	-0.611	0.081	-0.046
Ar	3.805	-1.518	-0.808	0.185	-0.110
O_2	3.900	-1.554	-0.848	0.164	-0.115
C_2H_6	8.095	-6.171	-14.350	67.600	-97.400
C_3H_8	11.250	-10.000	-43.140	-18.000	-165.000

Fugacity was used instead of pressure to handle with the gas phase non-ideality at higher pressures [**191**]. It was obtained from the virial equation for the bulk gas phase using

$$\ln\left(\frac{f}{P}\right) = \left[\frac{B^{gas}P}{RT}\right] \qquad 4.6$$

4.5 Different Types of Amount Adsorbed

In general, any experiments to measure adsorbed amount require a correction term (last term in Eq. 4.1) as discussed above. In adsorption literature several “types” of adsorption are defined based on the reference state to calculate the buoyancy volume or locating the so-called Gibbs

dividing surface. The common reference states used in adsorption literature are given in Figure 4.2 [**196**].

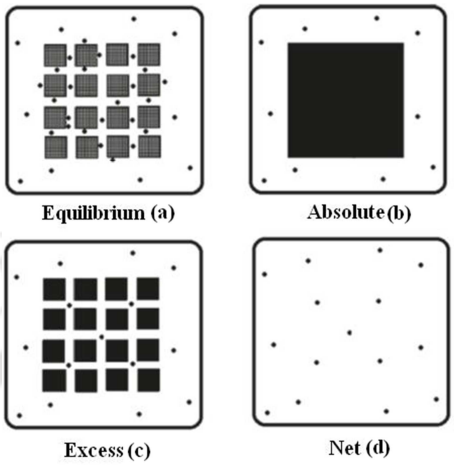

Figure 4.2: (a) Equilibrium between Adsorbate and Adsorbent; **(b)** Reference state for Absolute Adsorption; **(c)** Reference state for Excess Adsorption; **(d)** Reference state for net Adsorption Framework [**196**].

Absolute Adsorption

Figure 4.2 (b) shows the reference state for absolute adsorption. The gas molecules exist in the non-shaded "available" volume of the tank at the same conditions (temperature and pressure) as that in Figure 4.2 (a). Thus, the density of molecules in the non-shaded region of this figure is same as that of the bulk density in case (a). The shaded black region is considered to be unavailable for the gas at the reference state conditions. The difference between the number of gas molecules between the two cases (a) and (b) is called as the absolute amount adsorbed. On a normalized basis, the difference per unit mass of adsorbent is the so called specific absolute amount adsorbed.

Excess Adsorption

Figure 4.2 (c) (bottom left) shows the reference state for excess adsorption. The gas molecules exist in the non-shaded "available" volume of the tank at the same conditions (temperature and pressure) as that in Figure 4.2 (a). Thus, the density of molecules in the non-shaded region (including that inside the pores) of this Figure 4.2 (c) is same as that of the bulk density in case (equilibrium). The shaded black region is the so called "impenetrable solid volume" that is unavailable for the gas. The difference between the number of gas molecules between the two cases (a) and (c) is called as the excess amount adsorbed. Thus, excess amount is equivalent to the number of additional gas that can be accommodated in the "penetrable" region of the tank due to adsorption. By far this is the most commonly used reference state in adsorption literature.

Net Adsorption

Figure 4.2 (d) shows the reference state for net adsorption. The gas molecules exist in the total volume of the tank at the same conditions (temperature and pressure) as that in Figure 4.2 (a). Note that in this reference state the total volume of the tank is considered available to the gas unlike in the earlier two cases. Further, the density of molecules in the tank at the reference state is same as that of the bulk density in case (a). The difference between the number of gas molecules between the two cases (a) and (d) is called as the net amount adsorbed. Thus, net amount is equivalent to the number of additional gas that can be accommodated in the total volume of the tank (as opposed to that in the penetrable volume only for case of excess) due to adsorption.

4.5.1 Determination of Buoyancy Volume for Various Reference States

In order to calculate the amount adsorbed based on any one (absolute, excess or net) reference states, it is necessary to correct the microbalance signal with appropriate buoyancy correction term as described in Eq. 4.1.

The buoyancy volume for net adsorption is the buoyancy acting on the bucket alone (excluding the sample). This is usually obtained *via* Eq. 4.1, by using a convenient gas to record the microbalance signal of the bucket only (in the absence of any sample) at several densities of the surrounding bulk gas. In the absence of adsorbent sample, the change in microbalance signal is solely due to buoyancy of the bucket assembly (irrespective of the gas used) and hence LHS of Eq. 4.1 is zero. The slope of microbalance signal against bulk gas density is thus directly related to the buoyancy volume (of the bucket in this case, V_{bucket}). Argon was used as probe gas to obtain buoyancy of the bucket for data reported in this work. In net adsorption only bucket experience buoyancy force therefore

$$V_{buyoancy,\ net} = V_{bucket} \tag{4.7}$$

In case of excess adsorption the impenetrable solid volume also experiences the buoyancy force and

$$V_{buyoancy,\ excess} = V_{bucket} + V_s \tag{4.8}$$

where V_s is the impenetrable solid volume. The buoyancy volume is calculated again from the change in microbalance signal on the bucket and sample assembly. However, since a porous solid sample adsorbs the probe gas, LHS of Eq. 4.1 is non-zero unlike in the previous case when only the bucket is used to measure the buoyancy volume. LHS of Eq. 4.1 is zero in presence of a sample only if the sample does not adsorb the probe gas. Hence, helium is conventionally chosen as a non-adsorbing probe gas to obtain impenetrable solid volume (and hence $V_{buoyancy}$ for excess adsorption). With non-adsorbing helium assumption the LHS of Eq. 4.1 is zero; the slope of microbalance signal against helium density is related to the buoyancy volume for excess adsorption.

In case of absolute adsorption the impenetrable solid volume as well as the pores also experiences the buoyancy force. Thus the absolute amount adsorbed at a given condition is the amount of gas present in the solid adsorbent including that in the "pores".

$$V_{buyoancy,\,absolute} = V_{bucket} + V_s + V_p \qquad 4.9$$

where V_p is the pore volume of the adsorbent.

4.6 Conversion of Units

Generally "amount adsorbed" is expressed for per unit kilogram of adsorbent. However, in order to understand the effect of metal atom substitution in the framework, specific units are not suitable; since the molar masses of the different metal atoms are different, the formula mass of resultant unit cell also varies. Thus, the unit of "amount adsorbed" is converted from 'mol kg^{-1}' to 'molecules $unit\ cell^{-1}$' using.

$$N_u = \frac{NM_f}{1000} \qquad 4.10$$

where, N_u is amount adsorbed in molecules $unit\ cell^{-1}$, N is amount adsorbed in mol kg^{-1}, M_f is molecular weight of unit cell in g.

Amount adsorbed for per metal atom (N_m) can be further calculated from

$$N_m = \frac{N_u}{n} \qquad 4.11$$

where, n is the number of metal atoms in one unit cell.

Volumetric adsorption uptakes are also important for practical applications in gas storage and separation. Gravimetric uptakes (N) can easily be converted to volumetric uptakes (N_v) following Eq. 4.12.

$$N_v = N\rho_c \qquad 4.12$$

where, N_v (mol L^{-1}) is volumetric amount adsorbed, N is amount adsorbed in mol kg^{-1} and ρ_c (g cm^{-3}) is crystal density of the adsorbent.

It should be noted here that Eq. 4.12 is valid with the strict assumption of no void space between two crystals or two particles of adsorbent. In real scenario, there will be always some void fraction within the adsorbent material. Thus the volumetric uptake obtained from Eq. 4.12 is the maximum possible uptake. In reality, the experimentally achieved value of volumetric uptake is lower than that obtained through Eq. 4.12 and depends upon the packing of adsorbent [**146**].

4.7 Experimental Conditions

Adsorption equilibria of various gases on several MOFs were measured gravimetrically for a wide range of pressures and temperatures. The details of the experimental conditions at which adsorption measurements were performed, is given in Table 4.3.

Table 4.3: Experimental ranges for various adsorption isotherm measurements.

Adsorbent	Adsorbate	Temperatures (K)	Pressure Range (bar)
MIL-53(Al)	CO_2	293	0 – 26
	CH_4	293	0 – 26
	CO	293	0 – 26
	N_2	293	0 – 26
	O_2	293	0 – 26
M/DOBDC (M = Mg, Mn, Co, Ni)	CO_2	294, 315, 352	0 – 30
	CH_4	294, 315, 352	0 – 50
	CO	294, 315, 352	0 – 120
	N_2	294, 315, 352	0 – 120
	Ar	294, 315, 352	0 – 120
	C_2H_6	294, 315, 352	0 – 25
	C_3H_8	294, 315, 352	0 – 7
M/DABCO (M = Ni, Cu, Zn)	CO_2	294, 314, 350	0 – 26
	CH_4	294, 314, 350	0 – 26
	CO	294, 314, 350	0 – 26
	N_2	294, 314, 350	0 – 26

4.8 Purity of Gases

The purity of all the gases used in this work was more than 99%. No further purification of purchased gas was done. Purity detail of the studied gases is provided in Table 4.4.

Table 4.4: Details of gases used in this study.

Gas	**Supplier**	**Minimum Percentage Purity (Approximately)**
He	Assam Air Products	99.995
CO_2		99.9
N_2		99.99
O_2		99.9
Ar	BOC India Limited	99.995
CO	Vadilal Gases Limited, India	99.95
CH_4		99.95
C_2H_6		99.5
C_3H_8		99.5
n-C_4H_{10}		99.5
i-C_4H_{10}		99.5

4.9 Physical Properties of Gases Used

Physical properties of the gases used in this work are given in Table 4.5 [**193**].

Table 4.5: Physical properties of gases used in this study.

Gas	**Molecular Weight**	**Kinetic Diameter**	**Polarizability**	**Dipole Moment**	**Quadrupole Moment**
	(g mol^{-1})	(Å)	($\times 10^{25}$ cm^3)	($\times 10^{18}$ esu cm)	($\times 10^{40}$ C m^2)
He	4	2.58	2.06	0	0
CO_2	44	3.3	26.3	0.0	14.3
CH_4	16	3.8	26	0.0	0.0
CO	28	3.76	19.5	0.112	2.5
N_2	28	3.64	17.6	0.0	1.52
Ar	40	3.4	16.6	0.0	0.0
O_2	32	3.5	16	0.0	1.3
C_2H_6	30	4.4	44.7	0.0	0.65
C_3H_8	44	4.3	62.9	0.0	4.0

CHAPTER 5

STRUCTURAL TUNING OF FLEXIBLE MIL-53(Al) MOF

This chapter presents a systematic investigation on the effect of adsorption history on the structural transformation of flexible MIL-53(Al) MOF. By choosing a suitable history, the narrow pore form of MIL-53(Al) was stabilized at 293 K under vacuum. This narrow pore tuned form of MIL-53(Al) exhibited a significant increase in CO_2 loading and selectivity compared to un-tuned form at sub-atmospheric pressure and 293 K.

5.1 Background

Approximately, 80% of the total CO_2 emissions take place from the combustion of fossil fuels such as coal, oil, and natural gas. Thus the adaptation of cleaner energy sources instead of fossil fuels would be ideal way to control CO_2 emissions. However, on a short term basis, it is necessary to have efficient carbon capture from the existing emission sources. Absorption into aqueous amine solutions is one of the widely used techniques to capture CO_2; scientific community is actively involved in search of other alternatives due to known drawbacks of the amine absorption process such as solvent degradation, corrosion, high regeneration cost etc.

The development of an adsorption based process as an alternate technique for CO_2 capture is mostly driven by synthesis of novel adsorbent materials which can selectively adsorb reasonable amounts of CO_2. Metal organic frameworks (MOFs) are being widely investigated for their potential to efficiently remove of CO_2 from process streams [**36 – 38, 62, 67 – 69, 160**]. The

members of the MIL series [**201**], MIL-53 MOFs are among the few which are readily stable towards moisture [**41, 43**] but exhibit poor adsorption uptake and selectivity for CO_2 [**42**]. These MOFs were originally synthesized by Férey and co-workers [**39, 41**]. In these porous materials, connection between infinite trans-chains of M (M = Al^{3+} or Cr^{3+}) octahedra and BDC results a three dimensional framework with one-dimensional rhombic channels [**41**]. After removal of unreacted BDC molecules from MIL-53 (Al) structure by activating it at higher temperatures, channel dimensions are about 8.5×8.5 $Å^2$. However, a reversible adsorption of 1 water molecule per Al atom transforms its structure from **lp** (large pore) domain to **np** (narrow pore) domain of 2.6×13.6 $Å^2$ channel dimensions [**41**]. More structural details of both phases of this material are provided in Figure 5.1 and Table 5.1.

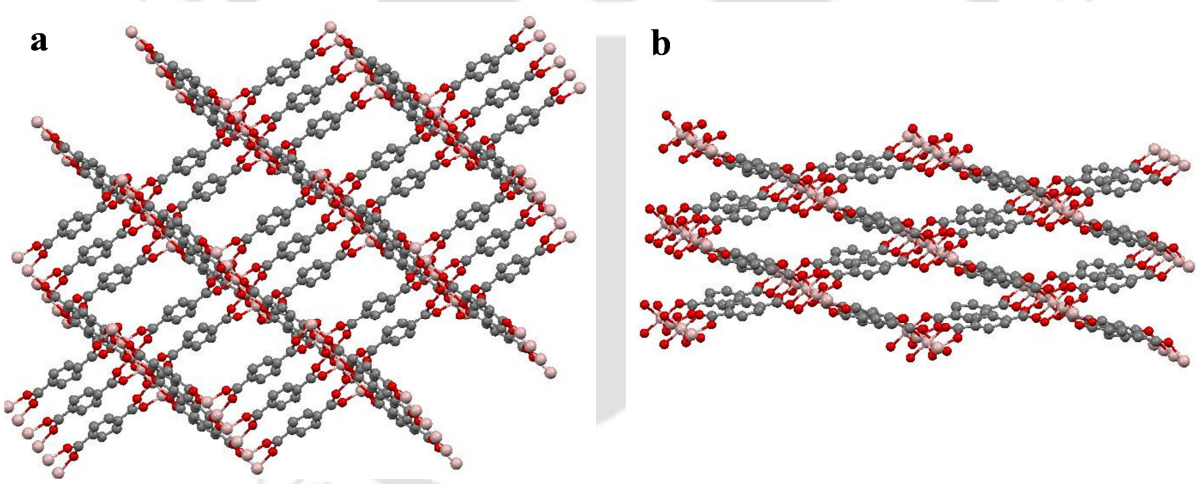

Figure 5.1: Crystal structure of MIL-53(Al) (**a**) in **lp** domain (sample $\mathbf{lp_0}$) and (**b**) in **np** domain (sample $\mathbf{np_0}$) (O, red; C, grey; Al, pink) [**41**].

Table 5.1: Structural details of MIL-53(Al) MOF [**41**].

Chemical formula of unit cell	Formula weight of unit cell (**g**)	Unit cell parameters		Cell volume (**Å^3**)	Crystal density (**g cm^{-3}**)	Conversion factor for mol kg^{-1} to molecule unit cell^{-1} conversion
		Cell lengths (**Å**)	Cell angles			
$Al_4O_{20}C_{32}H_{20}$ (**lp** phase)	832.44	a = 6.6085 b = 16.675 c = 12.813	α = 90 β = 90 γ = 90	1411.9	0.979	0.832
$Al_4O_{20}C_{32}H_{20}$ (**np** phase)	832.44	a = 19.513 b = 7.612 c = 6.576	α = 90 β = 104 γ = 90	946.8	1.460	0.832

Most of the MOF materials have rigid framework but MIL-53 MOFs are among few which have flexible structure and they exhibit structural transformation from **lp** domain to **np** domain and vice versa (so called breathing phenomena) upon adsorption of certain guest molecules (like CO_2, H_2O etc.) [**41, 42, 91, 138, 202 – 204**], by change in temperature [**88**] or by applying mechanical pressure [**92, 205, 206**]. Considerable amount of research work is published on these materials due to their fascinating breathing behavior and good stability. In their work on coadsorption measurements of CO_2 and CH_4 in MIL-53(Al), Ortiz et al. [**207**] state that the total amount adsorbed depends on history (*i.e.* whether the measurements were performed during so called pressure or composition swipes) of the system. However, the parent form of MIL-53 material has shown low CO_2 capacity and selectivity [**43**].

Attempts were made to exploit MIL-53 for adsorptive separation of gases like CO_2 and CH_4 by structural modification of the framework material. Hydrated [**170**] and functionalized [**208**] (using 2-amino terephthalate linkers) forms of MIL-53 have been used to enhance CO_2 selectivity by transforming its structure into the **np** form [**170, 208, 209**] (which exhibits negligible capacity for CH_4 at low pressures). The resultant materials showed higher CO_2 selectivity over CH_4. However, compared to parent MIL-53 material, the CO_2 adsorption capacity of the hydrated form decreased significantly [**170**]. In case of the amine functionalized form [**208**], at sub-atmospheric pressures a marginal increase in CO_2 uptake capacity was observed, while at higher pressures the gravimetric uptake was actually lower than that of parent material due to the presence of additional functional groups.

In this chapter, a technique is presented to tune MIL-53(Al) structure into its **np** domain at sub-atmospheric pressures to considerably increase both CO_2 capacity and selectivity. The tuning in this work is achieved by simply changing the history of the sample. Since functional groups and other guest molecules are not used in this methodology, there will be no negative effect on gravimetric uptake capacity, or competitive adsorption of the guest molecules. Generally, modifications (such as amine grafting or others) to enhance CO_2 uptakes at sub-atmospheric pressures also result higher enthalpy of adsorption; which means with increase of CO_2 uptake, the regeneration cost also increases. However, in this work using the method presented, enhancement of CO_2 uptake and selectivity on MIL-53(Al) will be achieved without additional energy penalty for regeneration.

5.2 Characterization of MIL-53(Al)

MIL-53(Al) MOF was synthesized following the procedure suggested by Férey and coworkers [**41**]. After synthesis, sample was subjected to DMF treatment followed by calcination at 553 K to remove the unreacted BDC molecules [**199**].

5.2.1 Thermogravimetric Analysis (TGA)

TGA of the synthesized MIL-53(Al) is shown in Figure 5.2. The TGA profile obtained in this work for MIL-53(Al) is similar to that reported in the literature [**41, 107**]. The initial weight loss below 373 K is due to the removal of water from the sample. Thereafter, the material continues to show stable weight up to ~ 723 K. The sharp increase in weight loss above 723 K is due to the collapse of MIL 53(Al) structure *i.e.* removal of structural BDC linkers from the framework [**41**]. Thermal stability of this MOF (723 K) is higher than most of the other MOFs such as Zn/DABCO [**79**], CuBTC [**125**], MIL-101 [**74**], MOF-210 [**38**], Mg/DOBDC [**97**] etc. Apart from good chemical stability, superior thermal stability is also an advantageous factor for MIL-53(Al).

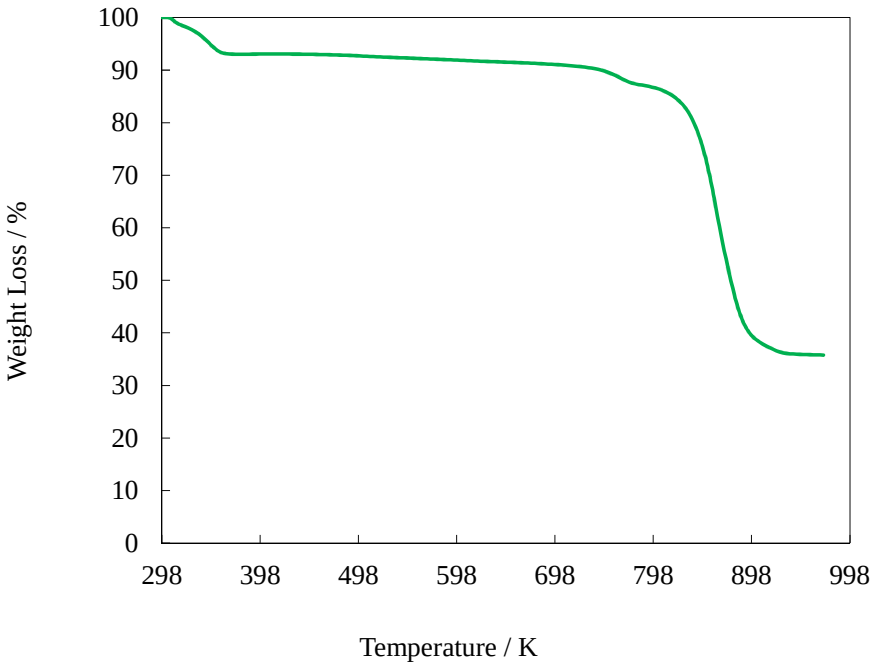

Figure 5.2: Thermogram of MIL-53(Al) at a heating rate of 5 K min^{-1} under a flow of 40 cm^3 min^{-1} of N_2.

5.2.2 X-ray Diffraction (XRD) Analysis

XRD analysis of MI-53(Al) sample was performed after activating it at higher temperature of 493 K. The obtained X-ray diffraction (XRD) patterns (Figure 5.3) indicate a good crystallanity for prepared MIL-53(Al) compound. These patterns are similar to the XRD pattern reported by Loisue et al. [**41**] for large pore (**lp**) domain of MIL-53(Al).

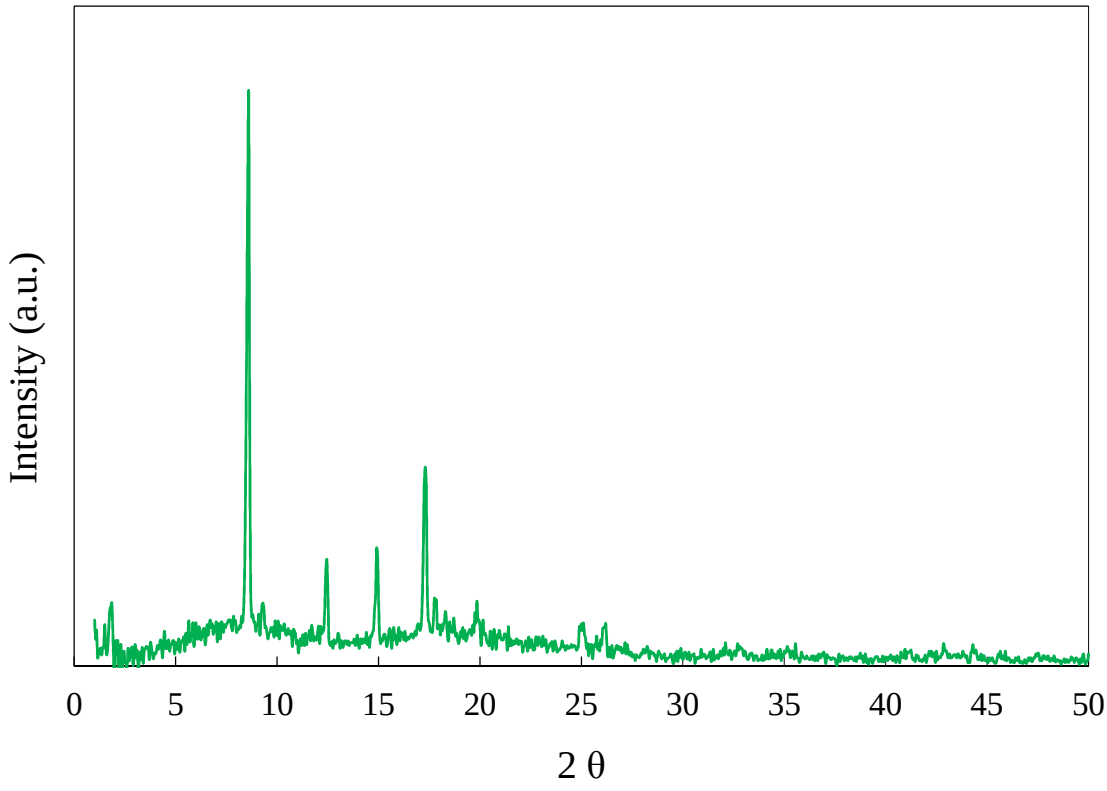

Figure 5.3: X-ray diffractogram of MIL-53(Al) after high temperature activation.

5.2.3 Surface Area and Pore Volume Analysis

Nitrogen physisorption at 77 K (Figure 5.4) is performed on MIL-53(Al) to calculate its surface area and pore volume. Prior to nitrogen physisorption, MIL-53(Al) sample was degassed at 493 K for 2 h. The BET surface area and pore volume were estimated to be 1284 m^2 g^{-1} and 0.64 cm^3 g^{-1} respectively. These values obtained in this work are comparable to those reported in the literature. The detailed comparison of these results with the existing literature is provided in the Table 5.2.

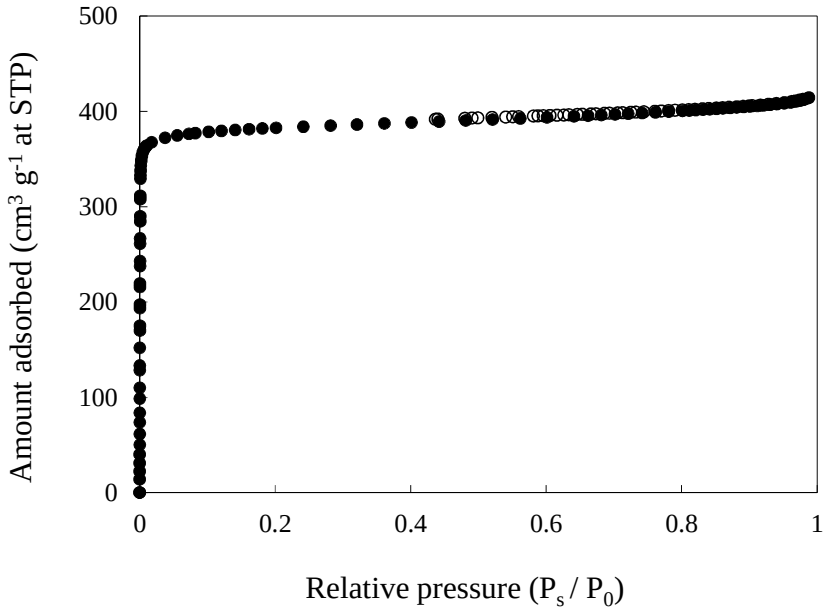

Figure 5.4: N_2 physisorption at 77 K on MIL 53(Al). (●) represents adsorption branch; (○) represents desorption branch.

Table 5.2: Surface area and pore volume of MIL-53(Al).

BET Surface area ($m^2 g^{-1}$)	**Pore volume ($cm^3 g^{-1}$)**	**Ref.**
1140	–	[**41**]
1235	–	[**107**]
1300	0.42	[**75**]
1664*	0.60	[**210**]
1284	0.64	This study

*** Langmuir surface area.**

The above TGA, XRD, and BET characterization results matched well with previous literature reports.

5.3 CO_2 Isotherms of MIL-53(Al)

Adsorption and desorption of CO_2 at 293 K on MIL-53(Al) is shown in Figure 5.5. Before performing the adsorption measurement of CO_2, MIL-53(Al) sample is activated at 493 K. Although MIL-53(Al) is a microporous material, the obtained isotherms are of type-IV with clear steps. The similar results for CO_2 adsorption on MIL-53(Al) have already been reported in the literature by Bourelly et al. [**42**] and Boutin et al. [**90**]. The steps in the isotherms are known to be attributed to the structural transformation of MIL-53(Al) or so called breathing phenomenon [**41, 42, 90**].

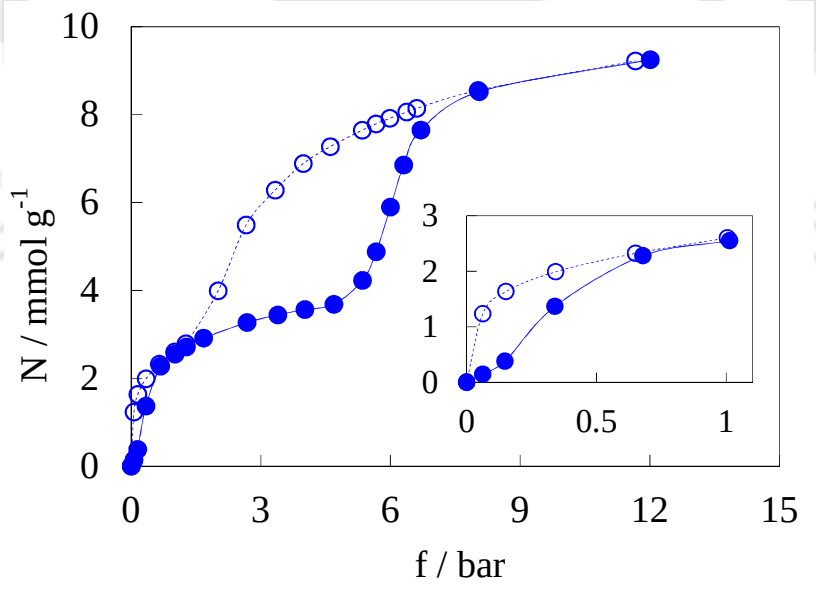

Figure 5.5: CO_2 isotherms at 293 K on MIL-53(Al) after activating it at higher temperature of 493 K (sample **lp$_0$**). ● represents adsorption; ○ represents desorption. Lines are drawn as a guide to the eye.

5.4 Identification of Different Phases of MIL-53(Al)

XRD patterns of MIL-53(Al) sample were measured at different stages *i.e.* after high temperature activation, after CO_2 adsorption up to 1 bar, after completely desorbing CO_2 under vacuum at 293 K and after performing N_2 adsorption at high pressure (*ca.* > 15 bar) at 293 K on CO_2 desorbed sample (Figure 5.6). The obtained patterns were matched with the existing patterns of different phases of MIL-53(Al) in the literature to identify the phase of the sample at above stages.

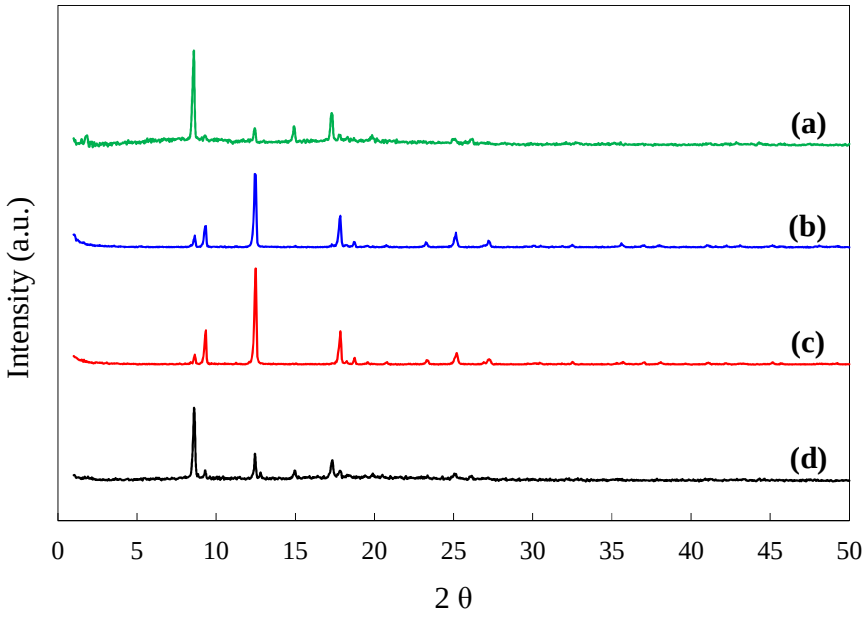

Figure 5.6: XRD patterns of (**a**) sample **lp$_0$**, (**b**) sample after **lp→np** transformation at about 1 bar of CO_2, (**c**) sample **np$_0$** and (d) sample after N_2 adsorption at high pressure (*ca.* > 15 bar) at 293 K on sample **np$_0$**.

An initial high temperature (493 K) activation of MIL-53(Al) yields the **lp** structure that is retained even after the sample is cooled to the experimental temperature (293 K) [**88, 90**]. The obtained XRD pattern (Figure 5.6a) of MIL-53(Al) at 293 K after high temperature activation (493 K) well matched the reported XRD pattern of **lp** phase of MIL-53(Al) [**41**]. We call this as

sample **lp$_0$** (material in its **lp** structure *in vacuo*). The CO_2 uptake (solid circles, Figure 5.5) for this material are also in good agreement with the earlier reported data [**41, 42, 90, 91**] and the predominance of **lp** phase is obvious initially. As the sample is exposed to CO_2, the first **lp→np** transformation takes place at low pressures (0 – 0.8 bar) [**211**], followed by a saturation in CO_2 capacity for the **np** structure at about 1 bar. The XRD pattern for the sample at this condition (Figure 5.6b) differs from that of sample **lp$_0$** and matched with the reported XRD pattern of **np** phase of MIL-53(Al) [**41**]. Thus majority of the sample exists in the **np** phase at 1 bar of CO_2. As CO_2 pressure is further increased, reverse transformation starts at about 4.5 bar, a step in the isotherm is observed accordingly. Finally, by about 8 bar the sample completely transforms into its **lp** form. During desorption, as the pressure is decreased, the sample will undergo a transformation back into the **np** structure. The two hysteresis loops observed (the low pressure hysteresis is prominent in inset of Figure 5.5) are attributed to the differences in the structure of the sample during adsorption and desorption branches [**90**].

CO_2 uptake at sub-atmospheric pressures merits focus (inset of Figure 5.5). In this region, while the adsorption branch includes the **lp→np** transition, during desorption the sample is continues to be in its **np** form. What happens when the sample is desorbed to very low pressure (say about 0.01 mbar)? As expected, the initial weight of the sample is regained (matching well with that of the **sample lp$_0$** *in vacuo*). However, we observed that the XRD pattern (Figure 5.6c) of the sample is similar to that of the **np** structure reported in literature [**41**]. This is to be expected because a hysteresis loop is observed in the low pressure region. While the existence of hysteresis in low pressure region has been reported elsewhere in literature [**90**], to the best of our knowledge no attempt has been made to correlate hysteresis with the phase of the sample (in this case, majority of the sample will be in the **np** domain). As we will demonstrate, this important

observation can be exploited to tune the adsorption characteristics of the material. We call this CO_2 desorbed sample as **sample np_0**.

5.5 Tuning of MIL-53(Al) Structure into Different Phases

From the above discussion it is clear that guest free MIL-53(Al) MOF can be stabilized to its **lp** as well as **np** phase at 293 K. In contrast to the earlier reported work, tuning to **np** phase in this work is done without inclusion of any extra functional groups or guest molecules. In brief, the activation (or desorption of guest molecules) at higher temperature (493 K) yields the material in its **lp** phase and adsorption of CO_2 followed by its complete desorption at 293 K yields **np** phase. The necessary steps involved to tune MIL-53(Al) into the desired structural form are summarized in Figure 5.7.

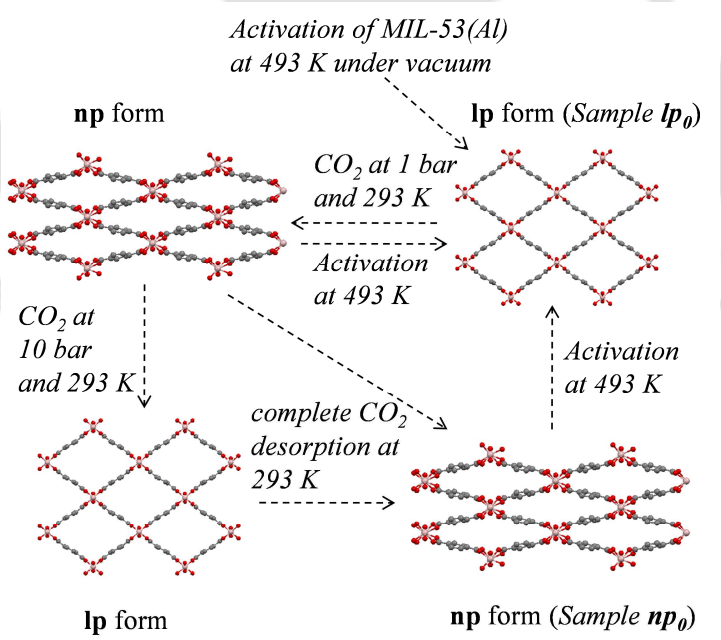

Figure 5.7: Structural transformations in MIL-53(Al).

5.6 Adsorption Characteristics of Different Phases

Adsorption and desorption branches of CO_2 isotherm at 293 K on both **lp** phase (sample **lp$_0$**) and **np** phase (sample **np$_0$**) of MIL-53(Al) MOF are shown in Figure 5.8.

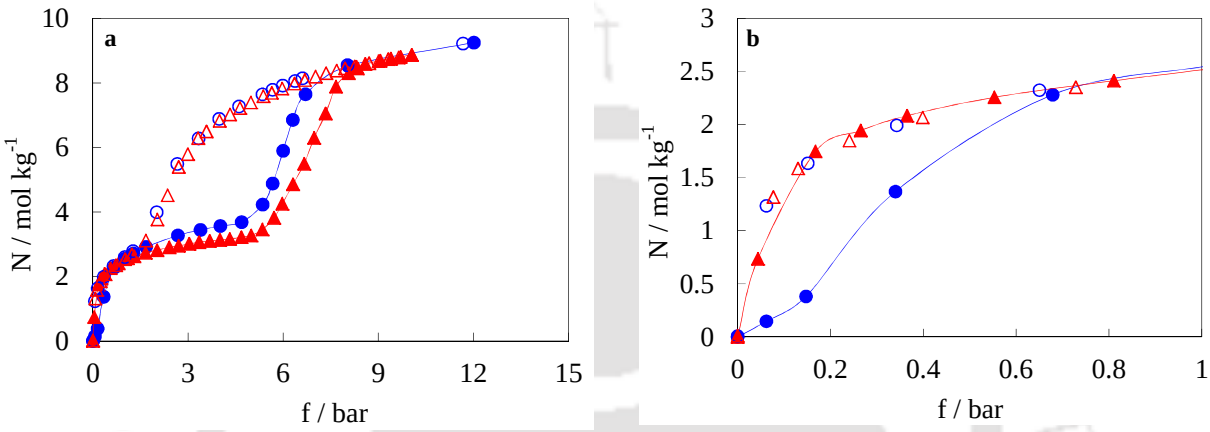

Figure 5.8: (**a**) CO_2 isotherms at 293 K on different structures of MIL-53(Al). (**b**) enlarged portion of the isotherms in the low pressure region. ● represents adsorption on sample **lp$_0$**; ○ represents desorption on sample **lp$_0$;** ▲ represents adsorption on sample **np$_0$**; Δ represents desorption on sample **np$_0$**. Lines are drawn as a guide to the eye.

Adsorption isotherm of CO_2 on the sample **np$_0$** (filled triangles, Figure 5.8) is different than that on sample **lp$_0$**. First, in the low pressure region the uptake of CO_2 on sample **np$_0$** increases as compared to that of sample **lp$_0$** and almost matches desorption branch of the isotherm on sample **lp$_0$** (Figure 5.8b). At about 0.17 bar, CO_2 loading capacity on sample **np$_0$** (1.75 mol kg^{-1}) is significantly higher than that on sample **lp$_0$** (0.42 mol kg^{-1}). The comparison is highlighted for this pressure due to its industrial relevance (in flue gases, partial pressure of CO_2 is typically between 0.12 – 0.20 bar). This increase in CO_2 loading on sample **np$_0$** is to be expected, since **np**

structure has larger Henry's constant [**209**]. Some of the earlier works have also attempted to exploit this feature of the **np** structure to enhance CO_2 loading at low pressure [**170, 208**]. However, such a high enhancement in CO_2 uptake has not been reported (possibly due to presence of guest molecules or functional groups in their samples). In addition, since the sample $\mathbf{np_0}$ is already in the **np** domain prior to adsorption, the first **lp→np** transition no longer occurs and corresponding hysteresis below 1 bar disappears (solid and open triangles in Figure 5.8b overlap). **np→lp** transformation occurs at slightly higher pressure for sample $\mathbf{np_0}$ because in this case, sample exists in its **np** form at the start of CO_2 adsorption resulting into a better stability of **np** phase. It is also worth mentioning that the enhancement of CO_2 capacity is achieved without any additional regeneration penalty, as the desorption branches on $\mathbf{lp_0}$ or $\mathbf{np_0}$ samples follow the same curve (open circles and triangles in Figure 5.8b).

Adsorption and desorption of other industrially important gases such as N_2, CH_4, CO and O_2 are also measured at 293 K on both **lp** phase (sample $\mathbf{lp_0}$) and **np** phase (sample $\mathbf{np_0}$) of MIL-53(Al) MOF sample (Figures 5.9 − 5.12).

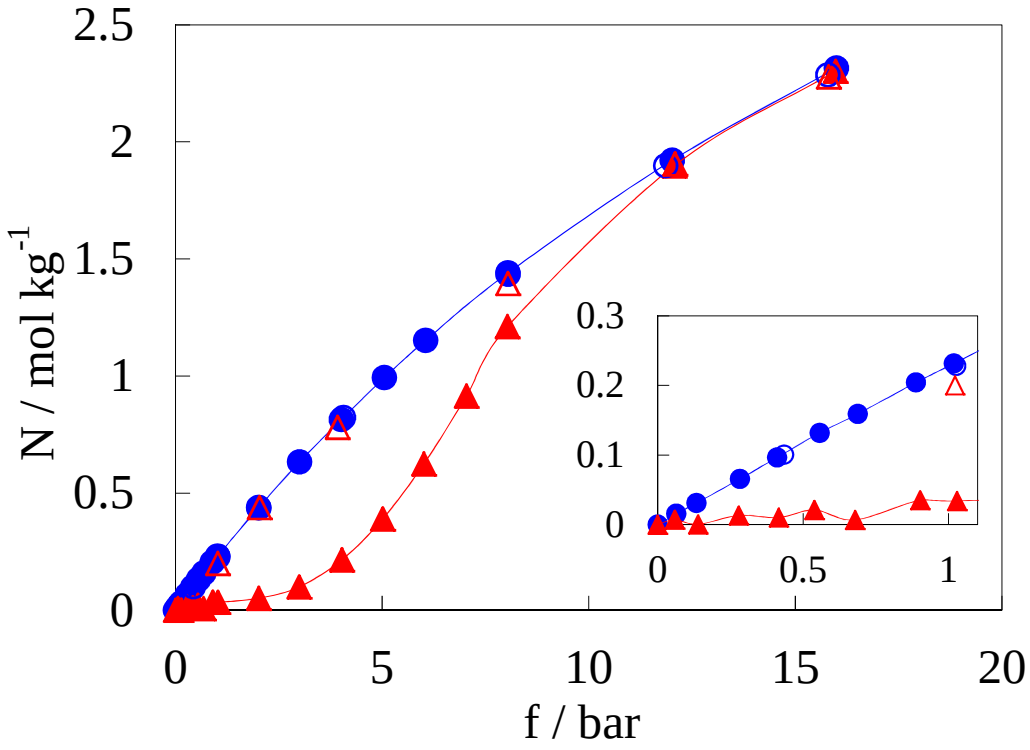

Figure 5.9: N_2 isotherms at 293 K on different structures of MIL-53(Al). ● represents adsorption on sample **lp$_0$**; ○ represents desorption on sample **lp$_0$;** ▲ represents adsorption on sample **np$_0$**; Δ represents desorption on sample **np$_0$**. Lines are drawn as a guide to the eye.

Adsorption and desorption isotherms of N_2 at 293 K on the samples **lp$_0$** and **np$_0$** have significant differences (Figure 5.9). As reported in literature [**90, 107**], structural transformation does not occur in case of sample **lp$_0$** and isotherm does not exhibit hysteresis. In contrast, isotherms on sample **np$_0$** show several interesting features. N_2 adsorption was negligible upto to a certain pressure (~*ca.* 1 bar), as the **np** form of the sample excludes N_2 molecules with larger kinetic diameter and low adsorption energies [**209**]. This is the lowest uptake reported for N_2 on non-hydrated and non-functionalized form of MIL-53(Al) at 293 K. At higher pressures, increase in adsorption may be readily attributed to the **np**→**lp** transformation of the sample. As a result of

this structural transformation, hysteresis is also observed in the isotherms (which was absent earlier in case of sample **lp$_0$**). After a certain pressure (*ca*. 12 bar), the transformation is complete and both the adsorption and desorption branches coincide with that on the **lp** structure. The predominance of **lp** phase for the sample equilibrated with N_2 at high pressure is further confirmed from the XRD pattern (Figure 5.6d). This behavior is also observed for other industrially important gases like CH_4, CO and O_2 (Figure 5.10 − 5.12). It is interesting to note that for all the four gases considered, the **np→lp** transformation is complete when loading is in between 1.5 and 2 mol kg^{-1}. Thus, the range of pressure at which the transformation occurs seems related to the adsorption affinity of these gases on to the sample. For example, the transformation during CH_4 adsorption occurs at a lower pressure compared to that occurring during adsorption of CO, O_2 or N_2. On the other hand, no transformation occurs even up to 25 bar when sample **np$_0$** is exposed to a non-adsorbing gas like healium. To the best of our knowledge, structural transformation of MIL-53(Al) upon adsorption of gases like CH_4, N_2, CO and O_2 at ambient temperature has not been reported so far.

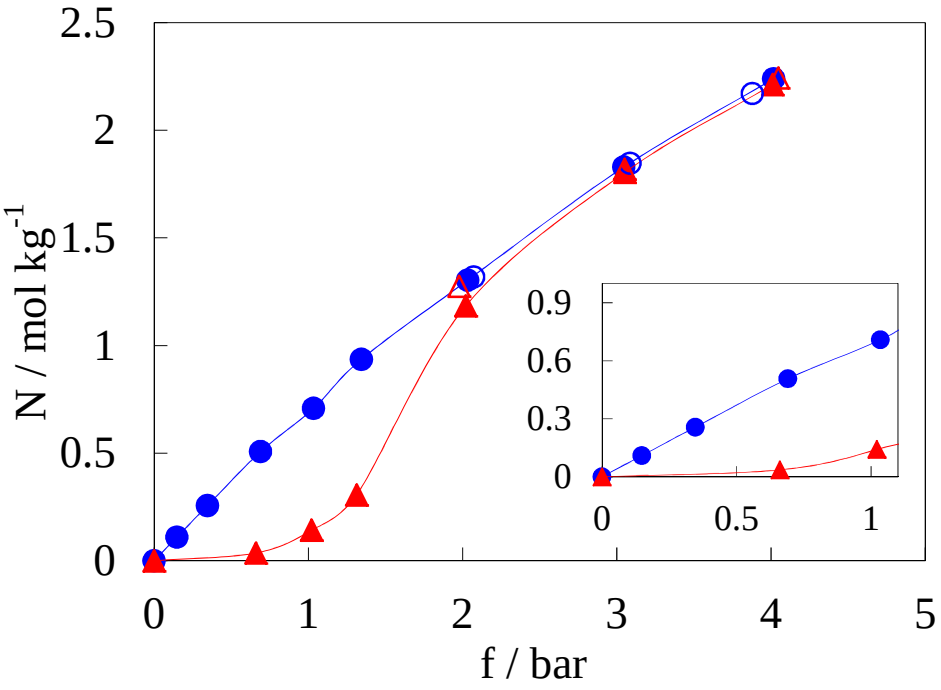

Figure 5.10: CH_4 isotherms at 293 K on different structures of MIL-53(Al). ● represents adsorption on sample **lp$_0$**; ○ represents desorption on sample **lp$_0$;** ▲ represents adsorption on sample **np$_0$**; Δ represents desorption on sample **np$_0$**. Lines are drawn as a guide to the eye.

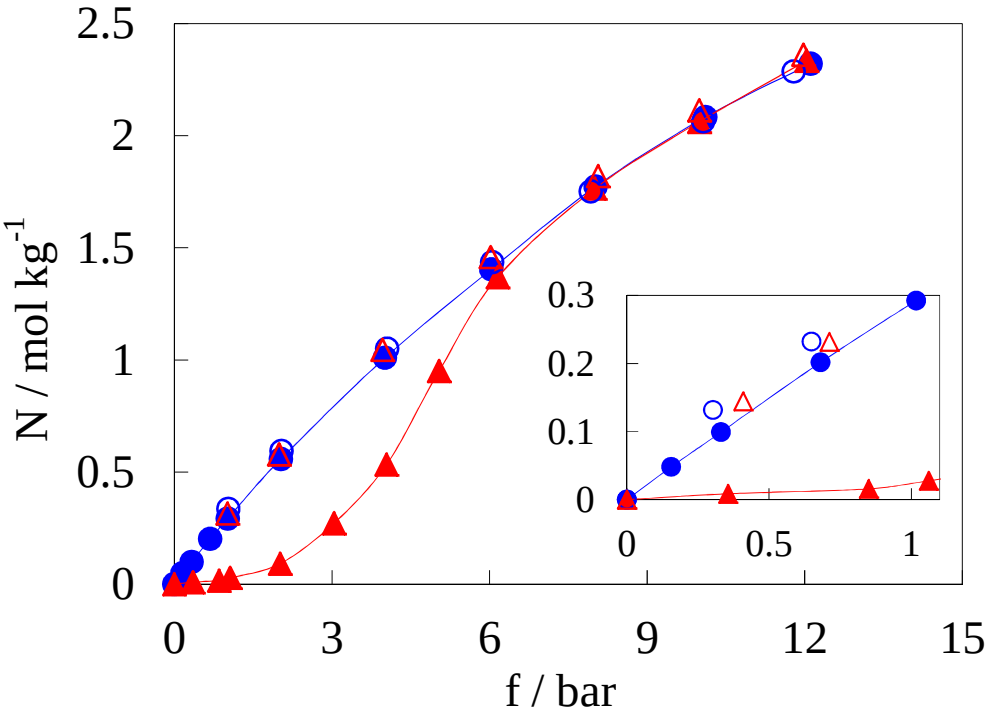

Figure 5.11: CO isotherms at 293 K on different structures of MIL-53(Al). ● represents adsorption on sample **lp$_0$**; ○ represents desorption on sample **lp$_0$;** ▲ represents adsorption on sample **np$_0$**; Δ represents desorption on sample **np$_0$**. Lines are drawn as a guide to the eye.

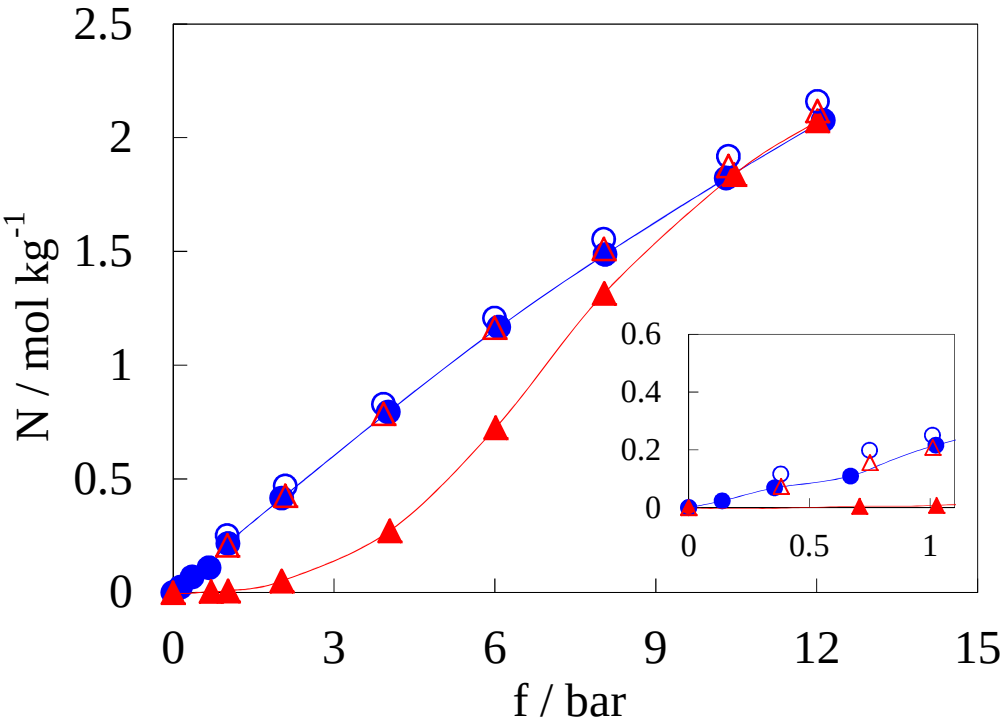

Figure 5.12: O_2 isotherms at 293 K on different structures of MIL-53(Al). ● represents adsorption on sample **lp$_0$**; ○ represents desorption on sample **lp$_0$;** ▲ represents adsorption on sample **np$_0$**; Δ represents desorption on sample **np$_0$**. Lines are drawn as a guide to the eye.

5.7 High Selectivity of CO_2 over CH_4, N_2, CO and O_2

Figure 5.13 highlights the usefulness of the **np** tuned form of MIL-53 (sample $\mathbf{np_0}$) for separations. Even though MIL-53(Al) has greater stability towards moisture, it has not gained much attention for CO_2 separation due to its poor capacity and selectivity on the **lp** structure [**42, 107, 202**]. However now, we have removed these limitations to a large extent, by tuning the pores into **np** domain; CO_2 capacity at about 0.17 bar (similar to its partial pressure in flue gas) is significantly higher (1.75 mol kg^{-1}) than those reported elsewhere (0.42 – 1.00 mol kg^{-1}) on any MIL-53 material (including the hydrated or functionalized forms) [**170, 208**]. At the same time, the **np** form shows near zero uptake for CH_4, N_2, CO and O_2 at pressures below 1 bar. Thus very high CO_2 selectivity is achieved. Since **np** phase of sample $\mathbf{np_0}$ is retained up to 1 bar during adsorption of all gases at 293 K, similar trend in CO_2 selectivity will be obtained at sub-atmospheric pressure even for multi-component adsorption of these gases. No further experiments (with relevant gas mixtures) are needed to validate selectivity trend shown in Figure 5.13.

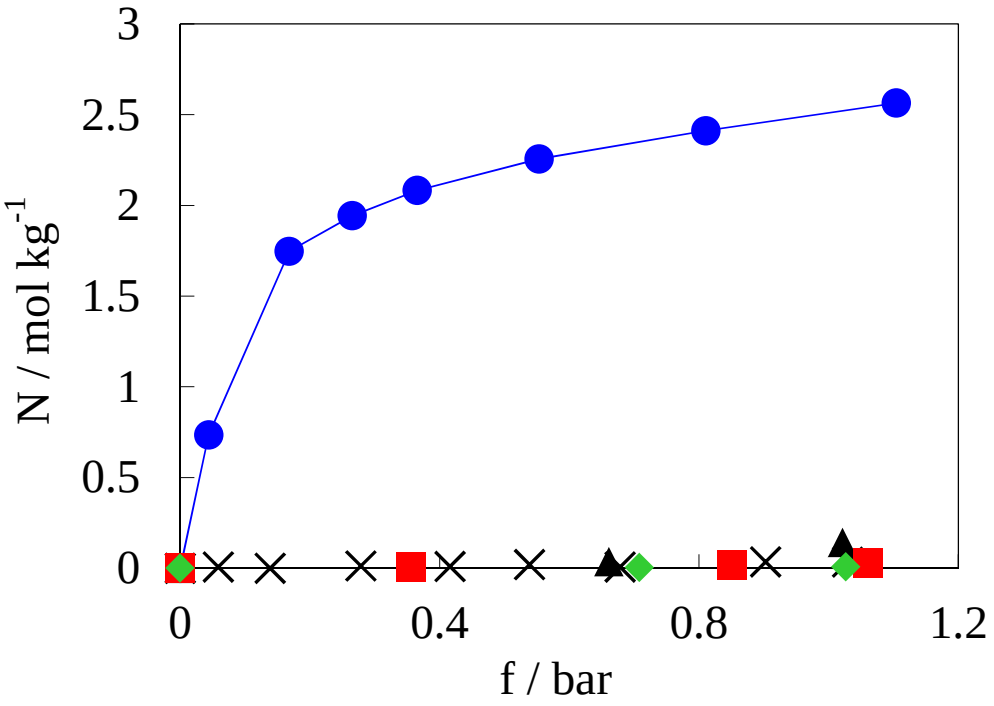

Figure 5.13: Adsorption capacities of CO_2 (●), N_2 (✕), CH_4 (▲), CO (■) and O_2 (♦) on **np** structured MIL-53(Al), sample $\mathbf{np_0}$ at 293 K. Lines are drawn as a guide to the eye.

5.8 Summary

It is widely believed that the structure of MIL-53(Al) depends on its equilibrium environment *i.e.* temperature and partial pressure of the adsorbate guest molecules. In this chapter, we have demonstrated that the adsorption and desorption history of the sample after the high temperature activation also strongly influence its structural transformation (and hence its adsorption properties). By choosing an appropriate *path*, the sample under vacuum was tuned into the **np** form which exhibits more than fourfold increase in CO_2 capacity (from 0.42 mol kg^{-1} to 1.75 mol kg^{-1} at about 0.17 bar and 293 K) along with exceptional enhancement in its selectivity over N_2, CH_4, CO and O_2 at sub-atmospheric pressures. MIL-53(Al) also exhibited structural transformation upon adsorption of N_2, CH_4, CO and O_2 at 293 K in its **np** form. We believe these results demonstrate a methodology that can be exploited to tune flexible materials for enhancement of adsorption capacity / selectivity and to design separation processes based on such adsorbents.

CHAPTER 6

ADSORPTION CHARACTERISTICS OF COORDINATIVELY UNSATURATED METAL SITES CONTAINING DOBDC MOFS

This chapter contains an adsorption analysis of M/DOBDC MOFs which have coordinatively unsaturated (cus) metal sites. An attempt is made to understand the effect of adsorbate polarity, polarizability, cus metal sites and different metal constituent in the framework on the adsorption characteristics of these MOFs.

6.1 Background

In previous chapter, effect of framework flexibility is investigated for the flexible MIL-53(Al) MOF. A methodology was presented to tune the flexible structure of MIL-53(Al) to enhance its adsorption uptake and selectivity for CO_2 in the sub-atmospheric region. In next two chapters, the effect of coordinatively unsaturated *(cus)* metal sites on the adsorption characteristics of the MOF is investigated. While in this chapter, MOFs with *cus* metal centers (M/DOBDC) are selected; in the next chapter M/DABCO MOFs with negligible *cus* metal centers are chosen. The effect of variation of metal constituent in the framework is also evaluated for each category of MOF. In addition, the effect of physical properties of adsorbate on adsorption characteristics is also highlighted.

The family of isostructural MOFs (M/DOBDC, M = Mg, Mn, Co, Ni and Zn), known to contain *cus* metal sites, has been recently reported in the literature [**63, 96, 97, 166 – 169**]. In these MOFs, metal atoms (M) are coordinatively bonded to the oxygen atoms of the carboxylate and hydroxylate groups of the 2,5-dihydroxy terephthalic acid ligand (Figure 6.1). This coordination results in occupation of five coordination positions of metal atom by the oxygen atoms. The sixth position is occupied by water molecule which can be removed by thermal treatment at higher temperature under vacuum making the metal site of framework coordinatively unsaturated [**168, 169**]. The structure of these MOFs is honeycomb-like with large one-dimensional pores of 11–12 **Å** diameter [**96**]. Unit cell parameters and other details of M/DOBDC frameworks are listed in Table 6.1.

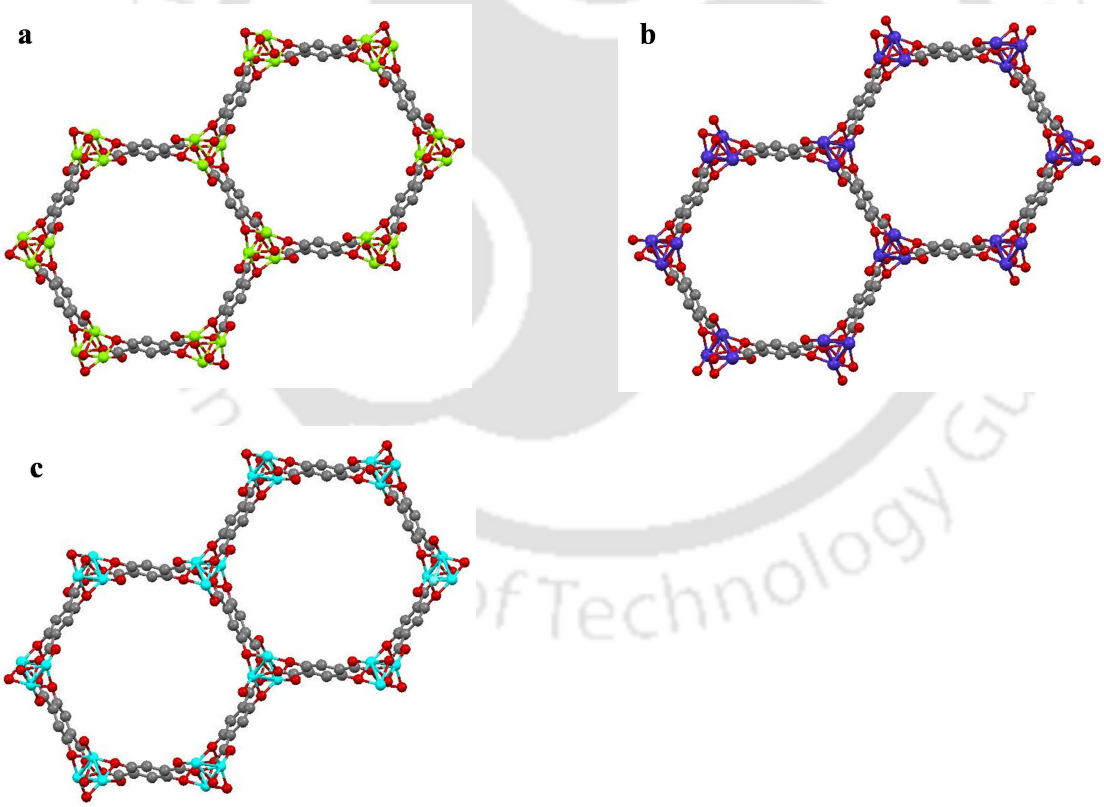

Figure 6.1: Crystal structure of (a) Mg/DOBDC [**169**], (b) Co/DOBDC [**166**] and (c) Ni/DOBDC [**167**] MOFs (O, red; C, grey; Mg, yellow; Co, violet; Ni, sky blue).

Table 6.1: Structural details of M/DOBDC MOFs [**166 – 169**].

Chemical formula of unit cell	Molecular weight of unit cell (**g**)	Unit cell parameters		Cell volume (**Å^3**)	Crystal density (**g cm^{-3}**)	Conversion factor for mol kg^{-1} to molecule unit cell^{-1} conversion
		Cell lengths (**Å**)	Cell angles			
$C_{72}H_{18}O_{54}Mg_{18}$	2184.7	a = 26.026 b = 26.026 c = 6.7587	α = 90 β = 90 γ = 120	3964.7	0.915	2.185
$C_{72}H_{18}O_{54}Mn_{18}$	2736.1	NA	NA	3964.7*	1.146*	2.736
$C_{72}H_{18}O_{54}Co_{18}$	2808.0	a = 25.885 b = 25.885 c = 6.8058	α = 90 β = 90 γ = 120	3949.0	1.180	2.808
$C_{72}H_{18}O_{54}Ni_{18}$	2803.6	a = 25.785 b = 25.785 c = 6.7701	α = 90 β = 90 γ = 120	3898.3	1.194	2.804

* Mg/DOBDC cell volume was used for the calculation

M/DOBDC MOFs have been investigated for gas storage and gas separation applications. Ni/DOBDC compound of this family exhibits very good storage performance for methane [**78**] and hydrogen [**147**]. On the other, CO_2 uptake and selectivity at flue gas conditions on Mg/DOBDC are better than that on other DOBDC compounds including Ni/DOBDC [**68, 97**]. Similarly, Fe/DOBDC is reported to be one of the best adsorbent for O_2/N_2 [**141**] and hydrocarbon [**133**] separation. Earlier studies in literature report the effect of substitution of various metal atoms on the adsorption characteristics of hydrogen and methane on DOBDC series of MOFs [**78, 147**]. It was also reported that structure of DOBDC frameworks decomposes

upon exposure to humid environment and the rate of decomposition is comparatively higher for Mg/DOBDC [**188**] compared to other M/DOBDC MOFs. These isostructural MOFs seem to be good candidates for studying the effect of metal atom substitution (in the framework) on the adsorption characteristics; the presence of a large number of *cus* metal sites will pronounce the effect of metal atoms. It would be interesting to systematically investigate the effect of metal atom in the framework on adsorption of several gases with varying polarity over a wide range of temperature and pressure conditions.

In this chapter, the adsorption properties of CO_2, CO, CH_4, N_2, Ar, C_2H_6 and C_3H_8 on M/DOBDC (M = Mg, Mn, Co, and Ni) MOFs at three temperatures (294, 315 and 352 K) and for a wide range of pressure are presented. Due to the change in the metal atoms and their corresponding ionic radii (Table 6.2), the electrostatic interactions of the *cus* metal centers in the framework with the adsorbate molecules are expected to be different, thereby affecting the adsorption characteristics. Thermodynamic properties such as the Henry's constant and enthalpy of adsorption were calculated for each MOF to highlight the effect of adsorbate properties and metal atom on the adsorption at different conditions. In addition, selectivities for various binary mixtures were also calculated using Ideal Adsorption Solution Theory (IAST) [**198**] to understand the effect of metal atom in the framework on this important thermodynamic property.

Table 6.2: Ionic radii of relevant divalent metal cations [**212**].

Metal	**Mg^{2+} (V)**	**Mn^{2+} (V)**	**Co^{2+} (V)**	**Ni^{2+} (V)**
Ionic radii, Å	0.66	0.75	0.67	0.63

6.2 Characterization of Frameworks Synthesized

Mg/DOBDC, Co/DOBDC and Ni/DOBDC frameworks were synthesized following the procedure reported in the literature as discussed in Section 4.1. The detailed description of synthesis procedures is provided in Section 4.1. Since these materials are highly sensitive towards moisture [**43, 188**], additional care has been taken to avoid any exposure of the synthesized samples in ambient environment. The synthesized samples were analyzed using thermogravimetry, powder XRD and BET surface area analysis.

6.2.1 Thermogravimetric Analysis (TGA)

Thermograms of all the M/DOBDC samples (M = Mg, Mn, Co and Ni) are shown in Figure 6.2. The temperature was ramped from 298 to 873 K with a heating rate of 5 K min^{-1}, and the measurements were performed under a nitrogen atmosphere. There are total three weight loss steps for each sample. The first weight loss step up to 377 K is relatively rapid, and corresponds to the removal solvent (methanol) and moisture. The second weight loss is due to detachment of coordinatively bonded water molecules; thus creating coordinatively unsaturated metal sites in the frameworks [**96**]. The final weight loss step corresponding to the decomposition and collapse of the framework varies for each sample (about 560 K for Co/DOBDC to ~700 K for Mg/DOBDC).

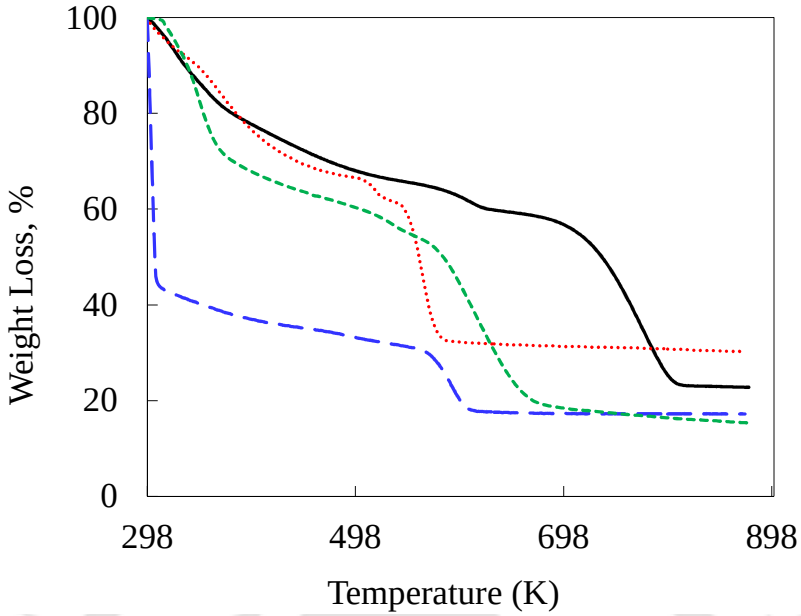

Figure 6.2: Thermogram of as-synthesized Mg/DOBDC (—), Mn/DOBDC (---), Co/DOBDC (···) and Ni/DOBDC (– –) at a heating rate of 5 K min^{-1} under flow of N_2.

6.2.2 Powder X-ray Diffraction (PXRD) Analysis

Powder XRD analysis (Figure 6.3) of synthesized M/DOBDC samples indicates very good crystallanity for these frameworks. In addition, the obtained results are similar to the PXRD pattern reported in the literature for M/DOBDC compounds [**147**] and also confirm the isostructural nature of the compounds.

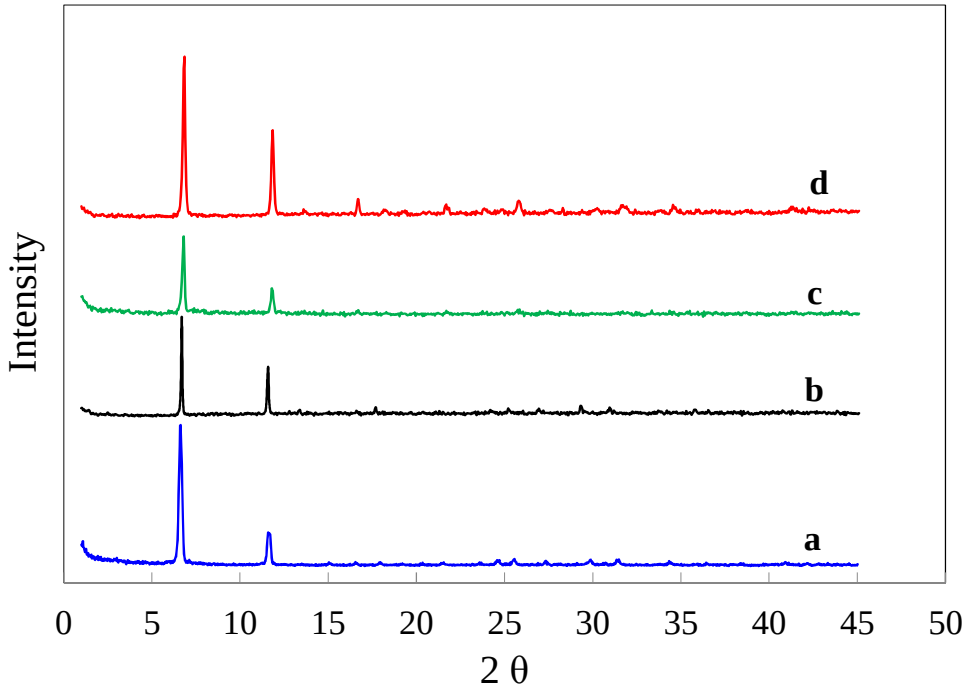

Figure 6.3: X-ray diffractogram of (a) Mg/DOBDC, (b) Mn/DOBDC, (c) Co/DOBDC and (d) Ni/DOBDC.

6.2.3 Surface Area and Pore Volume Analysis

The N_2 isotherms of the M/DOBDC samples at 77 K are shown in Figure 6.4. Mg/DOBDC exhibits the highest N_2 specific loadings per unit gram (Figure 6.4a). However, when loadings are converted to a unit cell basis, a significant change in the trend is observed (Figure 6.4b).

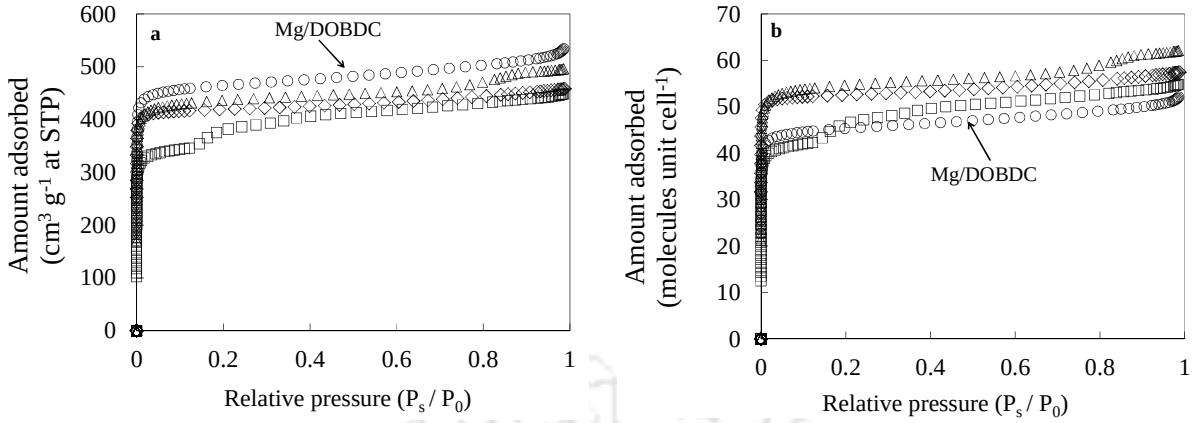

Figure 6.4: (**a**) Adsorption of N_2 on Mg/DOBDC (○), Mn/DOBDC (□), Co/DOBDC (◊) and Ni/DOBDC (Δ) at 77 K; (**b**) N_2 loadings are given for per unit cell.

The N_2 isotherms at 77 K were used to obtained surface area and pore volume for the frameworks. The surface area and pore volume of all the compounds on are given in Table 6.3. The surface area for Mg/DOBDC obtained in this work (1579 m^2 g^{-1}) is comparable to that obtained by Caskey et al. (1495 m^2 g^{-1}) [**97**]; however, it is lower than that reported by Herm et al. (1800 m^2 g^{-1}) [**67**] and is higher than that reported by Bae et al. (1206 m^2 g^{-1}) [**160**]. Similarly, the BET surface area obtained in this work for other three DOBDC frameworks are slightly higher than that observed by other researchers like Wu et al. [**78**] and Caskey et al. [**97**]. The surface area obtained in this work for Mg/DOBDC (1579 m^2 g^{-1}), Co/DOBDC (1428 m^2 g^{-1}) and Ni/DOBDC (1485 m^2 g^{-1}) are very close to the geometric surface area reported by Yazaydın et al. [**37**] for these frameworks (*i.e.* 1639, 1508 and 1456 m^2 g^{-1} for Mg/DOBDC, Co/DOBDC and Ni/DOBDC, respectively). Experimental values of surface area, such a close to geometric surface area are rarely reported in the literature.

Table 6.3: BET surface area and pore volume of the DOBDC series of MOFs used in this study.

Compound	Surface area		Pore volume	
	$m^2\ g^{-1}$	$nm^2\ uc^{-1}$	$cm^3\ g^{-1}$	$nm^3\ uc^{-1}$
Mg/DOBDC	1579	5.73	0.82	2.97
Mn/DOBDC	1304	5.92	0.69	3.15
Co/DOBDC	1428	6.66	0.71	3.30
Ni/DOBDC	1485	6.91	0.77	3.58

It is interesting to note that both the surface area and pore volume of unit cells vary linearly with the 2nd ionization energy of metal atom in the framework (Figure 6.5).

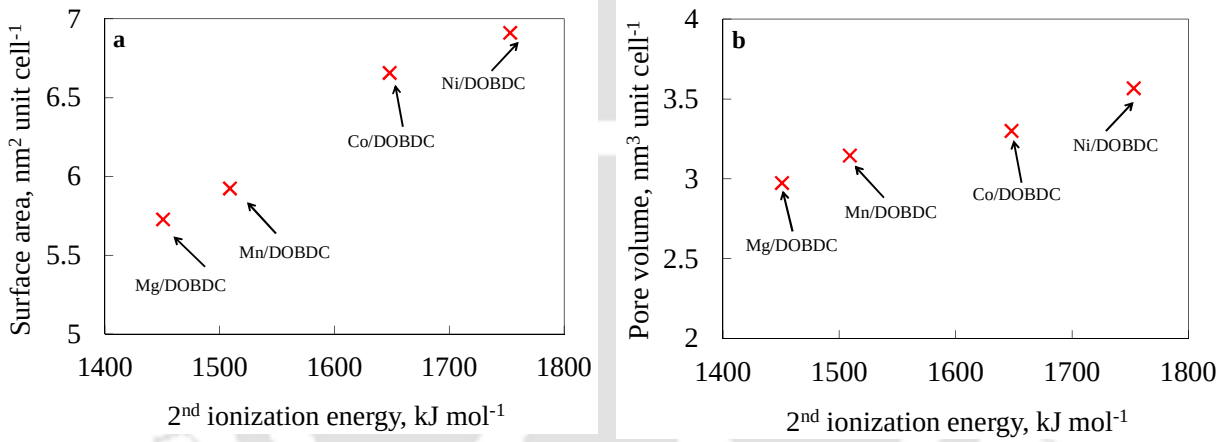

Figure 6.5: Variation of **(a)** surface area and **(b)** pore volume of unit cell with 2nd ionization energy of metal cation in DOBDC MOFs.

6.3 Adsorption Isotherms

As DOBDC frameworks have a large number of *cus* metal sites, electrostatic interactions are also expected to play a significant role on their adsorption characteristics. In order to understand the effect of both polarizability as well as polarity, adsorbates such as Ar, C_2H_6 and C_3H_8 are also included. The low pressure adsorption data was carefully measured to get accurate insights

of Henry's law region. All isotherms are plotted here in conventional [*N vs. f*] domain as well as in virial domain [ln(*f*/*N*) *vs. N*]. A virial domain plot is useful for analyzing the low pressure experimental data as mentioned in the Section 3.5.3.

6.3.1 CO_2 Isotherms

The CO_2 isotherms of Mg/DOBDC, Mn/DOBDC, Co/DOBDC and Ni/DOBDC samples at 294, 315 and 352 K are shown in Figures 6.6 − 6.7. Flue gas streams come out at about ambient pressure with CO_2 concentration of 12 − 20% which means the CO_2 partial pressure in flue gas streams ranges from 0.12 to 0.20 bar. Thus, it is desirable to have good CO_2 adsorption capacity in this pressure range for an adsorbent used for removal of CO_2 from the flue gas streams. CO_2 adsorption at 0.15 bar and 294 K is 5.07 mol kg^{-1} on Mg/DOBDC which is significantly higher than that on most of the MOFs and other adsorbents such as CuBTC (2.63 mol kg^{-1}) [**76**], MIL-101 (0.7 mol kg^{-1}) [**74**], MOF-5 (0.1 mol kg^{-1}) [**37**], UTSA-16 (2.1 mol kg^{-1}) [**160**], Ni/DABCO (0.28 mol kg^{-1}) [**75**], MIL-53(Al) (0.4 mol kg^{-1}) [**75**], NH_2-MIL-53(Al) (0.7 mol kg^{-1}) [**75**], MOF-177 (0.14 mol kg^{-1}) [**37**] , MIL-47 (0.25 mol kg^{-1}) [**37**] and Zeolite 13X (3.8 mol kg^{-1}) [**35**]. After Mg/DOBDC, NiDOBDC exhibits second highest CO_2 uptake of 3.75 mol kg^{-1} followed by Co/DOBDC (3.3 mol kg^{-1}) and Mn/DOBDC (2.6 mol kg^{-1}) at 0.15 bat and 294 K. Gravimetric CO_2 saturation uptake at 294 K on these samples ranges from 11.5 to 14 mol kg^{-1}; it is similar to that on other adsorbents compounds with similar surface area and pore volume like Ni/DABCO (14 mol kg^{-1}) [**75**], MIL-53(Al) (10.5 mol kg^{-1}) [**42**], MIL-47 (12.5 mol kg^{-1}) [**42**] and is significantly lower than that on MOFs with larger surface area and pore volume such as MIL-101 (22 mol kg^{-1}) [**74**], MOF-177 (34 mol kg^{-1}) [**62**], MOF-200 (55 mol kg^{-1}) [**38**], MOF-205 (33 mol kg^{-1}) [**38**], MOF-210 (53 mol kg^{-1}) [**38**].

Virial domain plot of CO_2 on Mg/DOBDC exhibit a clear inflection at ~ 8 mol kg^{-1} loading as shown in Figure 6.7. This behavior is typical for a heterogeneous adsorbent and usually cannot be observed when isotherm is plotted in conventional [*N* vs. *f*] domain. This inflection indicates that the adsorbent is energetically heterogeneous to adsorption of CO_2 on Mg/DOBDC. With the increase in temperature, this inflection decreases indicating the reduction in the heterogeneity to CO_2 adsorption on Mg/DOBDC at the higher temperature. Isotherms with such inflection cannot be modeled by a Langmuir equation.

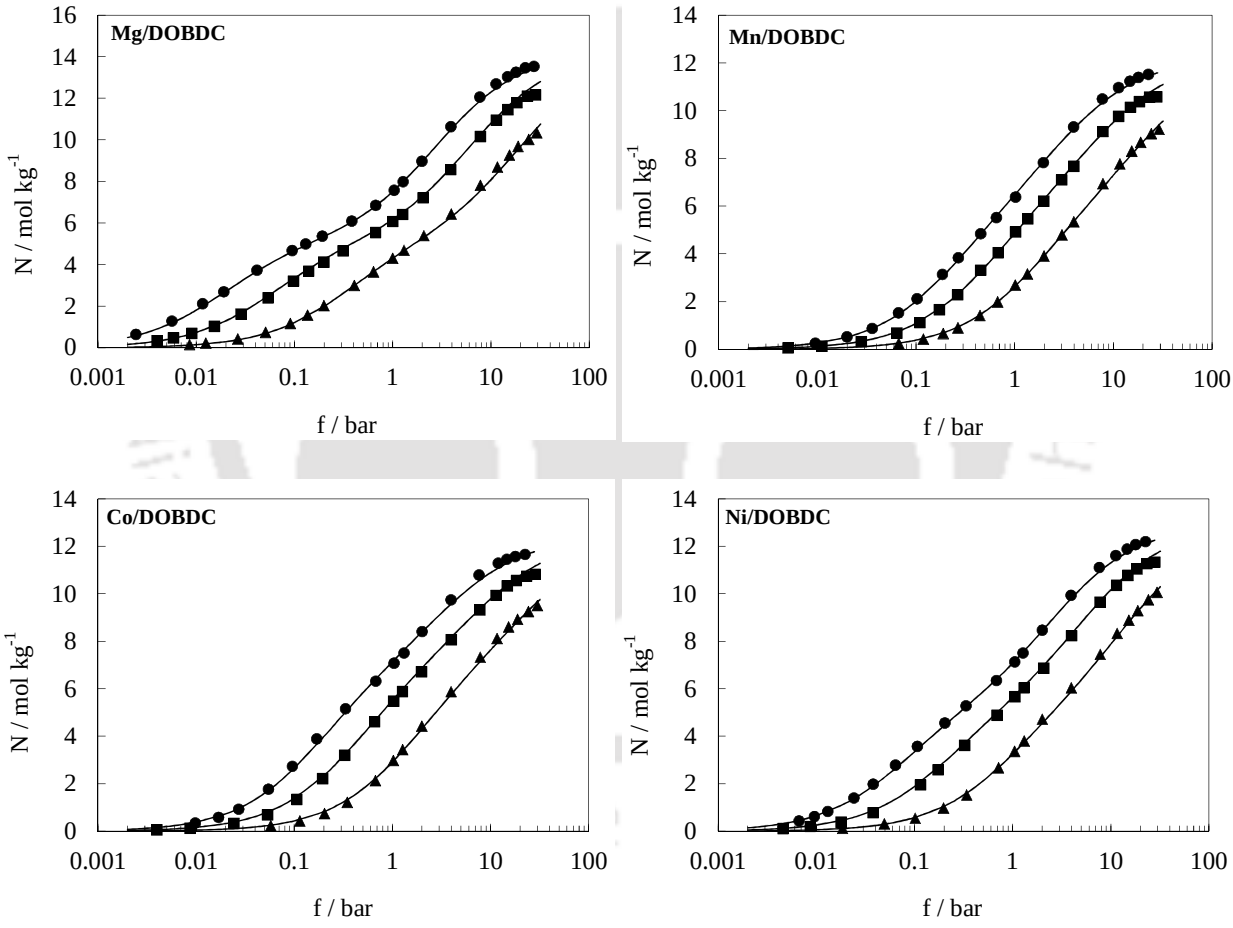

Figure 6.6: CO_2 isotherms of DOBDC MOFs. Symbols are experimental data at 294 K (●), 315 K (■) and 352 K (▲); lines are fits obtained using DSL isotherm parameters from Table 6.4.

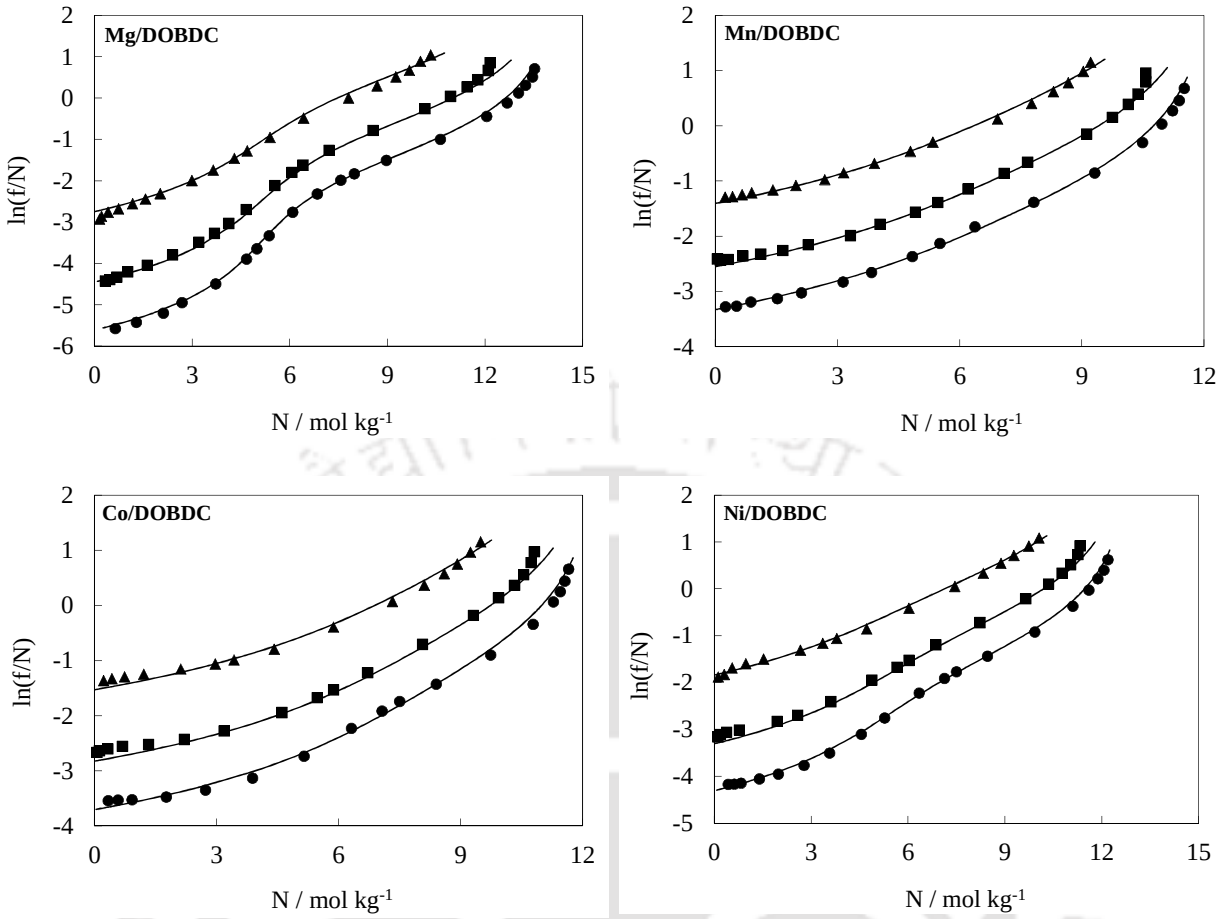

Figure 6.7: CO_2 isotherms of DOBDC MOFs in virial domain. Symbols are experimental data at 294 K (●), 315 K (■) and 352 K (▲); lines are fits obtained using DSL isotherm parameters from Table 6.4.

6.3.2 CO Isotherms

CO isotherms on MOFs are rarely reported although industrial need exists for separation of $CO_2/CH_4/CO$ gas mixtures [**213** – **214**] in processes like steam reforming. To the best of our knowledge, CO isotherms are reported only for Ni/DOBDC [**122**] among all four DOBDC frameworks and up to an atmospheric pressure only. Adsorption isotherms for CO on M/DOBDC frameworks are shown in Figures 6.8 − 6.9. Since these frameworks adsorbed a large amount of CO at low pressures, CO adsorption was measured at very low pressures such as 0.2 mbar in order to get the adsorption characteristics in Henry's law region. The obtained CO loading of ~4.7 mol kg^{-1} at 0.1 bar and 294 K on CoDOBDC and NiDOBDC is the highest known CO uptake on any adsorbent at similar conditions. Thus Ni/DOBDC and Co/DOBDC merit special attention for capturing CO from process streams. Even at ambient condition the CO uptakes on M/DOBDC samples is higher than most of the other adsorbents such Zn/DABCO [**121**], CuBTC, [**95**], MIL-101 [**95**], and NaX [**123**]. The virial domain plots of CO also exhibit inflection at about 6 – 7 mol kg^{-1} loading, demonstrates heterogeneity for adsorption of CO on M/DOBDC frameworks.

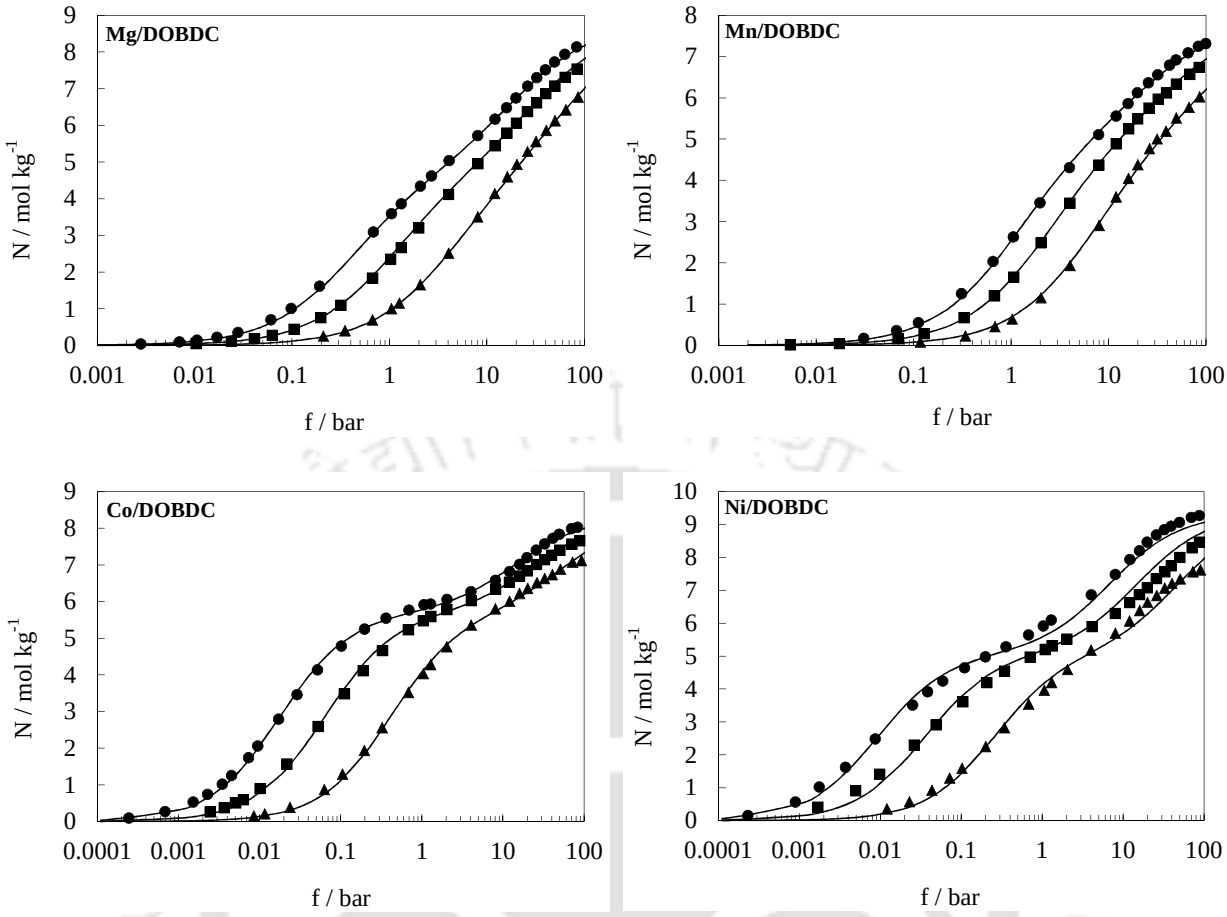

Figure 6.8: CO isotherms of DOBDC MOFs. Symbols are experimental data at 294 K (●), 315 K (■) and 352 K (▲); lines are fits obtained using DSL isotherm parameters from Table 6.5.

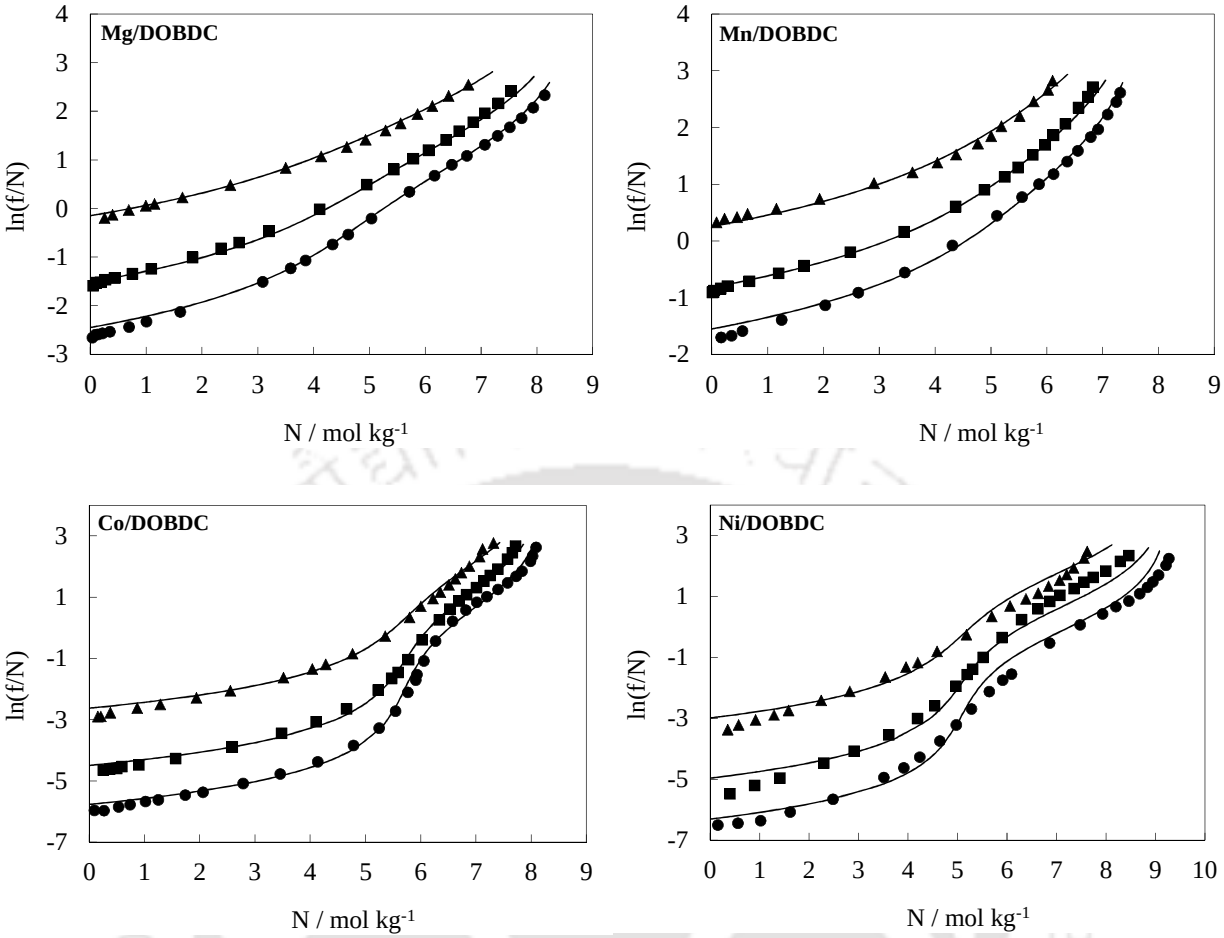

Figure 6.9: CO isotherms of DOBDC MOFs in virial domain. Symbols are experimental data at 294 K (●), 315 K (■) and 352 K (▲); lines are fits obtained using DSL isotherm parameters from Table 6.5.

6.3.3 CH_4 Isotherms

CH_4 isotherms on M/DOBDC frameworks at 294, 315 and 352 K are shown in Figures 6.10 − 6.11. CH_4 uptake at ambient condition on these frameworks ranges between 1.1 to 1.3 mol kg^{-1}; this value is slightly higher than that on MIL-101 [**74**], Zn/DABCO [**79**], MIL-53(Al) and MIL-47 [**42**] and is comparable to that on CuBTC [**76**]. The difference between the uptake of CH_4 on M/DOBDC compounds and that on other adsorbents near ambient conditions, is not as significant as in case of polar gases such as CO_2 and CO. At higher pressures, gravimetric uptake on M/DOBDC MOFs is considerably lower than that on NOTT-101 [**102**], MOF-177 [**38**], MOF-210 [**38**] and AX-21 activated carbon [**100**] due to lower pore volume of M/DOBDC frameworks. In contrast to CO_2 and CO, virial domain plot of CH_4 do not show any inflection for the experimental pressure and temperature range covered in this study. In fact, the other relatively non-polar gases (N_2, C_2H_6, C_3H_8 and Ar) also do not exhibit any inflection in their virial domain plot.

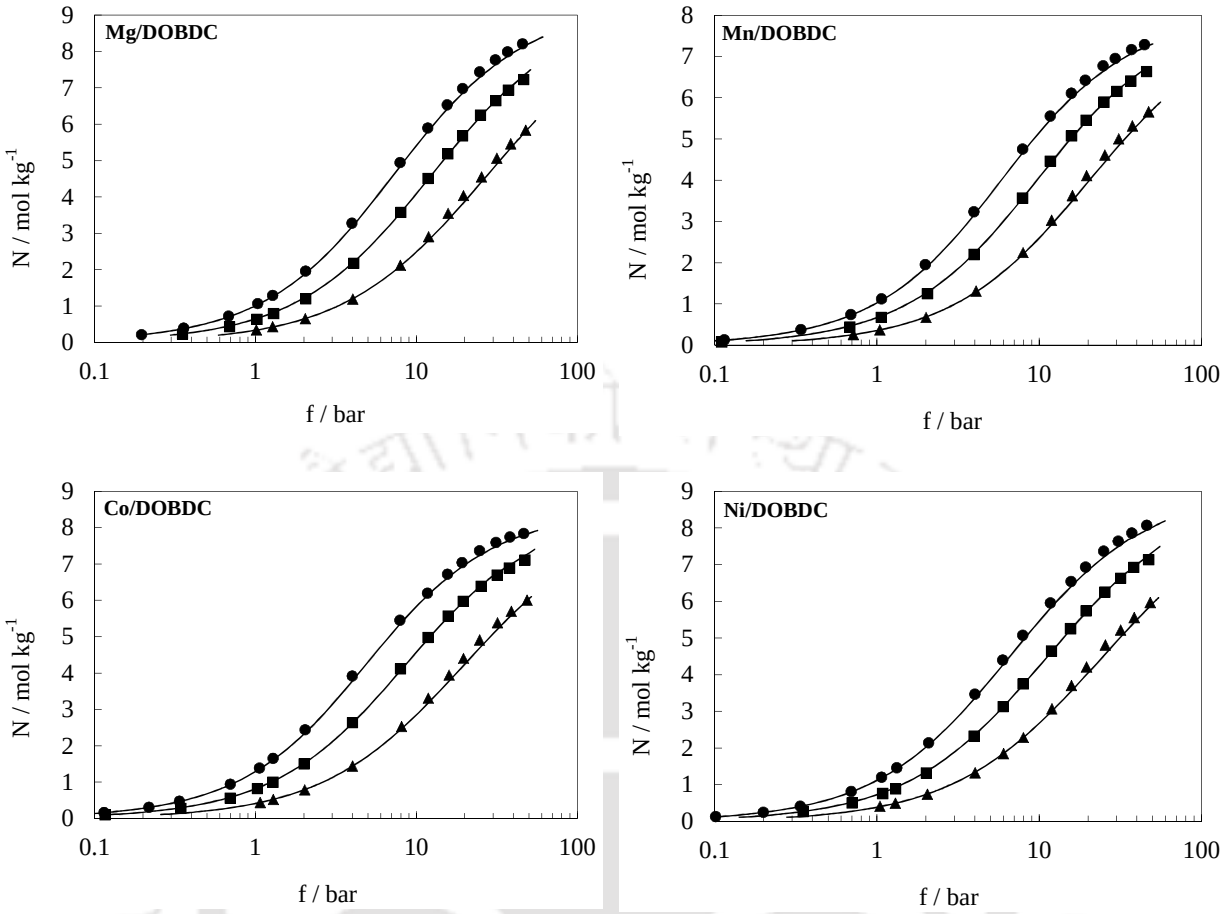

Figure 6.10: CH_4 isotherms of DOBDC MOFs. Symbols are experimental data at 294 K (●), 315 K (■) and 352 K (▲); lines are fits obtained using Langmuir-virial isotherm parameters from Table 6.6.

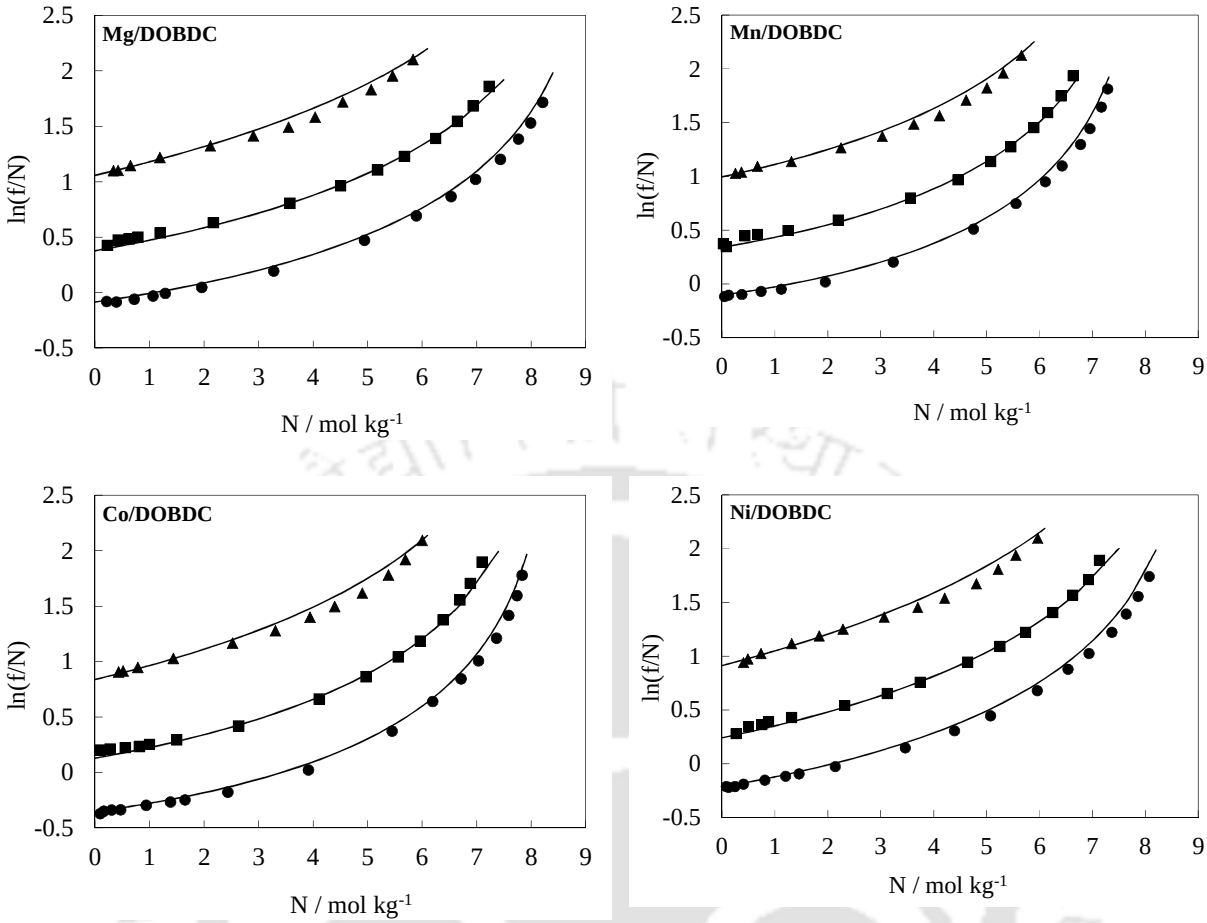

Figure 6.11: CH_4 isotherms of DOBDC MOFs in virial domain. Symbols are experimental data at 294 K (●), 315 K (■) and 352 K (▲); lines are fits obtained using Langmuir-virial isotherm parameters from Table 6.6.

6.3.4 N_2 Isotherms

The N_2 adsorption isotherms on all the four samples were measured up to ~ 100 bar (Figures 6.12 − 6.13). The uptake varied between 0.6 to 0.8 mol kg^{-1} at 294 K and 1 bar. This value is slightly higher than that on many adsorbents such as MIL-53 [**75**], MIL-47 [**37**], MOF-5 [**121**], MOF-177 [**68**], Ni/DABCO [**75**] and is comparable to CuBTC [**76, 121**]; N_2 adsorption data at higher pressure is rarely reported on MOFs.

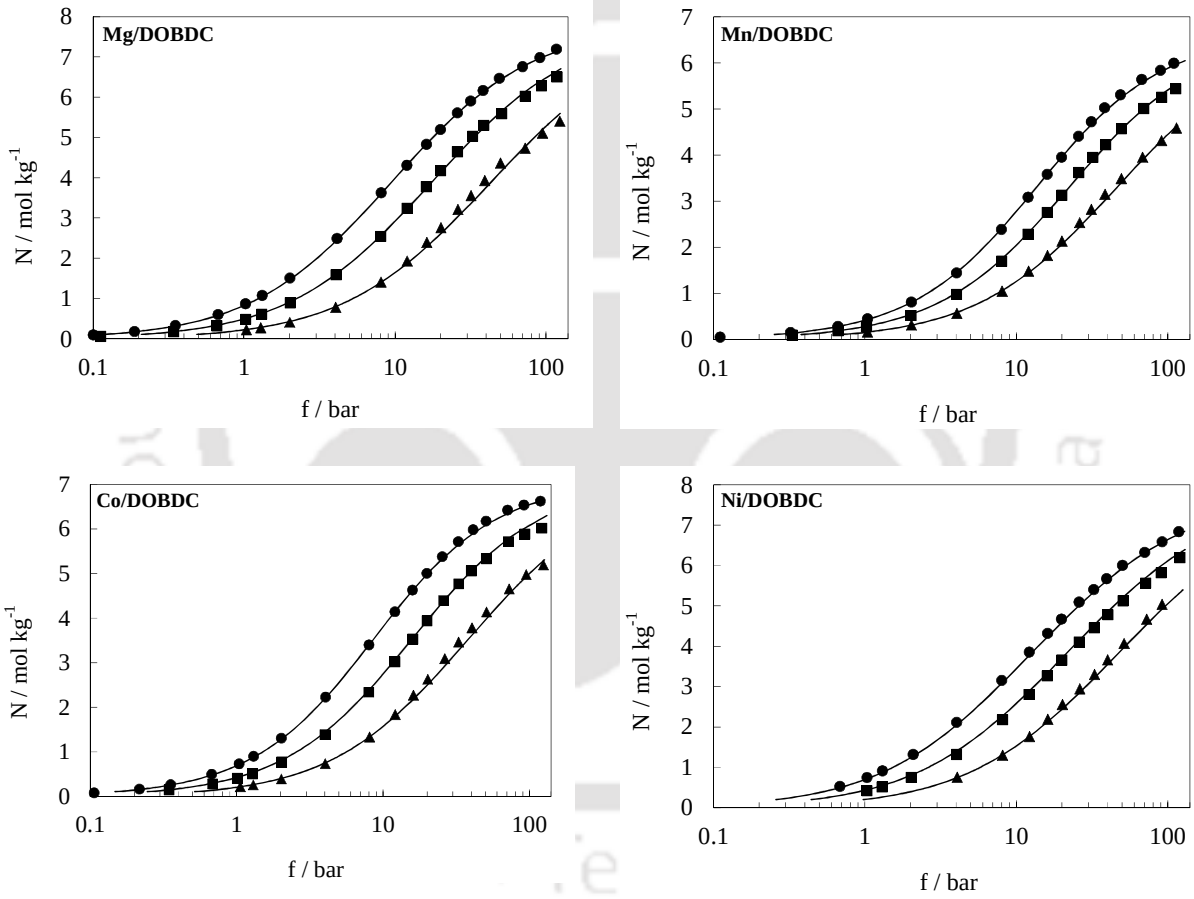

Figure 6.12: N_2 isotherms of DOBDC MOFs. Symbols are experimental data at 294 K (●), 315 K (■) and 352 K (▲); lines are fits obtained using Langmuir-virial isotherm parameters from Table 6.7.

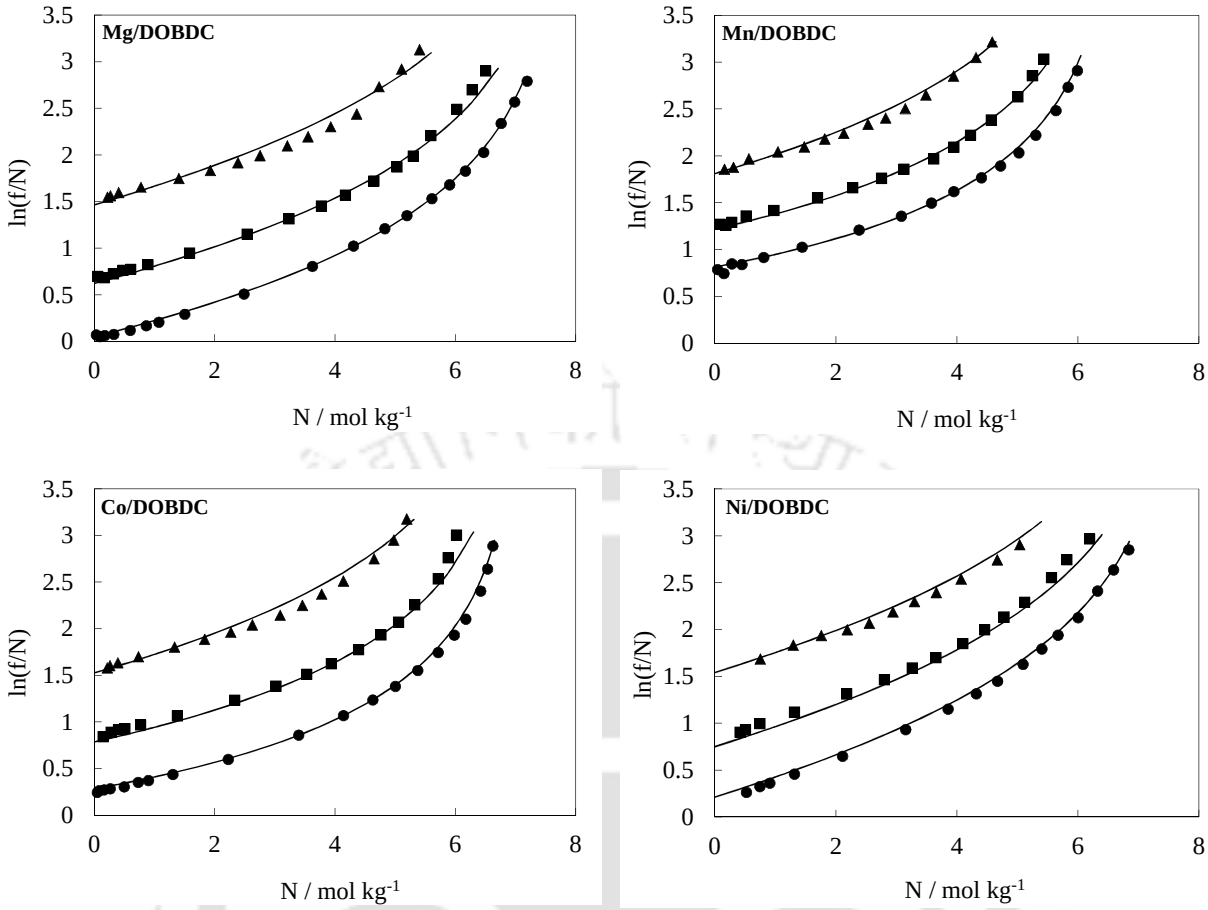

Figure 6.13: N_2 isotherms of DOBDC MOFs in virial domain. Symbols are experimental data at 294 K (●), 315 K (■) and 352 K (▲); lines are fits obtained using Langmuir-virial isotherm parameters from Table 6.7.

6.3.5 C_2H_6 Isotherms

C_2H_6 isotherms of all four M/DOBDC frameworks are shown in Figure 6.14 – 6.15. Isotherm at 294 K for Mg/DOBDC is similar to that reported by Bao et al. [**132**]. Adsorption loading at 294 K and 1 bar on M/DOBDC frameworks (~ 6 mol kg^{-1}) is comparable to that on Fe/DOBDC [**133**]; however, it is higher than that on Cu-BTC [**126**], MOF-5 [**130**], MIL-101 [**131**], Zeolite 13X [**134**] and silicalite [**99**]. As in case of CO_2, adsorption uptake at higher pressure on M/DOBDC frameworks (~ 8 mol kg^{-1} at 8.5 bar and 294 K) is lower than that on MIL-101(~ 15.5 mol kg^{-1} at 8.5 bar and 298 K) [**131**] due to lower pore volume of M/DOBDC frameworks.

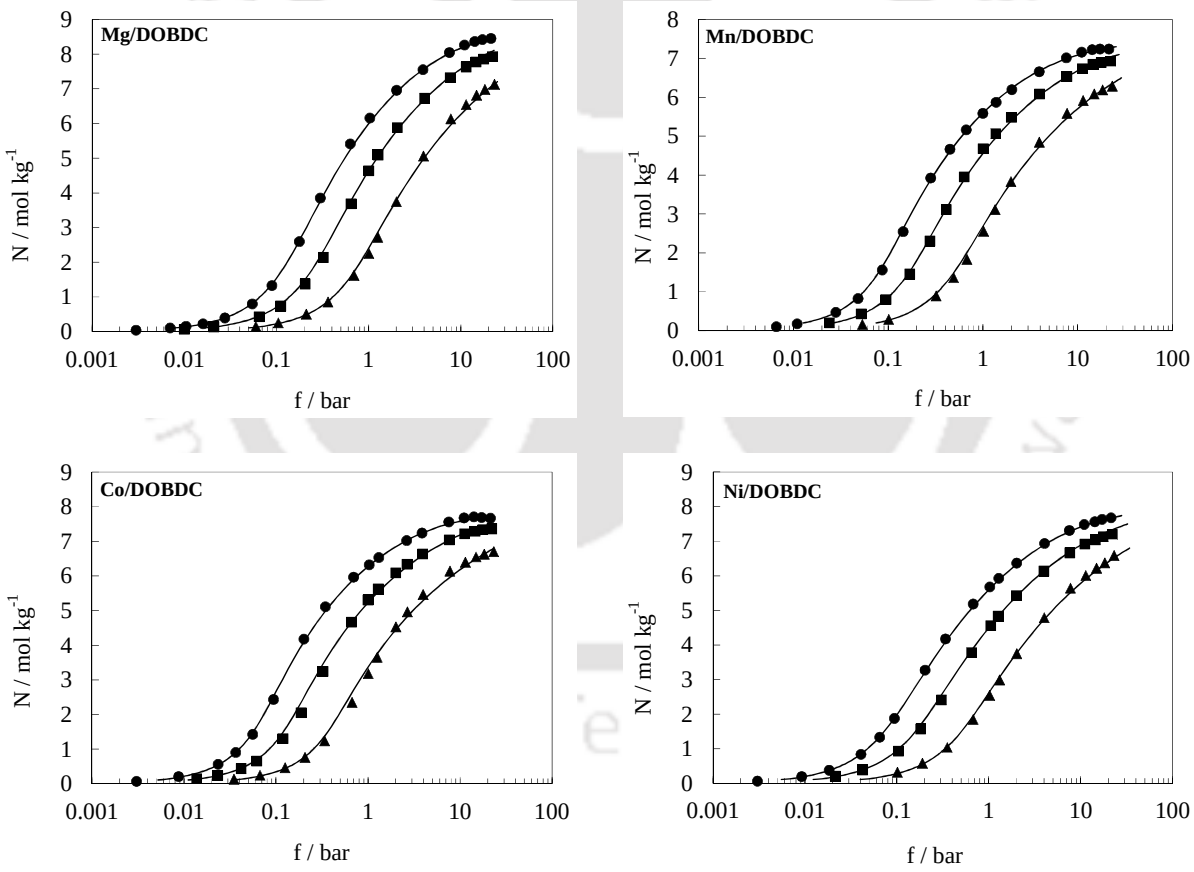

Figure 6.14: C_2H_6 isotherms of DOBDC MOFs. Symbols are experimental data at 294 K (●), 315 K (■) and 352 K (▲); lines are fits obtained using Langmuir-virial isotherm parameters from Table 6.8.

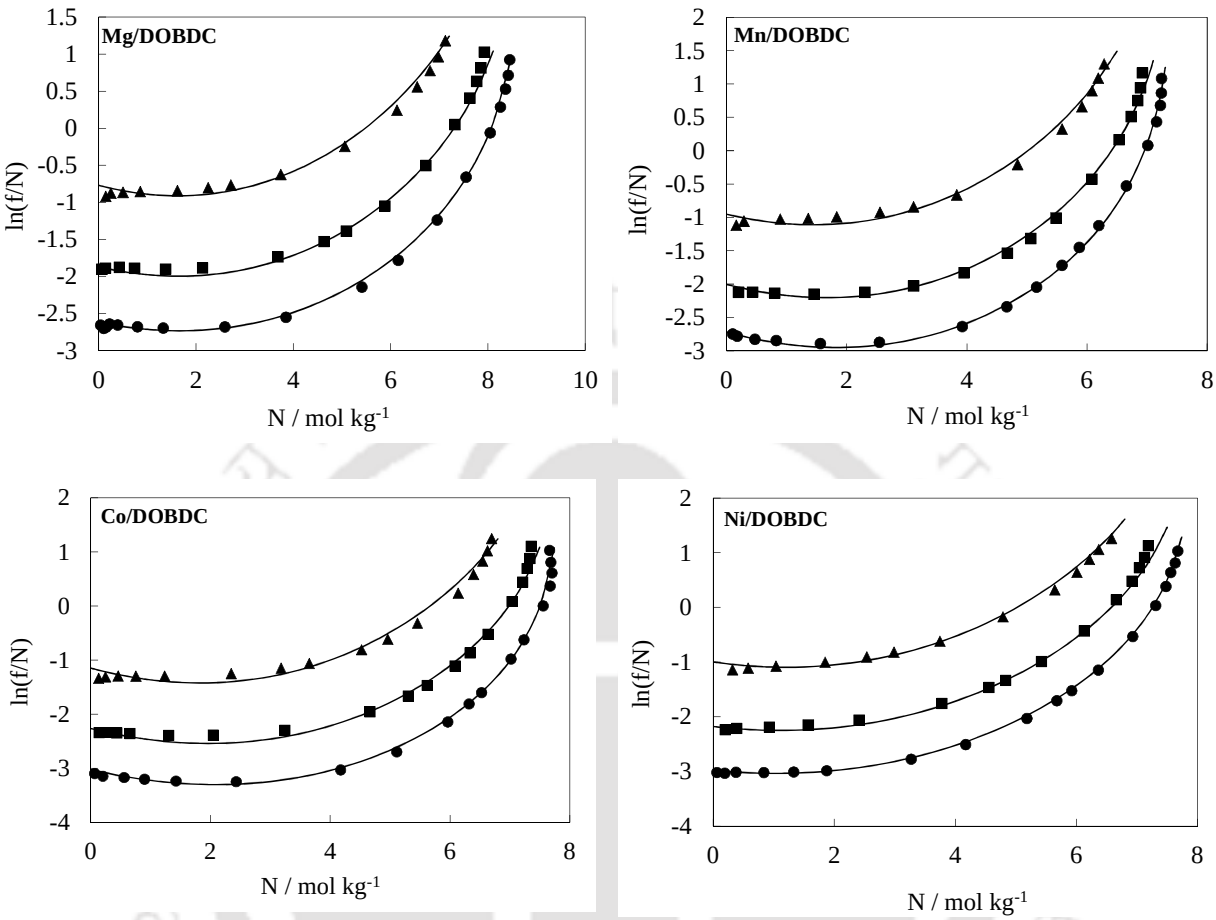

Figure 6.15: C_2H_6 isotherms of DOBDC MOFs in virial domain. Symbols are experimental data at 294 K (●), 315 K (■) and 352 K (▲); lines are fits obtained using Langmuir-virial isotherm parameters from Table 6.8.

6.3.6 C_3H_8 Isotherms

C_3H_8 isotherms obtained for all four M/DOBDC frameworks are shown in Figure 6.16 – 6.17. The isotherms obtained in this work at 294 K for M/DOBDC are similar to that reported by Bae et al. [**160**]. Adsorption loading at 294 K and 1 bar on Mg/DOBDC and Co/DOBDC frameworks (~ 6.5 mol kg^{-1}) are slightly higher than that on Fe/DOBDC [**133**]; it is also higher than that on Cu-BTC [**136**], MIL-53(Cr) [**138**], Zeolite NaX [**139**] and silicalite [**99**]. C_3H_8 isotherms are saturated at a relatively lower pressure due to its high polarizability.

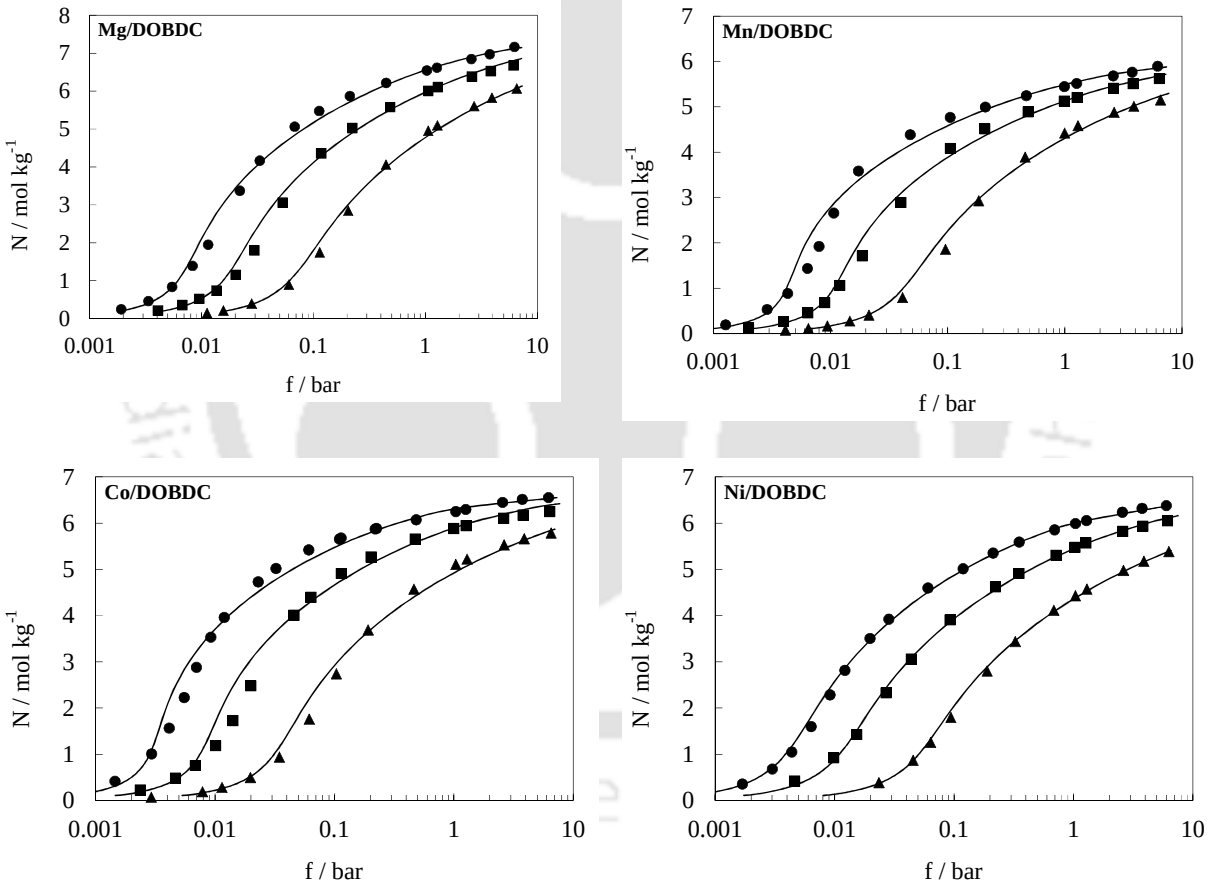

Figure 6.16: C_3H_8 isotherms of DOBDC MOFs. Symbols are experimental data at 294 K (●), 315 K (■) and 352 K (▲); lines are fits obtained using Langmuir-virial isotherm parameters from Table 6.9.

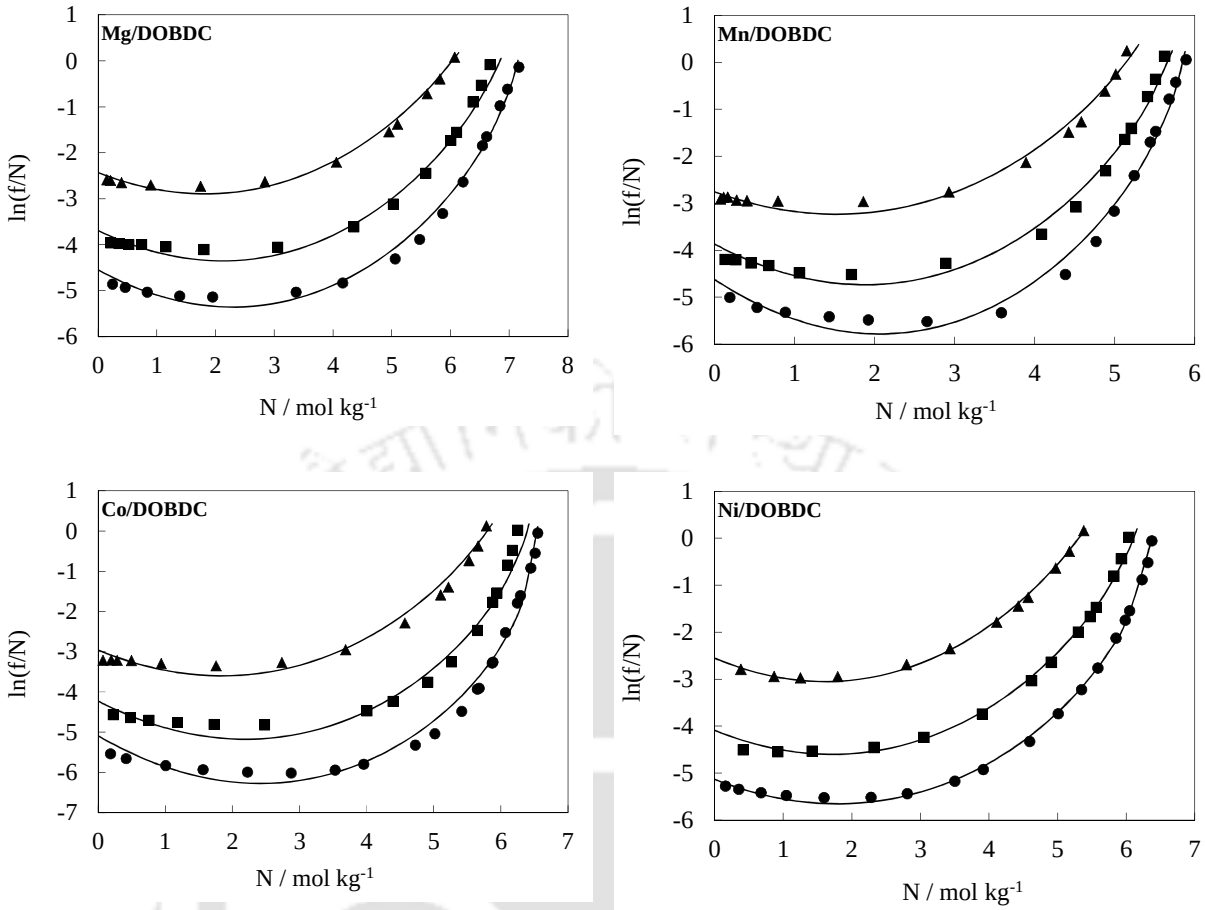

Figure 6.17: C_3H_8 isotherms of DOBDC MOFs in virial domain. Symbols are experimental data at 294 K (●), 315 K (■) and 352 K (▲); lines are fits obtained using Langmuir-virial isotherm parameters from Table 6.9.

6.3.7 Ar Isotherms

Ar isotherms for all four M/DOBDC frameworks are shown in Figure 6.18 – 6.19. The adsorption uptake at 294 K and ~ 100 bar on M/DOBDC frameworks is ~ 7 mol kg^{-1}; this value is significantly higher than that on Zeolite 13X (2.5 mol kg^{-1}) [**127**]. Ar isotherms do not saturate even at 100 bar due to its low polarizability.

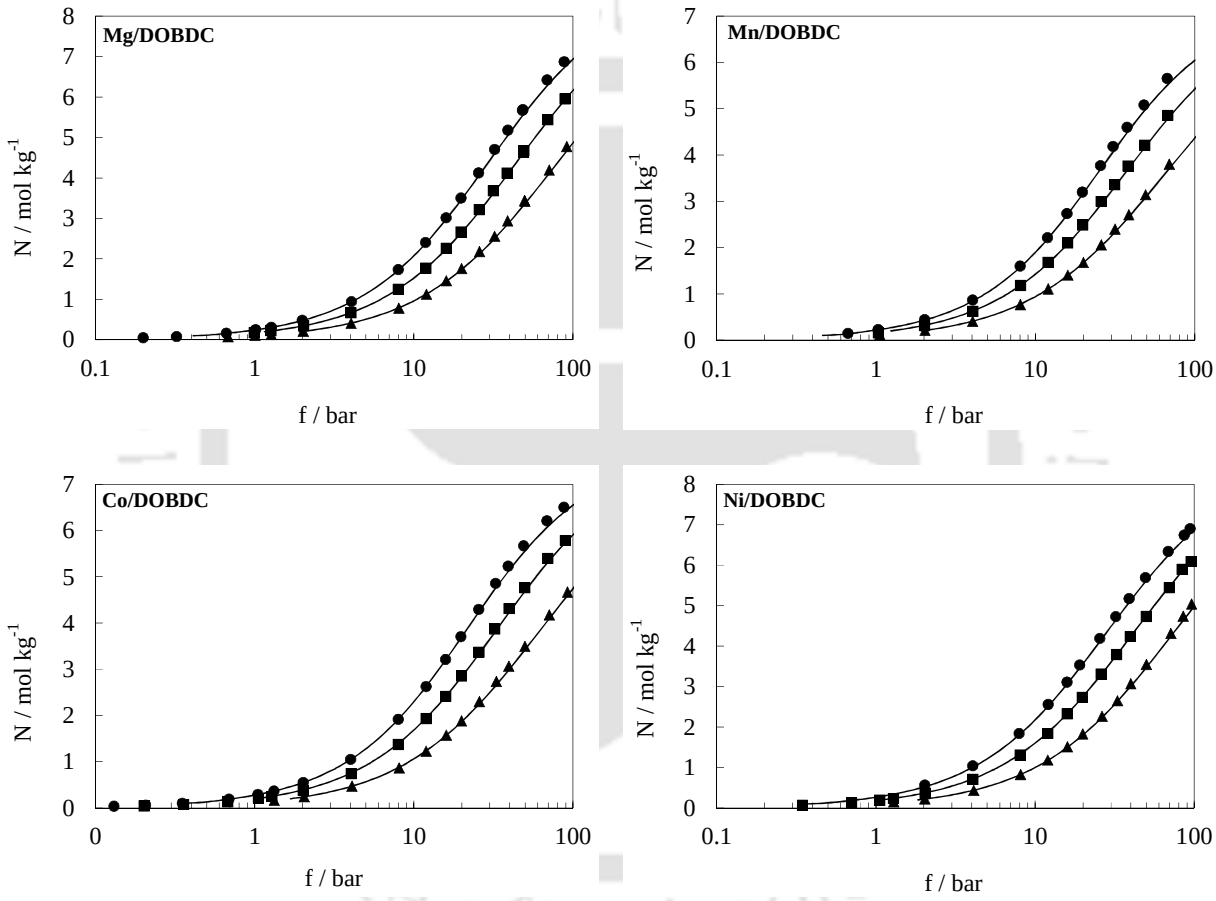

Figure 6.18: Ar isotherms of DOBDC MOFs. Symbols are experimental data at 294 K (●), 315 K (■) and 352 K (▲); lines are fits obtained using Langmuir-virial isotherm parameters from Table 6.10.

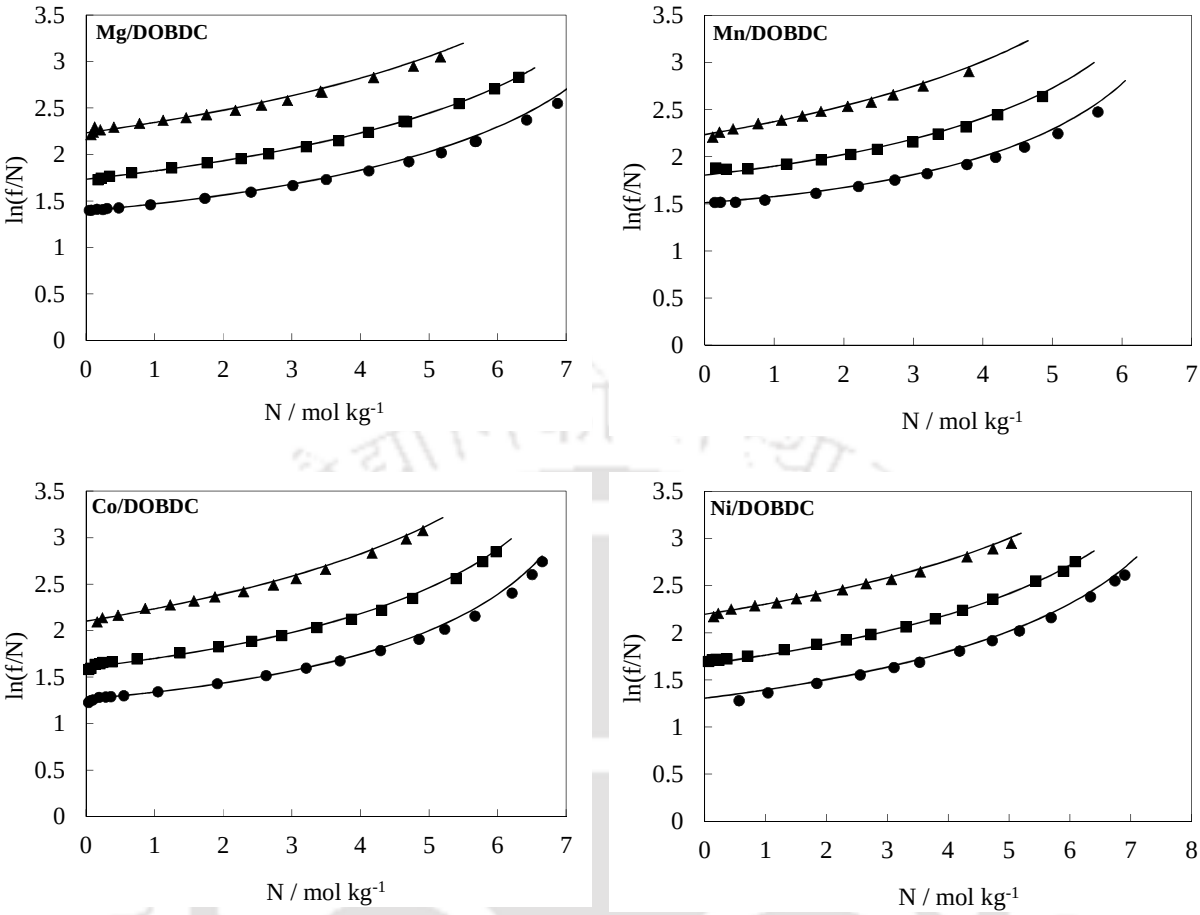

Figure 6.19: Ar isotherms of DOBDC MOFs in virial domain. Symbols are experimental data at 294 K (●), 315 K (■) and 352 K (▲); lines are fits obtained using Langmuir-virial isotherm parameters from Table 6.10.

6.4 Isotherm Modeling

In order to model the excess adsorption isotherms of various gases on M/DOBDC compounds attempts were made to fit the experimental data using several models. A Langmuir equation could not describe the adsorption behavior of M/DOBDC compounds due to the heterogeneity of the adsorbent surface. As in case of adsorption on other MOFs with *cus* metal centers [**68**], the isotherms for polar gases (CO_2 and CO in this case) on the four M/DOBDC frameworks considered in this work were well described by a dual site Langmuir (DSL) model (Eq. 3.8) with good statistical significance. Other sites with different energies may also exist but they are lumped into either of these two sites because they are energetically very close to one of these two sites [**74**]. For other relatively non-polar adsorbates (CH_4, N_2, C_2H_6, C_3H_8 and Ar), DSL equation was not required and Langmuir-virial isotherm (Eq. 3.13) was sufficient to model the experimental data. The results from the fits are included in Figures 6.6 – 6.19 along with the experimental data. The model parameters are given in Tables 6.4 – 6.10.

Table 6.4: Dual site Langmuir (DSL) isotherm model parameters for CO_2 adsorption on DOBDC MOFs.

Parameters	Mg/DOBDC Coefficient *(Std. Error)*	Mn/DOBDC Coefficient *(Std. Error)*	Co/DOBDC Coefficient *(Std. Error)*	Ni/DOBDC Coefficient *(Std. Error)*
N_1^{max}, mol kg^{-1}	5.19	6.18	7.00	5.39
	(0.10)	*(0.33)*	*(0.34)*	*(0.19)*
N_2^{max}, mol kg^{-1}	9.07	6.06	5.42	7.53
	(0.10)	*(0.27)*	*(0.26)*	*(0.14)*
$\beta_1^{(0)} \times 10^5$, bar^{-1}	0.132	3.520	0.964	0.322
	(0.052)	*(0.875)*	*(0.291)*	*(0.095)*
$\beta_1^{(1)}$, K	5142.6	3436.8	3901.3	4477.6
	(126.6)	*(76.9)*	*(96.9)*	*(95.6)*
$\beta_2^{(0)} \times 10^5$, bar^{-1}	0.239	0.323	0.248	0.805
	(0.050)	*(0.088)*	*(0.095)*	*(0.162)*
$\beta_2^{(1)}$, K	3508.2	3385.6	3424.8	3163.0
	(69.5)	*(89.3)*	*(131.6)*	*(71.2)*

.

Table 6.5: Dual site Langmuir (DSL) isotherm model parameters for CO adsorption on DOBDC MOFs.

Parameters	Mg/DOBDC Coefficient *(Std. Error)*	Mn/DOBDC Coefficient *(Std. Error)*	Co/DOBDC Coefficient *(Std. Error)*	Ni/DOBDC Coefficient *(Std. Error)*
N_1^{max}, mol kg^{-1}	4.68	5.13	5.70	5.08
	(0.10)	*(0.16)*	*(0.03)*	*(0.09)*
N_2^{max}, mol kg^{-1}	4.17	2.74	2.61	4.25
	(0.10)	*(0.11)*	*(0.06)*	*(0.14)*
$\beta_1^{(0)} \times 10^5$, bar^{-1}	0.169	1.431	0.029	0.019
	(0.032)	*(0.268)*	*(0.006)*	*(0.013)*
$\beta_1^{(1)}$, K	4167.6	3247.5	5611.5	5932.0
	(63.2)	*(60.5)*	*(62.2)*	*(224.2)*
$\beta_2^{(0)} \times 10^5$, bar^{-1}	2.502	0.987	1.108	0.116
	(0.434)	*(0.322)*	*(0.039)*	*(0.079)*
$\beta_2^{(1)}$, K	2253.7	2447.4	2581.5	3453.2
	(59.3)	*(106.5)*	*(116.4)*	*(226.8)*

Table 6.6: Langmuir-virial isotherm model parameters for CH_4 adsorption on DOBDC MOFs.

Parameters	Mg/DOBDC Coefficient *(Std. Error)*	Mn/DOBDC Coefficient *(Std. Error)*	Co/DOBDC Coefficient *(Std. Error)*	Ni/DOBDC Coefficient *(Std. Error)*
$\beta^{(0)}\times10^3$, mol kg^{-1} bar^{-1}	1.06	5.13	1.02	1.32
	(0.03)	*(0.04)*	*(0.03)*	*(0.03)*
$\beta^{(1)}$, K	2039.2	1962.2	2127.2	2010.8
	(53.4)	*(56.2)*	*(67.3)*	*(53.3)*
$b^{(0)}$, mol^{-1} kg	0.229	0.176	0.259	0.241
	(0.015)	*(0.049)*	*(0.056)*	*(0.046)*
$b^{(1)}$, mol^{-1} kg K	-78.0	-68.2	-91.1	-78.3
	(14.7)	*(15.8)*	*(18.0)*	*(14.7)*
N^{max}, mol kg^{-1}	9.33	8.07	8.52	9.10
	(0.09)	*(0.06)*	*(0.05)*	*(0.08)*

Table 6.7: Langmuir-virial isotherm model parameters for N_2 adsorption on DOBDC MOFs.

Parameters	Mg/DOBDC Coefficient *(Std. Error)*	Mn/DOBDC Coefficient *(Std. Error)*	Co/DOBDC Coefficient *(Std. Error)*	Ni/DOBDC Coefficient *(Std. Error)*
$\beta^{(0)}\times10^3$, mol kg^{-1} bar^{-1}	0.18	1.05	0.40	0.25
	(0.00)	*(0.03)*	*(0.01)*	*(0.01)*
$\beta^{(1)}$, K	2524.2	1776.9	2218.5	2371.0
	(67.4)	*(51.6)*	*(77.9)*	*(104.8)*
$b^{(0)}$, mol^{-1} kg	0.199	0.393	0.405	0.066
	(0.064)	*(0.057)*	*(0.077)*	*(0.097)*
$b^{(1)}$, mol^{-1} kg K	-47.4	-124.3	-126.3	2.5
	(20.2)	*(18.1)*	*(24.7)*	*(30.7)*
N^{max}, mol kg^{-1}	7.79	6.66	7.08	7.70
	(0.05)	*(0.04)*	*(0.04)*	*(0.09)*

Table 6.8: Langmuir-virial isotherm model parameters for C_2H_6 adsorption on DOBDC MOFs.

Parameters	Mg/DOBDC Coefficient *(Std. Error)*	Mn/DOBDC Coefficient *(Std. Error)*	Co/DOBDC Coefficient *(Std. Error)*	Ni/DOBDC Coefficient *(Std. Error)*
$\beta^{(0)}\times 10^3$, mol kg^{-1} bar^{-1}	0.184	0.335	0.235	0.117
	(0.008)	*(0.020)*	*(0.018)*	*(0.006)*
$\beta^{(1)}$, K	3298.2	3152.0	3345.2	3538.4
	(115.3)	*(149.1)*	*(207.7)*	*(143.9)*
$b^{(0)}$, mol^{-1} kg	-0.472	-0.189	-0.608	-0.557
	(0.295)	*(0.377)*	*(0.511)*	*(0.341)*
$b^{(1)}$, mol^{-1} kg K	65.1	-56.7	64.0	95.7
	(93.3)	*(119.8)*	*(164.2)*	*(107.6)*
$c^{(0)}$, mol^{-2} kg^2	0.109	0.102	0.170	0.128
	(0.039)	*(0.055)*	*(0.071)*	*(0.047)*
$c^{(1)}$, mol^{-2} kg^2 K	-22.4	-13.5	-34.6	-25.1
	(12.4)	*(17.6)*	*(22.8)*	*(15.0)*
N^{max}, mol kg^{-1}	8.79	7.47	7.88	7.98
	(0.05)	*(0.03)*	*(0.03)*	*(0.05)*

Table 6.9: Langmuir-virial isotherm model parameters for C_3H_8 adsorption on DOBDC MOFs.

Parameters	Mg/DOBDC Coefficient *(Std. Error)*	Mn/DOBDC Coefficient *(Std. Error)*	Co/DOBDC Coefficient *(Std. Error)*	Ni/DOBDC Coefficient *(Std. Error)*
$\beta^{(0)}\times10^3$, mol kg^{-1} bar^{-1}	0.247	1.240	0.390	0.027
	(0.025)	*(0.174)*	*(0.061)*	*(0.001)*
$\beta^{(1)}$, K	3778.3	3326.3	3804.3	4604.8
	(269.6)	*(306.9)*	*(397.5)*	*(173.4)*
$b^{(0)}$, mol^{-1} kg	0. 331	1.724	0.573	-0. 979
	(0.725)	*(1.012)*	*(1.078)*	*(0.451)*
$b^{(1)}$, mol^{-1} kg K	- 341.8	- 882.7	-496.9	73.6
	(230.5	*(323.5)*	*(341.4)*	*(140.6)*
$c^{(0)}$, mol^{-2} kg^2	0. 066	-0.145	0. 113	0.334
	(0.110)	*(0.183)*	*(0.171)*	*(0.073)*
$c^{(1)}$, mol^{-2} kg^2 K	21.3	115.8	20.4	-55.8
	(35.0)	*(58.3)*	*(53.8)*	*(22.7)*
N^{max}, mol kg^{-1}	7.39	6.02	6.61	6.51
	(0.06)	*(0.04)*	*(0.02)*	*(0.02)*

Table 6.10: Langmuir-virial isotherm model parameters for Ar adsorption on DOBDC MOFs.

Parameters	Mg/DOBDC Coefficient *(Std. Error)*	Mn/DOBDC Coefficient *(Std. Error)*	Co/DOBDC Coefficient *(Std. Error)*	Ni/DOBDC Coefficient *(Std. Error)*
$\beta^{(0)}\times10^3$, mol kg^{-1} bar^{-1}	1.53	2.74	1.76	1.22
	(0.01)	*(0.03)*	*(0.02)*	*(0.02)*
$\beta^{(1)}$, K	1495.2	1290.2	1492.6	1587.9
	(18.0)	*(23.9)*	*(20.3)*	*(35.2)*
$b^{(0)}$, mol^{-1} kg	0.183	0.353	0.301	0.082
	(0.019)	*(0.033)*	*(0.022)*	*(0.033)*
$b^{(1)}$, mol^{-1} kg K	-67.6	-127.8	-107.9	-34.3
	(6.3)	*(10.7)*	*(7.2)*	*(11.2)*
N^{max}, mol kg^{-1}	8.87	7.41	7.82	8.72
	(0.06)	*(0.10)*	*(0.04)*	*(0.11)*

The saturation uptakes (from the model parameter N^{max}) of all gases of different frameworks are plotted against unit cell pore volume of the frameworks in Figure 6.20. Two interesting observations can be made. First, the saturation uptake on all frameworks is the highest for CO_2 (which has the smallest kinetic diameter) and is the lowest for C_3H_8 (which has the largest kinetic diameter). Second, the saturation uptake of a given gas increases with the increase of pore volume of the framework. For all gases, the saturation uptake is highest on Ni/DOBDC followed by Co/DOBDC, Mn/DOBDC and Mg/DOBDC in that order. C_3H_8 slightly deviates from this order with a slightly higher saturation loading (~ 2.7 %) for Co/DOBDC compared to that of Ni/DOBDC.

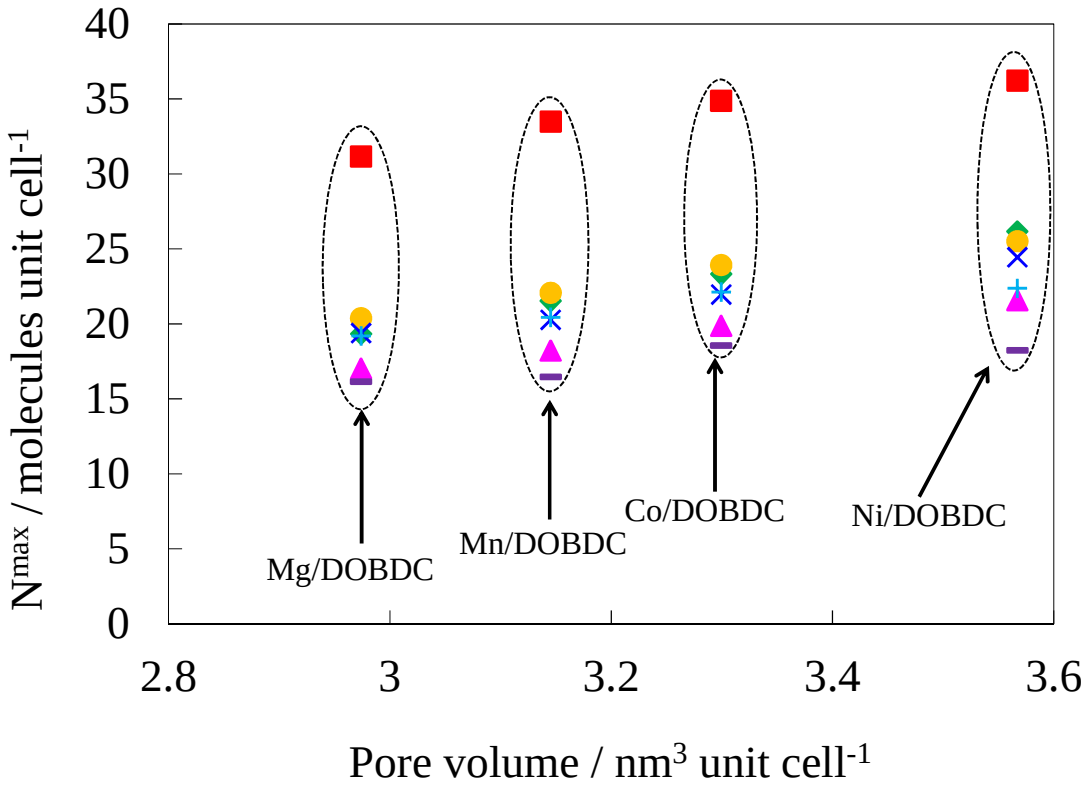

Figure 6.20: Variation of saturation uptake of CO_2 (■), CO (♦), CH_4 (●), N_2 (▲), Ar (×), C_2H_6 (+) and C_3H_8 (–) with pore volume for DOBDC MOFs.

6.5 Effect of Physical Properties of the Adsorbate

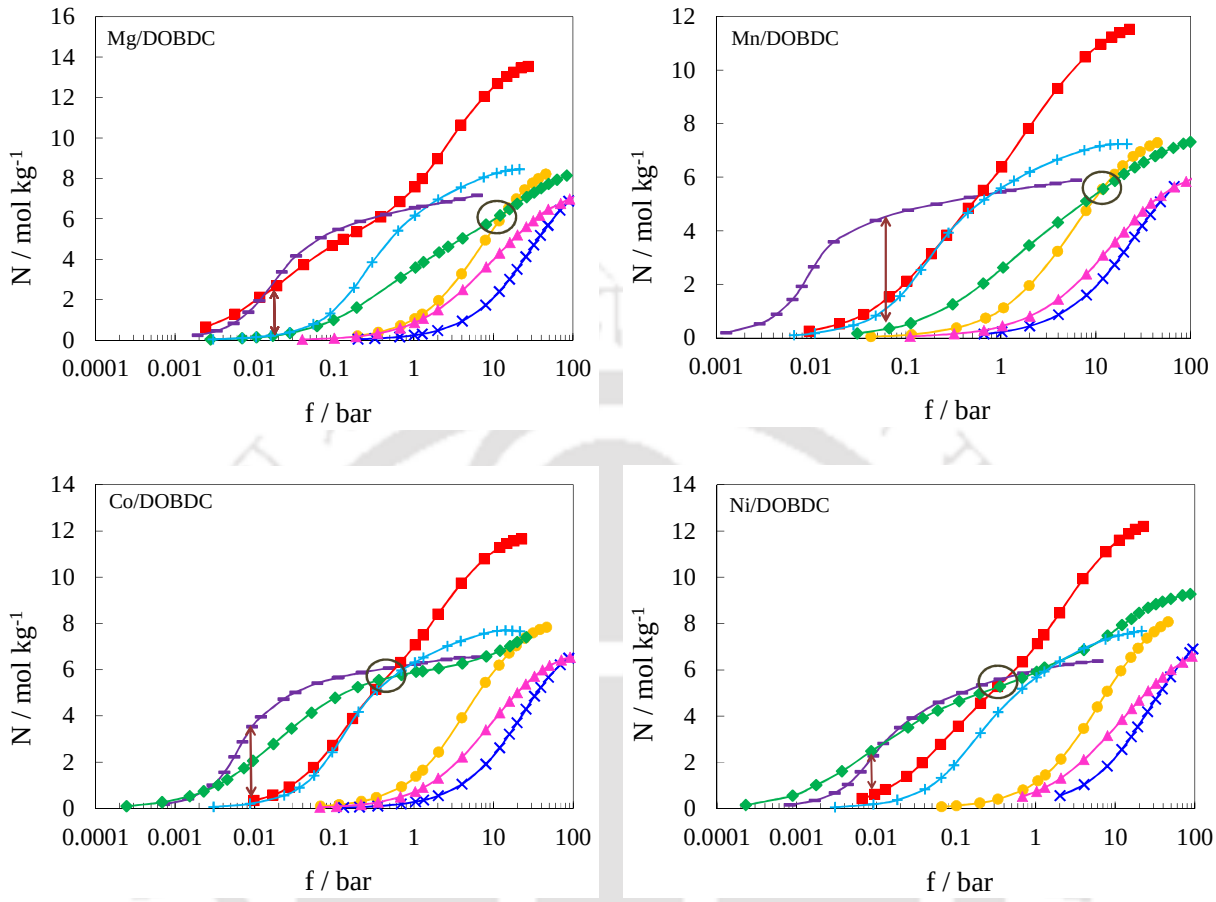

Figure 6.21: Adsorption isotherms of CO_2 (■), CO (♦), CH_4 (●), N_2 (▲), Ar (×), C_2H_6 (+) and C_3H_8 (–) at 294 K on DOBDC MOFs; lines are drawn as a guide to the eye.

The excess adsorption isotherms of CO_2, CO, CH_4, N_2, Ar, C_2H_6 and C_3H_8 on M/DOBDC frameworks at 294 K are shown in Figure 6.21. For all the samples, adsorption capacity of C_3H_8 is higher than that of CH_4, N_2, Ar and C_2H_6 at low pressure, due to its polarizability and slight quadrupole moment (Table 4.6). However, in case of Mg/DOBDC, adsorption uptakes of CO_2 at lower pressure are similar to that of C_3H_8 discounting the 2.4 fold difference between their polarizability values. This indicates strong electrostatic interactions between CO_2 molecules and Mg/DOBDC framework. Similarly in case of Co/DOBDC and Ni/DOBDC, low pressure CO

isotherms are comparable to C_3H_8 even though there is ~ 4 fold difference between the polarizability of these gases. The reasons behind this exceptional uptake for CO_2 on Mg/DOBDC and CO on Co/DOBDC and Ni/DOBDC will be discussed later. On the other hand, low pressure uptake of C_3H_8 is significantly higher than that of CO_2 or CO on Mn/DOBDC. This indicates that the strength of electrostatic interactions between CO_2 (or CO) and Mn/DOBDC framework are weaker than those on other frameworks. Carbon monoxide which has a dipole moment exhibits high loading initially (in the low pressure region) compared to that of CH_4 due to strong electrostatic interactions between polar CO molecules and *cus* metal centers of DOBDC frameworks. However, once these unsaturated metal centers are occupied by the adsorbate molecules, dispersion interactions dominate, resulting in preferential adsorption of CH_4 (which has higher polarizability) over CO. Although, C_2H_6 is relatively non-polar, its adsorption capacity on Mg/DOBDC and Mn/DOBDC is higher than that on CO, due to its significantly high polarizability. The lowest adsorption capacity of Ar on all samples can be readily attributed to its low polarizability and non-polar nature. Isotherms of all adsorbates (except Ar) on M/DOBDC frameworks saturate within the experimental pressure range, in contrast to isotherms of these gases on a large pore size MOF like MIL-101[**95**]. This difference in adsorption characteristics of M/DOBDC and MIL-101 MOF in the high pressure region is a result of better affinity (due to *cus* metal centers) and smaller pore volume of M/DOBDC. Saturation loading of CO_2 (12.2 − 14.2 mol kg^{-1}) is significantly higher than that of the other gases due to its smaller kinetic diameter. However, when compared to other adsorbents with large pore volumes such as MIL-101 [**95**], CuBTC [**95**], IRMOF-1 [**62**], IRMOF-3 [**62**], UMCM-1 [**215**] and MOF-177 [**62**], the gravimetric saturation loading for CO_2 on M/DOBDC frameworks is significantly lower.

6.5.1 On Henry's Constants and Adsorption Enthalpy

The Henry's constant (β) at 294 K and the adsorption enthalpy at zero coverage ($-\Delta h_{ads,0}$) of gases studied on M/DOBDC MOFs are shown in Figures 6.22 – 6.25. Both these quantities were obtained from the isotherm model parameters (Tables 6.4 – 6.10). These plots help in understanding the effect of polarity and polarizability on the adsorbate-adsorbent interactions. Both β and $-\Delta h_{ads,0}$, vary almost linearly with polarizability for relatively non-polar Ar, CH_4, C_2H_6 and C_3H_8 gases; this behavior is similar to that for silicalite [**99**], and MIL-101 [**74**]. However, for polar gases (CO_2, CO, N_2), higher values of β and $-\Delta h_{ads,0}$ are observed, highlighting the role of electrostatic interactions on the adsorption for these gases. The deviation from the trend for polar gases is larger in case of M/DOBDC frameworks than that for MIL-101 [**95**], indicating that the electrostatic interactions between polar gases and the *cus* metal sites is more pronounced in M/DOBDC frameworks.

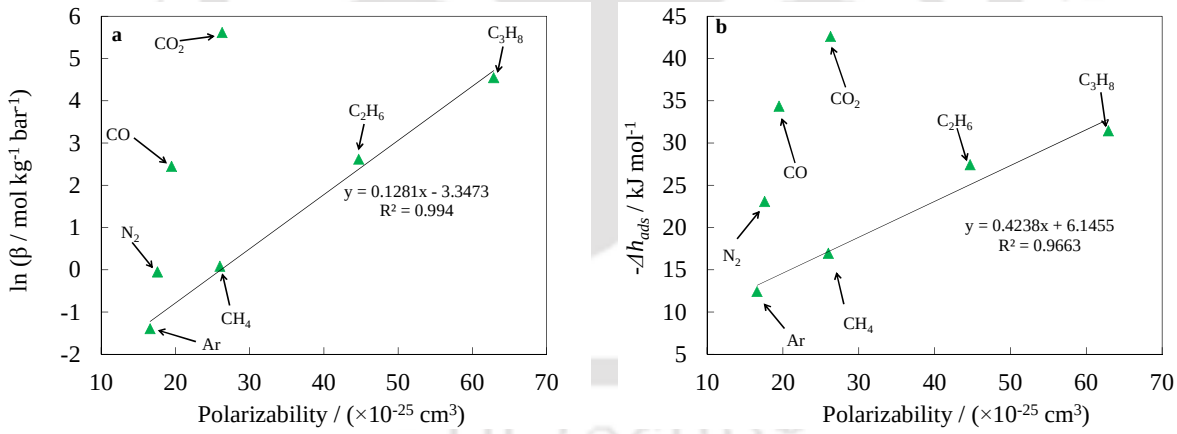

Figure 6.22: Variation of (**a**) Henry's constant at 294 K and (**b**) enthalpy of adsorption at zero occupancy with polarizability of the adsorbate for Mg/DOBDC adsorbent; linear trend lines for non-polar adsorbates are also shown.

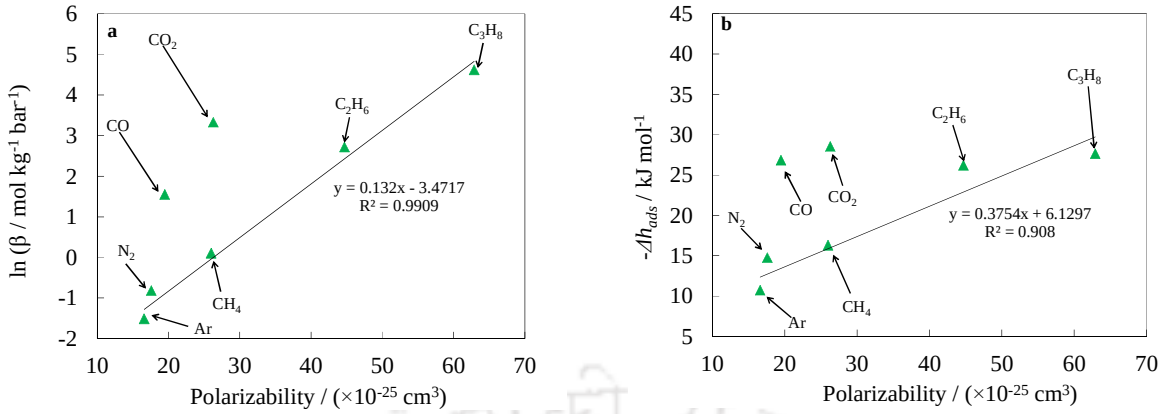

Figure 6.23: Variation of (**a**) Henry's constant at 294 K and (**b**) enthalpy of adsorption at zero occupancy with polarizability of the adsorbate for Mn/DOBDC adsorbent; linear trend lines for non-polar adsorbates are also shown.

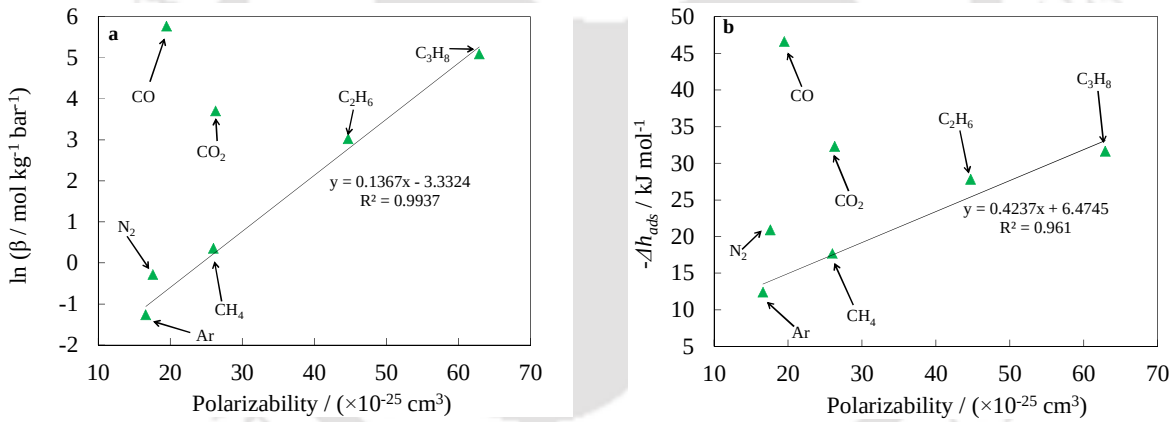

Figure 6.24: Variation of (**a**) Henry's constant at 294 K and (**b**) enthalpy of adsorption at zero occupancy with polarizability of the adsorbate for Co/DOBDC adsorbent; linear trend lines for non-polar adsorbates are also shown.

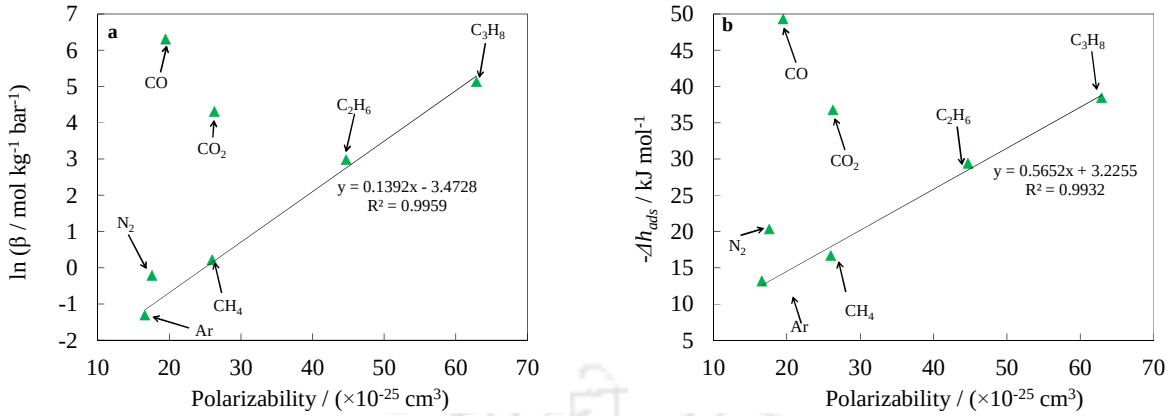

Figure 6.25: Variation of (**a**) Henry's constant at 294 K and (**b**) enthalpy of adsorption at zero occupancy with polarizability of the adsorbate for Ni/DOBDC adsorbent; linear trend lines for non-polar adsorbates are also shown.

Henry's constant for CO_2 at 294 K on the Mg/DOBDC MOF is higher than that on most of the other adsorbents such as CuBTC [**76, 216**], MIL-53(Al) [**42**], MIL-101 [**74, 94**], IRMOF-1, IRMOF-3 [**93**], MOF-177, silicalite [**99**], NaX [**139**], H-mordenite [**217**] and ZIF-8 [**37**]. However, Henry's constant for CH_4 at 294 K on M/DOBDC compounds is comparable to that on MOFs such as CuBTC [**216**] and MIL-101 [**74, 94**]. In addition, to the best of our knowledge, the Henry's constant obtained for CO on Ni/DOBDC sample is the highest reported so far (547.2 mol kg^{-1} bar^{-1} at 294 K). The reasons for such behavior are discussed in the next section. Similarly, Henry's constant for N_2 on DOBDC sample is also higher than most of the other solid adsorbents; however, the difference between Henry's constant of DOBDC MOFs and other adsorbents for N_2 is not as pronounced as that for polar gases such as CO_2 or CO.

Enthalpy of adsorption at zero loading ($-\Delta h_{ads,0}$) of CO_2 on the studied M/DOBDC frameworks (~28 – 42 kJ mol^{-1}) are higher than that on MOF-177 (~15 kJ mol^{-1}) [**68**]. $-\Delta h_{ads,0}$ of CO_2 on Mg/DOBDC (~42 kJ mol^{-1}) obtained in this work is similar to that reported in earlier literature [**68**]. It is also interesting to note that enthalpy of adsorption at zero coverage ($-\Delta h_{ads,0}$) for CO_2

on Mn/DOBDC (28 kJ mol^{-1}) is considerably lower than that on isostructural Mg/DOBDC (42 kJ mol^{-1}) indicating smaller energy penalty for regeneration, but at the same time loading is also significantly lower (2.6 mol kg^{-1} on Mn/DOBDC as opposed to 4.95 mol kg^{-1} on Mg/DOBDC at 0.15 bar and 294 K). On the other hand, at about the same conditions, a saturated metal site containing MOF like Ni/DABCO has a loading of 0.28 mol kg^{-1} and enthalpy of ~20 kJ mol^{-1}. Enthalpy of adsorption at zero coverage ($-\Delta h_{ads,0}$) of CO on Ni/DOBDC (~50 kJ mol^{-1}) is higher than that on most of the other MOFs such as MIL-101 (~45 kJ mol^{-1}) [**95**] and CuBTC (~24 kJ mol^{-1}) [**95**] . In case of CH_4 N_2, Ar, C_2H_6 and C_3H_8 adsorption on M/DOBDC samples, $-\Delta h_{ads,0}$ is comparable to that on MIL-101 [**95**], CuBTC [**95**].

Variation of Henry's constant with temperature is shown in Figure 6.26. As already mentioned, Henry's constant for CO_2 is larger on Mg/DOBDC at all the temperatures. Ni/DOBDC and Mn/DOBDC exhibit the highest Henry's constants for CO and C_3H_8 respectively at all the temperatures. This comparison indicates that the electrostatic interactions are least dominant in case Mn/DOBDC and is to be expected because of larger ionic radii of Mn^{2+} (Table 6.2). In case of Co/DOBDC, Henry's constant for CO was higher on than that for C_3H_8 at 294 and 315 K. At 352 K, Henry's constant of C_3H_8 surpassed Henry's constant of CO due to decrease in the electrostatic interactions between *cus* metal site and CO molecules. For all four DOBDC adsorbent considered, Henry's constant is lowest for Ar due to its non-polarity and low polarizability at all the three temperature studied in this work. With the increase in the temperature, the decrease in Henry's constant of polar gases (CO_2 and CO) is more pronounced than that of non-polar gases (Ar, CH_4). This can easily be attributed to the reduction in the electrostatic interactions between *cus* metal centers and polar adsorbates as temperature increases.

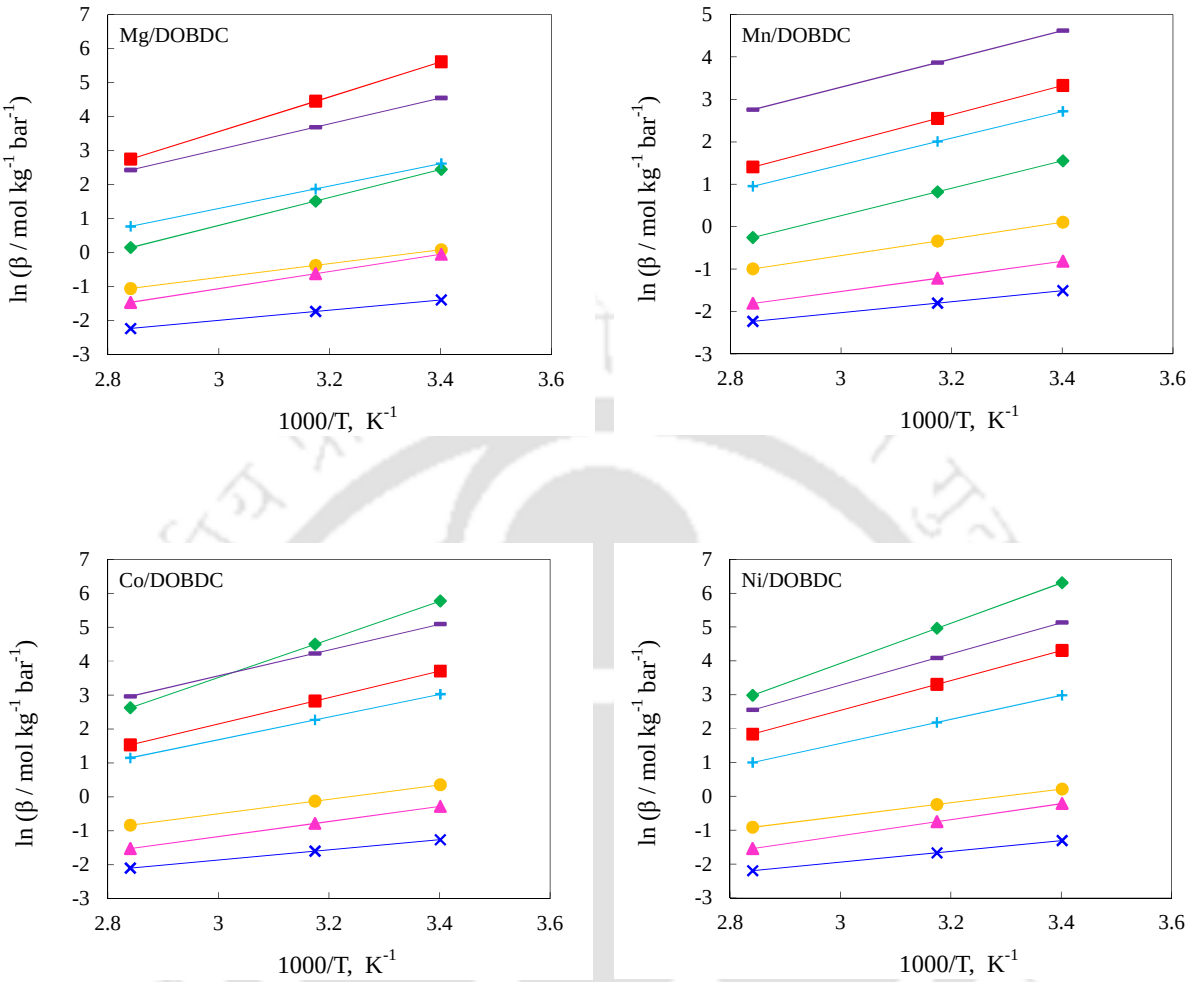

Figure 6.26: Variation of Henry's constant with temperature for CO_2 (■), CO (♦), CH_4 (●), N_2 (▲), Ar (×), C_2H_6 (+) and C_3H_8 (–) on DOBDC MOFs. Lines are drawn as a guide to the eye.

It is easier to understand the effect of *cus* site availability on adsorption properties by studying the variation in adsorption enthalpy with loading. The enthalpies of adsorption on all the four frameworks for CO_2, CO, CH_4 N_2, Ar, C_2H_6 and C_3H_8 were calculated from respective isotherm models (Table 6.4 – 6.10). The variation with loading is shown in Figure 6.27.

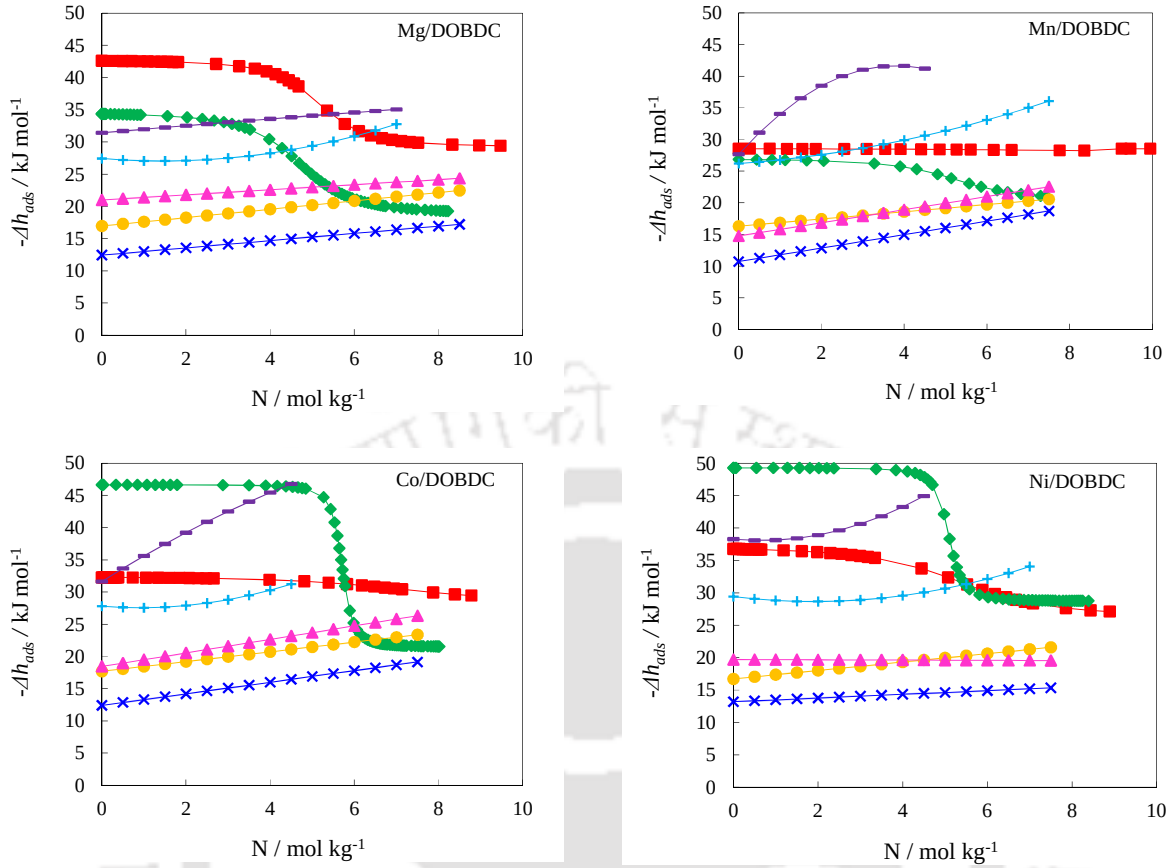

Figure 6.27: Variation of adsorption enthalpy with loading for CO_2 (■), CO (♦), CH_4 (●), N_2 (▲), Ar (×), C_2H_6 (+) and C_3H_8 (–) on DOBDC MOFs. Lines are drawn as a guide to the eye.

In case of CO_2 and CO, the adsorption enthalpy is initially high due to electrostatic interactions between *cus* metal centers and these gases. After certain loading (~18 molecules per unit cell or 1 molecule per metal atom) the adsorption enthalpy decreases sharply as the *cus* metal centers are progressively filled and attains a steady value. On other hand, with increase in loading, a slight increase in adsorption enthalpy is observed for Ar, N_2, CH_4, C_2H_6 and C_3H_8 and is attributed to the increase in lateral interactions between adsorbate molecules. It should be noticed here that the increase in adsorption enthalpy becomes more prominent as polarizability of adsorbates increases. For example, the increase in enthalpy with loading for C_3H_8 is much more pronounced than that for CH_4, N_2 or Ar.

6.6 Effect of Metal Cation in the Framework

Henry's constants, saturation adsorption uptakes and adsorption enthalpies of different DOBDC MOFs are compared for all the gases to investigate the role of metal cation on the adsorption characteristics of M/DOBDC MOFs.

6.6.1 On Henry's Constants

Henry's constant (β) is a measure of interactions between the adsorbate molecules and the solid surface. Henry's constants of all adsorbates at different temperatures for all the four frameworks studied in this work are plotted in Figures 6.28a – 6.28c. Several interesting features can be observed in these figures. First, the Henry's constant is relatively insensitive to the choice of metal atom in the framework for relatively non-polar gases like CH_4, C_2H_6, C_3H_8, N_2 and Ar at all temperatures due to negligible electrostatic interactions. Second, the Henry's constant for polar gases like CO_2 and CO is strongly dependent on the metal atom in the adsorbent framework; since the electrostatic interactions dominate in the low pressure region, differences in these electrostatic interactions of the adsorbate with different metal centers result in such a behavior. It can also be seen that the difference in Henry's constants for CO_2 (or CO) between the four DOBDC frameworks decreases as temperature increases because the electrostatic interactions become weaker with the increase of temperature and the effect of metal atom in the framework on the Henry's constant for these gases becomes less pronounced.

In general, framework containing the metal with the smallest ionic radius exhibits stronger affinity (and hence high Henry's constant) for the adsorbate molecules. However, two features merit special attention. First, as has been discussed earlier in literature [**97**], Mg/DOBDC framework exhibits superior affinity for CO_2 in the Henry's law region due to preference of the Mg^{2+} in the framework for oxygen-containing ligands. Second, in case of CO adsorption

Ni/DOBDC and Co/DOBDC frameworks exhibit significantly large values of Henry's constant for CO (surpassing that of even CO_2 and C_3H_8 on these frameworks). Ni/DOBDC (547 mol kg^{-1} bar^{-1} at 294 K) and Co/DOBDC (320 mol kg^{-1} bar^{-1} at 294 K) exhibit considerably higher Henry's constants than Mg/DOBDC (12 mol kg^{-1} bar^{-1} at 294 K) and Mn/DOBDC (5 mol kg^{-1} bar^{-1} at 294 K). The σ-donation [**122**] of electron lone pair by CO molecules to the Ni and Co metal ions results in this exceptional affinity of these frameworks for CO.

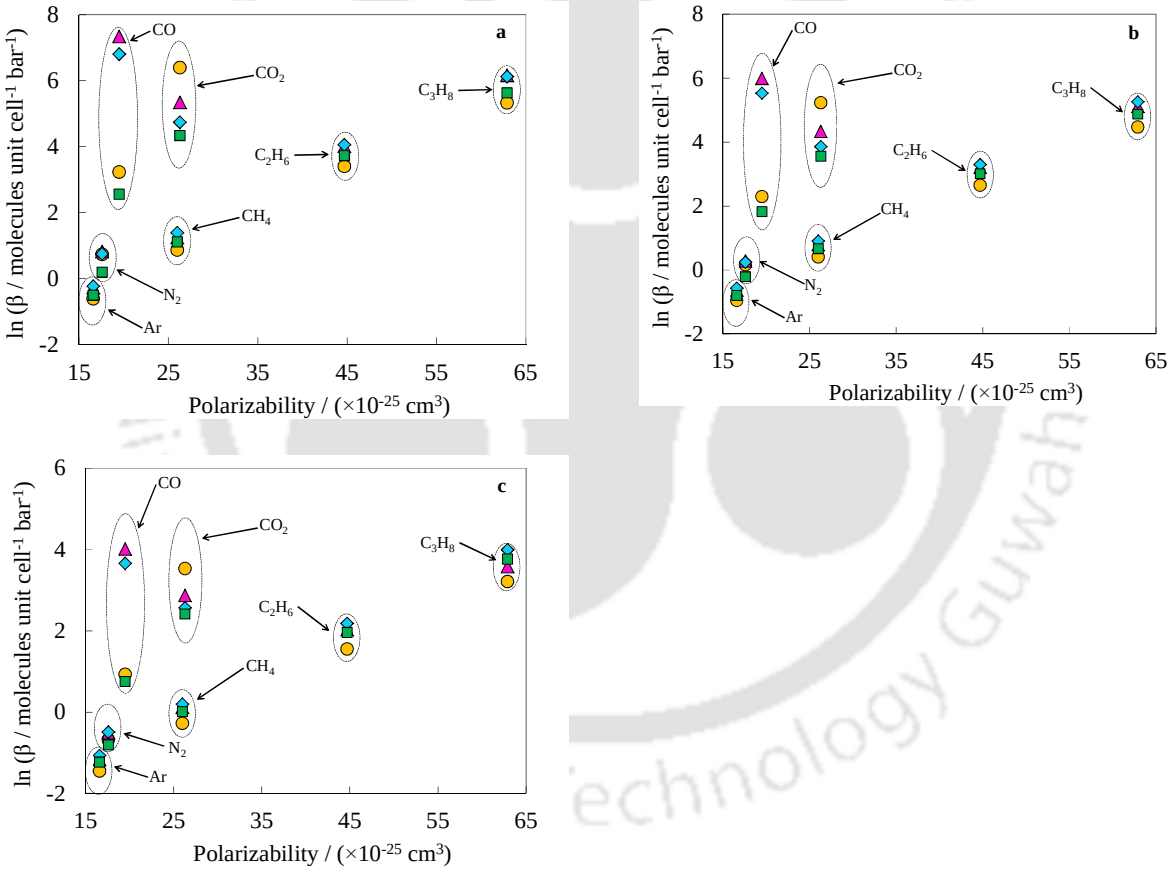

Figure 6.28: Variation of Henry's constants at **(a)** 294 K, **(b)** 315 K and **(c)** 352 K with polarizability for Mg/DOBDC (●), Mn/DOBDC (■), Co/DOBDC (♦) and Ni/DOBDC (▲).

6.6.2 On Adsorption Isotherms at High Pressures

6.6.2.1 On Isotherms of Non-polar Gases. CH_4 isotherms at 294 K on all the four adsorbent samples are compared in Figure 6.29. Due to negligible electrostatic interactions between *cus* metal sites of these frameworks and non-polar CH_4 molecules, the change of metal constituent in the framework has negligible effect on the adsorption characteristics in the low pressure region (*ca.* < 0.5 bar) (Figures. 6.29a). Thereafter (*ca.* above 1 bar), loading on these frameworks are related to their pore volumes; while the highest loading was observed for Ni/DOBDC (which has the highest pore volume), lowest capacity is observed for Mg/DOBDC (which has the lowest pore volume. In fact, the saturation uptake capacities vary almost linearly with pore volumes (Figure 6.29b) obtained from N_2 isotherm at 77 K. Isotherms for other relatively non-polar gas (Ar, C_2H_6 and N_2) also follow similar trends (Figures 6.30 – 6.32).

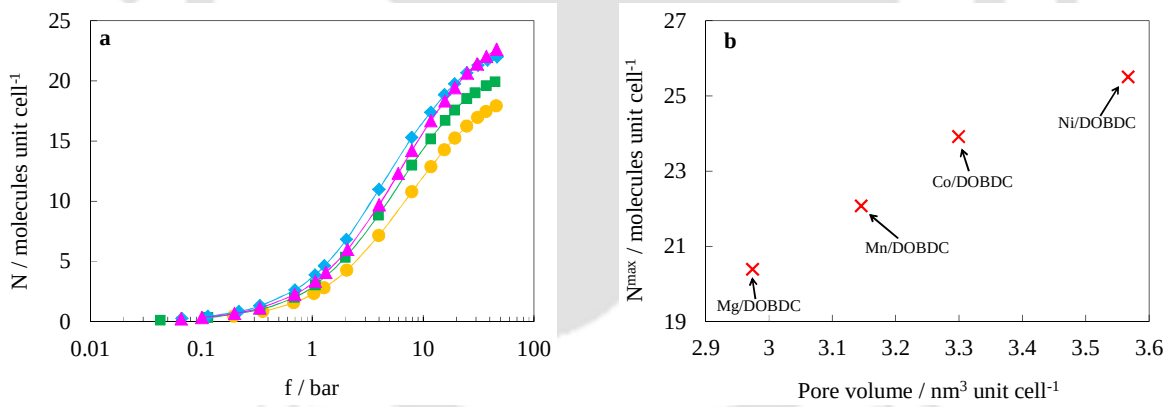

Figure 6.29: (**a**) CH_4 isotherms at 294 K on Mg/DOBDC (●), Mn/DOBDC (■), Co/DOBDC (♦) and Ni/DOBDC (▲). (**b**) Variation of CH_4 saturation uptake with pore volume of DOBDC MOFs.

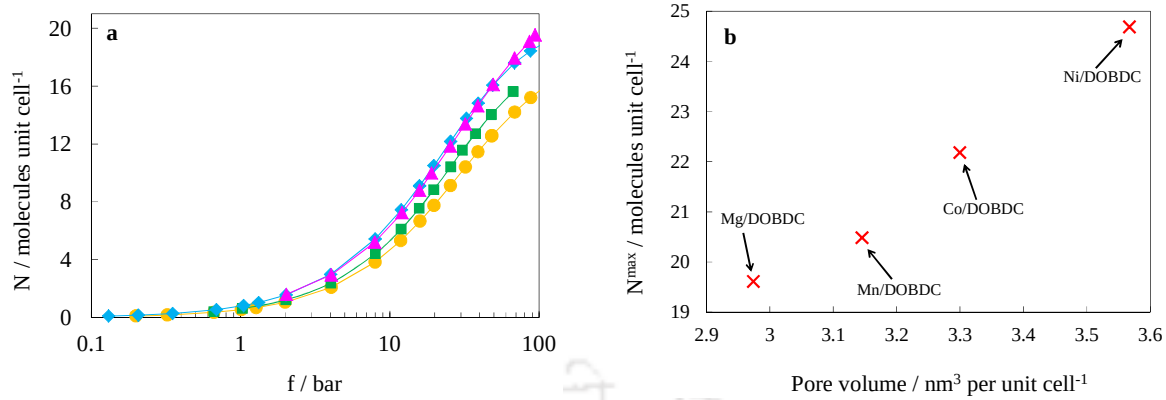

Figure 6.30: (**a**) Ar isotherms at 294 K on Mg/DOBDC (●), Mn/DOBDC (■), Co/DOBDC (♦) and Ni/DOBDC (▲). (**b**) Variation of Ar saturation uptake with pore volume of DOBDC MOFs.

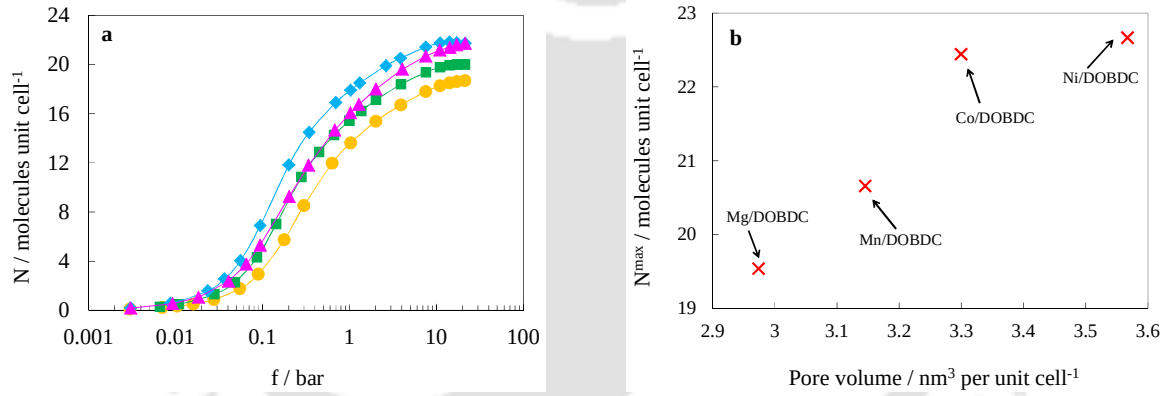

Figure 6.31: (**a**) C_2H_6 isotherms at 294 K on Mg/DOBDC (●), Mn/DOBDC (■), Co/DOBDC (♦) and Ni/DOBDC (▲). (**b**) Variation of C_2H_6 saturation uptake with pore volume of DOBDC MOFs.

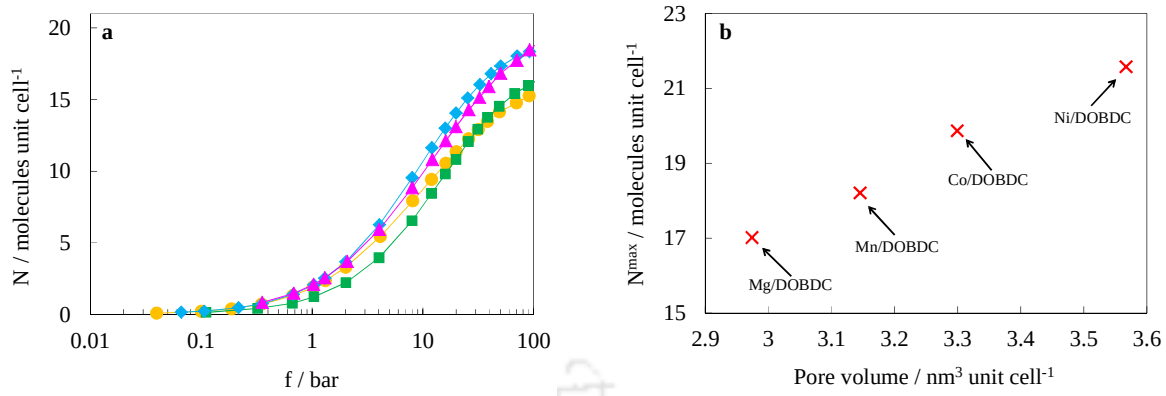

Figure 6.32: (**a**) N_2 isotherms at 294 K on Mg/DOBDC (●), Mn/DOBDC (■), Co/DOBDC (♦) and Ni/DOBDC (▲). (**b**) Variation of N_2 saturation uptake with pore volume of DOBDC MOFs.

6.6.2.2 On C_3H_8 Isotherms. C_3H_8 isotherms at 294 K on M/DOBDC compounds are shown in Figure 6.33. Comparison of C_3H_8 Henry's constants for M/DOBDC samples indicates the negligible role of metal constituent in the framework on C_3H_8 adsorption at low pressure. However, with increase of pressure, difference arises between adsorption capacity of different frameworks and Co/DOBDC exhibits higher uptake than that by other DOBDC frameworks at saturation. As in case of other gases, the N^{max} for all the frameworks are related to their pore volumes; however Co/DOBDC has slightly higher saturation loading (~ 2.7 %) compared to that of Ni/DOBDC. Repeated experiments confirm to these results and we are unable to offer any reasonable explanation for this anomaly at this stage. Molecular simulations may offer insight into this behavior.

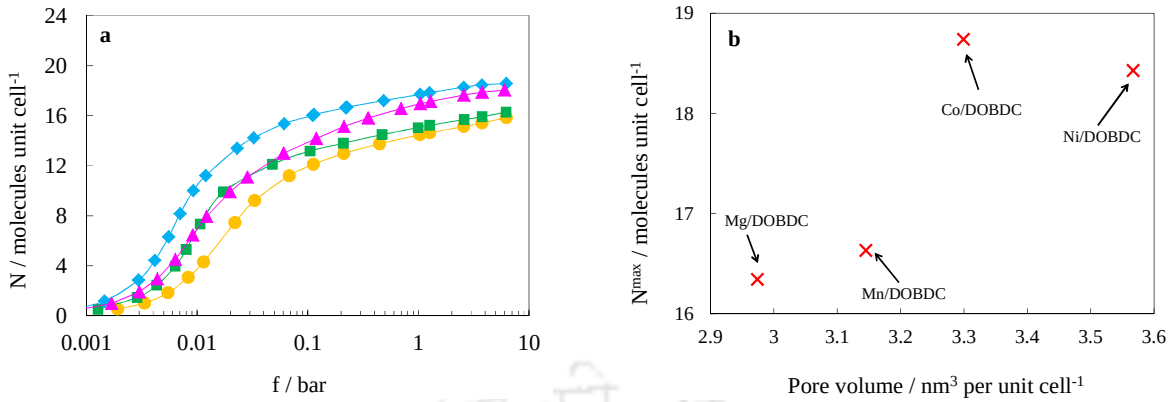

Figure 6.33: (**a**) C_3H_8 isotherms at 294 K on Mg/DOBDC (●), Mn/DOBDC (■), Co/DOBDC (♦) and Ni/DOBDC (▲). (**b**) Variation of C_3H_8 saturation uptake with pore volume of DOBDC MOFs.

6.6.2.3 On CO_2 Isotherms. CO_2 isotherms at 294 K on M/DOBDC MOFs are shown in Figure 6.34a. The CO_2 uptake capacities for these frameworks behave differently in two regions. As already discussed, in the Henry's law region the CO_2 uptakes follow the order Mg/DOBDC > Ni/DOBDC > CoDOBDC > Mn/DOBDC. As the pressure increases, the metal centers are progressively filled; at a loading of ~1 molecule per metal atom (18 molecules per unit cell) *cus* metal centers are saturated and hence the role of metal atom should be negligible. Accordingly in this region (highlighted region in Figure 6.34a), the difference between adsorption capacity of the four framework is negligible. As the pressure is further increased, the pore volume of the framework governs the adsorption capacity and as in case of non-polar gases, saturation loading on these frameworks varies linearly with pore volume (Figure 6.34b).

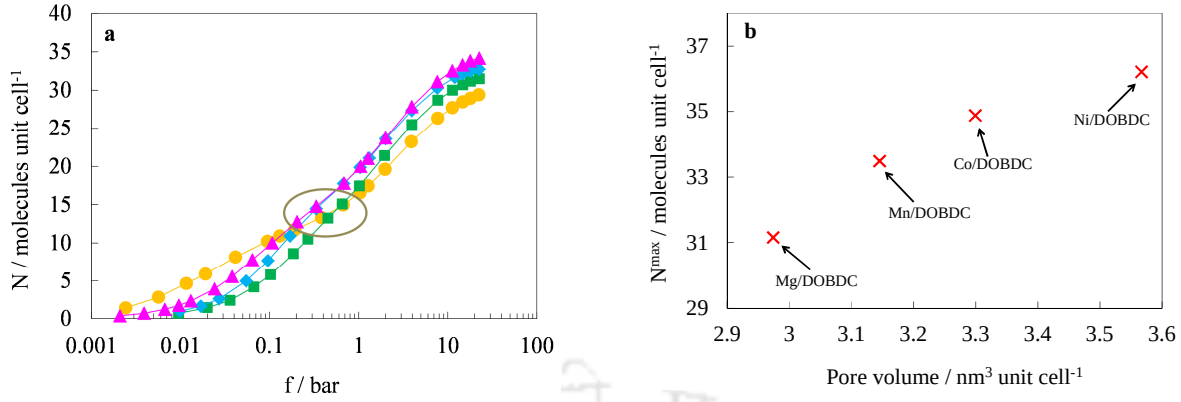

Figure 6.34: (**a**) CO_2 isotherms at 294 K on Mg/DOBDC (●), Mn/DOBDC (■), Co/DOBDC (♦) and Ni/DOBDC (▲). (**b**) Variation of CO_2 saturation uptake with pore volume of DOBDC MOFs.

6.6.2.4 On CO isotherms. Figure 6.35 reports the CO adsorption isotherms at 294 K on *cus* metal site containing M/DOBDC frameworks. At low pressure (*ca*. 0.01 bar), CO adsorption on Ni/DOBDC and Co/DOBDC is considerably higher than that on Mg/DOBDC and Co/DOBDC; the difference of this magnitude (~100 times) cannot be accounted by the slight difference in the ionic radii of different metals; since this can create only a small difference in electrostatic interactions. In literature, it is reported that CO molecules donate σ-electron lone pair to the Ni^{2+} [**122**]. Thus, exceptional CO adsorption uptake on Ni/DOBDC and Co/DOBDC is attributed to the σ-donation of electron lone pair by CO molecules to the *cus* Ni and Co metal centers. The difference between Ni/DOBDC or Co/DOBDC and the other two frameworks studied in this work are significant even at pressures as high as 10 bar (~ 2 times). Thereafter, as the *cus* metal centers are occupied, electrostatic interactions get weaker and similar to other gases, CO saturation capacities are found to be linearly related to the pore volume for these frameworks (Figure 6.35b).

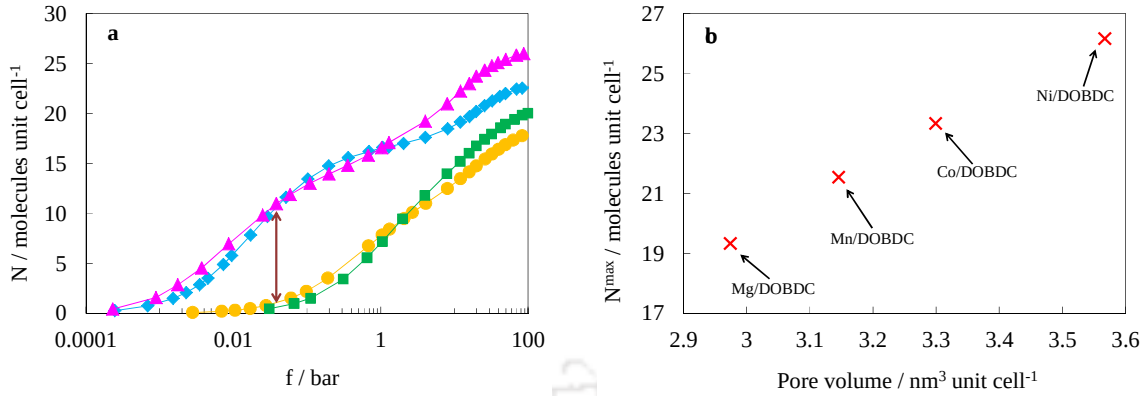

Figure 6.35: (**a**) CO isotherms at 294 K on Mg/DOBDC (●), Mn/DOBDC (■), Co/DOBDC (♦) and Ni/DOBDC (▲). (**b**) Variation of CO saturation uptake with pore volume.

The above results indicate that for non-polar gas, the metal atom in the framework plays negligible role; however, it plays an important role for polar gases like CO_2 and CO. While Mg/DOBDC exhibits significant high Henry's constant for CO_2, Ni/DOBDC and Co/DOBDC show large value of Henry's constant for CO due to σ-bonding. As the *cus* metal cations are filled, the difference between four frameworks becomes negligible for even polar gases. At high pressure pore volume of the framework governs the adsorption and is linearly related to the saturation capacity of the gas.

6.6.3 On Enthalpy of adsorption

The effect of metal constituent in the M/DOBDC frameworks on their adsorption characteristics is further elaborated by variation of adsorption enthalpy with loading (Figures 6.36 – 6.37).

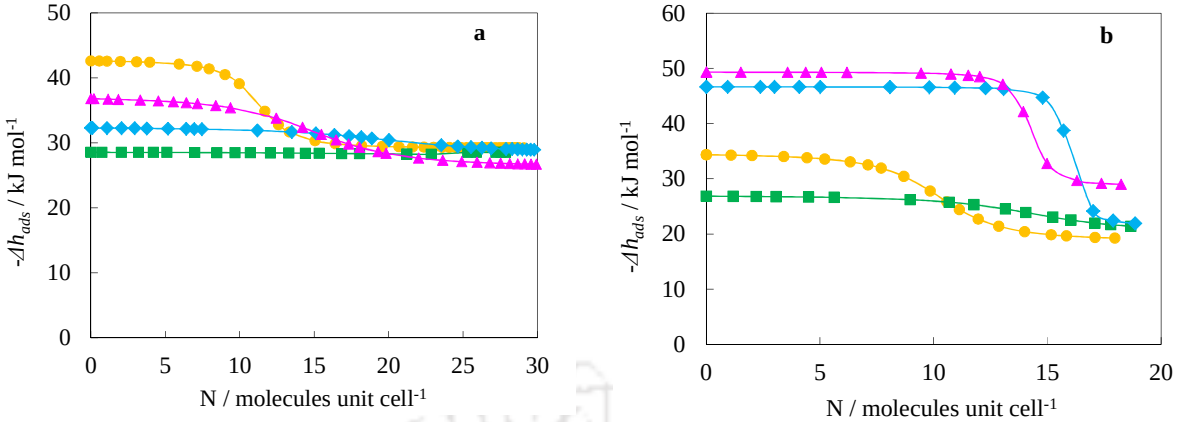

Figure 6.36: Variation of adsorption enthalpy of (**a**) CO_2 and (**b**) CO with loading for Mg/DOBDC (●), Mn/DOBDC (■), Co/DOBDC (♦) and Ni/DOBDC (▲)

At low loadings the enthalpy of CO_2 and CO varies significantly (Figure 6.36) with the metal atom in the framework due to differences in the adsorbate-adsorbent electrostatic interactions for different frameworks; thereafter, this difference vanishes and the enthalpy difference between various frameworks is negligible. At about 1 molecule per metal atom, CO_2 and CO enthalpies of all the frameworks are almost equal (due to complete occupation of *cus* metal sites and hence the effect of constituent metal in the framework vanishes). However, in case of non-polar gases such as (CH_4, N_2, Ar, C_2H_6 and C_3H_8) the enthalpy of adsorption is almost independent of the constituent metal atom in the framework for entire range of loadings (Figure 6.37).

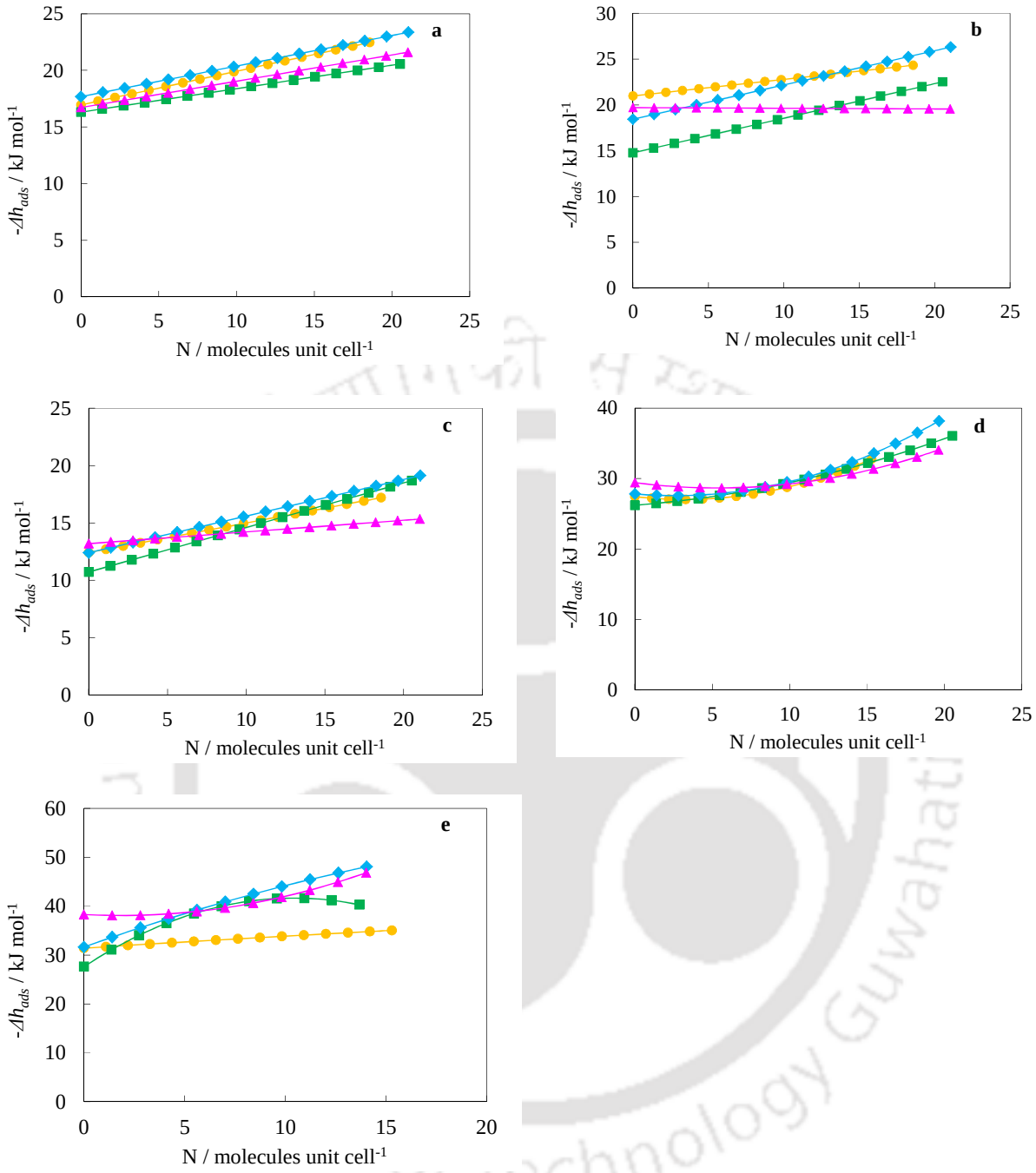

Figure 6.37: Variation of adsorption enthalpy of (**a**) CH_4, (**b**) N_2, (**c**) Ar, (**d**) C_2H_6 and (**e**) C_3H_8 with loading for Mg/DOBDC (●), Mn/DOBDC (■), Co/DOBDC (♦) and Ni/DOBDC (▲).

6.7 Prediction of Binary Selectivity using IAST

The selectivities of various binary mixtures are calculated using Ideal Adsorbed Solution Theory (IAST) [**198**] to understand the effect of adsorbate properties and metal constituent in the DOBDC framework on the binary adsorption. The variation in CO_2 selectivity over CH_4, N_2, and Ar with pressure from a 20% CO_2 in the binary mixture at 294 K is shown in Figures 6.38a – 6.38c. In case of non-polar gases, CO_2 selectivity is higher over the gas with lower polarizability (CO_2/Ar selectivity is higher than that of CO_2/CH_4). At sub-atmospheric pressures CO_2 selectivity over CH_4, N_2, and Ar is considerably higher in DOBDC frameworks than that on other adsorbents. This can be easily correlated to the strong electrostatic interactions between *cus* metal centers and CO_2 molecules. As already discussed due to exceptional preference of Mg^{2+} for oxygen-containing ligands, CO_2 selectivity on Mg/DOBDC is significantly higher than that on the other DOBDC frameworks. CO_2 selectivity over CH_4 at zero pressure and 294 K on Mg/DOBDC (250) is also significantly higher than that on most of other MOFs like IRMOF-1 (3) [**218**], PCN-6 (3) [**219**], CuBTC (4) [**219**], MIL-101 (4) [**220**], *soc*-MOF (20) [**219**], Li-IRMOF-1 (180) [**221**], NaX (55) [**158**], Ni/DOBDC (60), Mn/DOBDC (28) and Co/DOBDC (28). Similarly, CO_2 selectivity over N_2 at zero loading (294 K) on Mg/DOBDC (288) is significantly higher than that on most of other MOFs like IRMOF-1 (4) [**121**], IRMOF-3 (5) [**121**], CuBTC (20) [**121**], MOF-177 (7) [**159**], $Zn_2(BDC)_2DABCO$ (7) [**121**], MFI (10) [**159**], NaX (200) [**159**], bio-MOF-11 (100) [**159**], Ni/DOBDC (92), Mn/DOBDC (63) and Co/DOBDC (54); however, it comparable to UTSA-16 (300) [**159**].

At low pressure, CO_2 molecules experience strong electrostatic interactions with *cus* metal sites in M/DOBDC frameworks. As these sites are progressively filled, the electrostatic interactions weaken resulting into a considerable decrease in CO_2 selectivity with pressure. However, the magnitude of decrease in selectivity with pressure is different for each of the frameworks. For

example, in case of Mn/DOBDC the decrease in CO_2/N_2 selectivity with pressure is smaller (as compared to that in case of Mg/DOBDC), since the electrostatic interactions of CO_2 with this framework are weaker.

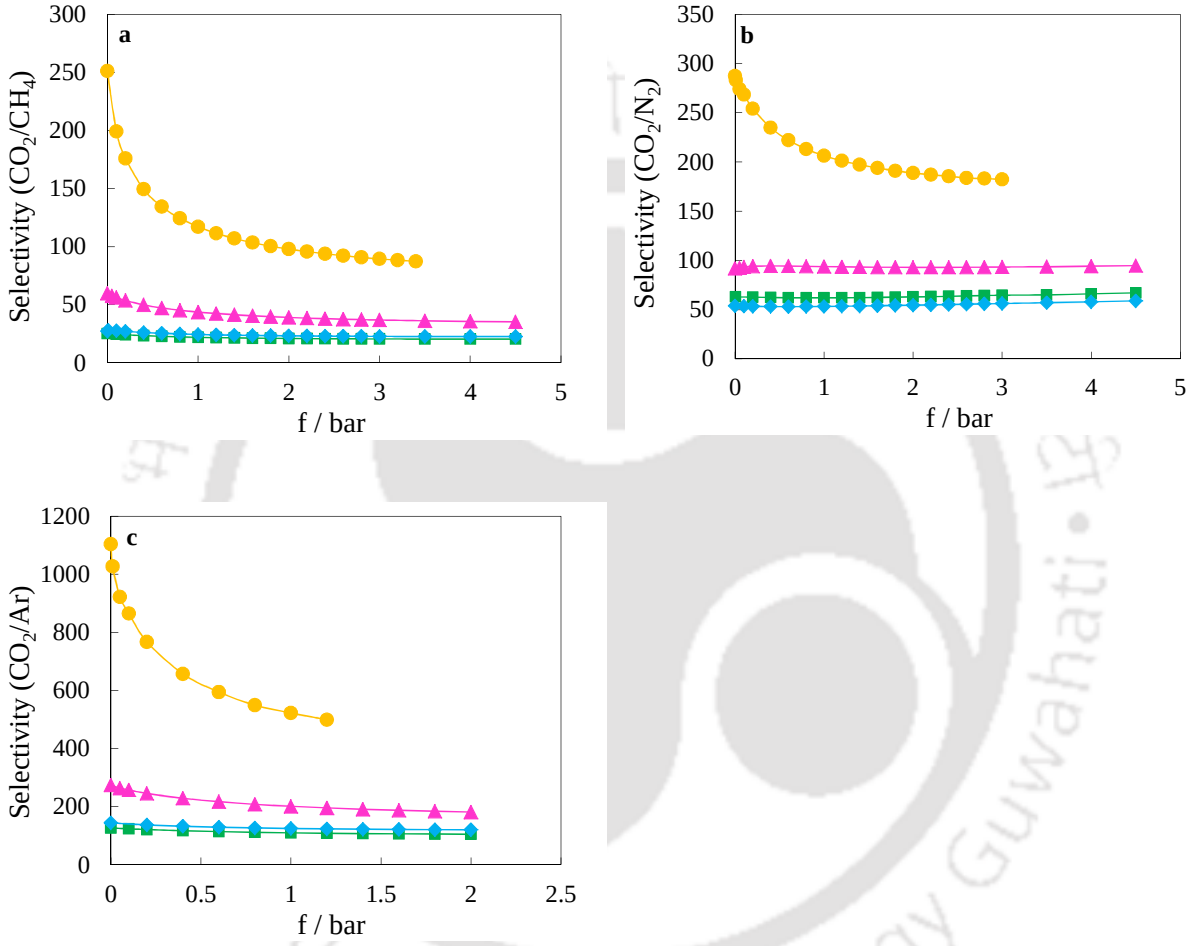

Figure 6.38: Variation of CO_2 selectivity over (**a**) CH_4, (**b**) N_2 and (**c**) Ar at 294 K with pressure on Mg/DOBDC (●), Mn/DOBDC (■), Co/DOBDC (♦) and Ni/DOBDC (▲). CO_2 mole fraction in all binary mixtures is 20%. Symbols are calculated values; lines are drawn as a guide to the eyes.

The variation in CO_2 selectivity over CO with pressure from a 20% CO_2 in the binary mixture at 294 K is shown in Figure 6.39. Several interesting observations can be highlighted in this figure.

In this case both CO_2 and CO molecules experience electrostatic interactions with *cus* metal centers of M/DOBDC frameworks and thus CO_2 selectivity for CO_2/CO binary mixture is considerably lower than for CO_2/CH_4, CO_2/N_2 and CO_2/Ar binary mixtures. Moreover, CO_2 selectivity over CO in the Mg/DOBDC framework does not change appreciably with pressure, since the decrease in electrostatic interactions occurs for both the gases as the *cus* sites are occupied. Mg/DOBDC and Mn/DOBDC frameworks are selective for CO_2 throughout the entire pressure range. In fact, CO_2 selectivity at zero coverage and 294 K on Mg/DOBDC (24) is higher than that on many MOFs such as Zn/DABCO (7) [**121**] and CuBTC (7) [**121, 158**]. But the selectivity of CO_2/CO mixture is lower than 1 at low pressures for Ni/DOBDC and Co/DOBDC samples, indicating that these samples are more selective to CO. In fact at zero loading the CO/CO_2 selectivity on these samples are as high as 7.5 (ratio of Henry's constants on these samples) and the samples remain selective to CO even up to 10 bar. However, as in the other cases, as the *cus* metal centers are filled with increasing pressure, the CO/CO_2 selectivity gradually decreases. At pressures higher than 16 bar, the samples have preferential selectivity for CO_2 over CO (since the saturation capacity of CO_2 is higher).

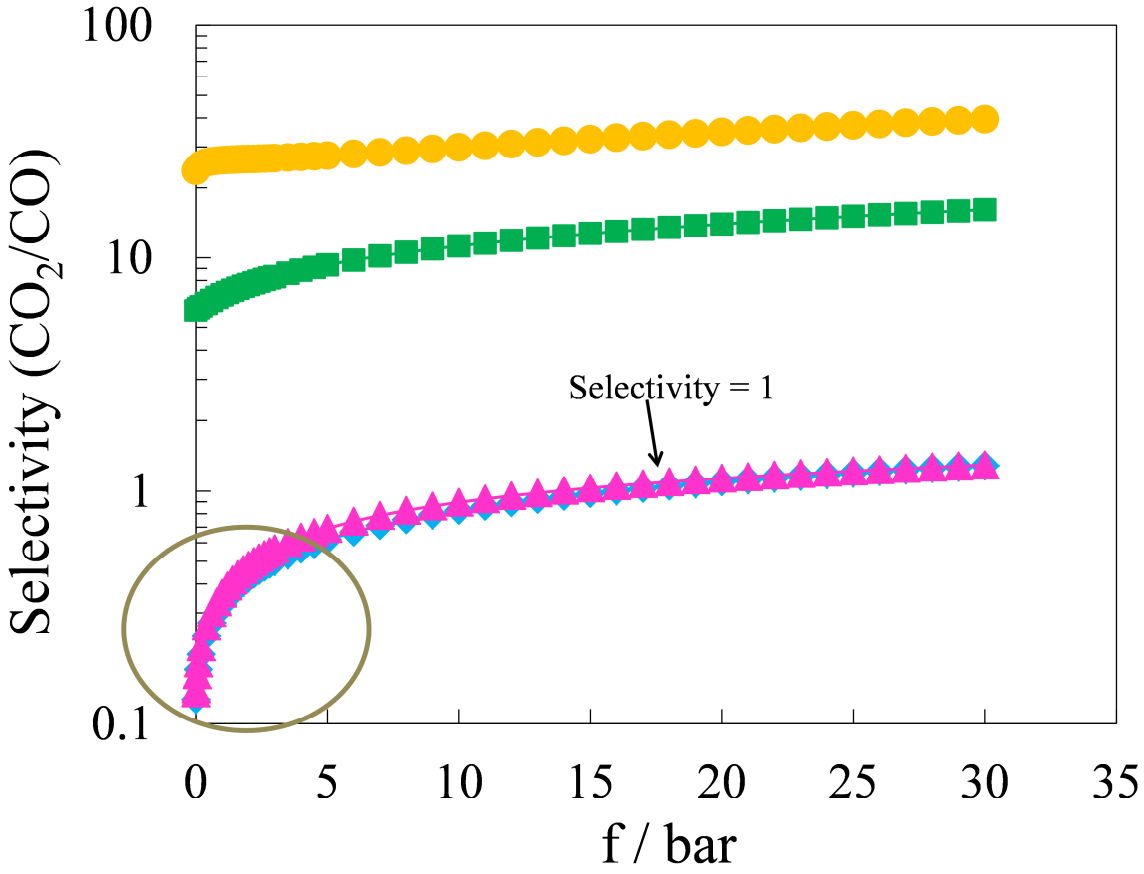

Figure 6.39: Variation of CO_2 selectivity over CO at 294 K with pressure on Mg/DOBDC (●), Mn/DOBDC (■), Co/DOBDC (♦) and Ni/DOBDC (▲). CO_2 mole fraction is 20%. Symbols are calculated values; lines are drawn as a guide to the eyes.

The DOBDC compounds are found to be selective for CO over CH_4 and N_2 (Figures 6.40) due to presence of electrostatic interactions in case of CO adsorption.

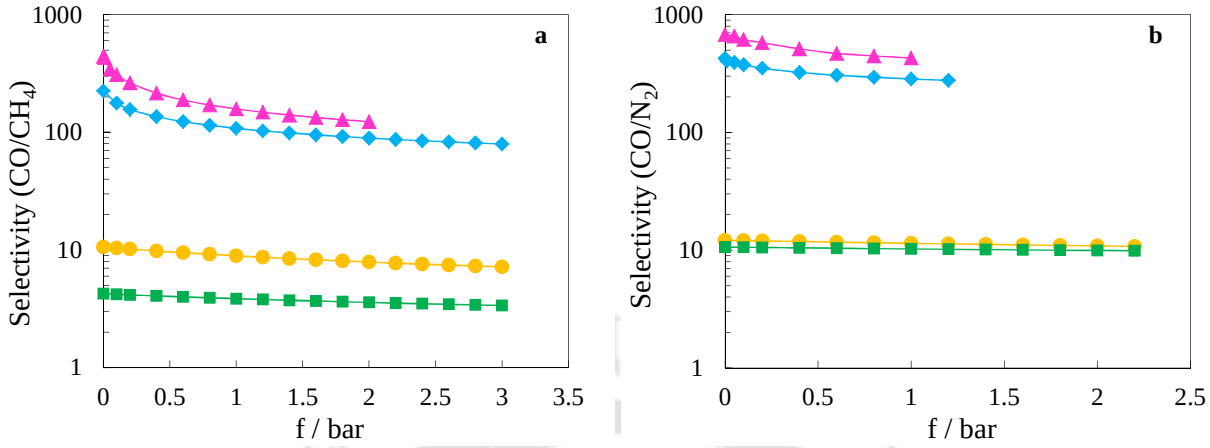

Figure 6.40: Variation of CO selectivity over (**a**) CH_4 and (**b**) N_2 at 294 K with pressure on Mg/DOBDC (●), Mn/DOBDC (■), Co/DOBDC (♦) and Ni/DOBDC (▲). CO mole fraction in all binary mixtures is 20%. Symbols are calculated values; lines are drawn as a guide to the eyes.

Both Ni and Co containing DOBDC frameworks, exhibit higher selectivity for CO over CH_4 and N_2 (Figures 6.40a – 6.40b) as compared to that by Mg/DOBDC and Mn/DOBDC. CO selectivity over CH_4 obtained in this work on Ni/DOBDC at zero loading and 294 K is 441; this value is much higher than that on MIL-101 (30) [**95**] and CuBTC (~1) [**71**]. CO selectivity over N_2 on Ni/DOBDC at zero loading and 294 K is even higher (677). As in case of CO_2, the selectivity of CO over CH_4 and N_2 decreases with pressure due to reduced electrostatic interactions. Decrease in CO selectivity over N_2 is lesser pronounced than that over CH_4, because of the quadrupole moment of N_2. For Mg/DOBDC and Mn/DOBDC samples, decrease in CO selectivity over CH_4 and N_2 with pressure, is less pronounced than in case of Ni/DOBDC and Co/DOBDC (which show exceptional Henry's constants for CO adsorption).

The effect of temperature on CO_2 selectivity over N_2 is shown in Figure 6.41a. CO_2 selectivity for a binary gas mixture (20% CO_2 at 1 bar) decreases by ~2.4 to 3 times when the temperature is increased from 294 to 352 K. This decrease can be readily attributed to the larger decrease in the electrostatic interactions for CO_2 molecules than that for N_2 molecules by the increase of temperature. Similar behavior is also observed for CO_2 selectivity over CH_4, Ar (Figure 6.41b – 6.41c) and for CO selectivity over CH_4, N_2 (Figure 6.42a – 6.42b). On the other hand, CO_2 selectivity over CO (Figure 6.41d) does not change appreciably since both of the gases have considerable polarity; thus the decrease in selectivity with (increasing) temperature will be smaller in case of a binary mixture containing two polar species than in case of a binary mixture containing one polar and one non-polar adsorbate.

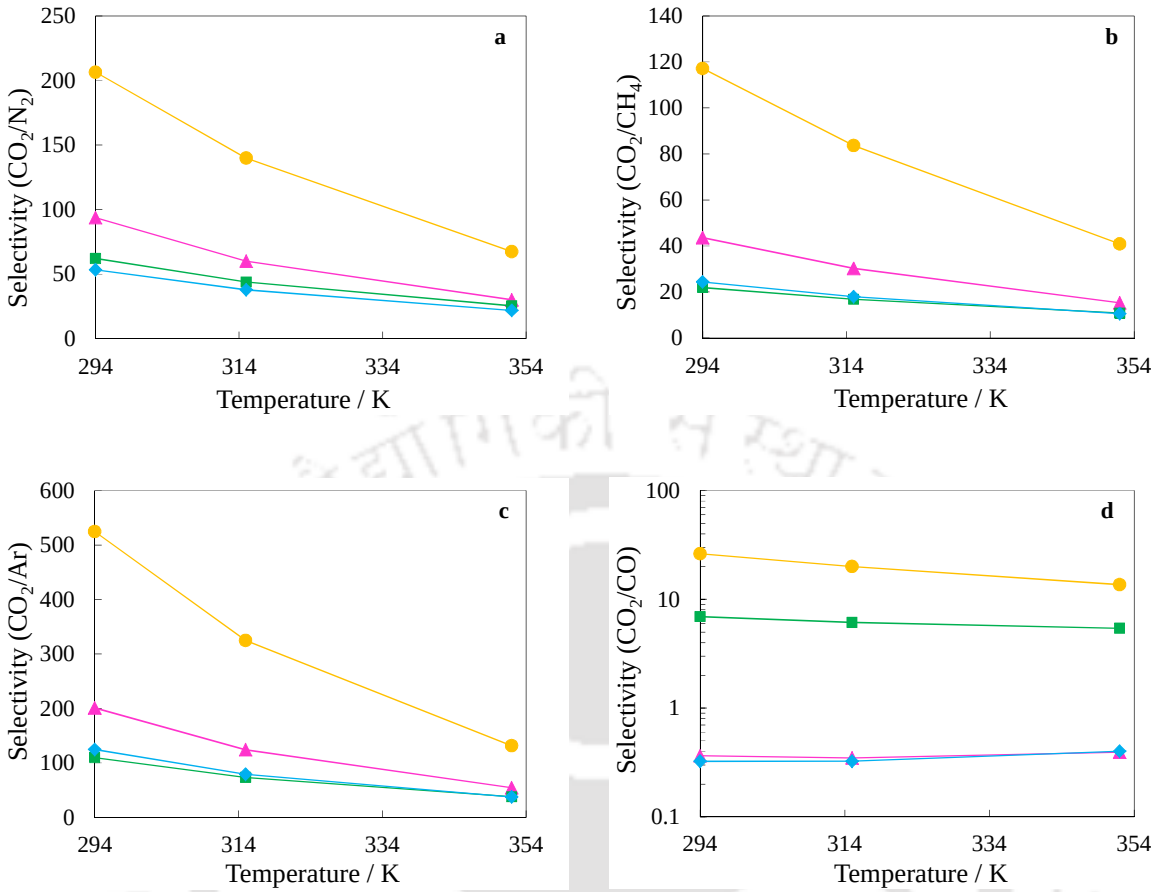

Figure 6.41: Effect of temperature on CO_2 selectivity (for 20% molar composition of CO_2) over (**a**) N_2, (**b**) CH_4 , (**c**) Ar and (**d**) CO at 1 bar total pressure for Mg/DOBDC (●), Mn/DOBDC (■), Co/DOBDC (♦) and Ni/DOBDC (▲). Symbols are calculated values; lines are drawn as a guide to the eyes.

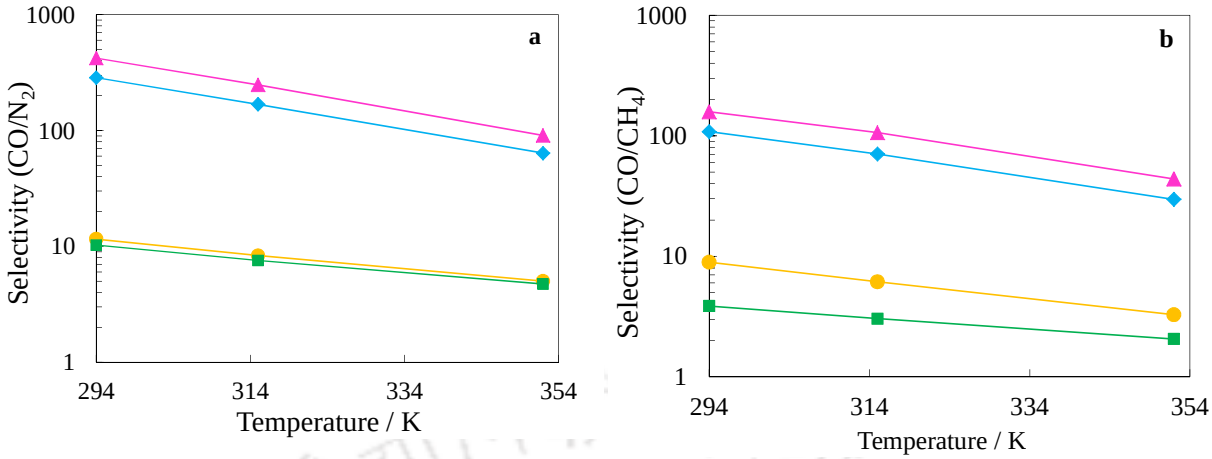

Figure 6.42: Effect of temperature on CO selectivity (for 20% molar composition of CO) over (**a**) N_2 and (**b**) CH_4 at 1 bar total pressure for Mg/DOBDC (●), Mn/DOBDC (■), Co/DOBDC (♦) and Ni/DOBDC (▲). Symbols are calculated values; lines are drawn as a guide to the eyes.

6.8 Stability of Frameworks upon Exposure to Different Adsorbates

For practical realization of any adsorptive separation processes, the adsorbent should be stable upon the exposure to gas mixtures. In most of the processes (especially for those involving removal of CO_2 from flue gas streams), moisture and oxygen are also present apart from major components such as CO_2, N_2, CH_4 etc. Kizzie et al. [**188**] have already performed the stability analysis of these M/DOBDC (M = Mg, Co, Ni, Zn) MOFs for their exposure to moisture. They observed that all of the M/DOBDC compounds are unstable to moisture exposure. They reported that Mg/DOBDC is highly unstable in humid environment compared to all other DOBDC MOFs.

In this work, the stability of M/DOBDC (M = Mg, Mn, Co, Ni) MOFs was evaluated upon their exposure to studied adsorbates *i.e.* CO_2, CO, CH_4, N_2, Ar, C_2H_6 and C_3H_8 at 294, 315 and 352 K. In addition, O_2 is also included because of its industrial relevance.

First, CO_2 adsorption uptake was measured at 294 K and 1 bar on a freshly prepared activated sample without exposing it to any other gases. Then all the high pressure adsorption measurements reported in the preceding sections for CO_2, CO, CH_4 N_2, Ar, C_2H_6 and C_3H_8 at 294, 315 and 352 K were measured on the sample (mimicking their exposure to these adsorbents). The CO_2 adsorption uptake was measured again at 294 K and 1 bar. Thereafter, the sample was exposed to O_2 at 294 K and ~ 100 bar; then followed by another CO_2 adsorption uptake measurement at 294 K and 1 bar. The O_2 exposure was repeated at 315 and 352 K followed by CO_2 adsorption uptake measurement at 294 K and 1 bar each time. The reduction in the measured CO_2 uptake at 294 K and 1 bar is correlated to the effect of O_2 on the framework stability. Stability upon exposure to O_2 at various temperatures is evaluated to see the role of temperature on framework stability during its exposure to O_2.

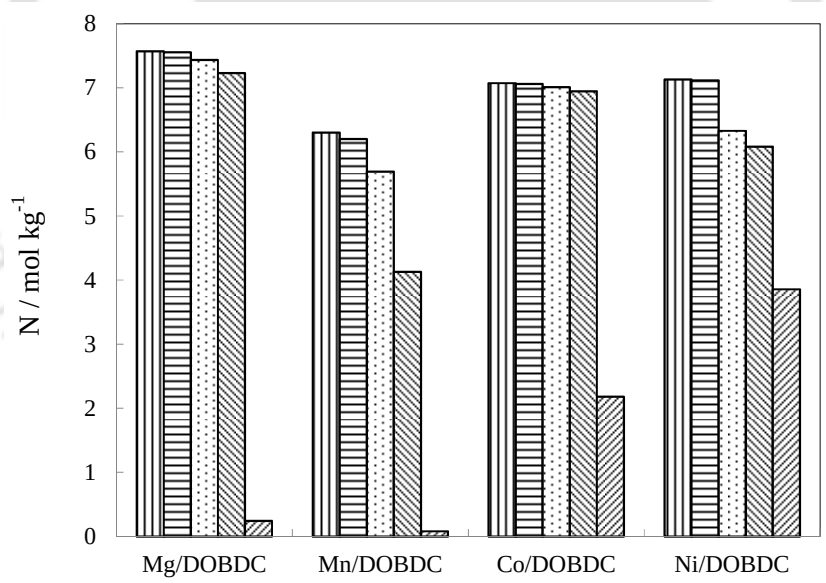

Figure 6.43: CO_2 uptake at 294 K and 1 bar on freshly prepared DOBDC samples (vertical lines); after performing adsorption measurements of CO_2, CO, CH_4 N_2, Ar, C_2H_6 and C_3H_8 (horizontal lines); after exposing to O_2 at 294 K (dots); after exposing to O_2 at 315 K (backward slashes); after exposing to O_2 at 352 K (forward slashes).

CO_2 uptake before and after adsorption measurements of CO_2, CO, CH_4 N_2, Ar, C_2H_6 and C_3H_8 matches exactly for all samples (Figure 6.43). This confirms no change in adsorption characteristics of frameworks up on their exposure to these gases. CO_2 uptake slightly decreases after exposure to O_2 at 294 K indicating instability for M/DOBDC samples in O_2 environment at 294 K. However, with increasing temperature of exposure (to O_2), decrease in CO_2 uptake becomes more pronounced. After O_2 exposure at 352 K, CO_2 uptake reduces considerably indicating the collapse of structure. M/DOBDC frameworks are reported to be unstable in the humid [**188**] and in the steam [**222**] environment. In addition, this work demonstrates that M/DOBDC (M = Mg, Mn, Co, Ni) frameworks are also unstable in the oxygen environment especially at higher temperature.

6.9 Summary

DOBDC MOFs exhibit significantly higher adsorption uptake for the polar CO_2 and CO gases compared to that for other relatively gases such as Ar, N_2, CH_4 in the Henry's region due to the strong electrostatic interactions between polar adsorbate molecules and *cus* metal centers. However, as the *cus* metal centers are filled, the variation of adsorption enthalpy with loading manifests a prominent inflection at a loading of about 1 molecule per metal atom in case of CO_2 and 0.8 molecule per metal atom in case of CO and approaches to that of other relatively non-polar gases with similar polarizability; this highlights the prominent role of *cus* metal sites on the adsorption characteristics of M/DOBDC frameworks for polar adsorbates. The adsorption characteristics of *cus* metal sites containing DOBDC frameworks can be dramatically altered for polar adsorbates by change of metal constituents in the frameworks. CO_2 adsorption at low pressures follows the order Mg/DOBDC > Ni/DOBDC > Co/DOBDC > Mn/DOBDC with adsorption enthalpies ranging between 42 and 28 kJ mol^{-1}. Ni and Co/DOBDC frameworks exhibit preferential selectivity for CO over all other gases due to its favorable interactions with the *cus* Ni and Co metal centers and also show higher adsorption enthalpy (> 46 kJ mol^{-1}). The metal atom in the framework has negligible effect on adsorption loading of non-polar adsorbates in the Henry's region. For both polar and non-polar adsorbates, the saturation loadings correlate well with the pore volumes of the respective frameworks. M/DOBDC MOFs were found to be stable up on exposure to CO_2, CO, CH_4 N_2, Ar, C_2H_6 and C_3H_8. However, exposure to O_2 at high temperatures significantly affects the adsorption characteristics of these MOFs.

CHAPTER 7

ADSORPTION CHARACTERISTICS OF COORDINATIVELY SATURATED METAL SITES CONTAINING M/DABCO MOFS

This chapter reports the adsorption isotherms of CO_2, CH_4, CO and N_2 at 294, 314 and 350 K upto ~ 25 bar on saturated metal sites containing M/DABCO MOFs. Similar to DOBDC MOFs, effect of adsorbate properties and metal cation in the framework is investigated on the adsorption characteristics of DABCO MOFs. The work also highlights the role of having cus metal sites on the adsorption of different gases.

7.1 Background

In previous chapter, the effect of metal atom variation in the M/DOBDC MOFs on their adsorption characteristics was studied. A significant variation is observed in the adsorption characteristics for polar adsorbates because electrostatic interactions between adsorbate molecules and coordinatively unsaturated *(cus)* metal centers of these MOFs vary with the change of metal atom in the framework. In this chapter, we study the effect of metal constituent in the framework and adsorbate physical properties on the adsorption characteristics of M/DABCO MOFs.

The DABCO MOFs have negligible coordinatively unsaturated *(cus)* metal centers; hence, they are expected to behave differently than DOBDC MOFs. The first member of DABCO MOFs *i.e.*

Cu/DABCO was synthesized by Seki et al. [**54**] forming a paddle wheel of two copper(II) atoms, two benzene dicarboxylate molecules and one 1,4-diazabicyclo[2.2.2]octane (DABCO) molecule. Later, isostructural Zn/DABCO and Ni/DABCO were synthesized by Dybtsev et al. [**55**] and Arstad et al. [**75**], respectively. In these MOFs, DABCO molecule acts as a pillar to a two-dimensional layer of metal dicarboxylate (Figure 7.1). There are two distinct pore sizes (7.5 Å × 7.5 Å along the *c*-axis and 4.8 Å × 3.2 Å along *a*- and *b*- axes) [**55, 223**]. The mass and the volume of a unit cell of Zn/DABCO MOF are 9.48×10^{-22} g and 1147.6 $Å^3$ respectively [**55**], which correspond to a crystal density of 0.826 g cc^{-1}.

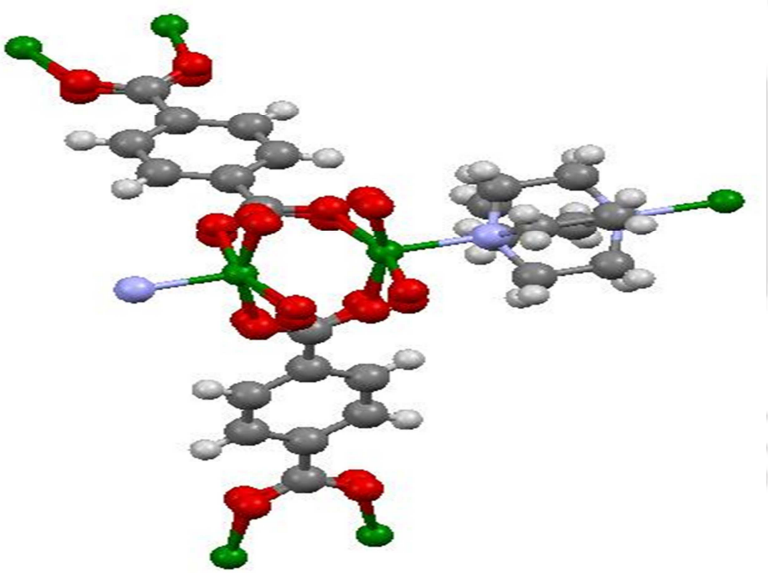

Figure 7.1: Crystal structure of Zn/DABCO MOF (O, red; C, grey; H, white; N, violet; Zn, green) [**55**].

All metal atoms are coordinatively saturated in M/DABCO MOFs. While small pore sizes in these MOFs are favorable for enhancement of vertical interactions between the adsorbent and the adsorbate, the absence of *cus* metal centers results in negligible electrostatic interactions [**71,**

121] and hence in smaller Henry's constant and enthalpy of adsorption. The lower enthalpy values are indeed beneficial for easier regeneration in an adsorption process. Some of the earlier studies for gas adsorption on DABCO MOFs are available in the literature. Senkovska et al. [**224**] have studied CH_4 adsorption on Zn/DABCO framework at 303 K up to 175 bar. They found complete reversibility for the adsorption/desorption branch and reported the stability of the framework upon adsorption of CH_4 at higher pressure. Arstad et al. [**75**] have measured CO_2 adsorption on Ni/DABCO at 298 K. Arstad et al. [**75**] have also functionalized the DABCO MOF with amine groups in order to enhance its CO_2 uptake at sub-atmospheric pressures. Karra et al. [**121**] have performed GCMC simulation for CO_2, CO and N_2 adsorption in Zn/DABCO. In another important progress, Liang et al. [**79**] have reported CO_2, N_2 and CH_4 adsorption on Zn/DABCO and Ni/DABCO up to 15 bar. They obtained unchanged CO_2 uptake after water sorption at 30% relative humidity and 298 K; however CO_2 uptake decreased after water sorption at 60% humidity. In comparison to other well studied MOFs such as CuBTC, MOF-5, MIL-101 etc. adsorption studies on these MOFs are limited. Comprehensive investigation of adsorption characteristics of these MOFs involving various adsorbates as well as a large range of temperature and pressure will be beneficial in understanding the adsorption behavior of MOFs with coordinatively saturated metal centers. While the earlier literature suggests the absence of electrostatic interactions and low enthalpy values for adsorption on these MOFs it will be interesting to systematically investigate and compare the adsorption characteristics of these MOFs with the coordinatively unsaturated metal site containing DOBDC MOFs studied in the previous chapter. Effect of metal cation variation in the DABCO MOFs on the adsorption characteristics will also be examined.

7.2 Characterization of Frameworks Synthesized

Three M/DABCO samples (M = Ni, Cu and Zn) were synthesized as detailed in Section 4.1. The synthesized samples are characterized by performing thermogravimetric and BET surface area analyses.

7.2.1 Thermogravimetric Analysis (TGA)

The thermo-gravimetric analyses (TGA) of all three M/DABCO samples are shown in Figure 7.2. The first weight loss for samples occurs between 360 and 450 K, corresponds to the removal of solvent DMF molecules. In between 405 and 560 K, the mass of the sample is relatively stable; hence during the adsorption measurements, the materials were activated at temperature between 450 and 500 K. The final weight loss step corresponding to the decomposition of the sample and collapse of the crystal structure starts about 573 K for Cu/DABCO and Zn/DABCO and at about 680 K for Ni/DABCO.

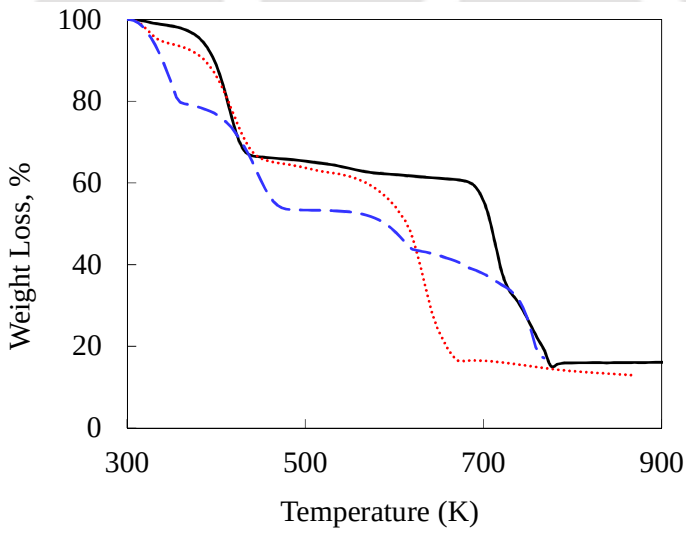

Figure 7.2: Thermogram of Ni/DABCO (——), Cu/DABCO (·····) and Zn/DABCO (– – –) at a heating rate of 5 K min^{-1} under flow of N_2.

7.2.2 Surface Area and Pore Volume Analysis

N_2 physisorption isotherms at 77 K (Figure 7.3a) were used for the calculation of BET surface area and pore volume. Prior to measurement of N_2 adsorption at 77 K, all the samples were degassed by heating them at 453 K under vacuum. N_2 loadings at 77 K were converted into amount adsorbed per unit cell (Figure 7.3b) to eliminate the effect of formula weight of the unit cell. The comparison of BET surface area and pore volume with existing literature is listed in Table 7.1. The obtained surface area and pore volume for these compounds are similar to that reported in literature earlier; slight difference between the results of different research groups is common in MOF literature and is attributed to the presence of impurities including the solvent molecules in these samples. The same reason is attributed for somewhat lower surface area exhibited by Cu/DABCO material. Even after several attempts, we were unable to improve the surface area of Cu/DABCO MOF. Indeed it is interesting to note that one other reported literature on Cu/DABCO also lists a surface area of 1400 $m^2 g^{-1}$.

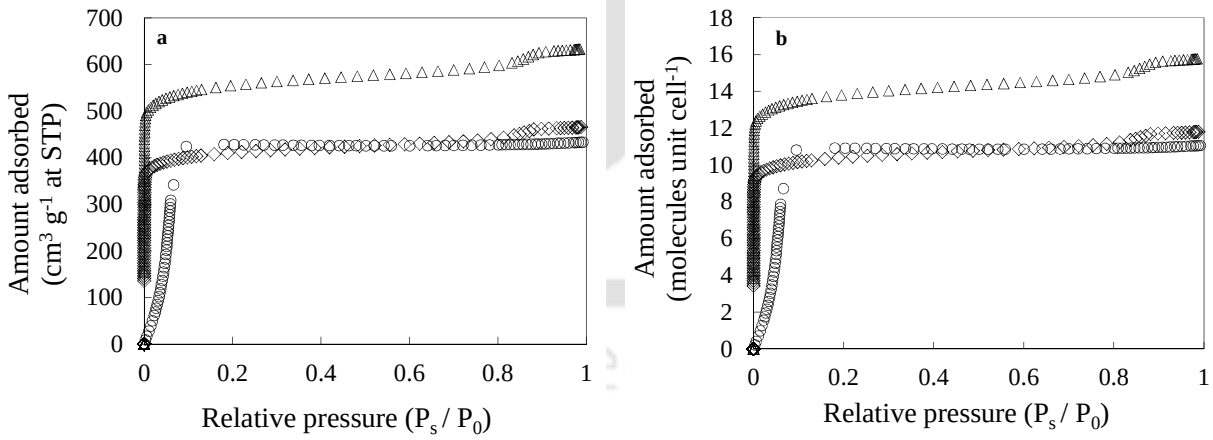

Figure 7.3: (**a**) N_2 adsorption at 77 K on Ni/DOBDC (Δ), Cu/DOBDC (◊) and Zn/DOBDC (○); (**b**) N_2 loadings per unit cell.

Table 7.1: Surface area and pore volume of Ni/DABCO, Cu/DABCO and Zn/DABCO MOFs.

Compound	Surface area $m^2\ g^{-1}$	$nm^2\ uc^{-1}$	Pore volume $cm^3\ g^{-1}$	$nm^3\ uc^{-1}$	Reference
Ni/DABCO	1904	1.76	0.98	0.91	this work
	1705	–	0.82	–	[**79**]
	1925	–	0.74	–	[**75**]
Cu/DABCO	1415	1.33	0.72	0.68	this work
	1400	–	0.71	–	[**80**]
Zn/DABCO	1863	1.77	0.67	0.64	this work
	1450	–	–	–	[**55**]
	1725	–	0.85	–	[**79**]

7.3 Adsorption Isotherms

In order to evaluate the role of both electrostatic and dispersion interactions on adsorption characteristics of M/DABCO MOFs, the adsorption measurement of four gases (CO_2, CH_4, CO and N_2) with varying polarity and polarizability were performed on these MOFs.

7.3.1 CO_2 Isotherms

Adsorption isotherms of CO_2 on all samples at 294, 314 and 350 K are shown in Figure 7.4. All isotherms exhibit type-I shape which is to be expected as M/DABCO adsorbents are microporous in nature. CO_2 loading on Ni/DABCO measured in this work is slightly higher than that reported by Liang et al. [**79**] and comparable to that reported by Arstad et al. [**75**]. CO_2 capacities obtained on Zn/DABCO at ambient temperature are slightly lower than that reported by Karra et al. [**121**] and comparable to that reported by Liang et al. [**79**]. In addition, to the best of our knowledge CO_2 isotherms on Cu/DABCO are measured first time in this work.

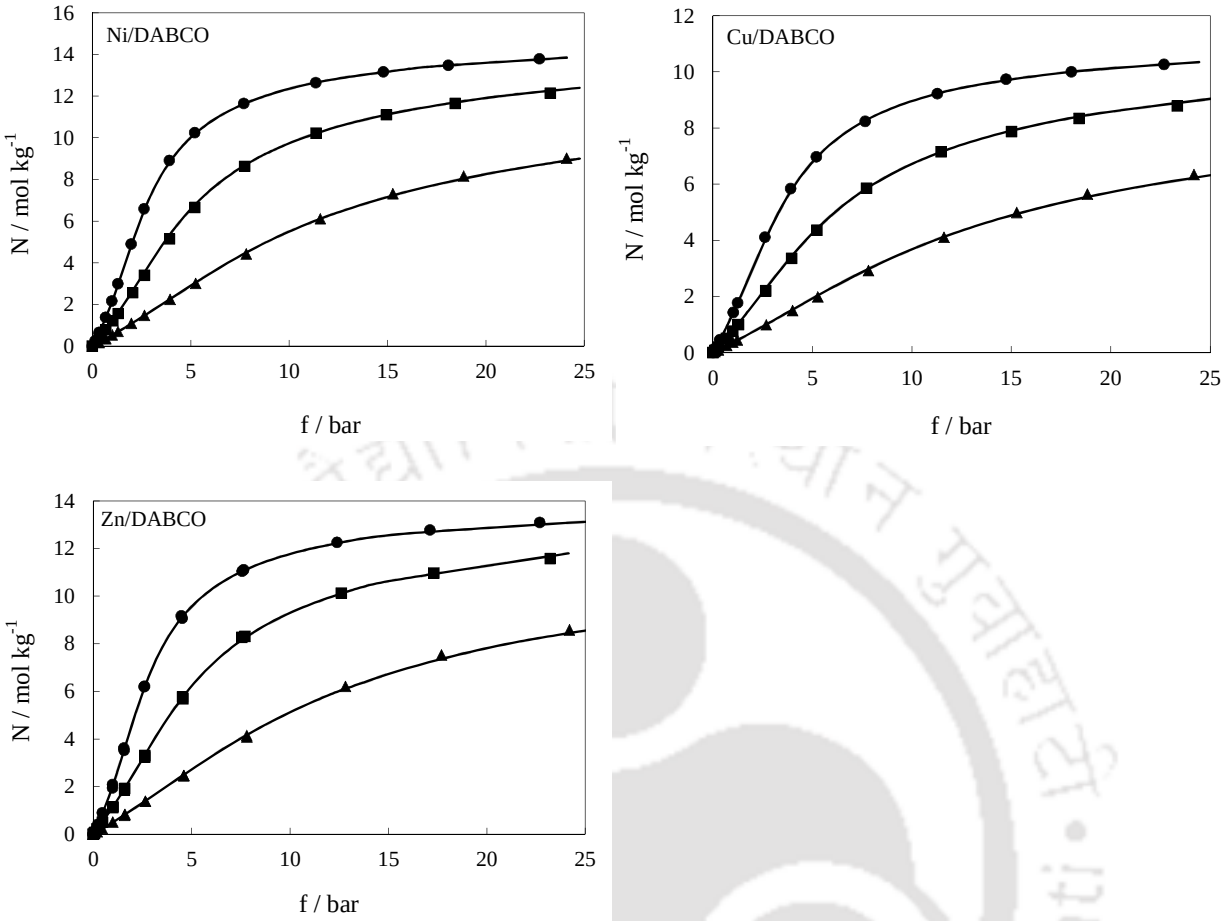

Figure 7.4: Isotherms of CO_2 on DABCO MOFs. Symbols: experimental data at 294 K (●), 314 K (■) and 350 K (▲); lines are fits using Langmuir-virial isotherm parameters from Table 7.2.

CO_2 loading at 294 K and 0.1 bar on DABCO compounds is only ~ 0.2 mol kg^{-1}; this adsorption uptake is significantly lower than that on previously studied DOBDC compounds (2.1 – 4.7 mol kg^{-1}). However, at 25 bar, loading on DABCO MOFs (11 – 14 mol kg^{-1}) is similar to that on DOBDC frameworks. CO_2 loading on DABCO MOFs at about ambient conditions (1.4 – 2.2 mol kg^{-1}) is higher than that on IRMOF-1 (0.98 mol kg^{-1}). Though both DABCO MOFs as well as IRMOF-1 do not have open metal sites, smaller pore diameter for DABCO MOFs (~7.6 Å) compared to that for IRMOF-1 (~14.5 Å) results into better adsorption uptake on DABCO MOFs at lower pressure. CO_2 loading on Ni/DABCO (2.2 mol kg^{-1}) and Zn/DABCO (2.13 mol kg^{-1}) at

about ambient conditions is also higher than that on IRMOF-3 (1.4 mol kg^{-1}), MOF-177 (1.1 mol kg^{-1}), ZIF-8 (1.3 mol kg^{-1}) [**37**], MIL-47 (1.5 mol kg^{-1}) [**42**]; it is comparable to that on AC (Norit R1) (2.2 mol kg^{-1}) [**128**], H-mordenite (2.2 mol kg^{-1}) [**217**], Na-ZSM-5 (1.9 mol kg^{-1} at 0.72 bar) [**32**] and silicalite (2.3 mol kg^{-1}) [**99**]. The loading on these DABCO MOFs for CO_2 at ambient conditions is lower than that on MOFs containing open metal sites (such as CuBTC (5.5 mol kg^{-1}) [**76**], MIL-101 (2.5 mol kg^{-1}) [**74**] and MgDOBDC (7.8 mol kg^{-1}) [**97**]). While the loading in the low pressure region is lower for the DABCO MOFs compared to that of CuBTC [**95**], as the pores are gradually filled this difference decreases since pore volume of these MOFs are comparable. On the other hand, the pore volume of MIL-101 [**95**] is considerably higher and hence it exhibits a higher saturation capacity than DABCO MOFs (Figure 7.5).

CO_2 loading on Cu/DABCO is somewhat lower than that on Ni/DABCO and Zn/DABCO throughout the entire measurement conditions due to smaller surface area. Nevertheless, as in case of Ni/DABCO and Zn/DABCO, Cu/DABCO also has better CO_2 adsorption capacity (1.4 mol kg^{-1}) at ambient condition than MOFs like IRMOF-1 [**37**], MOF-177 [**37**], ZIF-8 [**37**] etc.

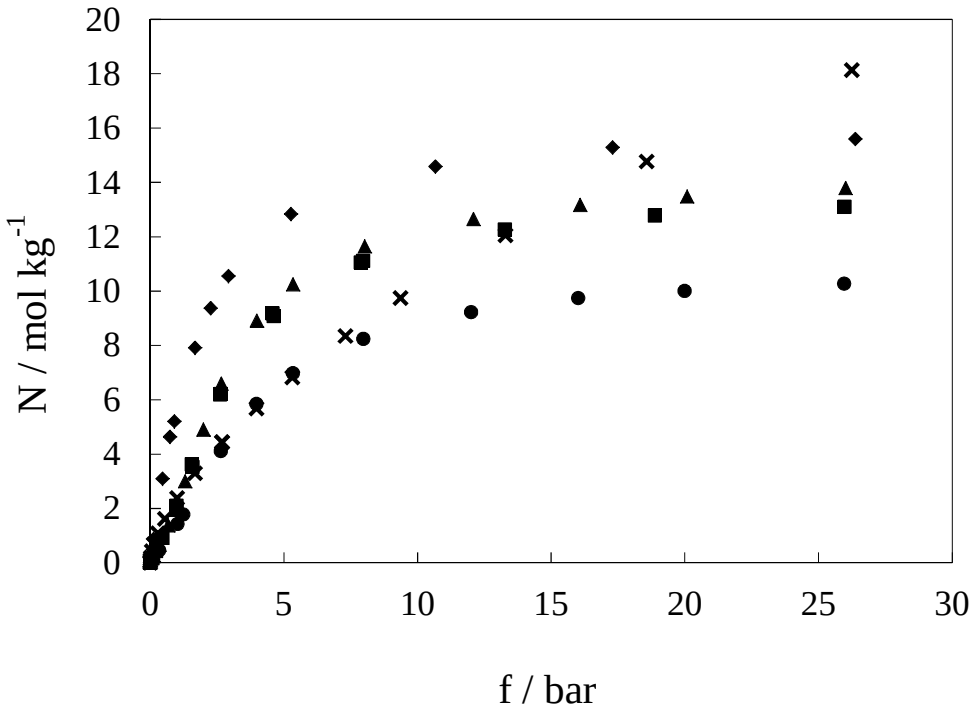

Figure 7.5: Comparision of CO_2 isotherms on Ni/DABCO (▲), Cu/DABCO (●), Zn/DABCO (■), at 294 K, CuBTC (♦) [**95**] and MIL-101 (×) [**95**], at 295 K.

7.3.2 CH_4 Isotherms

Figure 7.6 shows adsorption of CH_4 on DABCO MOFs at three different temperatures. As in case of CO_2, isotherms are of type-I. CH_4 adsorption capacities, measured in this work on Zn/DABCO are similar to that reported by Liang et al. [**79**]; however in case of Ni/DABCO, slightly higher adsorption capacities are obtained in this work. In contrast to CO_2, CH_4 loading on DABCO MOFs are comparable to that on DOBDC MOFs (studied in the previous chapter) over the entire range of pressure and temperature. Ni/DABCO and Zn/DABCO show higher saturation gravimetric capacity (~11 mol kg^{-1}, obtained from model parameter) for CH_4 at 294 K than zeolites like 13X (2.9 mol kg^{-1}) [**35**], 4A (1.5 mol kg^{-1}) and 5A (2.9 mol kg^{-1}) [**225**]. But saturation gravimetric capacities on these MOFs are lower than that on MOF-200 (8.17 mol kg^{-1}) [**38**], MOF-205 (10.77 mol kg^{-1}) [**38**], MOF-210 (9.36 mol kg^{-1}) [**38**], MIL-101 (7.1 mol kg^{-1})

[**74, 94**] and activated carbon (AX-21) (11.59 mol kg^{-1}) [**100**] due to the smaller pore volume of DABCO MOFs. On the other hand, volumetric saturation uptake of CH_4 on Zn/DABCO MOFs (~9 mol L^{-1}) is substantially higher than that on MOFs with large void fraction such as MOF-200 (1.8 mol L^{-1}) [**38**], MOF-205 (4.08 mol L^{-1}) [**38**], MOF-210 (2.4 mol L^{-1}) [**38**], MIL-101 (3.2 mol L^{-1}) [**74, 94**], and activated carbons (5.7 mol L^{-1}) (AX-21) [**100**].

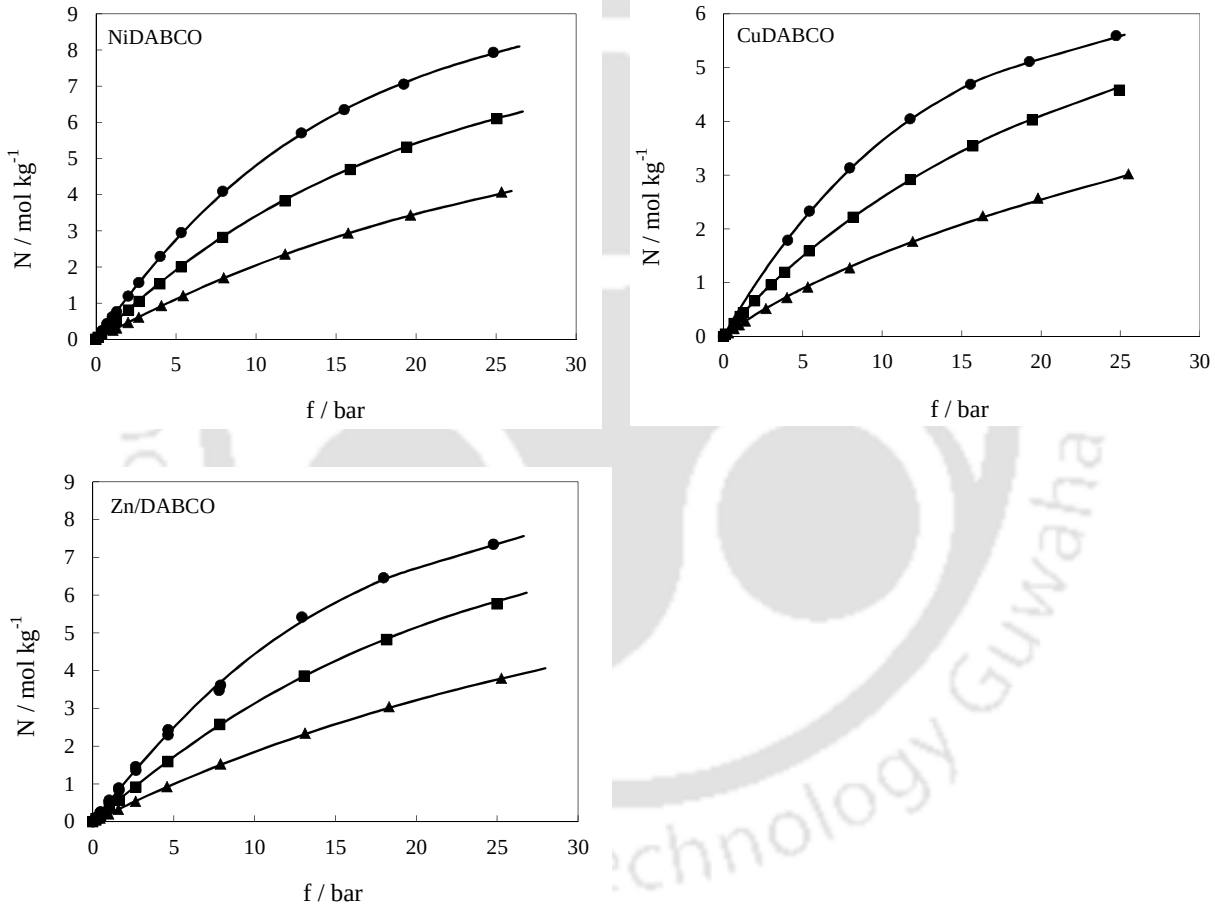

Figure 7.6: Isotherms of CH_4 on DABCO MOFs. Symbols: experimental data at 294 K (●), 314 K (■) and 350 K (▲); lines are fits using Langmuir-virial isotherm parameters from Table 7.3.

7.3.3 CO Isotherms

Adsorption isotherms of CO on DABCO MOFs at all three temperatures studied are shown in Figure 7.7. These isotherms do not reach the saturation uptake capacity within the experimental pressure range. The adsorption capacities measured in this work for CO on Zn/DABCO at 294 K are slightly lower than those reported by Karra et al. [**121**]. CO adsorption isotherms for Ni/DABCO and Cu/DABCO are not reported in the literature to the best of our knowledge. Similar to CO_2, adsorption uptake of CO on DABCO samples is substantially lower compared to that on DOBDC samples; this trend continues and even at 25 bar loading on DABCO samples is lower. CO adsorption uptake at 294 K and 1 bar on Ni/DABCO and Zn/DABCO (0.25 mol kg^{-1}) is comparable to uptake on silicalite (0.27 mol kg^{-1}) [**124**], IRMOF-1 (~0.2 mol kg^{-1}) [**121**], IRMOF-3 (~0.25 mol kg^{-1}) [**121**]; however it is substantially lower than that on Zeolite 5A (~1 mol kg^{-1}) [**226**], CuBTC (1.43 mol kg^{-1}) and MIL-101 (0.89 mol kg^{-1}) [**95**]. Adsorption uptakes of CO on DABCO MOFs at high pressure (*ca.* 25 bar) and 294 K temperature (~4 mol kg^{-1}) are comparable to IRMOF-1 (~4 mol kg^{-1}) [**121**], IRMOF-3 (~4 mol kg^{-1}) [**121**] and MIL-101 (~4 mol kg^{-1}) [**95**] but these uptakes are lower compared to corresponding uptakes on M/DOBDC (~7 mol kg^{-1}) [**227**] and Cu-BTC (~8 mol kg^{-1}) [**95**].

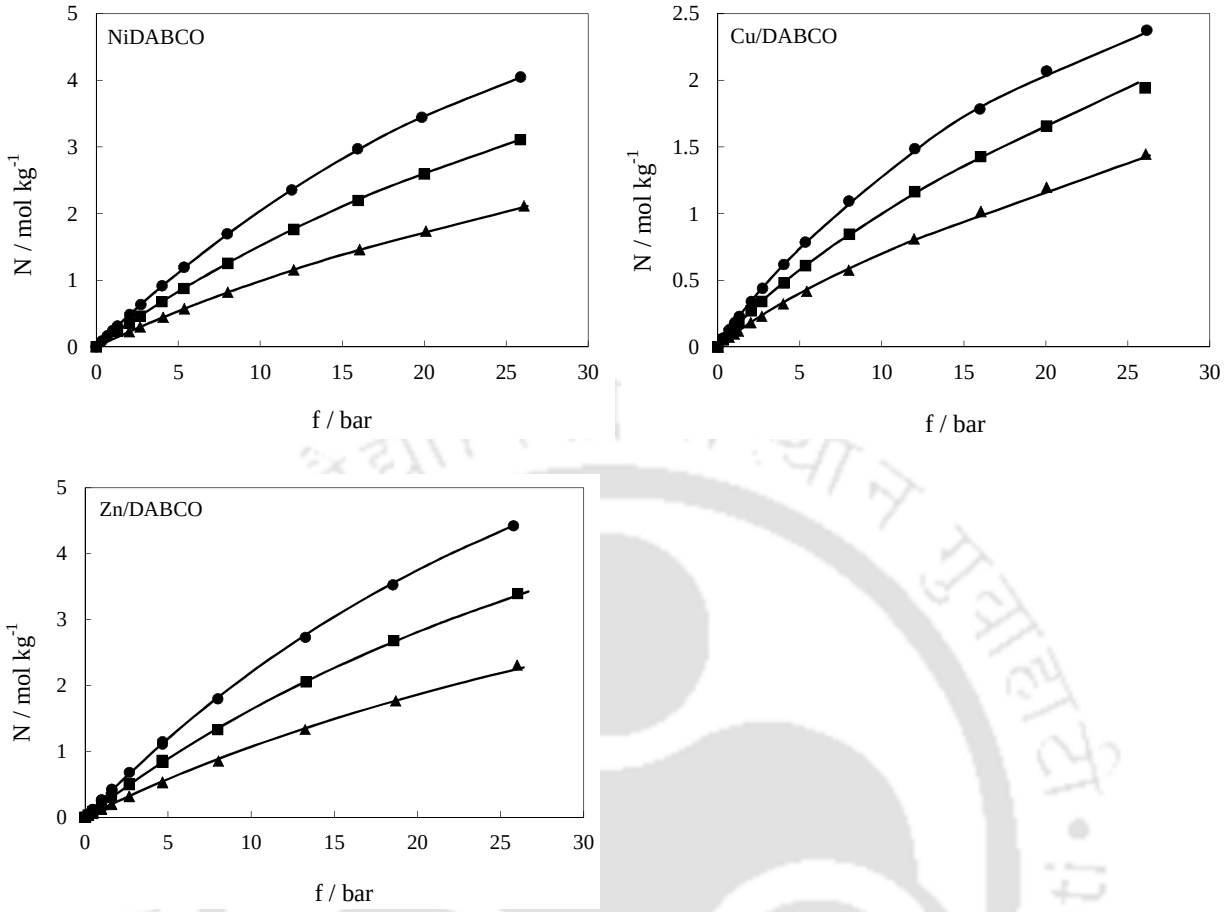

Figure 7.7: Isotherms of CO on DABCO MOFs. Symbols: experimental data at 294 K (●), 314 K (■) and 350 K (▲); lines are fits using Langmuir-virial isotherm parameters from Table 7.4.

7.3.4 N_2 Isotherms

N_2 isotherms of DABCO MOFs are shown in Figure 7.8. As in case of CO, the isotherms for N_2 do not reach their corresponding saturation capacities within the experimental pressure range. The capacities obtained in this work for N_2 on Zn/DABCO at 294 K are slightly lower than those reported by Karra et al. [**121**]. On the other hand, N_2 capacities on Ni/DABCO are slightly higher than those reported by Liang et al. [**79**]. Adsorption uptake of N_2 is also lower for DABCO compounds than that for DOBDC compound in the Henry's region; however, at 25 bar only marginal difference exists between adsorption uptakes of these compounds. N_2 loading at 294 K and 1 bar on DABCO MOFs vary between 0.09 to 0.14 mol kg^{-1}; this value is comparable to that on silicalite (~0.2 mol kg^{-1}) [**126**], MOF-177 (0.2 mol kg^{-1}) [**68**], and is lower than that on MIL-53(Al) (0.3 mol kg^{-1}) [**107**] and Zeolite 13X (~0.4 mol kg^{-1}) [**35**].

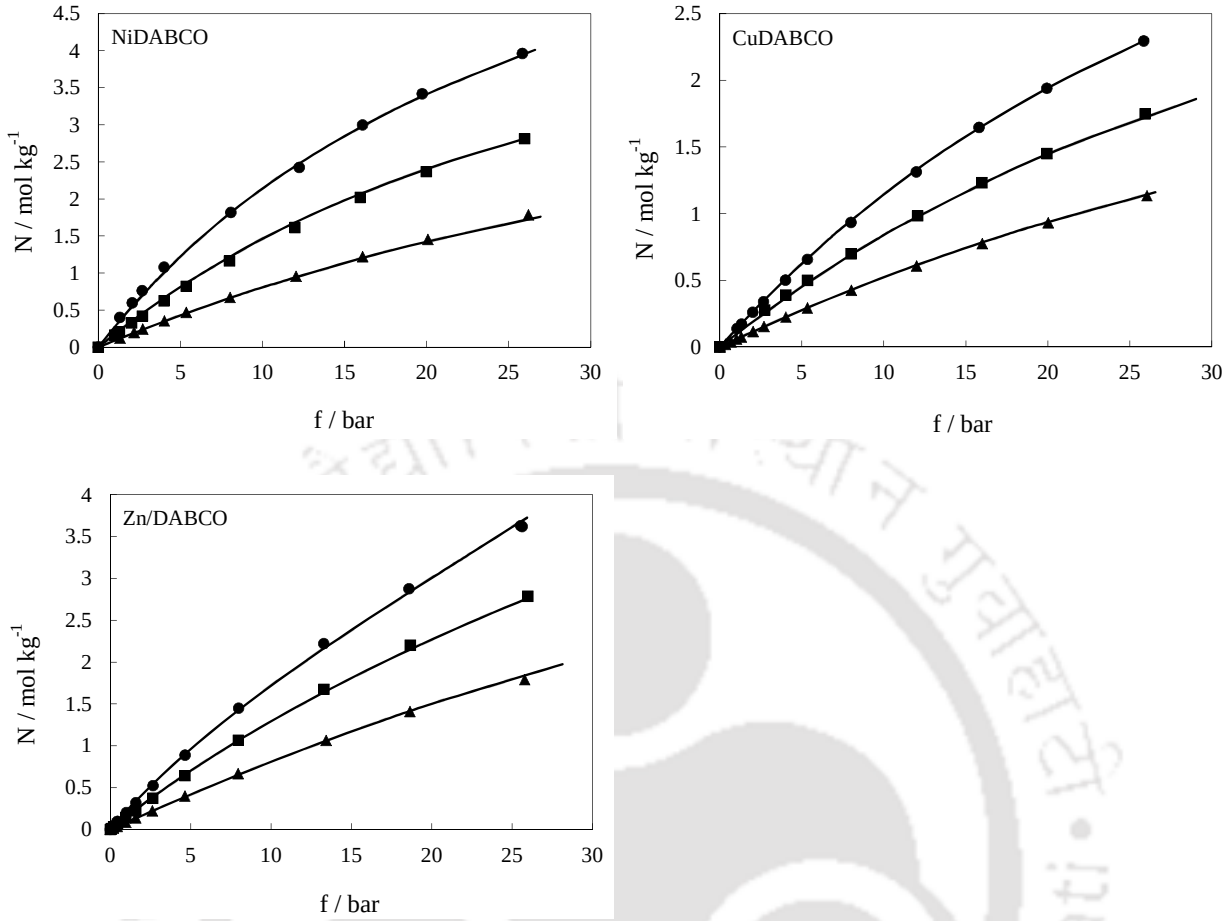

Figure 7.8: Isotherms of N_2 on DABCO MOFs. Symbols: experimental data at 294 K (●), 314 K (■) and 350 K (▲); lines are fits using Langmuir-virial isotherm parameters from Table 7.5.

7.4 Isotherm Modeling

The modeling of adsorption isotherms provides a useful insight into the adsorption energetics [**74**]. A simple Langmuir equation did not fit the adsorption isotherms indicating the heterogeneity which is likely to exist because of the inherent nature of MOFs (with several functional groups in their structure). So, a Langmuir-virial isotherm was used to model adsorption of CO_2, CO and CH_4 on these materials (Eq. 3.13). As N_2 isotherm does not exhibit saturation behavior within the experimental range, any attempt to model it with Eq. 3.13 yields statistically insignificant value for the saturation loading (N^{max}). Hence, only a simple virial isotherm (Eq. 3.11) with three parameters was used to describe the adsorption behavior of N_2. The parameters for isotherm models of the four gases on the three DABCO MOFs studied in this work are given in Tables 7.2 − 7.5.

Table 7.2: Langmuir-virial isotherm model parameters for CO_2 adsorption on DABCO MOFs.

Parameters	Ni/DABCO Coefficient *(Std. Error)*	Cu/DABCO Coefficient *(Std. Error)*	Zn/DABCO Coefficient *(Std. Error)*
$\beta^{(0)}\times10^4$, mol kg^{-1} bar^{-1}	6.63	4.19	6.33
	(0.10)	*(0.07)*	*(0.09)*
$\beta^{(1)}$, K	2320	2354	2328.5
	(36)	*(45)*	*(33)*
$b^{(0)}$, mol^{-1} kg	− 0.070	− 0.212	0.020
	(0.059)	*(0.103)*	*(0.059)*
$b^{(1)}$, mol^{-1} kg K	− 29.1	10.8	− 55.4
	(18.8)	*(33.0)*	*(18.6)*
$c^{(0)}$, mol^{-2} kg^2	0.036	0.079	0.030
	(0.006)	*(0.014)*	*(0.006)*
$c^{(1)}$, mol^{-2} kg^2 K	− 9.2	− 22.1	− 7.4
	(1.8)	*(4.4)*	*(1.9)*
N^{max}, mol kg^{-1}	15.0	11.3	14.2
	(0.1)	*(0.1)*	*(0.1)*

Table 7.3: Langmuir-virial isotherm model parameters for CH_4 adsorption on DABCO MOFs.

Parameters	Ni/DABCO Coefficient *(Std. Error)*	Cu/DABCO Coefficient *(Std. Error)*	Zn/DABCO Coefficient *(Std. Error)*
$\beta^{(0)}\times10^4$, mol kg^{-1} bar^{-1}	16.38	25.91	18.14
	(0.26)	*(0.49)*	*(0.35)*
$\beta^{(1)}$, K	1743	1562	1670
	(32)	*(37)*	*(38)*
$b^{(0)}$, mol^{-1} kg	0.073	1.126	0.284
	(0.107)	*(0.127)*	*(0.061)*
$b^{(1)}$, mol^{-1} kg K	− 38.4	− 345.1	− 107.2
	(32.6)	*(40.7)*	*(20.0)*
$c^{(0)}$, mol^{-2} kg^2	0.050	− 0.153	−
	(0.019)	*(0.030)*	−
$c^{(1)}$, mol^{-2} kg^2 K	− 14.7	41.4	−
	(6.2)	*(9.9)*	−
N^{max}, mol kg^{-1}	11.6	7.2	10.7
	(1.0)	*(0.2)*	*(0.5)*

Table 7.4: Langmuir-virial isotherm model parameters for CO adsorption on DABCO MOFs.

Parameters	Ni/DABCO Coefficient *(Std. Error)*	Cu/DABCO Coefficient *(Std. Error)*	Zn/DABCO Coefficient *(Std. Error)*
$\beta^{(0)}\times10^4$, mol kg^{-1} bar^{-1}	22.32	34.5	31.58
	(0.17)	*(0.87)*	*(0.47)*
$\beta^{(1)}$, K	1387	1188	1296
	(15)	*(45)*	*(0.27)*
$b^{(0)}$, mol^{-1} kg	0.342	1.455	0.580
	(0.095)	*(0.487)*	*(0.080)*
$b^{(1)}$, mol^{-1} kg K	− 114.4	− 382.6	− 181.8
	(28.3)	*(152.0)*	*(28.7)*
$c^{(0)}$, mol^{-2} kg^2	0.036	− 0.584	−
	(0.033)	*(0.283)*	−
$c^{(1)}$, mol^{-2} kg^2 K	− 16.7	120.1	−
	(10.6)	*(91.7)*	−
N^{max}, mol kg^{-1}	6.4	3.2	10.0
	(0.4)	*(0.2)*	*(2.1)*

Table 7.5: Virial isotherm model parameters for N_2 adsorption on DABCO MOFs.

Parameters	Ni/DABCO Coefficient *(Std. Error)*	Cu/DABCO Coefficient *(Std. Error)*	Zn/DABCO Coefficient *(Std. Error)*
$\beta^{(0)}\times 10^4$, mol kg^{-1} bar^{-1}	2.20	6.67	4.91
	(0.10)	*(0.11)*	*(0.13)*
$\beta^{(1)}$, K	2103	1560	1806
	(122)	*(39)*	*(66)*
$b^{(0)}$, mol^{-1} kg	0.016	0.363	−0.758
	(0.651)	*(0.375)*	*(0.495)*
$b^{(1)}$, mol^{-1} kg K	23.6	−78.2	282.6
	(200.9)	*(117.0)*	*(151.8)*
$c^{(0)}$, mol^{-2} kg^2	0.262	0.334	0.273
	(0.259)	*(0.256)*	*(0.224)*
$c^{(1)}$, mol^{-2} kg^2 K	−72.7	−87.4	−86.3
	(77.1)	*(76.9)*	*(66.7)*

7.5 Effect of Physical Properties of the Adsorbate

The excess adsorption isotherms of CO_2, CO, CH_4 and N_2 on M/DABCO MOFs at 294 K are shown in Figure 7.9. The trends of the isotherms are similar for all the three frameworks. The adsorption capacities follow the order CO_2>CH_4>CO>N_2 over the entire experiment range for all samples. Lower adsorption capacities of CO, CH_4 and N_2 gases compared to that of CO_2 can easily be attributed to the smaller polarizability and bigger kinetic diameter of these gases (Table 4.6). Although CO has a permanent dipole, its adsorption uptake is lower than that of CH_4 (which is non-polar but has higher polarizability) on these MOFs; this indicates the negligible role of electrostatic interactions between CO molecules and M/DABCO frameworks due to coordinative saturation of metal atoms in these frameworks. Simulation results of Karra et al. [**121**] also show similar observations. However, this trend is very different to the adsorption of

CH_4 and CO on previously studied M/DOBDC MOFs with open metal sites where electrostatic interaction of CO with metal centers also plays an important role. In addition, the isotherms for CO and N_2 (both these gases have polarizability and kinetic diameter close to one another) on all the three MOFs almost overlap again confirming the negligible role of the electrostatic interactions between CO and the framework in the adsorption on DABCO MOFs.

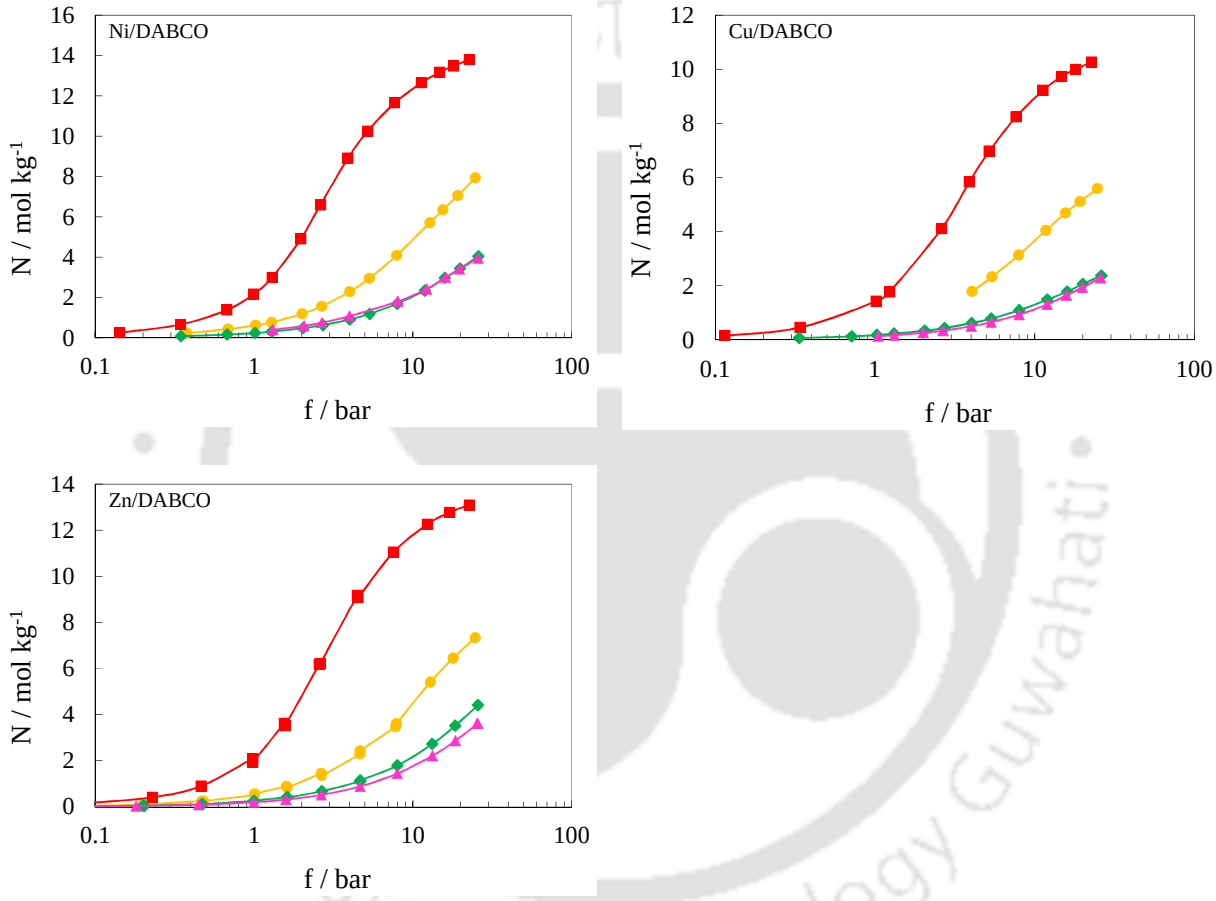

Figure 7.9: Adsorption isotherms of CO_2 (■), CO (♦), CH_4 (●) and N_2 (▲) on DABCO MOFs at 294 K; lines are drawn as a guide to the eyes.

7.5.1 On Henry's Constants and Adsorption Enthalpy

Variation of Henry's constant of all gases with the temperature is plotted in Figure 7.10 for M/DABCO MOFs. This quantity is useful for understanding the adsorbate-adsorbent interactions

at zero loading. In these DABCO MOFs, the effect of temperature on Henry's constant of both polar (CO_2 and CO) and non-polar (CH_4) gases is almost similar. This is in contrast to open metal sites containing M/DOBDC MOFs where electrostatic interactions dominate.

Henry's constant for CO_2 is higher than that for other gases for DABCO MOFs due to its higher polarizability. For M/DOBDC MOFs studied in the previous chapter, the Henry's constant is larger for CO than that for CH_4 due to the electrostatic interactions between polar CO molecules and *cus* metal sites of these MOFs. In contrast, DABCO MOFs exhibit higher Henry's constants for CH_4; this trend confirms the dominance of dispersion interactions and the negligible role of electrostatic interactions in adsorption on DABCO MOFs. With the increase in polarizability of adsorbates, Henry's constants increase.

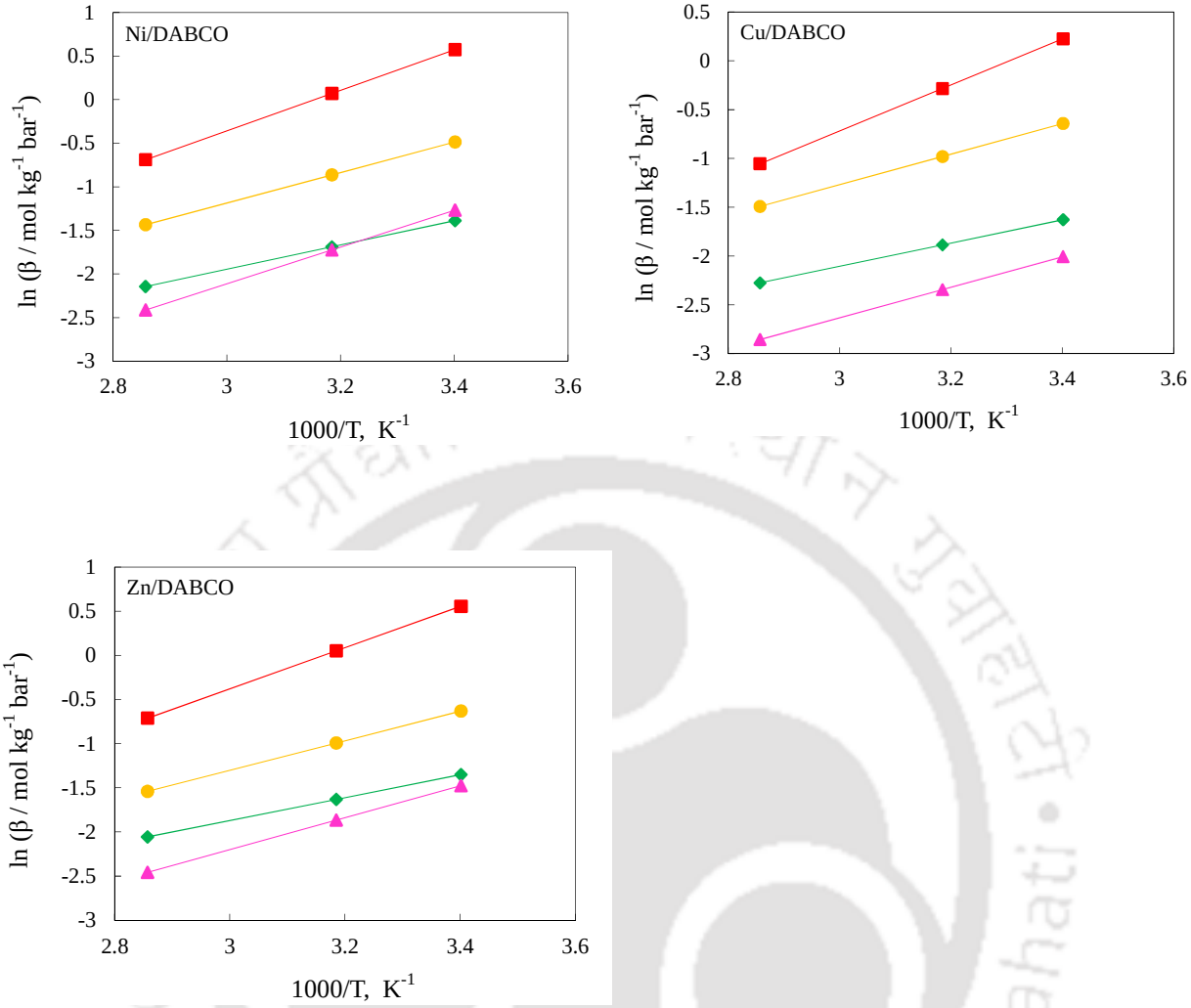

Figure 7.10: Variation of Henry's constant with temperature for CO_2 (■), CO (♦), CH_4 (●) and N_2 (▲) on DABCO MOFs. Lines are drawn as a guide to the eye.

The Henry's constant for CO_2 at 294 K on the DABCO MOFs is higher than that on large pore MOFs like IRMOF-1, IRMOF-3 [**93**], MOF-177 [**37**] and ZIF-8 [**37**]. It is however, lower than that on zeolites like silicalite [**99**], NaX [**139**] and H-mordenite [**217**] and on MOFs with open metal sites like Mg/DOBDC [**227**], Mn/DOBDC [**227**], Co/DOBDC [**227**], Ni/DOBDC [**227**], CuBTC [**76, 216**], MIL-53(Al) [**42**] and MIL-101 [**74, 94**]. The Henry's constant for CH_4 at 294 K is comparable to that on silicalite [**124**]. It is lower than that on CuBTC [**216**], MIL-101 [**74, 94**] and activated carbon (Norit R1) [**128**]. However, DABCO MOFs show higher capacity for

CH_4 than silicalite [**124**], zeolites like 13X [**35**], 4A [**225**] and 5A [**225**] due to their larger pore volume. The Henry's constant for CO is comparable to that on silicalite [**124**]; however it is lower than that on Zeolite 5A [**226**], MOFs like M/DOBDC [**227**], CuBTC [**121, 216, 71**] and MIL-101 [**74**] which contain open metal sites. Finally, the Henry's constant for nitrogen is comparable to that on silicalite [**124, 142**] and MOF-177 [**68**]; however, it is lower than that on M/DOBDC [**227**], CuBTC [**35, 93, 126, 216**], zeolites like 5A [**143, 228**] and 13X [**35, 127, 225**].

The variation of adsorption enthalpy ($-\Delta h_{ads}$) with loading is shown in Figure 7.11 for M/DABCO MOFs. Since the isotherms of CO and N_2 cover a loading of only about 2 − 3 mol kg^{-1} at 350 K, enthalpy plots for these gases are limited to only 2 − 3 mol kg^{-1} loading to avoid any extrapolation of data. Adsorption enthalpy at zero coverage ($-\Delta h_{ads,0}$) for CO_2 is higher than that for other gases. Polar CO exhibits lower enthalpy ($-\Delta h_{ads,0}$) than non-polar CH_4. For all gases, an increase in adsorption enthalpy is observed with increase in loading. This increase is due to increased lateral interactions between adsorbate moleclues. These results for enthalpy closely follow the reported values from GCMC simulations by Karra et al. [**121**] on Zn/DABCO MOF for CO_2, CO and N_2. This is in contrast to DOBDC MOFs where enthalpy decreases sharply for polar gases after the open metal sites are filled.

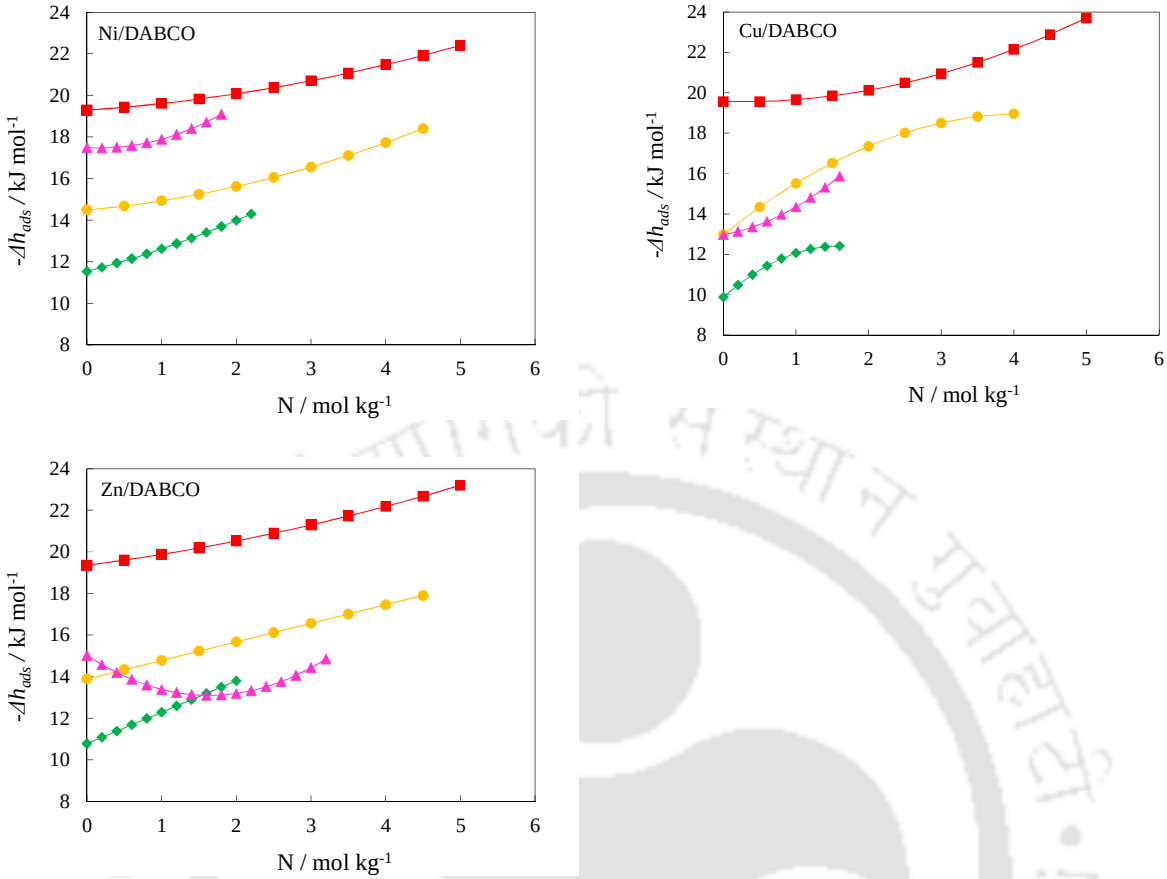

Figure 7.11: Variation of adsorption enthalpy with loading for CO_2 (■), CO (♦), CH_4 (●) and N_2 (▲) on DABCO MOFs. Lines are drawn as a guide to the eye.

The adsorption enthalpy ($-\Delta h_{ads}$) for CO_2 on DABCO MOFs varies between 19.4 to 24.7 kJ mol^{-1} and is similar to that reported by Liang et al. [**79**] on these materials. This is about 1.7 times lower than that on Mg/DOBDC MOF studied in the previous chapter. This value is also lower than that on MOFs like CuBTC [**35**], MIL-100, MIL-101 [**94**] and zeolites like 13X [**32**]. This difference is mainly due to absence of unsaturated metal sites and electrostatic interactions. The adsorption enthalpy ($-\Delta h_{ads}$) for CH_4 varies between 13.9 and 19 kJ mol^{-1} and is comparable to that on M/DOBDC (studied in the previous chapter) [**227**], 13 X [**127**], AS activated carbon [**127**], MIL-53 [**42**], MIL-100 [**86**], IRMOF-3 [**93**], NaX [**145, 229**] and NaY [**145, 229**] but slightly higher than that on large pore MOF like IRMOF-1 [**93**]. The enthalpies of adsorption at

zero loading for CO on DABCO MOFs ($-\Delta h_{ads,0}$ between 10 – 12 kJ mol^{-1}) is about 4 times lower that on Ni/DOBDC MOF (reported in previous chapter.) It is also lower than that on zeolite like 5A [**217**] and H-mordernite [**217**], but it is comparable to that on silicalite [**126**]. Finally, the enthalpy of adsorption for N_2 varies between 13.3 and 15.1 kJ mol^{-1} and comparable to that on silicalite [**126**]. It is higher than that on large pore MOFs like IRMOF-1 and IRMOF-3 [**93**] but lower than that on M/DOBDC (studied in the previous chapter) [**227**], CuBTC [**93, 230**], silicalite [**93, 230**] and CaA [**93, 230**].

The lower values of enthalpy of adsorption for these MOFs in general would make it easier to regenerate these materials. However, it must be emphasized that low enthalpy of adsorption at zero coverage implies weak adsorbate-adsorbent interactions and hence results into low loading in the low pressure region. The design of an efficient adsorption process requires consideration of several aspects and has been discussed elsewhere in literature [**158, 231 − 233**] in detail.

7.6 Effect of Metal Cation in the Framework

The effect of different metal cations in the M/DABCO (M = Ni, Cu and Zn) frameworks on their adsorption characteristics is evaluated by comparing the Henry's constants, the adsorption uptakes at higher pressures and adsorption enthalpies.

7.6.1 On Henry's Constants

Henry's constants of all adsorbates for all the three DABCO frameworks studied in this work are plotted in Figure 7.12. Henry's constants of all gases are similar for Ni/DABCO and Zn/DABCO and it can be concluded that metal atoms have negligible role on adsorption characteristics of DABCO MOFs. This trend is opposite to that obtained in the previous chapter for DOBDC

MOFs where metal constituent of the framework has a decisive role on adsorption characteristics of polar gases. Marginally lower values of Henry's constants are obtained for Cu/DABCO possibly due to presence of left over impurities from the synthesis in this framework as already discussed. Difference between Henry's constant at 294 K and 350 K for same gas (say CO_2 for example) on different MOFs does not change with temperature also indicates the negligible contribution of electrostatic interactions.

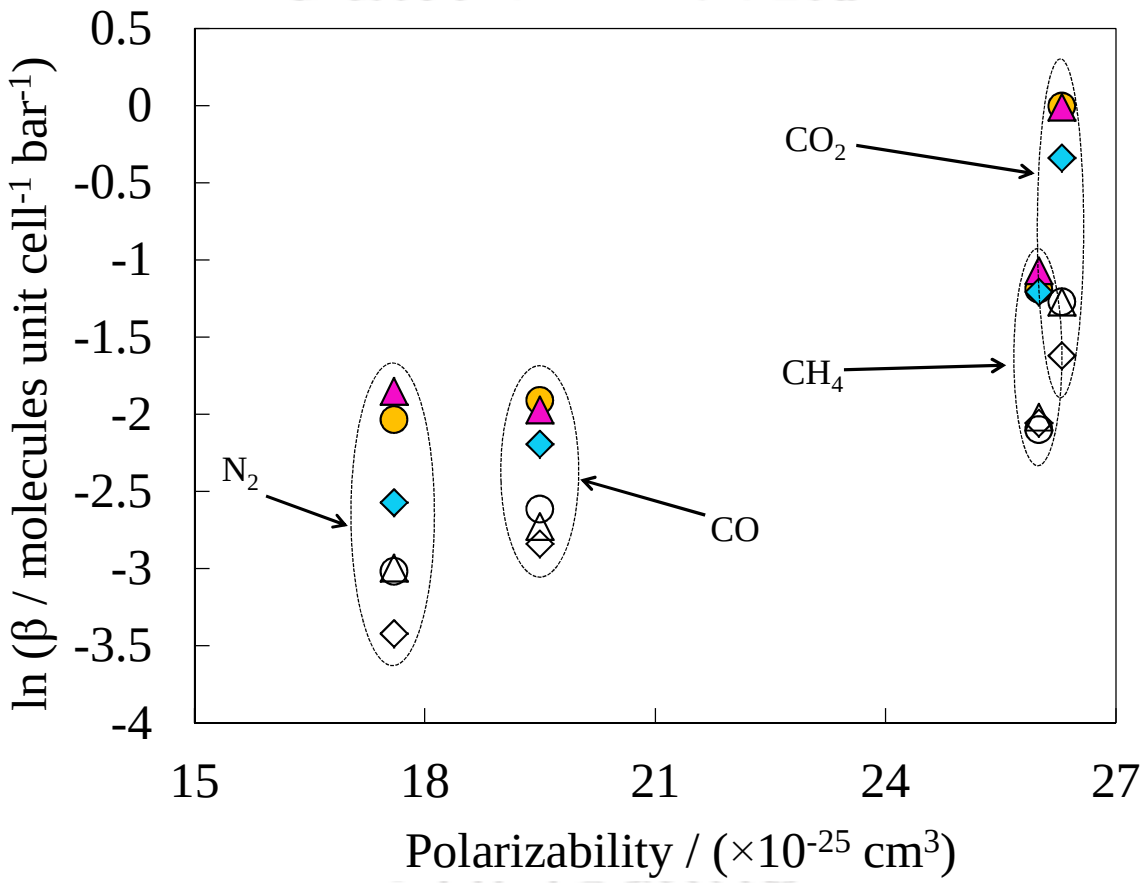

Figure 7.12: Variation of Henry's constants with polarizability for Ni/DABCO (▲), Cu/DABCO (♦) and Zn/DABCO (●); solid symbols represent the values at 294 K and open symbol represent the values at 350 K.

7.6.2 On Adsorption Isotherms at High Pressures

Isotherms of various gases on the three DABCO at 294 K over a wide pressure range are compared in Figure 7.13. As already discussed, the isotherms in the low pressure region are governed by the adsorbent-adsorbate interactions (corresponding to the Henry's constant) while that near the saturation loading are governed by the pore volume of the respective MOFs. Accordingly, Zn/DABCO and Ni/DABCO plots closely follow each other throughout the entire pressure range indicating negligible effect of metal atoms even on saturation loading. However, the capacities on Cu/DABCO are lower than that on Ni/DABCO and Zn/DABCO due to possibly presence of some impurities in Cu/DABCO structure as stated earlier.

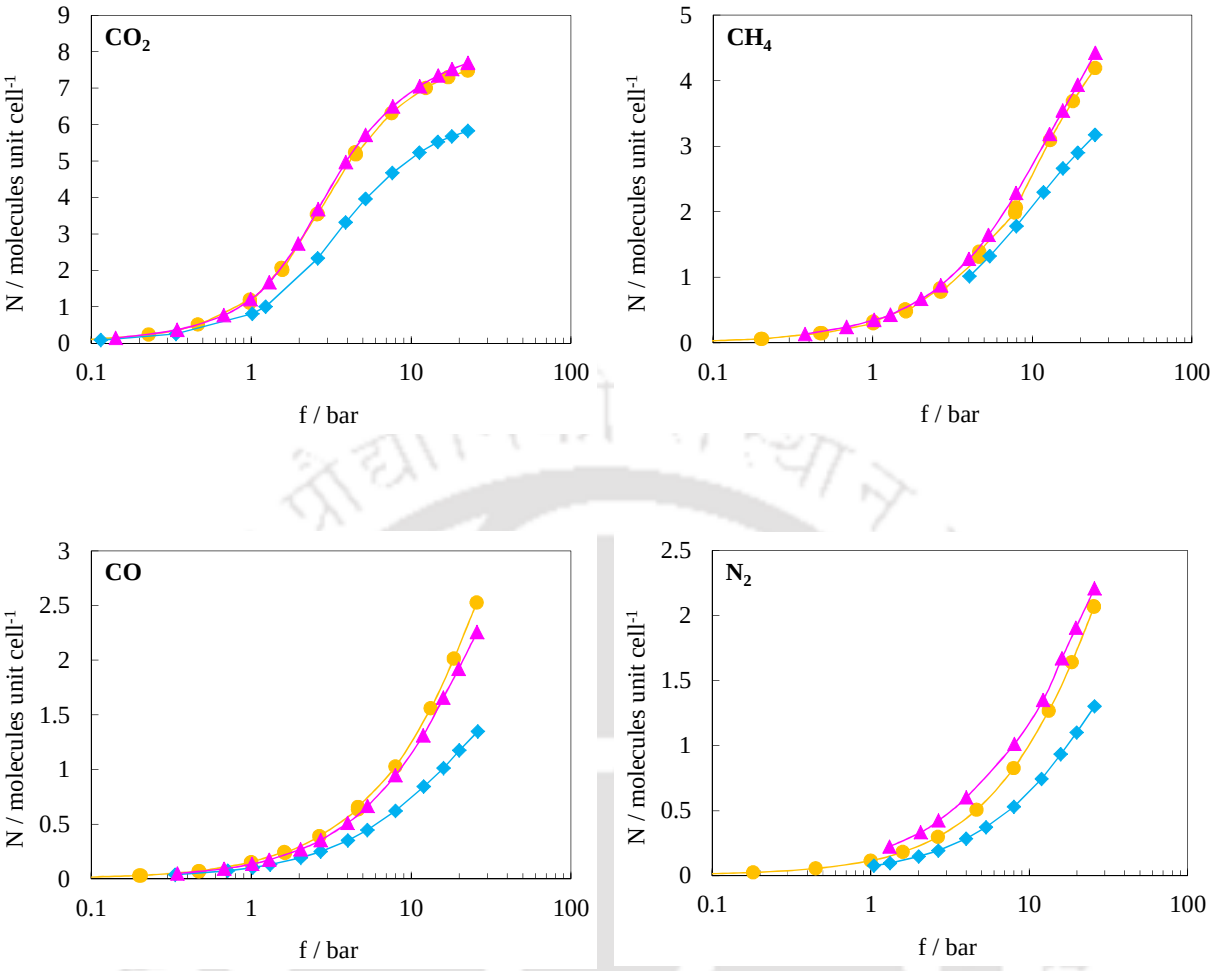

Figure 7.13: Adsorption isotherms of studied gases at 294 K on Ni/DABCO (▲), Cu/DABCO (♦) and Zn/DABCO (●).

7.6.3 On Enthalpy of adsorption

The variation of adsorption enthalpy with loading reveals the strength of host-guest interactions as a function of coverage. The variation in enthalpy of the four gases with loading is plotted for M/DABCO samples (Figure 7.14). The enthalpies on all the three samples for a given gas not only match at zero loading, but they also closely follow one another over the loading range shown.

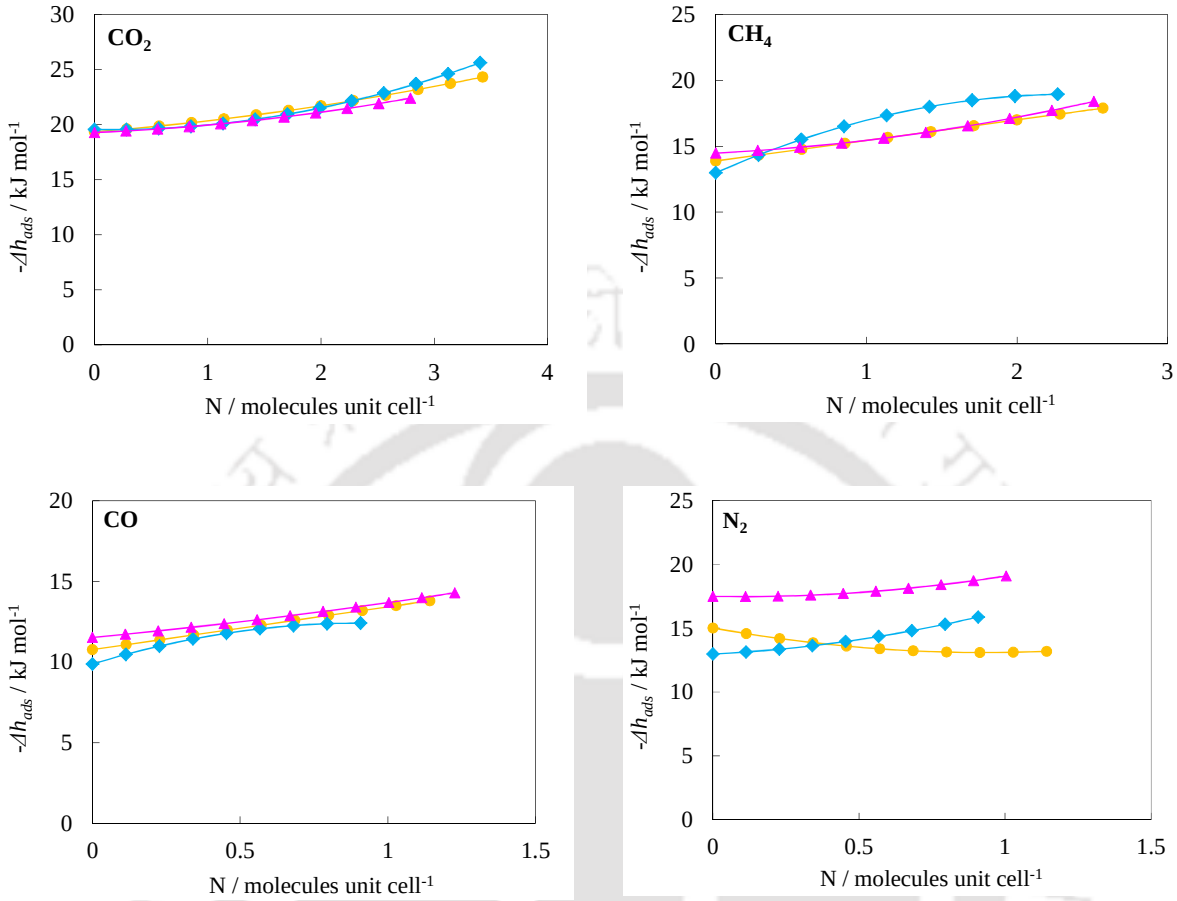

Figure 7.14: Variation of adsorption enthalpy of studied gases with loading for Ni/DABCO (▲), Cu/DABCO (♦) and Zn/DABCO (●).

7.7 Prediction of Binary Selectivity using IAST

The selectivities for different binary mixtures such as CO_2/CO, CO_2/CH_4, CO_2/N_2 and CH_4/CO mixtures at 294 K were predicted using Ideal Adsorbed solution Theory [**198**]. Three different compositions were considered to see its effect for each case.

7.7.1 CH_4 selectivity over CO

In contrast to M/DOBDC MOFs (Figure 6.40), DABCO compounds are found to be selective for CH_4 over CO (Figure 7.15) due to absence of electrostatic interactions and higher dispersion interactions for CH_4 (as it has higher polarizability). The selectivity predicted by IAST for CH_4/CO mixture on DABCO varies between 2 and 3.8 at 294 K for the pressure ranges considered. This selectivity value is higher than that reported on CuBTC (~1) [**71**] and Ni/DOBDC (~0.0022) [**227**]. In case of CuBTC, the selectivity of CH_4/CO mixture is close to unity; even though CO has lower polarizability than CH_4, its dipole moment (and thereby the electrostatic interactions with the open metal centers in the framework) enhances its adsorption. In case of Ni/DOBDC, the adsorbent is strongly selective for CO over CH_4 (with selectivity of ~ 441) due to the strong electrostatic interactions between CO molecules and *cus* Ni metal centers **[227]**. On the other hand, in case of DABCO MOFs, absence of open metal centers result in the MOF being more selective for CH_4 (which has a higher polarizability). In general, the CH_4 selectivity increases with the increase of pressure or increase in composition of CH_4.

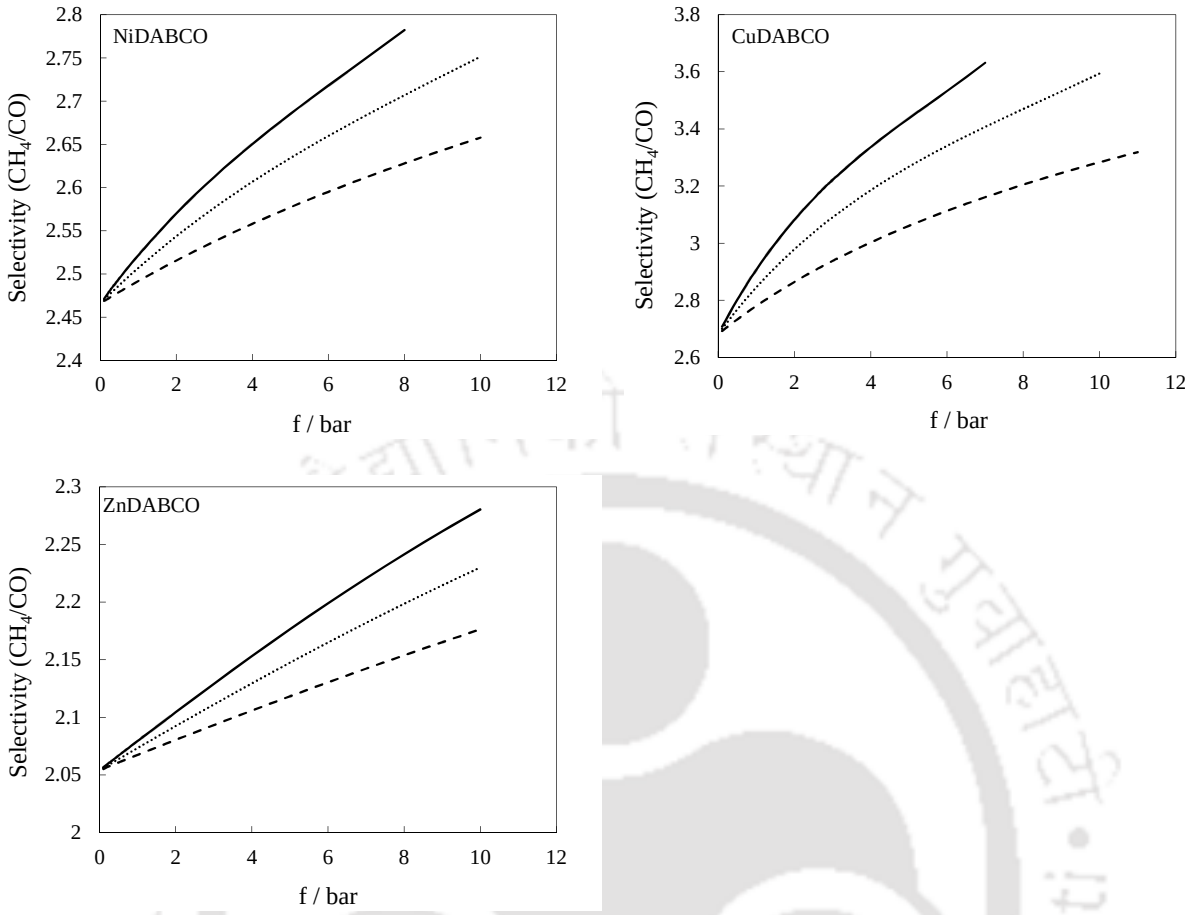

Figure 7.15: Variation of selectivity of CH_4 with pressure at 294 K for different CO compositions: 5 % CO (——), 50 % CO (·····) and 95 % CO (----).

7.7.2 CO_2 selectivity over N_2

The selectivity of CO_2/N_2 binary mixtures is shown in Figure 7.16. The selectivity obtained for Zn/DABCO MOF in this work, is similar to that reported by Karra et al. [**121**]. Selectivity at zero pressure and 294 K on Zn/DABCO is 7.6; it is slightly higher than that on Ni/DABCO (6.3) and is slightly lower than that on Cu/DABCO (9.3). These selectivity values are comparable to that on MOF-177 (7) [**159**] and MFI (10) [**159**]; they are higher than that on large pore MOFs like IRMOF-1 (4) [**159**] and IRMOF-3 (5) [**159**]. But, they are significantly lower than that on

CuBTC (20) [**159**], NaX (200) [**159**], bio-MOF-11 (100) [**159**], Mg/DOBDC (288) [**227**] and UTSA-16 (300) [**159**].

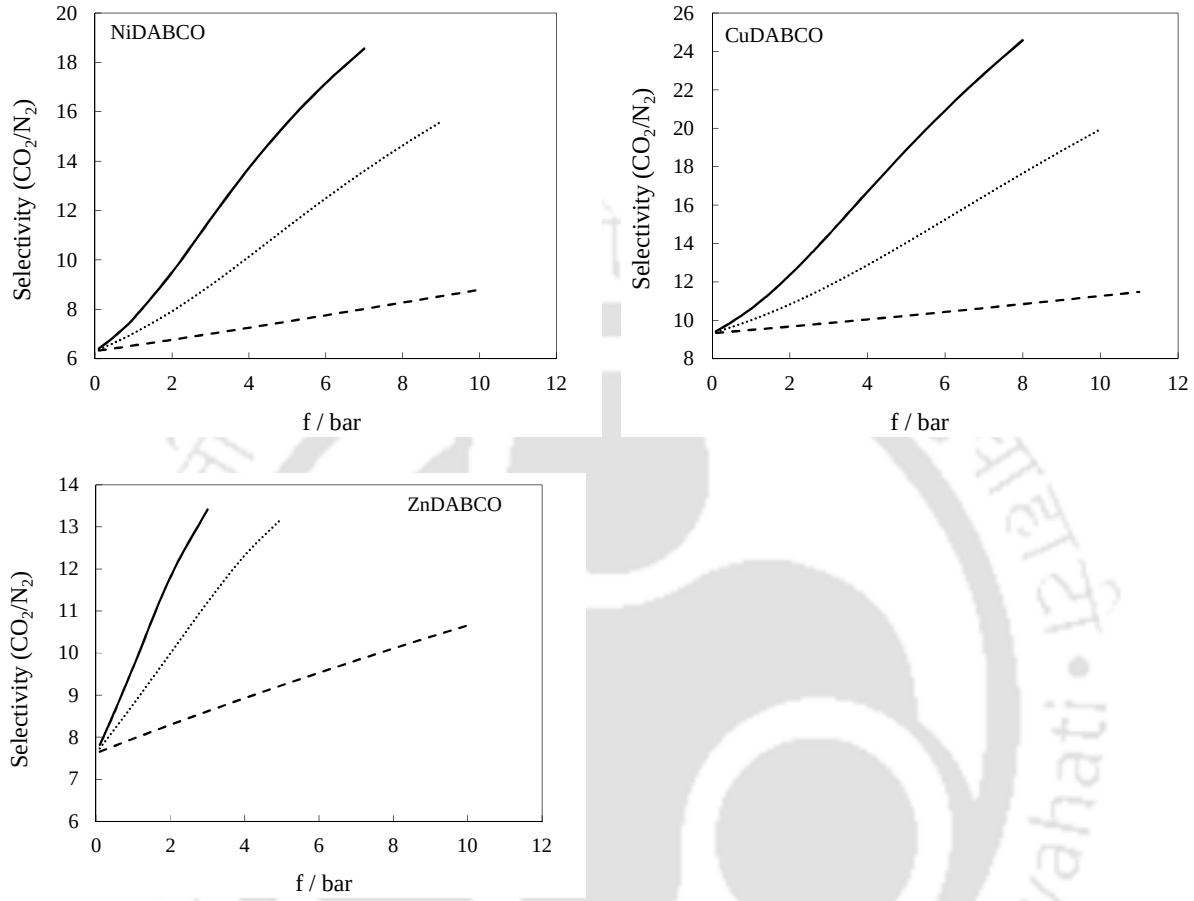

Figure 7.16: Variation of selectivity of CO_2 with pressure at 294 K for different N_2 compositions: 5 % N_2 (——), 50 % N_2 (·····) and 95 % N_2 (----).

In all the MOFs, with increase in pressure or composition of the CO_2, selectivity increases. At higher compositions of CO_2, contributions from lateral interactions between the adsorbed CO_2 molecules increase, thereby increasing the selectivity [**71**]. A similar effect of pressure and composition on CO_2 selectivity was observed by Karra et al. [**121**] for CuBTC. However, this trend is opposite to that obtained for M/DOBDC frameworks in the previous chapter, where CO_2 selectivity decreases with increase of pressure due to a reduction in the electrostatic interactions.

In order to understand the effect of metal atom variation in the DABCO framework on the binary selectivity, CO_2 selectivity over N_2 at 294 K for equimolar binary mixture is shown in Figure 7.17 for the three DABCO MOFs. Although, there is slight difference (< 15%) between the selectivities of different DABCO adsorbents, the nature and trend is almost same with respect to the pressure and composition.

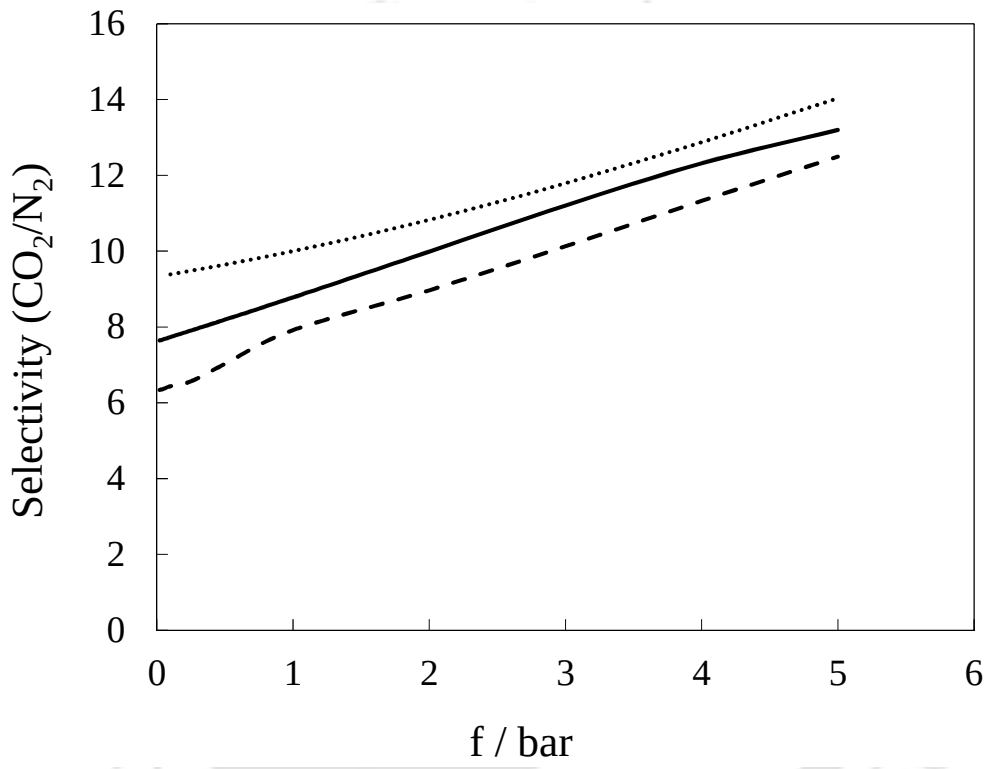

Figure 7.17: Variation of CO_2 selectivity over N_2 with pressure in equimolar binary mixture at 294 K for Ni/DABCO (----), Cu/DABCO (·····) and Zn/DABCO (——).

7.7.3 CO_2 selectivity over CH_4

CO_2 selectivity over CH_4 on the three studied DABCO sample at 294 K for binary mixtures of 5%, 50% and 95% CH_4 is plotted in Figure 7.18. The selectivity obtained in this work is comparable to that obtained on Zn/DABCO by Chen et al. [**234**] and Liu et al. [**235**]. CO_2

selectivity at zero coverage and 294 K on these frameworks is approximately 3, which is comparable to IRMOF-1 [**218**], PCN-6 and CuBTC [**219**]; however, it is lower than that on MIL-101 (4) [**220**], *soc*-MOF (20) [**219**], Li-IRMOF-1 (180) [**221**], M/DOBDC (25 – 250) [**227**]. CO_2 selectivity for CO_2/CH_4 mixture increases with increasing pressure. In general, the strength of vertical interactions decreases with increasing pressure. However, due to absence of *cus* metal sites in the DABCO based MOFs this decrease in vertical interactions will be small. On the other hand, lateral interactions increase with increasing pressure and this increase will be higher for CO_2 than that for CH_4. This trend is opposite to that observed for *cus* metal sites containing M/DOBDC MOFs studied in the previous chapter, wherein with increasing pressure, the decrease in vertical interactions for CO_2 is higher compared to the increase in lateral interactions. Increase in CO_2 selectivity with increase in pressure or composition of the CO_2, is less pronounced for CO_2/CH_4 mixture than for CO_2/N_2 mixture due to larger difference in polarizability of CO_2 and N_2. The effect of metal change in the framework is minimal for CO_2/CH_4 binary mixture (Figure 7.19), as in case of CO_2/N_2 binary mixture.

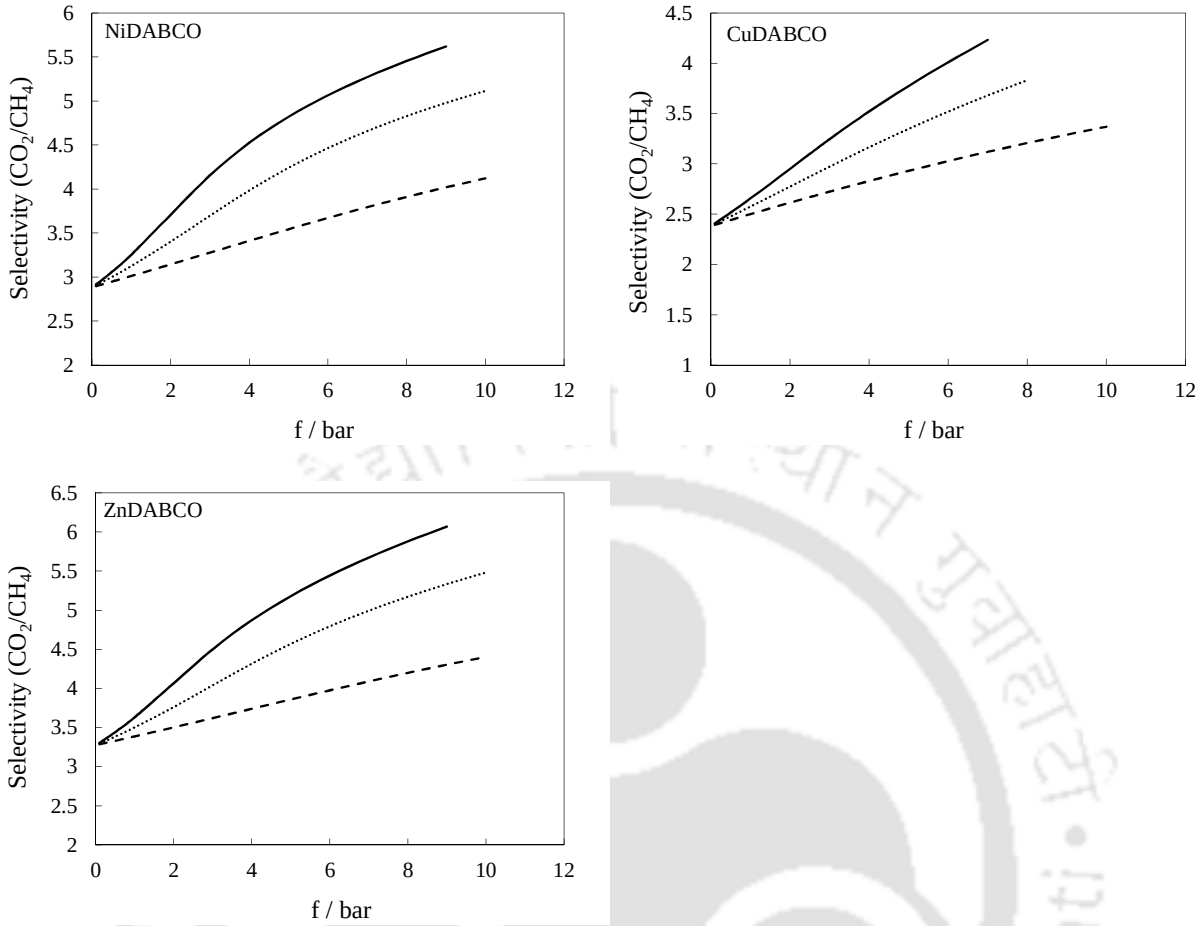

Figure 7.18: Variation of selectivity of CO_2 with pressure at 294 K for different CH_4 compositions: 5 % CH_4 (——), 50 % CH_4 (·····) and 95 % CH_4 (----).

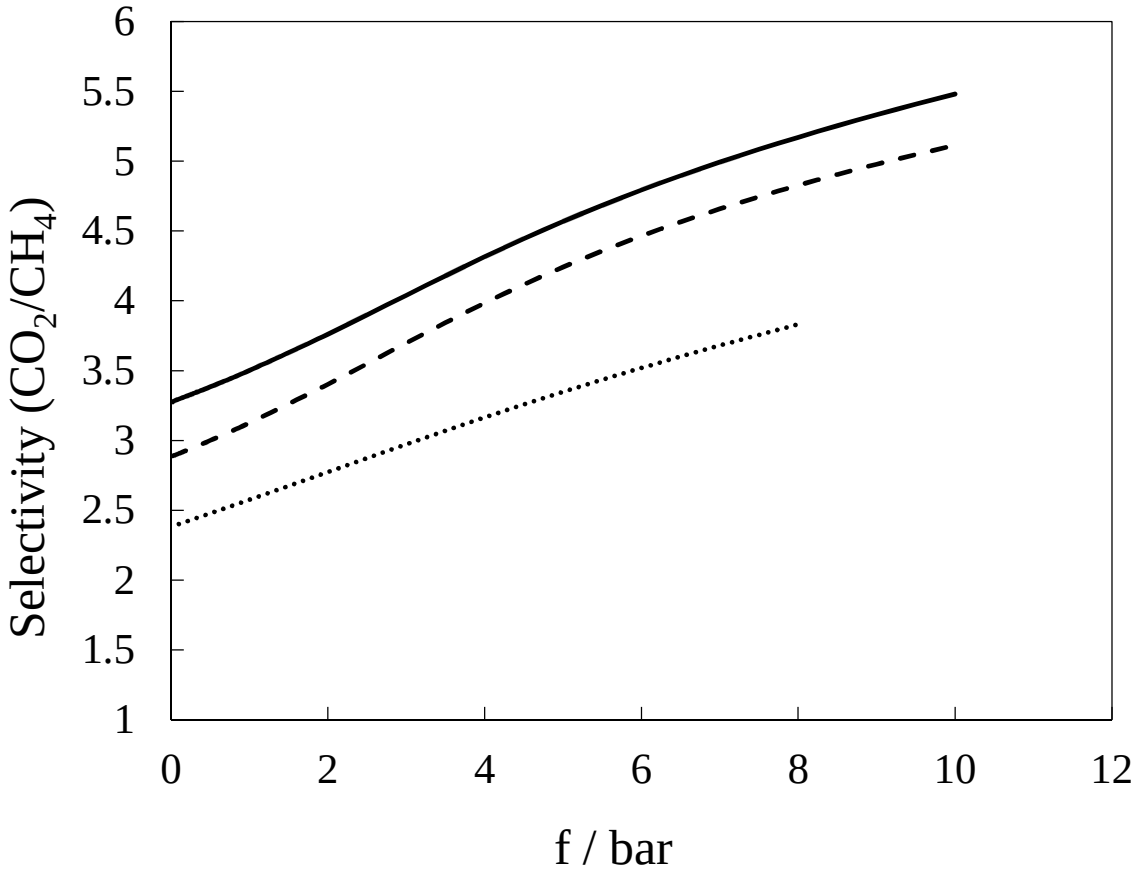

Figure 7.19: Variation of CO_2 selectivity over CH_4 with pressure in equimolar binary mixture at 294 K for Ni/DABCO (----), Cu/DABCO (·····) and Zn/DABCO (——).

7.7.4 CO_2 selectivity over CO

Although CO is polar, DABCO MOFs exhibit good CO_2 selectivity of ~7 over CO at zero coverage and 294 K (Figure 7.20). This value is slightly higher than that obtained by Karra et al. [**121**] on Zn/DABCO. This value is comparable to that on CuBTC (~7) [**121, 158**] and Mn/DOBDC (6) [**227**], but it is lower that on NaX (36) [**158**] and Mg/DOBDC (24) [**227**]. In contrast to these MOFs, Ni/DOBDC and Co/DOBDC compounds studied previous chapter are selective for CO over CO_2 with a selectivity value of ~ 7.5 at zero pressure and 294 K. The increase in CO_2 selectivity with increase in pressure or composition of the CO_2 for CO_2/CO

binary mixture is similar to that for CO_2/N_2 binary mixture. As in earlier cases, the effect of metal variation in the framework has negligible effect on CO_2 selectivity over CO for low pressures (Figure 7.21). However at higher pressures, some difference between CO_2 selectivity of Ni/DABCO, Cu/DABCO and Zn/DABCO is observed due to considerable difference in their saturation capacities for CO.

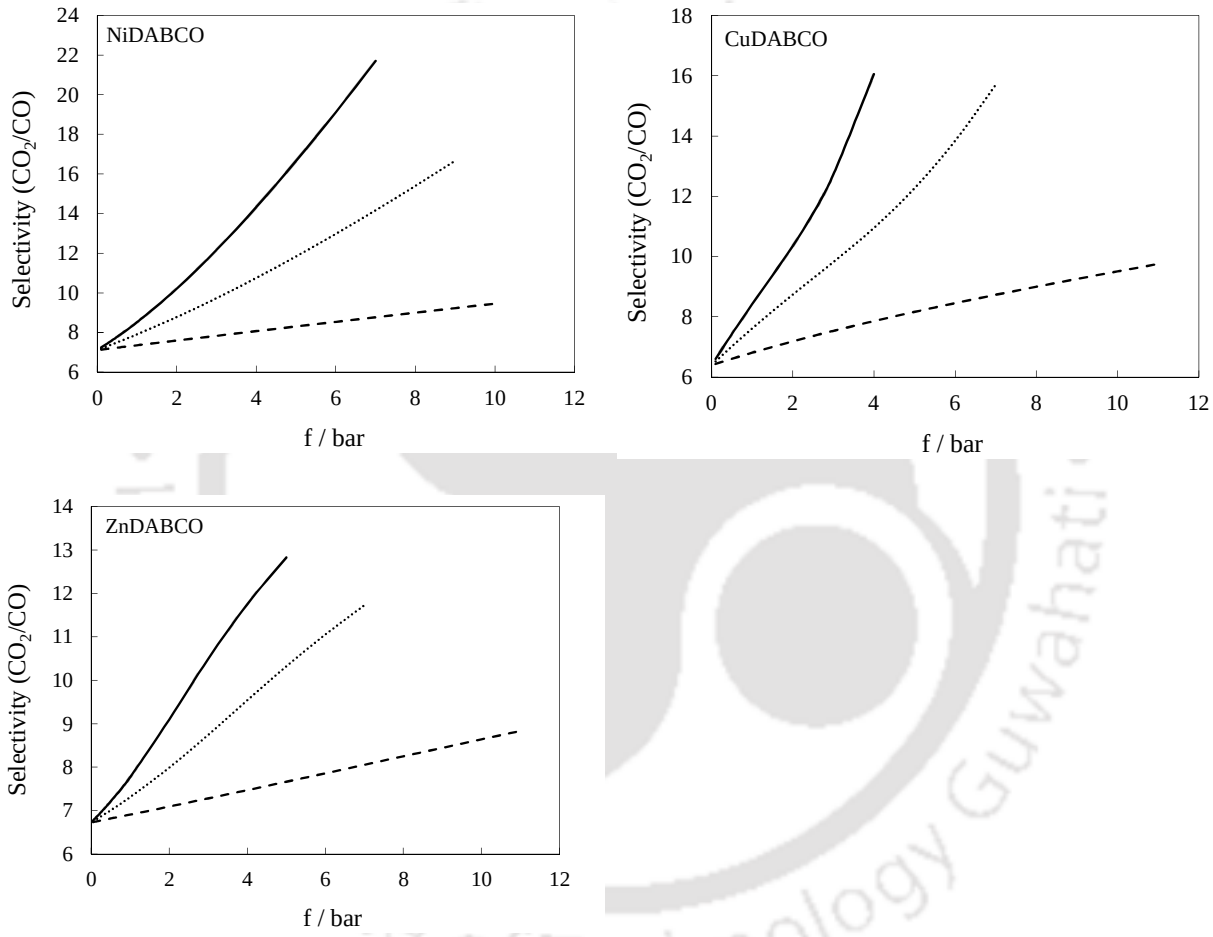

Figure 7.20: Variation of selectivity of CO_2 with pressure at 294 K for different CO compositions: 5 % CO (——), 50 % CO (·····) and 95 % CO (----).

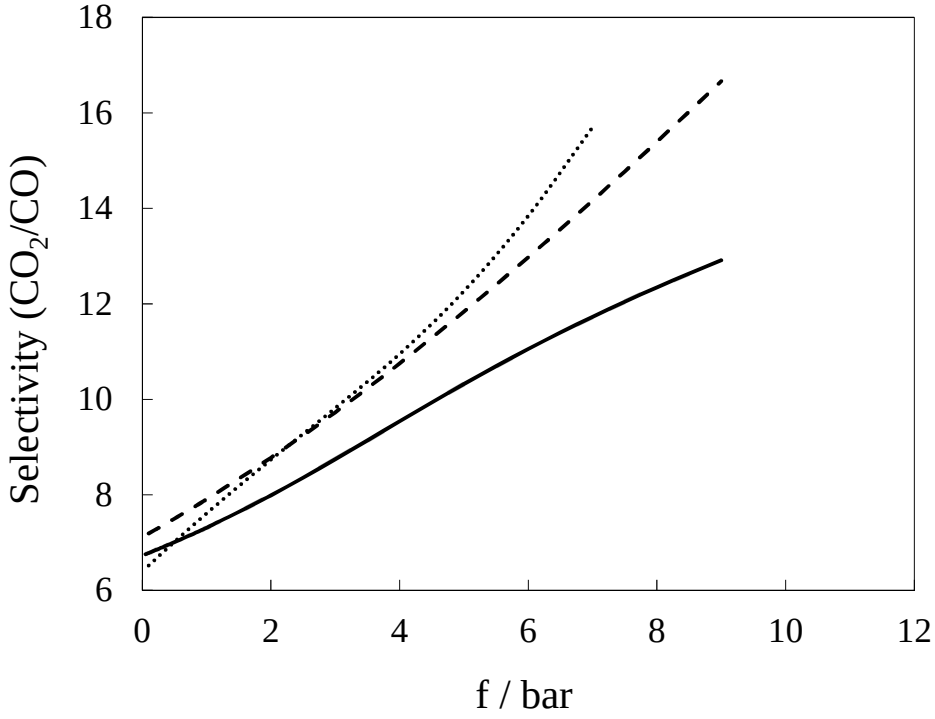

Figure 7.21: Variation of CO_2 selectivity over CO with pressure in equimolar binary mixture at 294 K for Ni/DABCO (----), Cu/DABCO (·····) and Zn/DABCO (——).

7.8 Effect of *cus* Metal Sites on Adsorption Characteristics

Ni/DOBDC studied in the previous chapter and Ni/DABCO studied in this work chapter may be chosen as representing candidate to understand the effect of having *cus* metal sites in the framework on the adsorption characteristics. Both these MOFs have same metal atom and similar surface area / pore volume; however, while Ni/DOBDC contains a large number of *cus* metal sites, Ni/DABCO has its metal sites coordinatively saturated. Adsorption enthalpy and selectivity of Ni/DOBDC and Ni/DABCO are compared to highlight the effect of *cus* metal sites on the adsorption characteristics.

7.8.1 Adsorption Enthalpy

The variation of adsorption enthalpy ($-\Delta h_{ads}$) of CO_2, CO, CH_4 and N_2 on Ni/DOBDC and Ni/DABCO is plotted in Figure 7.22. $-\Delta h_{ads}$ of CO_2 and CO at zero coverage are substantially higher on Ni/DOBDC than that on Ni/DABCO. As already discussed, *cus* Ni metal centers in Ni/DOBDC compound generate a strong electrostatic interactions with polar adsorbate molecules resulting into a higher $-\Delta h_{ads}$ values for them on this compound. A sharp decrease in $-\Delta h_{ads}$ of CO_2 and CO occurs once the *cus* metal centers of Ni/DOBDC are filled. On the other hand, no such trend is observed for Ni/DABCO due to negligible electrostatic interactions. For relatively non-polar gases such as CH_4 and N_2, the difference between $-\Delta h_{ads}$ of the two frameworks is smaller.

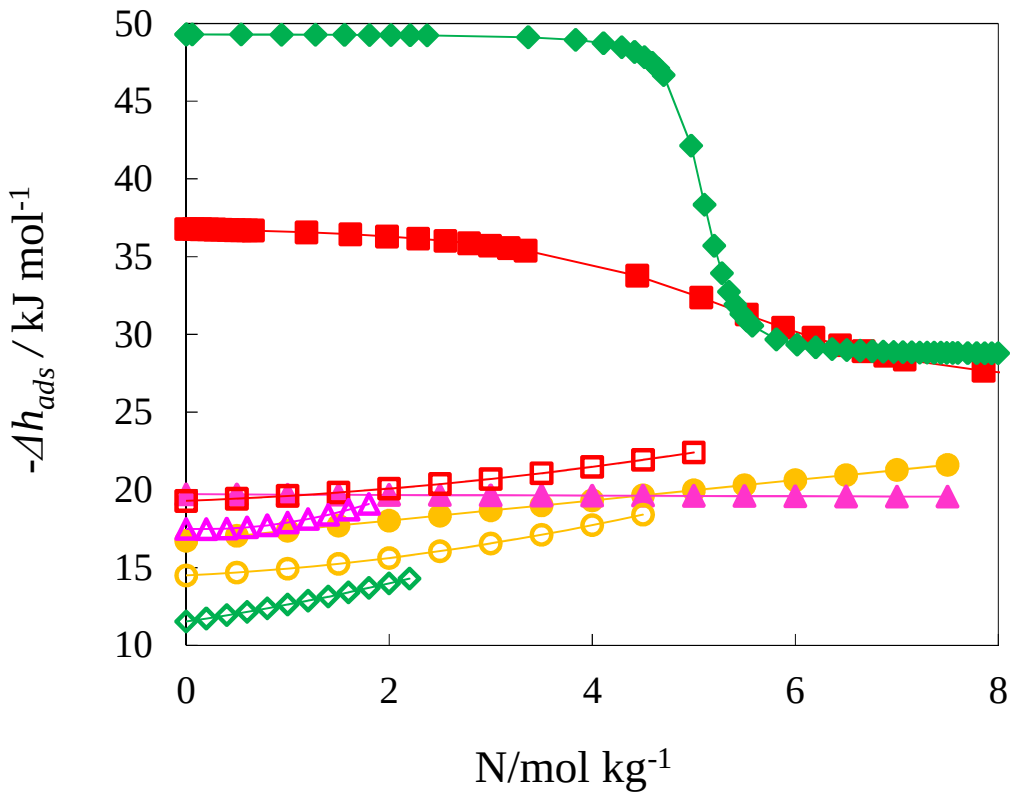

Figure 7.22: Variation of enthalpy of adsorption with loading for CO_2 (■, □), CO (♦, ◊), CH_4 (●, ○), N_2 (▲, Δ); closed symbols represent Ni/DOBDC and open symbols represent Ni/DABCO.

7.8.2 Selectivity of Binary Mixtures

The selectivities at 294 K for different equimolar binary mixtures on Ni/DOBDC and Ni/DABCO are shown in Figure 7.23. As expected, CO_2 selectivity ove CH_4 on Ni/DOBDC is considerably higher than that on Ni/DABCO (Figure 7.23a) due to the electrostatic interactions between CO_2 molecules and *cus* Ni metal centers of Ni/DOBDC framework. Similarly, CO selectivity over CH_4 (Figure 7.23b) at 294 K on Ni/DOBDC is ~400 times higher than that on Ni/DABCO in the low pressure region. In contrast, CH_4 selectivity over N_2 on Ni/DOBDC is slightly lower than that on Ni/DABCO (Figure 7.23c) because *cus* metal sites in Ni/DOBDC have slight electrostatic interactions with N_2 molecules reducing its selectivity for CH_4.

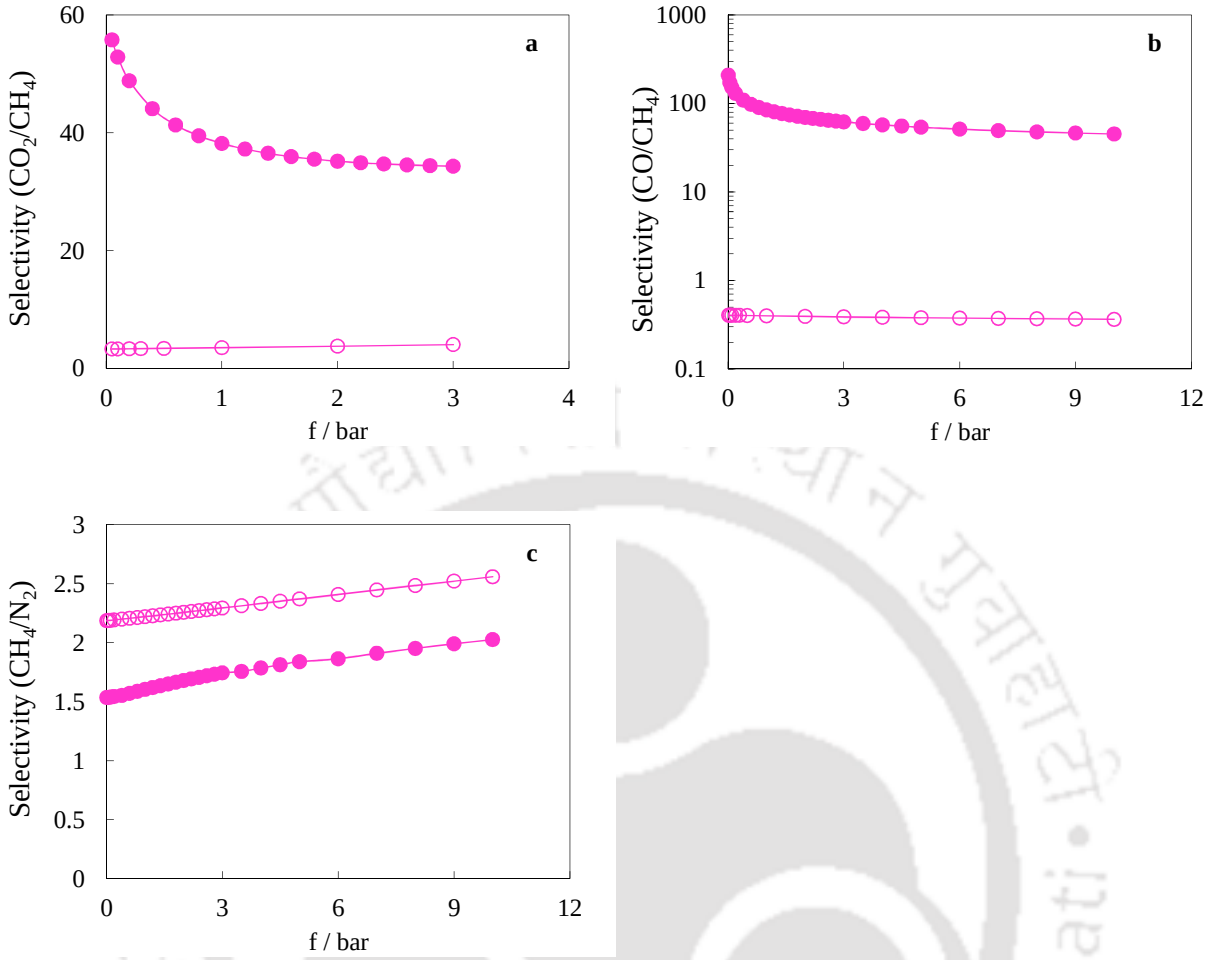

Figure 7.23: Variation of (**a**) CO_2/CH_4, (**b**) CO/CH_4 and (**c**) CH_4/N_2 selectivity with pressure at 294 K for equimolar binary mixtures on Ni/DOBDC (●) and Ni/DABCO (○).

7.9 Summary

In this work, we studied the adsorption characteristics of four industrially relevant gases (CO_2, CH_4, CO and N_2) on Ni/DABCO, Cu/DABCO and Zn/DABCO metal organic frameworks. Adsorption data was compared with the available literature data for a variety of adsorbents. Virial and Langmuir-virial models were used to model the experimental isotherms. Henry's constant and enthalpy of adsorption were calculated from the model parameters. CO_2 exhibits higher Henry's constant and enthalpy of adsorption compared to other studied gases. The enthalpy of adsorption and Henry's constant for polar gases (CO_2 and CO) on DABCO MOFs are lower than that on open metal centers containing M/DOBDC MOFs studied in the previous chapter due to absence of electrostatic interactions. This property of DABCO MOFs should make it easier to regenerate them at milder conditions. However, CO_2 uptake at ambient condition and selectivity for CO_2/CH_4 and CO_2/N_2 binary mixtures is found to be poor in DABCO MOFs compared to that in the M/DOBDC MOFs with *cus* metal sites. In contrast to M/DOBDC MOFs, the metal atoms in the adsorbent framework and polarity of the adsorbate play negligible role in the adsorption on the DABCO MOFs. IAST predicts enhancement in CO_2 selectivity with pressure and CO_2 mole-fraction. M/DABCO MOFs are found to be selective for CH_4 over CO (with a selectivity between 2 and 3.8), which is not very common in adsorption literature. The adsorption characteristics of Ni/DOBDC and Ni/DABCO MOFs were compared to highlight the role of *cus* metal sites on the adsorption characteristics of MOFs.

CHAPTER 8

CONCLUSIONS AND FUTURE SCOPE

This chapter summarizes the major inferences drawn from the research work presented in this dissertation and recommendations for further extension of this work in future.

8.1 Conclusions

The main objective of this work was to systematically investigate the adsorption characteristics of selected metal organic frameworks (MOFs). MOFs from various categories were judicially chosen to represent framework flexibility, presence of coordinatively unsaturated (*cus*) metal sites and absence of *cus* metal centers. Accordingly, MIL-53(Al) MOF studied in the first part of this work is flexible, while the frameworks of the MOFs considered later (*viz.* DOBDC and DABCO MOFs) are rigid but differ in availability of the *cus* metal centers. Several industrially important gases (*viz.* CO_2, CO, CH_4, N_2, Ar, C_2H_6, C_3H_8 and O_2) representing a wide range of polarity and polarizability were chosen for study. Adsorption isotherm measurements of the considered gases were performed on these MOFs to correlate their adsorption characteristics with the adsorbate physical properties. The salient accomplishments and major conclusions from this work are summarized in the following sections.

8.1.1 Structural Tuning of MIL-53 (Al) Flexible MOF

As stated in literature a high temperature activation (493 K) yields large pore structure for MIL-53(Al) that is retained after cooling the sample to 293 K under vacuo **(**denoted as **sample lp_0**). In line with the earlier works, **sample lp_0** exhibits structural transformations first from large pore (**lp**) domain to narrow pore (**np**) domain in the sub-atmospheric region and then from the **np** to the **lp** domain at higher pressures (> 4.5 bar) upon adsorption of CO_2 at 293 K. During desorption structural transformation occurs at different pressure conditions resulting into two hysteresis loops. On the other hand, no such transformation was observed during adsorption of CH_4, N_2, CO and O_2 on this sample at 293 K. In this work, **sample lp_0** was tuned first into the **np** phase at room temperature under vacuum, since **np** phase is known to adsorb higher amounts of CO_2 at low pressures compared to that of the **lp** phase. This tuning was achieved by equilibrating the sample **lp_0** with CO_2 at a pressure of ~ 1 bar at 293 K. Then, instead of high temperature treatment, CO_2 was completely desorbed from the sample by just applying vacuum (below 0.01 mbar) at room temperature. This CO_2 desorbed MIL-53(Al) sample show narrow pore structure and is denoted as **sample np_0**.

In contrast to **sample lp_0**, first hysteresis below 1 bar during CO_2 adsorption at 293 K disappears for **sample np_0** and a significant enhancement in adsorption uptake of CO_2 is obtained in the sub-atmospheric regime. In fact, CO_2 uptake capacity increases fourfold from 0.42 mol kg^{-1} to 1.75 mol kg^{-1} at 0.17 bar (this pressure is chosen to make the comparison because in flue gases partial pressure of CO_2 ranges between 0.12 to 0.20 bar). As CO_2 desorption branch for both **sample lp_0** and **sample np_0** overlap each other, it can be further concluded that the enhancement in CO_2 uptake on **Sample np_0** is obtained without any extra regeneration penalty (as compared to **sample lp_0**).

Other gases (CH_4, N_2, CO and O_2) adsorbs negligibly on **sample np_0** below 1 bar and 293 K; thus, **sample np_0** obtained by the tuning method proposed in this work not only exhibits enhancement in CO_2 adsorption uptake but also shows high selectivity for CO_2 over the other gases considered in the sub-atmospheric region at 293 K. At higher pressure as **sample np_0** transforms from **np** to **lp** structure, and hysteresis (which was otherwise absent earlier for **sample lp_0**) is observed in isotherm of CH_4, N_2, CO and O_2 on **Sample np_0**. The **np** tuned form of MIL-53(Al) thus exhibits better CO_2 capacity and selectivity at sub-atmospheric condition.

8.1.2 Adsorption Characteristics of DOBDC MOFs

Adsorption isotherm measurements of CO_2, CO, CH_4, N_2, Ar, C_2H_6 and C_3H_8 are performed on *cus* metal sites containing M/DOBDC (M = Mg, Mn, Co, and Ni) MOFs over a wide range of temperature and pressure. The CO_2 adsorption uptake obtained at 0.15 bar and 294 K on Mg/DOBDC (5.07 mol kg^{-1}) is considerably higher than that on most of the other adsorbents including other DOBDC frameworks. Similarly Ni/DOBDC and Co/DOBDC MOFs possess high CO loading (~ 4.8 mol kg^{-1}) at 0.1 bar and 294 K compared to that on the other adsorbents reported in the literature. On the other hand, the gravimetric adsorption loading of relatively non-polar CH_4 and N_2 in the sub-atmospheric region on the DOBDC frameworks are comparable to that on other adsorbents. Significantly higher adsorption uptake in the low pressure region for CO_2 and CO gases on these M/DOBDC frameworks is attributed to the strong electrostatic interactions between polar adsorbate molecules and *cus* metal centers. Isotherms of CO_2 and CO on the DOBDC MOFs follow a dual site Langmuir isotherms model in which high energy site corresponds to the *cus* metal sites. In contrast, a Langmuir-virial isotherm successfully describes the adsorption behavior of other (relatively non-polar) gases.

The change of metal constituent in the framework dramatically alters the adsorption characteristics of DOBDC MOFs for polar CO_2 and CO gases. For example, Henry's constant of CO_2 for Mg/DOBDC is about 4 to10 times higher than that for other frameworks due to due to preference of the Mg^{2+} ions for oxygen-containing ligands; similarly, Henry's constant for CO on Ni/DOBDC at 294 K is about 116 times larger than that on Mn/DOBDC. The σ-donation of electron lone pair by CO molecules to the Ni ions results in this exceptionally higher Henry's constant value for CO on Ni/DOBDC. However, as *cus* metal centers are progressively filled with the increase pressuring, effect of constituent metal atom in the framework decreases and saturation adsorption capacities of these gases vary almost linearly with the pore volume of M/DOBDC compounds. Interestingly, there is no difference between the Henry's constants of DOBDC compounds studied for other gases indicating the negligible role of metal cation on the adsorption of non-polar gases in the low pressure regime. But as in case of CO_2 and CO, saturation adsorption capacities of these gases also vary almost linearly with the pore volume of M/DOBDC compounds.

IAST predicts good selectivity for CO_2 over CH_4, CO, Ar and N_2 on Mg/DOBDC. At zero coverage and 294 K, Mg/DOBDC exhibits CO_2 selectivity of 24 (for CO) and 1104 (for Ar). In contrast to this, Ni/DOBDC and Co/DOBDC display preferential selectivity for CO over other gases including CO_2. For example at 294 K, Ni/DOBDC shows CO selectivity of 677 for N_2 and 7.5 for CO_2 at zero coverage.

M/DOBDC compounds are found to be stable upon exposure to all the gases studied. However, they display instability upon exposure to O_2 especially at higher temperatures. While good selectivity and loading of CO_2 and CO on M/DOBDC MOFs make them highly potential candidates for separation of these gases, high enthalpy of adsorption and poor stability upon exposure to O_2 still remain to be addressed.

8.1.3 Adsorption Characteristics of DABCO MOFs

Adsorption characteristics of coordinatively saturated metal sites containing M/DABCO MOFs are studied by performing adsorption of CO_2, CH_4, CO and N_2 at 294, 314 and 350 K in the range of 0 – 25 bar. Adsorption uptake of CO_2 in the sub-atmospheric region (for example at 0.15 bar and 294 K) on M/DABCO MOFs ranges 0.2 to 0.3 mol kg^{-1} which is considerably lower compared to corresponding uptake on M/DOBDC MOFs (2.7 – 5.1 mol kg^{-1}); this difference in adsorption uptake can easily be attributed to the absence of *cus* metal sites (and hence electrostatic interactions) for M/DABCO MOFs. Similarly, loading of another polar gas CO at 294 K and 1 bar on M/DABCO MOFs is substantially lower (only ~ 0.2 mol kg^{-1}). In fact, for M/DABCO MOFs, Henry's constant and adsorption enthalpy of polar CO are lower than those of non-polar CH_4 (Henry's constants of CO and CH_4 at 294 K are ~ 0.25 mol kg^{-1} bar^{-1} and ~ 0.55 mol kg^{-1} bar^{-1} respectively); this indicates negeligble electrostatic interactions between polar CO molecules and metal centers of DABCO frameworks. In contrast, saturation uptake of CO_2 at higher pressure on M/DABCO frameworks (~ 11 – 15 mol kg^{-1}) are comparable to that on M/DOBDC frameworks due similar pore volumes. Adsorption enthalpies of CO_2 (~ 19 kJ mol^{-1}) and CO (~ 11 kJ mol^{-1}) at zero loading on the DABCO MOFs are significantly lower than that on other MOFs like MIL-101, CuBTC, M/DOBDC etc. This property should make the regeneration of DABCO frameworks easier. DABCO MOFs are found to be selective for CH_4 over CO (with a selectivity value between 2 and 3.8) due to higher polarizability for CH_4 and negligible electrostatic interactions; this trend is not very common in adsorption literature.

Adsorption enthalpy and selectivities of binary mixtures on *cus* metal sites containing Ni/DOBDC and are compared with that on Ni/DABCO to highlight the role of *cus* metal sites on the adsorption characteristics of MOFs. Adsorption enthalpy of CO at zero coverage on Ni/DOBDC (> 46 kJ mol^{-1}) is considerably higher than that on Ni/DABCO (~ 11 kJ mol^{-1}).

Similarly, CO_2 selectivity over N_2 is almost 15 times higher on Ni/DOBDC. Although lower adsorption enthalpy for DABCO compounds is attractive from regeneration point of view, lower adsorption uptakes in the Henry's low regime and poor selectivities do not make these MOFs suitable candidates for CO_2 separation applications.

8.2 Recommendation for Future Works

This work presents a systematic and detailed investigation to understand the adsorption characteristics of different categories MOFs. There are certainly several areas which merit further research attention.

- **np** tuned form of MIL-53(Al) sample has shown a very good adsorption capacity and almost infinite CO_2 selectivity in the pressure range equivalent to flue gas conditions. Moreover, this MOF is known to have very good stability. However, in this work only single component adsorption measurements were performed on this interesting form of MIL-53(Al). So we strongly recommend that this **np** tuned form of MIL-53(Al) can be further studied in a vacuum swing adsorption (VSA) process for CO_2 capture from flue gas. The obtained economics for **np** tuned form of MIL-53(Al) may be compared with that for benchmark Zeolite 13X.
- Though M/DOBDC compounds have shown very good adsorption uptake and selectivity for polar CO_2 and CO gases, these MOFs are susceptible to humid and oxygen environment. It would be interesting to improve the stability of these frameworks may be by functionalization of organic ligand. In fact, similar type of attempt has been made by Walton and coworkers [**189**] to enhance the stability of pillared DABCO MOFs. The effect of such functionalization on other adsorption characteristics needs to be investigated.
- While M/DOBDC MOFs seem to be attractive in adsorption uptake and selectivity perspective, M/DABCO MOFs have advantage of easier regeneration. So the performance of all of these MOFs in the real time processes (PSA/TSA/VSA) should be evaluated for various industrial separation applications to identify MOFs suitable for various application.

REFERENCES CITED

[1] Schuth, F.; Sing, K. S. W.; Weitkamp, J. Handbook of Porous Solids; *Wiley-VCH: New York,* **2002**.

[2] Valtchev, V.; Mintova, S.; Tsapatsis, M. Ordered Porous Solids: Recent Advances and Prospects; *Elsevier B.V.: Oxford,* **2009**.

[3] Li, J. R.; Sculley, J.; Zhou, H. C. Metal_Organic Frameworks for Separations. *Chem. Rev.* **2012**, *112***,** 869–932.

[4] Yang, R. T. Gas Separation by Adsorption Processes, Chapter-1; *Imperial College Press, London,* **1997**.

[5] Tondeur, D. in Percolation Processes: Theory and Applications; Rodrigues, A. E. and Tondeur, D. [eds.] NATO ASI No. 33; Sijthoff and Noordhoff, Alphen van Rijn, p. 517, *Holland,* **1981**.

[6] Ruthven, D. M. and Sun, M. S. Principle of Adsorption and Adsorption Processes, Chapter-1; *Wiley-Interscience, New York,* **1984**.

[7] Ruthven, D. M.; Farooq, S; Knaebel, Pressure Swing Adsorption, *Wiley-VCH, New York,* **1993**.

[8] http://en.wikipedia.org/wiki/Physisorption.

[9] Klaus, R.; Aiken, R. C.; Rippin, D. W. T. Simulated binary isothermal adsorption on activated carbon in periodic countercurrent column operation. *AIChE J.* **1977,** *23,* 579–586.

[10] Wang, Y. and LeVan, M. D. Adsorption Equilibrium of Carbon Dioxide and Water Vapor on Zeolites 5A and 13X and Silica Gel: Pure Components. *J. Chem. Eng. Data* **2009,** *54,* 2839–2844.

[11] Wilmer, C. E.; Leaf, M.; Lee, C. Y.; Farha, O. K.; Hauser, B. G.; Hupp, J. T.; Snurr, R. Q. Large-scale screening of hypothetical metal–organic frameworks. *Nature Chemistry* **2012,** *4,* 83–89.

[12] Guisnet, M. and Gilson, J. P. Zeolites for Cleaner Technologies, p. 1–2; *Imperial College Press, London,* **2002**.

[13] Szostak, R. Molecular Sieves Principles of Synthesis and Identification, p. 3; *Blackie Academic & Professional, London,* **1998**.

[14] Yang, R. T. Adsorbents: Fundamentals and Applications, p. 17-18; *Wiley-Interscience, New-Jersey,* **2003**.

[15] Tranchemontagne, D. J.; Mendoza-Cortes, J. L.; O'Keeffe, M.; Yaghi, O. M. Secondary building units, nets and bonding in the chemistry of metal–organic frameworks. *Chem. Soc. Rev.* **2009,** *38,* 1257–1283.

[16] Wang, Z.; Cohen, S. M. Postsynthetic modification of metal–organic frameworks. *Chem. Soc. Rev.* **2009,** *38,* 1315–1329.

[17] Férey, G.; Serre, C.; Devic, T.; Maurin, G.; Jobic, H.; Llewellyn, P. L.; DeWeireld, G.; Vimont, A.; Daturi, M.; Chang, J. -S. Why hybrid porous solids capture greenhouse gases? *Chem. Soc. Rev.* **2011,** *40,* 550–562.

[18] D'Alessandro, D. M.; Smit, B.; Long, J. R. Carbon Dioxide Capture: Prospects for New Materials. *Angew. Chem., Int. Ed.* **2010,** *49,* 6058–6082.

[19] Li, J. R.; Ma, Y.; McCarthy, M. C.; Sculley, J.; Yu, J.; Jeong, H. K.; Balbuena, P. B.; Zhou, H. C. Carbon dioxide capture-related gas adsorption and separation in metal-organic frameworks. *Coord. Chem. Rev.* **2011,** *255,* 1791–1823.

[20] Wang, Z.; Chen, G.; Ding, K. L. Self-Supported Catalysts. *Chem. Rev.* **2009,** *109,* 322–359.

[21] Corma, A.; Garcia, H.; Xamena, F. X. L. Engineering Metal Organic Frameworks for Heterogeneous Catalysis. *Chem. Rev.* **2010,** *110,* 4606–4655.

[22] Horcajada, P.; Serre, C.; Vallet-Regi, M.; Sebban, M.; Taulelle, F.; Férey, G. Metal–Organic Frameworks as Efficient Materials for Drug Delivery. *Angew. Chem., Int. Ed.* **2006,** *45,* 5974–5978.

[23] Huxford, R. C.; Della Rocca, J.; Lin, W. B. Metal-organic frameworks as potential drug carriers. *Curr. Opin. Chem. Biol.* **2010,** *14,* 262–268.

[24] Della Rocca, J.; Liu, D.; Lin, W. Nanoscale Metal–Organic Frameworks for Biomedical Imaging and Drug Delivery. *Acc. Chem. Res.* **2011,** *44,* 957–968.

[25] Zhao, D.; Yuan, D. Q.; Zhou, H. C. The current status of hydrogen storage in metal–organic frameworks. *Energy Environ. Sci.* **2008,** *1,* 222–235.

[26] Hu, Y. H.; Zhang, L. Hydrogen Storage in Metal–Organic Frameworks. *Adv. Mater.* **2010,** *22,* E117–E130.

[27] Murray, L. J.; Dinca, M.; Long, J. R. Hydrogen storage in metal–organic frameworks. *Chem. Soc. Rev.* **2009,** *38,* 1294–1314.

[28] Dinca, M.; Long, J. R. Hydrogen Storage in Microporous Metal–Organic Frameworks with Exposed Metal Sites. *Angew. Chem., Int. Ed.* **2008,** *47,* 6766–6779.

[29] Romano, M. C.; Anantharaman, R.; Arastoc, A.; Ozcan, D. C.; Ahn, H.; Dijkstra, J. W.; Carbo, M.; Boavida. D. Application of advanced technologies for CO_2 capture from industrial sources. *Energy Procedia* **2013,** *37,* 7176–7185.

[30] Ezhova, N. N.; Sudareva, S. V. Modern Methods for Removing Carbon Dioxide from Flue Gases Emitted by Thermal Power Stations. *Thermal Engineering* **2009,** *56,* 15–21.

[31] Figueroa, J. D.; Fout, T.; Plasynski, S.; McIlvried, H.; Srivastava, R. D. Advances in CO_2 capture technology – The U.S. Department of Energy's Carbon Sequestration Program. *International Journal of Green House Gas Control* **2008,** *2,* 9–20.

[32] Dunne, J. A.; Rao, M.; Sircar, S.; Gorte, R. J.; Myers, A. L. Calorimetric heats of adsorption and adsorption isotherms. 2. O_2, N_2, Ar, CO_2, CH_4, C_2H_6, and SF_6 on NaX, H-ZSM-5, and Na-ZSM-5 zeolites. *Langmuir* **1996,** *12,* 5896–5904.

[33] Li, M.; Liu, J.; Wang, T. L. Adsorption Equilibria of Carbon Dioxide and Ethane on Graphitized Carbon Black. *J. Chem. Eng. Data* **2010,** *55,* 4301–4305.

[34] Himeno, S; Komatsu, T.; Fujita, S. High-Pressure Adsorption Equilibria of Methane and Carbon Dioxide on Several Activated Carbons. *J. Chem. Eng. Data* **2005,** *50,* 369–376.

[35] Liang, Z.; Marshall, M.; Chaffee, A. L. CO_2 Adsorption-Based Separation by Metal Organic Framework [Cu-BTC] versus Zeolite [13X]. *Energy & Fuels* **2009,** *23,* 2785–2789.

[36] Li, H.; Eddaoudi, M.; O'Keeffe, M.; Yaghi, O. M. Design and synthesis of an exceptionally stable and highly porous metal-organic framework. *Nature.* **1999**, *402***,** 276–279.

[37] Yazaydin, A. O.; Snurr, R. Q.; Park, T. –H.; Koh, K.; Liu, J.; LeVan, M. D.; Benin, A. I.; Jakubczak, P.; Lanuza, M.; Galloway, D. B.; Low, J. J.; Willis, R. R. Screening of Metal Organic

Frameworks for Carbon Dioxide Capture from Flue Gas Using a Combined Experimental and Modeling Approach. *J. Am. Chem. Soc.* **2009,** *131,* 18198–18199.

[38] Furukawa, H.; Ko, N.; Go, Y. B.; Aratani, N.; Choi, S. B.; Choi, E.; Yazaydin, A. O.; Snurr, R. Q.; O'Keeffe, M.; Kim, J.; Yaghi, O. M. Ultra high Porosity in Metal–Organic Frameworks. *Science* **2010,** *329,* 424–428.

[39] Serre, C.; Millange, F.; Thouvenot, C.; Noguès, M.; Marsolier, G.; Louër, D.; Férey, G. Very Large Breathing Effect in the First Nanoporous Chromium(III)-Based Solids: MIL-53 or $Cr^{III}(OH)\cdot\{O_2C-C_6H_4-CO_2\}\cdot\{HO_2C-C_6H_4-CO_2H\}_x\cdot H_2O_y$. *J. Am. Chem. Soc.* **2002**, *124*, 13519–13526.

[40] Yaghi, O. M.; O'Keeffe, M.; Ockwig, N. W.; Chae, H. K.; Eddaoudi, M.; Kim, J. synthesis and the design of new materials. *Nature* **2003**, *423,* 705–714.

[41] Loiseau, T.; Serre, C.; Hugueanrd, C.; Fink, G.; Taulelle, F.; Henry, M.; Bataille, T.; Férey, G. A rationale for the large breathing of the porous Aluminum Terephthalate [MIL-53] upon hydration. *Chem.–Eur. J.* **2004,** *10,* 1373–1382.

[42] Bourrelly, S.; Llewellyn, P. L.; Serre, C.; Millange, F.; Loiseau, T. Férey, G. Different adsorption behaviors of methane and carbon dioxide in the isotypic nanoporous Metal Terephthalates MIL-53 and MIL-47. *J. Am. Chem. Soc.* **2005**, *127*, 13519–13521.

[43] Sumida, K.; Rogow, D. L.; Mason, J. A.; McDonald, T. M.; Bloch, E. D.; Herm, Z. R.; Bae, T. -H.; Long, J. R. Carbon dioxide capture in Metal-Organic Frameworks. *Chem. Rev.* **2012**, *112,* 724–781.

[44] Kreno, L. E.; Leong, K.; Farha, O. K.; Allendorf, M.; Van Duyne, R. P.; Hupp, J. T. Metal–Organic Framework Materials as Chemical Sensors. *Chem. Rev.* **2012,** *112,* 1105–1125.

[45] Kitagawa, S.; Kitaura, R.; Noro, S. Functional Porous Coordination Polymers. *Angew. Chem., Int. Ed.* **2004,** *43,* 2334–2375.

[46] Ma, S. Q. and Zhou, H. C. A Metal−Organic Framework with Entatic Metal Centers Exhibiting High Gas Adsorption Affinity. *J. Am. Chem. Soc.* **2006,** *128,* 11734–11735.

[47] Liu, Y. L.; Kravtsov, V. C.; Larsen, R.; Eddaoudi, M. Molecular building blocks approach to the assembly of zeolite-like metal–organic frameworks (ZMOFs) with extra-large cavities. *Chem. Commun.* **2006,** 1488–1490.

[48] Lin, J. B.; Zhang, J. P.; Chen, X. M. Nonclassical Active Site for Enhanced Gas Sorption in Porous Coordination Polymer**.** *J. Am. Chem. Soc.* **2010,** *132,* 6654–6656.

[49] Park, K. S.; Ni, Z.; Cote, A. P.; Choi, J. Y.; Huang, R. D.; Uriberomo, F. J.; Chae, H. K.; O'Keeffe, M.; Yaghi, O. M. Exceptional chemical and thermal stability of zeolitic imidazolate frameworks. *Proc. Natl. Acad. Sci. U.S.A.* **2006,** *103,* 10186–10191.

[50] Hoskins, B. F. and Robson, R. Design and construction of a new class of scaffolding-like materials comprising infinite polymeric frameworks of 3D-linked molecular rods. A reappraisal of the zinc cyanide and cadmium cyanide structures and the synthesis and structure of the diamond-related frameworks $[N(CH_3)_4][Cu^{I}Zn^{II}(CN)_4]$ and Cu^{I}[4,4',4",4"'-tetracyanotetraphenylmethane]$BF_4.xC_6H_5NO_2$. *J. Am. Chem. Soc.* **1990,** *112,* 1546–1554.

[51] Chui, S. S. Y.; Lo, S. M. F.; Charmant, J. P. H.; Orpen, A. G.; Williams, I. D. A chemically functionalizable nanoporous material $[Cu_3(TMA)_2(H_2O)_3]_n$. *Science* **1999,** *283,* 1148–1150.

[52] Férey, G.; Mellot-Draznieks, C.; Serre, C.; Millange, F.; Dutour, J.; Surble, S.; Margiolaki, I. A Chromium Terephthalate-Based Solid with Unusually Large Pore Volumes and Surface Area. *Science* **2005,** *309,* 2040–2042.

[53] Eddaoudi, M.; Kim, J.; Rosi, N.; Vodak, D.; Wachter, J.; O'Keefe, M.; Yaghi, O. M. Systematic Design of Pore Size and Functionality in Isoreticular MOFs and Their Application in Methane Storage. *Science* **2002,** *295*, 469–472.

[54] Seki, K. and Mori, W. Syntheses and Characterization of Microporous Coordination Polymers with Open Frameworks. *J. Phys. Chem. B* **2002,** *106*, 1380–1385.

[55] Dybtsev, D. N.; Chun, H.; Kim, K. Rigid and Flexible: A Highly Porous Metal–Organic Framework with Unusual Guest-Dependent Dynamic Behavior. *Angew. Chem., Int. Ed.* **2004,** *43*, 5033–5036.

[56] Yaghi, O. M.; Li, H.; Davis, C.; Richardson, D.; Groy, T. L. Synthetic strategies, structure patterns, and emerging properties in the chemistry of modular porous solids. *Acc. Chem. Res.* **1998,** *31*, 474–484.

[57] Rosi, N. L.; Eckert, J.; Eddaoudi, M.; Vodak, D. T.; Kim, J.; O'Keefe, M.; Yaghi, O. M. Hydrogen storage in microporous metal-organic frameworks. *Science* **2003,** *300*, 1127–1129.

[58] Eddaoudi, M.; Moler, D. B.; Li, H; Chen, B.; Reineke, T. M.; O'Keeffe, M.; Yaghi, O. M. Modular chemistry: Secondary building units as a basis for the design of highly porous and robust metal−organic carboxylate frameworks. *Acc. Chem. Res.* **2001,** *34*, 319–330.

[59] Eddaoudi, M.; Li, H.; Yaghi, O. M.; Highly porous and stable metal−organic frameworks: Structure design and sorption properties. *J. Am. Chem. Soc.* **2000,** *122*, 1391–1397.

[60] Chen, B.; Eddaoudi, M.; Hyde, S. T.; O'Keeffe, M.; Yaghi, O. M. Interwoven Metal-Organic Framework on a periodic minimal surface with extra-large pores. *Science* **2001**, *291***,** 1021–1023.

[61] Wong-Foy, A. G.; Matzger, A. J.; Yaghi O. M. Exceptional H_2 saturation uptake in microporous metal−organic frameworks. *J. Am. Chem. Soc.* **2006,** *128*, 3494–3495.

[62] Millward, A. R.; Yaghi, O. M. Metal Organic Frameworks with Exceptionally High Capacity for Storage of Carbon Dioxide at Room Temperature. *J. Am. Chem. Soc.* **2005,** *127*, 17998–17999.

[63] Rosi, N.; Kim, J.; Eddaoudi, M.; Chen, B.; O'Keeffe, M.; Yaghi, O. M. Rod Packings and Metal−Organic Frameworks Constructed from Rod-Shaped Secondary Building Units. *J. Am. Chem. Soc.* **2005,** *127*, 1504–1518.

[64] Dϋren, T.; Sarkisov, L.; Yaghi, O. M.; Snurr, R. Q. Design of new materials for methane storage. *Langmuir* **2004,** *20*, 2683–2689.

[65] Farha, O. K.; Yazaydın, A. Ö; Eryazici, I.; Malliakas, C. D.; Hauser, B. G.; Kanatzidis, M. G.; Nguyen, S. T.; Snurr, R. Q.; Hupp, J. T. *De novo* synthesis of a metal–organic framework material featuring ultrahigh surface area and gas storage capacities. *Nature Chemistry* **2010,** *2*, 944–948.

[66] Wilmer, C. E.; Farha, O. K.; Bae, Y. -S.; Hupp, J. T.; Snurr, R. Q. Structure–property relationships of porous materials for carbon dioxide separation and capture. *Energy Environ. Sci.* **2012,** *5*, 9849–9856.

[67] Herm, Z. R.; Swisher, J. A.; Smit, B.; Krishna, R.; Long, J. R. Metal–Organic Frameworks as Adsorbents for Hydrogen Purification and Precombustion Carbon Dioxide Capture. *J. Am. Chem. Soc.* **2011,** *133*, 5664–5667.

[68] Mason, J. A.; Sumida, K.; Herm, Z. R.; Krishna, R.; Long, J. R. Evaluating metal–organic frameworks for post-combustion carbon dioxide capture via temperature swing adsorption. *Energy Environ. Sci.* **2011,** *4*, 3030–3040.

[69] Herm, Z. R.; Krishna, R.; Long, J. R. CO_2/CH_4, CH_4/H_2 and $CO_2/CH_4/H_2$ separations at high pressures using Mg_2(dobdc). *Microporous and Mesoporous Materials* **2012,** *151*, 481–487.

[70] Keskin, S.; Liu, J.; Rankin, R. B.; Johnson, J. K.; Sholl, D. S. Progress, Opportunities, and Challenges for Applying Atomically Detailed Modeling to Molecular Adsorption and Transport in Metal-Organic Framework Materials. *Ind. Eng. Chem. Res.* **2009,** *48*, 2355–2371.

[71] Karra, J. R.; Walton, K. S. Effect of open metal sites on adsorption of polar and nonpolar molecules in metal−organic framework Cu-BTC. *Langmuir* **2008,** *24*, 8620–8626.

[72] Perry, J. J.; Perman, J. A.; Zaworotko, M. Design and synthesis of metal-organic frameworks using metal-organic polyhedra as supermolecular building blocks. *J. Chem. Soc. Rev.* 2009, **38,** 1400–1417.

[73] Li, C. P.; Du, M. Role of solvents in coordination supramolecular systems. *Chem. Commun.* **2011,** *47*, 5958–5972.

[74] Chowdhury, P.; Bikkina, C.; Gumma, S. Gas adsorption properties of the Chromium-Based Metal Organic Framework MIL-101. *J. Phys. Chem.C.* **2009**, *113*, 6616–6621.

[75] Arstad, B.; Fjellvåg, H.; Kongshaug, K.; Swang, O.; Blom, R. Amine functionalised metal organic frameworks (MOFs) as adsorbents for carbon dioxide. *Adsorption* **2008,** *14*, 755–762.

[76] Chowdhury, P.; Bikkina, C; Meister, D; Dreisbach, F.; Gumma, S. Comparison of adsorption isotherms on Cu-BTC metal organic frameworks synthesized from different routes. *Microporous and Mesoporous Materials* **2009,** *117*, 406–413.

[77] Sumida, K.; Her, J.-H.; Dinc_a, M.; Murray, L. J.; Schloss, J. M.; Pierce, C. J.; Thompson, B. A.; FitzGerald, S. A.; Brown, C. M.; Long, J. R. A Metal-Organic Framework with Exposed Cr^{2+} Sites. *J. Phys. Chem. C* **2011,** *115*, 8414–8421.

[78] Wu, H.; Zhou, W.; Yildirim, T. High-Capacity Methane Storage in Metal–Organic Frameworks M_2(dhtp): The Important Role of Open Metal Sites. *J. Am. Chem. Soc.* **2009,** *131*, 4995–5000.

[79] Liang, Z.; Marshall, M.; Chaffee, A. L. CO_2 adsorption, selectivity and water tolerance of pillared-layer metal organic frameworks. *Microporous and Mesoporous Materials* **2010,** *132*, 305–310.

[80] Achmann, S.; Hagen, G.; Hämmerle, M.; Malkowsky, I.; Kiener, C.; Moos, R. Sulfur Removal from Low-Sulfur Gasoline and Diesel Fuel by Metal-Organic Frameworks. *Chem. Eng. Technol.* **2010,** *33*, 275–280.

[81] Allen, M. P.; Tildesley, D. J. *Computer Simulation of Liquids*; Oxford University Press: New York, **1987**.

[82] Frenkel, D.; Smit, B. *Understanding Molecular Simulation: From Algorithms to Applications*, 2nd ed.; Academic Press: San Diego, **2002**.

[83] Li, H.; Eddaoudi, M.; Groy, T. L.; Yaghi, O. M. Establishing microporosity in open metal-organic frameworks: gas sorption isotherms for Zn(BDC) (BDC ¼ 1,4-benzenedicarboxylate). *J. Am. Chem. Soc.* **1998,** *120*, 8571–8572.

[84] Kim, J.; Chen, B.; Reineke, T. M.; Li, H.; Eddaoudi, M.; Moler D. B.; O'Keeffe, M.; Yaghi, O. M. Assembly of metal-organic frameworks from large organic and inorganic secondary

building units: new examples and simplifying principles for complex structures. *J. Am. Chem. Soc.* **2001,** *123,* 8239–8247.

[85] Stock, N.; Biswas, S. Synthesis of Metal-Organic Frameworks (MOFs): Routes to Various MOF Topologies, Morphologies, and Composites *Chem. Rev.* **2012,** *112*, 933–967.

[86] Huang, L.; Wang, H.; Chen, J.; Wang, Z.; Sun, J.; Zhao, D.; Yan, Y. Synthesis, morphology control, and properties of porous metal–organic coordination polymers. *Microporous Mesoporous Mater.* **2003,** *58*, 105–114.

[87] Shono, T.; Mingos, D. M. P.; Baghurst, D. R.; Lickiss, P. D. Novel Energy Sources for Reactions. In *The New Chemistry;* Hall, N., Ed.; The Press Syndicate of the University of Cambridge: Cambridge, 2000, Chapter 4.

[88] Liu, Y.; Her, J. -H.; Dailly, A.; Ramirez-Cuesta, A. J.; Neumann, D. A.; Brown, C. M. Reversible structural transition in MIL-53 with large temperature hysteresis. *J. Am. Chem. Soc.* **2008**, *130***,** 11813–11818.

[89] Serre, C.; Mellot-Draznieks, C.; Surble´, S.; Audebrand, N.; Filinchuk, Y.; Férey, G. Role of Solvent-Host Interactions That Lead to Very Large Swelling of Hybrid Frameworks. *Science* **2007**, *315*, 1828–1831.

[90] Boutin, A.; Coudert, F. -X.; Springuel-Huet, M. -A.; Neimark, A. V.; Férey, G.; Fuchs, A. H. The behavior of flexible MIL-53(Al) upon CH_4 and CO_2 adsorption. *J. Phys. Chem. C.* **2010**, *114***,** 22237–22244.

[91] Serre, C.; Bourrelly, S.; Vimont, A.; Ramsahye, N. A.; Maurin, G.; Llewellyn, P. L.; Daturi, M.; Filinchuk, Y.; Leynaud, O.; Barnes, P.; Férey G. An Explanation for the Very Large

Breathing Effect of a Metal–Organic Framework during CO_2 Adsorption. *Adv. Mater.* **2007,** *19,* 2246–2251.

[92] Beurroies, I.; Boulhout, M.; Llewellyn, P. L.; Kuchta, B.; Férey, G.; Serre, C.; Denoyel, R. Using Pressure to Provoke the Structural Transition of Metal–Organic Frameworks. *Angew. Chem., Int. Ed.* **2010**, *49,* 7526–7529.

[93] Farrusseng, D.; Daniel, C.; Gaudillere, C.; Ravon, U.; Schuurman, Y.; Mirodatos, C.; Dubbeldam, D.; Frost, H.; Snurr, R.Q. Heats of Adsorption for Seven Gases in Three Metal-Organic Frameworks: Systematic Comparison of Experiment and Simulation. *Langmuir*, **2009,** *25,* 7383–7388.

[94] Llewellyn, P. L.; Bourrelly, S.; Serre, C.; Vimont, A.; Daturi, M.; Hamon, L.; Weireld, G. D.; Chang, J.-S.; Hong, D.-Y.; Hwang, Y. K.; Jhung, S. H.; Fe´rey, G. High Uptakes of CO_2 and CH_4 in Mesoporous Metals Organic Frameworks MIL-100 and MIL-101. *Langmuir* **2008**, *24*, 7245–7250.

[95] Chowdhury, P.; Mekala, S.; Dreisbach, F.; Gumma, S. Adsorption of CO, CO_2 and CH_4 on Cu-BTC and MIL-101 metal organic frameworks: Effect of open metal sites and adsorbate polarity. *Microporous and Mesoporous Materials* **2012,** *152,* 246–252.

[96] Dietzel, P. D. C.; Besikiotis, V.; Blom, R. Application of metal–organic frameworks with coordinatively unsaturated metal sites in storage and separation of methane and carbon dioxide. *J. Mater. Chem.*, **2009,** *19,* 7362–7370.

[97] Caskey, S. R.; Wong-Foy, A. G.; Matzger, A. J. Dramatic Tuning of Carbon Dioxide Uptake via Metal Substitution in a Coordination Polymer with Cylindrical Pores. *J. Am. Chem. Soc.* **2008,** *130,* 10870–10871.

[98] Naik, S. P.; Chiang, S. T.; Thompson, R. W.; Huang, F. C. Formation of Silicalite-1 Hollow Spheres by the Self-assembly of Nanocrystals. *Chem. Mater.* **2003,** *15,* 787–792.

[99] Sun, M. S.; Shah, D. B.; Xu, H. H.; Talu, O. Adsorption equilibria of C_1 to C_4 alkanes, CO_2, and SF_6 on silicalite. *J. Phys. Chem. B* **1998,** *102,* 1466–1473.

[100] Mason, J. A.; Veenstrab, M.; Long, J. R. Evaluating metal–organic frameworks for natural gas storage. *Chem. Sci.* **2014,** *5,* 32–51.

[101] Lu, Z.; Du, L.; Tang, K.; Bai, High H_2 and CH_4 Adsorption Capacity of a Highly Porous (2,3,4)-Connected Metal–Organic Framework. *J. Cryst. Growth Des.* **2013,** *13,* 2252–2255.

[102] He, Y.; Zhou, W.; Yildirim, T.; Chen, B. A series of metal-organic frameworks with high methane uptake and an empirical equation for predicting methane storage capacity. *Energy Environ. Sci.* **2013,** *6,* 2735–2744.

[103] Guo, Z.; Wu, H.; Srinivas, G.; Zhou, Y.; Xiang, S.; Chen, Z.; Yang, Y.; Zhou, W.; O'Keeffe, M.; Chen, B. A metal-organic framework with optimized open metal sites and pore spaces for high methane storage at room temperature. *Angew. Chem. Int. Ed.* **2011,** *50,* 3178–3181.

[104] Wang, X. -S.; Ma, S; Rauch, K.; Simmons, J. M.; Yuan, D.; Wang, X.; Yildirim, T.; Cole, W. C; L´opez, J. J.; Meijere, A.; Zhou, H. -C. Metal−Organic Frameworks Based on Double-Bond-Coupled Di-Isophthalate Linkers with High Hydrogen and Methane Uptakes. *Chem. Mater.* **2008,** *20,* 3145–3152.

[105] Sun, D.; Ma, S.; Simmons, J. M.; Li, J. -R.; Yuan D.; Zhou, H.-C. An Unusual Case of Symmetry-Preserving Isomerism. *Chem. Commun.* **2010,** *46,* 1329–1331.

[106] Lin, X.; Telepeni, I.; Blake, A. J.; Dailly, A.; Brown, C. M.; Simmons, J. M.; Zoppi, M.; Walker, G. S.; Thomas, K. M.; Mays, T. J.; Hubberstey, P.; Champness, N. R.; Schröder, M. High capacity hydrogen adsorption in Cu(II) tetracarboxylate framework materials: the role of pore size, Ligand functionalization and exposed metal sites. *J. Am. Chem. Soc.* **2009,** *131,* 2159–2171.

[107] Rallapalli, P.; Prasanth, K. P.; Patil, D.; Somani, R. S.; Jasra, R. V.; Bajaj, H. C. Sorption studies of CO_2, CH_4, N_2, CO, O_2 and Ar on nanoporous aluminum terephthalate [MIL-53(Al)]. *J. Porous Mater*. **2011**, *18,* 205–210.

[108] Wilmer, C. E.; Farha, O. K.; Yildirim, T.; Eryazici, I.: Krungleviciute, V.; Sarjeant, A. A.; Snurr, R. Q.; Hupp, J. T. Gram-scale, high-yield synthesis of a robust metal–organic framework for storing methane and other gases. *Energy Environ. Sci.* **2013,** *6,* 1158–1163.

[109] Wiersum, A. D.; Chang, J. -S.; Serre C.; Llewellyn, P. L. An Adsorbent Performance Indicator as a First Step Evaluation of Novel Sorbents for Gas Separations: Application to Metal–Organic Frameworks. *Langmuir* **2013,** *29,* 3301–3309.

[110] Rowsell, J. L. C.; Yaghi, O. M. Effects of Functionalization, Catenation, and Variation of the Metal Oxide and Organic Linking Units on the Low-Pressure Hydrogen Adsorption Properties of Metal-Organic Frameworks. *J. Am. Chem. Soc.* **2006,** *128,* 1304–1315.

[111] He, Y.; Furukawa, H.; Wu, C.; O'Keeffe, M.; Krishna R.; Chen, B. Low-energy regeneration and high productivity in a lanthanide-hexacarboxylate framework for high-pressure CO_2-CH_4-H_2 separation. *Chem. Commun.* **2013,** *49,* 6773–6775.

[112] Peng, Y.; Srinivas, G.; Wilmer, C. E.; Eryazici, I.; Snurr, R. Q.; Hupp, J. T.; Yildirim, T.; Farha, O. K. Simultaneously high gravimetric and volumetric methane uptake characteristics of the metal–organic framework NU-111. *Chem. Commun.* **2013,** *49*, 2992–2994.

[113] Yuan, D.; Zhao, D.; Sun, D.; Zhou, H. -C. An Isoreticular Series of Metal–Organic Frameworks with Dendritic Hexacarboxylate Ligands and Exceptionally High Gas-Uptake Capacity. *Angew. Chem. Int. Ed.* **2010,** *49*, 5357–5361.

[114] Klein, N.; Senkovska, I.; Baburin, I. A.; Grünker, R.; Stoeck, U.; Schlichtenmayer, M.; Streppel, B; Mueller, U.; Leoni, S.; Hirscher, M.; Kaskel, S. Route to a Family of Robust, Non-interpenetrated Metal–Organic Frameworks with pto-like Topology. *Chem.–Eur. J.* **2011,** *17*, 13007–13016.

[115] Prasad, T. K.; Suh, M. P. Control of Interpenetration and Gas-Sorption Properties of Metal–Organic Frameworks by a Simple Change in Ligand Design. *Chem.–Eur. J.* **2012,** *18*, 8673–8680.

[116] Perez-Pellitero, J.; Amrouche, H.; Siperstein, F. R.; Pirngruber, G.; Nieto-Draghi, C.; Chaplais, G.; Masseron, A. S.; Bachi, D. B.; Peralta, D.; Bats, N. Adsorption of CO_2, CH_4, and N_2 on Zeolitic Imidazolate Frameworks: Experiments and Simulations. *Chem.–Eur. J.* **2010,** *16*, 1560–1571.

[117] Feldblyum, J. I.; Dutta, D.; Wong-Foy, A. G.; Dailly, A.; Imirzian, J.; Gidley, D. W.; Matzger, A. J. Interpenetration, porosity, and high-pressure gas adsorption in Zn_4O(2,6-naphthalene dicarboxylate)$_3$. *Langmuir* **2013,** *29*, 8146–8153.

[118] Yan, Y.; Yang, S.; Blake, A. J.; Lewis, W.; Poirier, E.; Barnett, S. A.; Champness, N. R.; Schröder, M. A Mesoporous Metal-Organic Framework Constructed From A Nanosized C3-

Symmetric Linker and [Cu_{24}(Isophthalate)$_{24}$] Cuboctahedra. *Chem. Commun.* **2011,** *47,* 9995–9997.

[119] Rolniak, P. D.; Kobayashi, R. Adsorption of Methane and Several Mixtures of Methane and Carbon Dioxide at Elevated Pressures and Near Ambient Temperatures on 5A and 13X Molecular Sieves by Tracer Pertubation Chromatography. *AIChE J.* **1980,** *26,* 616–625.

[120] Dirar, Q. H.; Loughlin, K. F. Intrinsic Adsorption Properties of CO_2 on 5A and 13X Zeolite. *Adsorption* **2013,** *19,* 1149–1163.

[121] Karra, J. R.; Walton, K. S. Molecular Simulations and Experimental Studies of CO_2, CO, and N_2 Adsorption in Metal Organic Frameworks. *J. Phys. Chem. C* **2010**, *114,* 15735–15740.

[122] Chavan, S.; Vitillo, J. G.; Groppo, E.; Bonino, F.; Lamberti, C.; Dietzel, P. D. C.; Bordiga, S. CO Adsorption on CPO-27-Ni Coordination Polymer: Spectroscopic Features and Interaction Energy. *J. Phys. Chem. C* **2009,** *113,* 3292–3299.

[123] Belmabkhout, Y.; Pirngruber, G.; Jolimaitre, E.; Methivier, A. A complete experimental approach for synthesis gas separation studies using static gravimetric and column breakthrough experiments. *Adsorption* **2007,** *13,* 341–349.

[124] Golden, T. C.; Sircar, S. Gas Adsorption on Silicalite. *J. Coll. Inter. Sci.* **1994,** *162,* 182–188.

[125] Liu, J.; Culp, J.T.; Natesakhawat, S.; Bockrath, B.C.; Zande, B.; Sankar, S.G.; Garberoglio, G.; Karl Johnson, J. Experimental and Theoretical Studies of Gas Adsorption in Cu3(BTC)2: An Effective Activation Procedure *J. Phys. Chem. C.* **2007,** *111,* 9305–9313.

[126] García-Pérez, E.; Gascón, J.; Morales-Flórez, V.; Castillo, J.M.; Kapteijn, F.; Calero, S.; Identification of Adsorption sites in Cu-BTC by Experimentation and Molecular Simulation. *Langmuir* **2009,** *25,* 1725–1731.

[127] Salem, M.M.K.; Braeuer, P.; Szombathely, M.V.; Heuchel, M.; Harting, P.; Quitzsch, K.; Jaroniec, M. Thermodynamics of High-Pressure Adsorption of Argon, Nitrogen, and Methane on Microporous adsorbents. *Langmuir*, **1998,** *14*, 3376–3389.

[128] Dreisbach, F.; Staudt, R.; Keller, J. U. High Pressure Adsorption Data of Methane, Nitrogen, Carbon Dioxide and their Binary and Ternary Mixtures on Activated carbon. *Adsorption* **1999,** *5,* 215–227.

[129] Belmabkhout, Y.; De Weireld, G.; and Frère, M.; High-Pressure Adsorption Isotherms of N_2, CH_4, O_2, and Ar on Different Carbonaceous Adsorbents. *J. Chem. Engg. Data,* **2004,** *49,* 1379–1391.

[130] Stallmach, F.; Groger, S.; Kunzel, V.; Karger, J.; Yaghi, O. M.; Hesse, M.; Muller, U. NMR Studies on the Diffusion of Hydrocarbons on the Metal-Organic Framework Material MOF-5. *Angew. Chem. Int. Ed.* **2006,** *45,* 2123–2126.

[131] Pires, J.; Pinto, M. L. Granadeiro, C. M.; Barbosa, A.D. S.; Cunha-Silva, L.; Balula, S. S.; Saini, V. K. Effect on selective adsorption of ethane and ethylene of the polyoxometalates impregnation in the metal-organic framework MIL-101. *Adsorption* **doi:** 10.1007/s10450-013-9592-6.

[132] Bao, Z.; Alnemrat, S.; Yu, L.; Vasiliev, I.; Ren, Q.; Lu, X.; Deng, S. Adsorption of Ethane, Ethylene, Propane, and Propylene on a Magnesium-Based MetalOrganic Framework. Langmuir 2011, 27, 13554–13562.

[133] Bloch, E. D.; Queen, W. L.; Krishna, R.; Zadrozny, J. M.; Brown, C. M.; Long, J. R. Hydrocarbon Separations in a Metal-Organic Framework with Open Iron(II) Coordination Sites. *Science* **2012,** *335*, 1606–1610.

[134] Hyun, S. H.; Danner, R. P. Equiilbrium Adsorption of Ethane, Ethylene, Isobutane, Carbon Dioxide, and Their Binary Mixtures on 13X Molecular Sieves. J. *Chem. Eng. Data* **1982,** *27*, 196–200.

[135] Nam, Gi-M.; Jeong, Byung-M.; Kang, Seok-H.; Lee, Byung-K.; Choi, Dae-K. Equilibrium Isotherms of CH_4, C_2H_6, C_2H_4, N_2, and H_2 on Zeolite 5A Using a Static Volumetric Method. J. *Chem. Eng. Data* **2005,** *50*, 72–76.

[136] Rubes, M.; Wiersum, A. D.; Llewellyn, P. L.; Grajciar, L.; Bludsky, O.; Nachtigall, P. Adsorption of Propane and Propylene on CuBTC Metal−Organic Framework: Combined Theoretical and Experimental Investigation. *J. Phys. Chem. C* **2013,** *117*, 11159–11167.

[137] Jiang, J.; Sandler, S. I. Monte Carlo Simulation for the Adsorption and Separation of Linear and Branched Alkanes in IRMOF-1. Langmuir 2006, 22, 5702–5707.

[138] Llewellyn, P. L.; Horcajada, P.; Maurin, G.; Devic, T.; Rosenbach, N.; Bourrelly, S.; Serre, C.; Vincent, D.; Loera-Serna, S.; Filinchuk, Y.; Férey, G. Complex Adsorption of Short Linear Alkanes in the Flexible Metal-Organic-Framework MIL-53(Fe). *J. Am. Chem. Soc.* **2009**, *131***,** 13002–13008.

[139] Siperstein, F. R.; Myers, A.L. Mixed-Gas Adsorption. *AIChE J.* **2001,** *47*, 1141–1159.

[140] Herden, H.; Loffler, U.; Schollner, R. Adsorption of Hydrocarbons on Activated Carbons. Journal of Colloid and Interface Science 1991, 144, 477–482.

[141] Bloch, E. D.; Murray, L. J.; Queen, W. L.; Chavan, S.; Maximoff, S. N.; Bigi, J.P.; Krishna, R.; Peterson, V. K.; Grandjean, F.; Long, G.; Smit, B.; Bordiga, S.; Brown, C. M.; Long, J. R. Selective Binding of O_2 over N_2 in a Redox–Active Metal–Organic Framework with Open Iron(II) Coordination Sites. *J. Am. Chem. Soc.* **2011,** *133,* 14814–14822.

[142] Dunne, J.A.; Mariwala, R.; Rao, M.; Sircar, S.; Gorte, R.J.; Myers A. L. Calorimetric Heats of Adsorption and adsorption Isotherms. 1. O_2, N_2, Ar, CO_2, CH_4, C_2H_6, and SF_6 on Silicalite. *Langmuir* **1996,** *12,* 5888–5895.

[143] Talu, O.; Li, J.; Kumar, R.; Mathias, P. M.; Moyer, J. D. Jr; Schork, J. M. Measurement and analysis of oxygen/nitrogen/5A-zeolite adsorption equilibria for air separation. *Gas. Sep. Purif.* **1996,** *10,* 149–159.

[144] Alternative Fuels Data Center – Fuel Properties Comparison, 2013, http://www.afdc.energy.gov/fuels/fuel_comparison_chart.pdf.

[145] Ma, S.; Sun, D.; Simmons, J. M.; Collier, C. D.; Yuan, D.; Zhou, H.-C. Metal-Organic Framework from an Anthracene Derivative Containing Nanoscopic Cages Exhibiting High Methane Uptake. *J. Am. Chem. Soc.* **2008,** *130,* 1012–1016.

[146] Peng, Y.; Krungleviciute, V.; Eryazici, I.; Hupp, J. T.; Farha, O. K.; Yildirim, T. Methane Storage in Metal–Organic Frameworks: Current Records, Surprise Findings, and Challenges. *J. Am. Chem. Soc.* **2013,** *135,* 11887–11894.

[147] Zhou, W.; Wu, H.; Yildirim, T. Enhanced H_2 Adsorption in Isostructural Metal Organic Frameworks with Open Metal Sites: Strong Dependence of the Binding Strength on Metal Ions. *J. Am. Chem. Soc.* **2008,** *130,* 15268–15269.

[148] Suh, M. P.; Park, H. J.; Prasad, T. K.; Lim D. W. Hydrogen Storage in Metal–Organic Frameworks. *Chem. Rev.* **2012**, *112*, 782–835.

[149] Hugle, T.; Hartl, M.; Lentz, D. The Route to a Feasible Hydrogen-Storage Material: MOFs versus Ammonia Borane. *Chem.—Eur. J.* **2011,** *17,* 10184–10207.

[150] Zhang, Y.-H. P. Renewable carbohydrates are a potential high density hydrogen carrier. *Int. J. Hydrogen Energy* **2010,** *35,* 10334–10342.

[151] Chen, J.; Wu, F. Review of hydrogen storage in inorganic fullerene-like nanotubes. *Appl. Phys. A: Mater. Sci. Process.* **2004,** *78,* 989–994.

[152] Strobel, R.; Garche, J.; Moseley, P. T.; Jorissen, L.; Wolf, G. Hydrogen storage by carbon materials. *J. Power Sources* **2006,** *159,* 781–801.

[153] Wang, Z.; Tanabe, K. K.; Cohen, S. M. Tuning Hydrogen Sorption Properties of Metal-Organic Frameworks by Postsynthetic Covalent Modification. *Chem. –Eur. J.* **2010,** *16,* 212–217.

[154] Kosal, M. E.; Chou, J.-H.; Wilson, S. R.; Suslick, K. S. A Functional Zeolite Analogue Assembled From Metalloporphyrins. *Nat. Mater.* **2002,** *1,* 118–121.

[155] Zimmer, B.; Hutin, M.; Bulach, V.; Hosseini, M. W.; Cian, A. D.; Kyritsakas, A 3-D network based on porphyrin and copper : an interpla y between coordination bonding, P-P interactions and H-bonding. *N. New. J. Chem.* **2002,** *26,* 1532–1535.

[156] Deiters, E.; Bulach, V.; Hosseini, M. W. Reversible single-crystal-to-single-crystal guest exchange in a 3-D coordination network based on a zinc porphyrin. *Chem. Commun.* **2005,** 3906–3908.

[157] Kuhn, E.; Bulach, V.; Hosseini, M. W. Molecular tectonics: control of pore size and polarity in 3-D hexagonal coordination networks based on porphyrins and Zinc cation. *Chem. Commun.* **2008,** 5104–5106.

[158] Krishna, R. Adsorptive separation of $CO_2/CH_4/CO$ gas mixtures at high pressures. *Microporous and Mesoporous Materials* **2012,** *156,* 217–223.

[159] Xiang, S.; He, Y.; Zhang, Z.; Wu, H.; Zhou, W.; Krishna, R.; Chen, B. Microporous metal-organic framework with potential for carbon dioxide capture at ambient conditions. *Nat. Commun.* **2012**, *3,* 954–962.

[160] Bae, Y. -S.; Lee, C. Y.; Kim, K. C.; Farha, O. K.; Nickias, P.; Hupp, J. T.; Nguyen, S. B. T.; Snurr, R. Q. High Propene/Propane Selectivity in Isostructural Metal–Organic Frameworks with High Densities of Open Metal Sites. *Angew. Chem., Int. Ed.* **2012,** *51,* 1857–1860.

[161] Wang, Z.; Cohen, S. M. Postsynthetic Covalent Modification of a Neutral Metal−Organic Framework. *J. Am. Chem. Soc.* **2007,** *129,* 12368–12369.

[162] Tanabe, K. K.; Wang, Z.; Cohen, S. M. Systematic functionalization of a metal-organic framework via a postsynthetic modification approach. *J. Am. Chem. Soc.* **2008,** *130,* 8508–8517.

[163] Biswas, S.; Ahnfeldt, T.; Stock, N. New functionalized flexible Al-MIL-53-X (X = -Cl, -Br, $-CH_3$, $-NO_2$, $-(OH)_2$) solids: syntheses, characterization, sorption, and breathing behavior. *Inorg Chem.* **2011,** *50,* 9518–9526.

[164] Himsl, D.; Wallacher, D.; Hartmann, M. Improving the Hydrogen-Adsorption Properties of a Hydroxy-Modified MIL-53(Al) Structural Analogue by Lithium Doping. *Angew. Chem. Int. Ed.* **2009,** *48,* 4639–4642.

[165] Xiang, Z.; Hua, Z.; Yang, W.; Cao, D. Lithium doping on metal-organic frameworks for enhancing H_2 Storage. *International Journal of Hydrogen Energy* **2012,** *37*, 946–950.

[166] Dietzel, P. D. C.; Morita, Y.; Blom, R.; Fjellvag, H. An In Situ High-Temperature Single-Crystal Investigation of a Dehydrated Metal–Organic Framework Compound and Field-Induced Magnetization of One-Dimensional Metal–Oxygen Chains. *Angew. Chem., Int. Ed.* **2005,** *44*, 6354–6358.

[167] Dietzel, P. D. C.; Panella, B.; Hirscher, M.; Blom, R.; Fjellvag, H. Hydrogen adsorption in a nickel based coordination polymer with open metal sites in the cylindrical cavities of the desolvated framework. *Chem. Commun.* **2006,** 959–961.

[168] Chavan, S.; Vitillo, J. G.; Larabi, C.; Quadrelli, E. A.; Dietzel, P. D. C.; Bordiga, S. Functionalization of CPO-27-Ni through metal hexacarbonyls: The role of open Ni^{2+} sites. *Microporous and Mesoporous Materials* **2012,** *157*, 56–61.

[169] Dietzel, P. D. C.; Johnsen, R. E.; Blom, R.; Fjellvag, H. Structural Changes and Coordinatively Unsaturated Metal Atoms on Dehydration of Honeycomb Analogous Microporous Metal–Organic Frameworks. *Chem. Eur. J.* **2008,** *14*, 2389–2397.

[170] Llewellyn, P. L.; Bourrelly, S.; Serre, C.; Filinchuk, Y.; Férey, G. How hydration drastically improves adsorption selectivity for CO_2 over CH_4 in the flexible chromium terephthalate MIL-53. *Angew. Chem. Int. Ed.* **2006,** *45*, 7751–7754.

[171] Comotti, A.; Bracco, S.; Sozzani, P.; Horike, S.; Matsuda, R.; Chen, J.; Takata, M.; Kubota, Y.; Kitagawa, S. Nanochannels of Two Distinct Cross-Sections in a Porous Al-Based Coordination Polymer. *J. Am. Chem. Soc.* **2008,** *130*, 13664–13672.

[172] Alaerts, L.; Maes, M.; van der Veen, M. A.; Jacobs, P. A.; De Vos, D. E. Metal–organic frameworks as high-potential adsorbents for liquid-phase separations of olefins, alkylnaphthalenes and dichlorobenzenes. *Phys. Chem. Chem. Phys.* **2009,** *11,* 2903–2911.

[173] Maes, M.; Vermoortele, F.; Alaerts, L.; Couck, S.; Kirschhock, C. E. A.; Denayer, J. F. M.; De Vos, D. E. Separation of styrene and ethylbenzene on metal-organic frameworks: analogous structures with different adsorption mechanisms. *J. Am. Chem. Soc.* **2010,** *132,* 15277–15285.

[174] Kanoh, H.; Kondo, A.; Noguchi, H.; Kajiro, H.; Tohdoh, A.; Hattori, Y.; Xu, W. C.; Moue, M.; Sugiura, T.; Morita, K.; Tanaka, H.; Ohba, T.; Kaneko, K. Elastic layer-structured metal organic frameworks (ELMs). *J. Colloid Interface Sci.* **2009,** *334,* 1–7.

[175] Kitaura, R.; Seki, K.; Akiyama, G.; Kitagawa, S. Porous Coordination-Polymer Crystals with Gated Channels Specific for Supercritical Gases. *Angew. Chem. Int. Ed.* **2003,** *42,* 428–431.

[176] Henke, S.; Fischer, R. A. Gated channels in a honeycomb-like zinc-dicarboxylate-bipyridine framework with flexible alkyl ether side chains. *J. Am. Chem. Soc.* **2011,** *133,* 2064–2067.

[177] Ma, S.; Sun, D.; Wang, X. S.; Zhou, H. C. Mesh-Adjustable Molecular Sieve for General Use in Gas Separation. *Angew. Chem. Int. Ed.* **2007,** *46,* 2458–2462.

[178] Ma, S. Q.; Sun, D. F.; Yuan, D. Q.; Wang, X. S.; Zhou, H. C. he Preparation and Gas Adsorption Studies of Three Mesh-Adjustable Molecular Sieves with a Common Structure. *J. Am. Chem. Soc.* **2009,** *131,* 6445–6451.

[179] Yang, Q.; Liu, D.; Zhong, C.; Li, J. -R. Development of Computational Methodologies for Metal−Organic Frameworks and Their Application in Gas Separations. *Chem. Rev.* **2013,** *113,* 8261–8323.

[180] Frost, H.; Dùren, T.; Snurr, R. Q. Effects of surface area, free volume, and heat of adsorption on hydrogen uptake in metal-organic frameworks. *J. Phys. Chem. B* **2006,** *110,* 9565–9670.

[181] Getman, R. B.; Bae, Y.-S.; Wilmer, C. E.; Snurr, R. Q. Review and analysis of molecular simulations of methane, hydrogen, and acetylene storage in metal-organic frameworks. *Chem. Rev*. **2012,** *112,* 703–723.

[182] Lochan, R. C.; Head-Gordon, M. Computational studies of molecular hydrogen binding affinities: The role of dispersion forces, electrostatics, and orbital interactions. *Phys. Chem. Chem. Phys.* **2006,** *8,* 1357–1370.

[183] Dùren, T.; Bae, Y.-S.; Snurr, R. Q**.** Using molecular simulation to characterise metal–organic frameworks for adsorption applications. *Chem. Soc. Rev.* **2009,** *38,* 1237–1247.

[184] Krishna, R. Diffusion in porous crystalline materials. *Chem. Soc. Rev.* **2012,** *41,* 3099–3118.

[185] Jhon, Y. H.; Cho, M.; Jeon, H. R.; Park, I.; Chang, R.; Rowsell, J. L. C.; Kim, J. Simulations of methane adsorption and diffusion within alkoxy-functionalized IRMOFs exhibiting severely disordered crystal structures. *J. Phys. Chem. C* **2007,** *111,* 16618–16625.

[186] Liu, B. and Smit, B. Comparative molecular simulation study of CO_2/N_2 and CH_4/N_2 separation in zeolites and metal-organic frameworks. *Langmuir* **2009,** *25,* 5918–5926.

[187] Cychosz, K. A.; Matzger, A. J. Water Stability of Microporous Coordination Polymers and the Adsorption of Pharmaceuticals from Water. *Langmuir* **2010,** *26,* 17198–17202.

[188] Kizzie, A. C.; Wong-Foy, A. G.; Matzger, A. J. Effect of humidity on the performance of microporous coordination polymers as adsorbents for CO_2 capture. *Langmuir* **2011**, *27***,** 6368–6373.

[189] Jasuja, H.; Huang, Y.; Walton, K. S. Adjusting the Stability of Metal−Organic Frameworks under Humid Conditions by Ligand Functionalization. *Langmuir* **2012**, *28***,** 16874–16880.

[190] Smith, J. M. and Van Ness H. C. Introduction to Chemical Engineering Thermodynamics. *Fourth Edition, McGraw-Hill, New York,* **1987**.

[191] Talu, O. Needs,status,techniques and problems with binary gas adsorption experiments. *Advances in Colloid and Interface Science* **1998,** *76-77,* 227–269.

[192] Barton, T. J.; Bull, L. M.; Klemperer, W. G.; Loy, D. A.; McEnaney, B.; Misono, M.; Monson, P. A.; Pez, G.; Scherer, G. W.; Vartuli, J. C.; Yaghi, O. M. Tailored Porous Materials. *Chem. Mater*. **1999,** *11,* 2633–2656.

[193] Chowdhury, P. Gas Adsorption on Cu-BTC and Cr-BDC Metal Organic Frameworks (MOFs). **PhD Dissertation,** *Indian Institute of Technology, Guwahati* (**2010**).

[194] Van Ness, H. C. Adsorption of gases on solids. *I & EC Fundamentals* **1969,** *8,* 464–473.

[195] Steele,W.A. The interaction of gases with solid surfaces. *Pergamon press New York,* **1974**.

[196] Gumma, S.; Talu, O. Net Adsorption: A Thermodynamic Framework for Supercritical Gas Adsorption and Storage in Porous Solids. *Langmuir* **2010**, *26,* 17013–12023.

[197] Gumma, S. On Measurement, Analysis and Modeling of Mixed gas Adsorption Equilibria. **PhD Dissertation,** *Cleveland State University* (**2003**).

[198] Myers, A. L.; Prausnitz, J. M. Thermodynamics of Mixed Gas Adsorption. *AIChE J.* **1965,** ***11***,121–127.

[199] Trung, T. H.; Trens, P.; Tanchoux, N.; Bourrelly, S.; Llewellyn, P. L.; Loera-Serna, S.; Serre, C.; Loiseau, T.; Fajula, F.; Férey, G. Hydrocarbon adsorption in the flexible Metal Organic Frameworks MIL-53(Al, Cr). *J. Am. Chem. Soc.* **2008,** *130***,** 16926–16932.

[200] http://dippr.byu.edu/student.asp.

[201] Küsgens, P.; Rose, M.; Senkovska, I.; Fröde, H.; Henschel, A.; Siegle, S.; Kaskel, S. Characterization of metal-organic frameworks by water adsorption. *Microporous and Mesoporous Materials* **2009**, *120***,** 325–330.

[202] Hamon, L.; Llewellyn, P. L.; Devic, T.; Ghoufi, A.; Clet, G.; Guillerm, V.; Pirngruber, G.D.; Maurin, G.; Serre, C.; Driver, G.; Beek, W.; Jolimaître, E.; Vimont, A.; Daturi, M.; Férey, G. Co-adsorption and Separation of CO_2−CH_4 Mixtures in the Highly Flexible MIL-53(Cr) MOF. *J. Am. Chem. Soc.* **2009,** *131***,** 17490–17499.

[203] Serra-Crespo, P.; Gobechiya, E.; Ramos-Fernandez, E. V.; Juan-Alcańiz, J.; Martinez-Joaristi, A.; Stavitski, E.; Kirschhock, C. E. A.; Martens, J. A.; Kapteijn, F.; Gascon, J. Interplay of Metal Node and Amine Functionality in NH_2-MIL-53: Modulating Breathing Behavior through Intra-framework Interactions. *Langmuir* **2012**, *28***,** 12916–12922.

[204] Devic, T.; Salles, F.; Bourrelly, S.; Moulin, B.; Maurin, G.; Horcajada, P.; Serre, C.; Vimont, A.; Lavalley, J.-C.; Leclerc, H.; Clet, G.; Daturi, M.; Llewellyn, P. L.; Filinchuk, Y.; Férey, G. Effect of the organic functionalization of flexible MOFs on the adsorption of CO_2. *J. Mater. Chem.* **2012,** *22*, 10266–10273.

[205] Neimark, A.V.; Coudert, F. -X.; Triguero, C.; Boutin, A.; Fuchs, A. H.; Beurroies, I.; Denoyel, R. Structural Transitions in MIL-53(Cr): View from Outside and Inside. *Langmuir* **2011**, *27***,** 4734–4741.

[206] Ortiz. A. U.; Boutin, A.; Fuchs, A. H.; Coudert, F. -X. Anisotropic Elastic Properties of Flexible Metal-Organic Frameworks: How Soft are Soft Porous Crystals?. *Phys. Rev. Lett.* **2012**, *109***,** 195502 (1–5).

[207] Ortiz. A. U.; Springuel-Huet, M. A.; Coudert, F. -X.; Fuchs, A. H.; Boutin, A. Predicting Mixture Coadsorption in Soft Porous Crystals: Experimental and Theoretical Study of CO_2/CH_4 in MIL-53(Al). *Langmuir* **2012**, *28***,** 494–498.

[208] Couck, S.; Denayer, J. F. M.; Baron, G. V.; Rémy, T.; Gascon, J.; Kapteijn, F. An amine-functionalized MIL-53 Metal-Organic Framework with large separation power for CO_2 and CH_4. *J. Am. Chem. Soc.* **2009,** *131*, 6326–6327.

[209] Stavitski, E.; Pidko, E. A.; Couck, S.; Rémy, T.; Hensen, E. J. M.; Weckhuysen, B. M.; Denayer, J.; Gascon, J.; Kapteijn, F. Complexity behind CO_2 capture on NH_2-MIL-53(Al). *Langmuir* **2011**, *27***,** 3970–3976.

[210] Springuel-Huet, M. A.; Nossov, A.; Adem, Z.; Guenneau, F.; Volkringer, C.; Loiseau, T.; Férey, G.; Gédéon, A. Bourrelly, S.; Llewellyn, P. L.; Serre, C.; Millange, F.; Loiseau, T. ^{129}Xe NMR Study of the Framework Flexibility of the Porous Hybrid MIL-53(Al). *J. Am. Chem. Soc.* **2010**, *132*, 11599–11607.

[211] Coudert, F. -X.; Jeffroy, M.; Fuchs, A. H.; Boutin, A.; Mellot-Draznieks, C. Thermodynamics of guest-induced structural transitions in hybrid organic−inorganic frameworks. *J. Am. Chem. Soc.* **2008**, *130***,** 14294–14302.

[212] Shannon, R. D. Revised effective ionic radii and systematic studies of interatomic distances in halides and chalcogenides. *Acta Crystallogr*. **1976,** *A32*, 751–767.

[213] Walton, K. S.; LeVan, M. D. A Novel Adsorption Cycle for CO_2 Recovery: Experimental and Theoretical Investigations of a Temperature Swing Compression Process. *Sep. Sci. Technol.* **2006,** *41*, 485–500.

[214] Hamon, L.; Jolimaitre, E.; Pirngruber, G. CO_2 and CH_4 Separation by Adsorption Using Cu-BTC Metal−Organic Framework. *Ind. Eng. Chem. Res.* **2010,** *49*, 7497–7503.

[215] Galli, S.; Masciocchi, N.; Tagliabue, G.; Sironi, A.; Navarro, J. A. R.; Salas, J. M.; Mendez-Liñan, L.; Domingo, M.; Pérez-Mendoza, M.; Barea, E. Polymorphic Coordination Networks Responsive to CO_2, Moisture, and Thermal Stimuli: Porous Cobalt(II) and Zinc(II) Fluoropyrimidinolates. *Chem. –Eur. J.* **2008,** *14*, 9890–9901.

[216] Wang, Q. M.; Shen, D.; Bülow, M.; Lau, M. L.; Deng, S.; Fitch, F. R.; Lemcoff, N. O.; Semanscin, J. Metallo-organic molecular sieve for gas separation and purification. *Microporous and Mesoporous Materials* **2002,** *55*, 217–230.

[217] Talu, O.; Zwiebel, I. Multicomponent adsorption equilibria of nonideal mixtures. *AIChE J.* **1986,** *32*, 1263–1276.

[218] Babarao, R.; Hu, Z. Q.; Jiang, J. W.; Chempath, S.; Sandler, S. I. Storage and separation of CO_2 and CH_4 in silicalite, C168 schwarzite, and IRMOF-1: a comparative study from Monte Carlo simulation. *Langmuir* **2007,** *23*, 659–666.

[219] Babarao, R.; Jiang, J. W.; Sandler, S. I. Molecular simulations for adsorptive separation of CO_2/CH_4 mixture in metal-exposed, catenated, and charged metal-organic frameworks. *Langmuir* **2009,** *25*, 5239–5247.

[220] Chen, Y. F.; Babarao, R.; Sandler, S. I.; Jiang, J. W. Metal-organic framework MIL-101 for adsorption and effect of terminal water molecules: from quantum mechanics to molecular simulation. *Langmuir* **2010,** *26*, 8743–8750.

[221] Xu, Q.; Liu, D. H.; Yang, Q. Y.; Zhong, C. L.; Mi, J. G. Li-modified metal–organic frameworks for CO_2/CH_4 separation: a route to achieving high adsorption selectivity. *J. Mater. Chem*. **2010,** *20*, 706–714.

[222] Liu, J.; Benin, A.; Furtado, A. M. B.; Jakubczak, P.; Willis, R. R.; LeVan, M. D. Stability Effects on CO_2 Adsorption for the DOBDC Series of Metal–Organic Frameworks. *Langmuir* **2011,** *27*, 11451–11456.

[223] Lee, J. Y.; Olson, D. H.; Pan, L.; Emge, T. J.; Li, J. Microporous metal–organic frameworks with high gas sorption and separation capacity. *Ad. Funct. Mater.* **2007,** *17*, 1255–1262.

[224] Senkovska, I.; Kaskel, S. High pressure methane adsorption in the metal-organic frameworks $Cu_3(btc)_2$, $ZN_2(bdc)_2$dabco, and $Cr_3F(H_2O)_2O(bdc)_3$. *Microporous and Mesoporous Materials* **2008,** *112*, 108–115.

[225] Vermesse, J.; Vidal, D.; Malbrunot, P. Gas adsorption on zeolites at high pressure. *Langmuir* **1996**, *12*, 4190–4196.

[226] Pakseresht, S.; Kazemeini, M.; Akbarnejad, M. M. Equilibrium isotherms for CO, CO_2, CH_4 and C_2H_4 on the 5A molecular sieve by a simple volumetric apparatus. *Sep. Purf. Tech.* **2002,** *28*, 53–60.

[227] Mishra, P.; Edubilli, S.; Mandal, B.; Gumma, S. Adsorption Characteristics of Metal Organic Frameworks Containing Coordinatively Unsaturated Metal Sites: Effect of Metal Cations and Adsorbate Properties. *J. Phys. Chem. C* **2014,** *118,* 6847–6855.

[228] Voorde, M. V.; Verelst, H.; Baron, G. V.; Measurement of O_2-N_2 binary sorption on 5A zeolite by isotope tracer and perturbation chromatography. *J. Porous Materials* **1995,** *2,* 51–57.

[229] Myers, A. L. Characterization of nanopores by standard enthalpy and entropy of adsorption of probe molecules. *Colloids and Surfaces A* **2004,** *241,* 9–14.

[230] Shen, D.; Bülow, M.; Siperstein, F.; Engelhard, M.; Myers, A. L. Comparison of experimental techniques for measuring isosteric heat of adsorption. *Adsorption* **2000,** *6,* 275–286.

[231] Krishna, R.; Long, J. R. Screening Metal-Organic Frameworks by Analysis of Transient Breakthrough of Gas Mixtures in a Fixed Bed Adsorber. *J. Phys. Chem. C* **2011,** *115,* 12941–12950.

[232] Krishna, R.; van Baten, J. M. A comparison of the CO_2 capture characteristics of zeolites and metal–organic frameworks. *Sep. Purif. Technol.* **2012,** *87,* 120–126.

[233] Krishna, R.; van Baten, J. M. In silico screening of metal-organic frameworks in separation applications. *Phys. Chem. Chem. Phys.* **2011,** *13,* 10593–10616.

[234] Chen, Y. F.; Lee, J. Y.; Babarao, R.; Li, J.; Jiang, J. W. A Highly Hydrophobic Metal-Organic Framework Zn(bdc)(ted)0.5 for Adsorption and Separation of CH_3OH/H_2O and CO_2/CH_4: Integrated Experimental and Simulation Studies. *J. Phys. Chem. C* **2010,** *114,* 6602–6609.

[235] Liu, Y.; Liu, H. L.; Hu, Y.; Jiang, J. W. Density Functional Theory for Adsorption of Gas Mixtures in Metal−Organic Frameworks. *J. Phys. Chem. B* **2010,** *114,* 2820–2827.

APPENDIX: A

Detail of the Experimental Protocol followed for Adsorption Measurement

Experimental Protocol

The gravimetric adsorption measurement unit used for this work has also been used by an earlier doctorate student (*Dr. Pradip Chowdhaury*) of our group [**193**]. The necessary steps involved in the operation of this unit are elaborately presented by him in his dissertation [**193**]. After that only slight modifications in this gravimetric adsorption measurement unit are made during present work and schematic of latest form of the setup is shown in Figure 4.1. The steps followed during gas adsorption measurements in this unit are presented below.

Before going into details of the experimental protocol, some procedures can be defined as follows.

Procedure - Vent

1) Open H5, H6, H8, M3 in order
2) If P3 > 760 torr, follow below steps; else close H5, H6, H8, M3
3) Open H12 and wait till P3 reaches < 1000 torr
4) Open H4 and wait till P3 reaches 760 torr
5) Close H4, H5, H6, H8, H12, M3

Procedure - Vacuum

1) Open H5, H6, H8, M3
2) If P3 =< 760 torr, directly follow below steps 3 to 7

   Else

   (a) First, follow *procedure - vent*

   (b) Open H5, H6, H8, M3

   (c) Follow steps 3 to 7

3) Switch on vacuum pump and open H13

4) Wait till P3 reaches < 20 torr

5) Open H4 and wait till P3 reaches 0 torr

6) Close H4, H5, H6, H8, H13, M3

7) Switch off vacuum pump

Procedure - Pressure Charge

1) Select a particular gas and connect it to H2 or H3 (say H2 for example)

2) Open gas cylinder regulator and start the weight measurement at three positions of balance *i.e.* ZP (zero point position), MP1 (when only bucket was lifted) and MP2 (when bucket and sinker both were lifted). Online measurement of these weights was done throughout whole experiment by software.

3) Open H4, H5 and H8

4) Open H2 and close this valve after getting the desired pressure inside the balance assembly

5) For the sake of safety of pressure transducers and accuracy in the measurements, open and monitor the transducers as following

If P4 < 350 psi, open M3; else monitor P4

If P3 < 1000, open M2; else monitor P3

If P2 < 10, open M1, H11 and monitor P1; else monitor P2

6) After injecting the gas wait for sufficient time to attain equilibrium. The time needed to gat equilibrium is not fixed and depends upon solid adsorbents and adsobate gas. Usually if the change in sample weight is less than 1 mg for 15 minutes, equilibrium was assumed.

7) Once the equilibrium was achieved, balance readings at ZP, MP1 and MP2 were manually noted down. Pressure and temperatures readings were also taken.

8) Adsorption readings corresponding to the next subsequent pressures were obtained by following steps 4 - 7 in loop.

The complete experimental protocol is divided into various sub-sections as following

(i) Sample loading

1) Open the balance and take out the bucket
2) Take the weights of empty bucket and glass wool
3) Load the adsorbent sample into bucket
4) Mount the bucket into the balance
5) The balance chamber is then sealed and whole system was ensured to be leaks free

(ii) Activation of sample

Activation of adsorbent sample was done prior to every isotherm measurement to remove adsorbed impurities from the sample. These impurities can be anything such as foreign gas molecules, moisture and left over solvents from the synthesis. Below steps were followed to do the activation. If nothing is mentioned about any valve or other part, by default that is in closed position.

1) Follow *procedure - vacuum*
2) Switch on vacuum pump
3) Open regulator (upto ~2 bar) of Helium cylinder connected to H1 through mass flow controller
4) Open H1, H5, H8, M3

5) If P3 > 760 torr, open H12 till P3 reaches ~760 torr, then close H12 and open H13

Else, directly open H13

6) Wait till flow rate in mass flow controller stabilizes at set value of 30 cc min^{-1}.

7) Open H4, close H5 and open H6 in order

8) Put Heater surrounding to balance and set the desired temperature

9) Open the software and observe the weight change

10) Activation was considered to be complete once the change in sample weight was less than 10 μg (resolution of the balance) for approximately 30 minutes.

11) Close software, H1, H4, H6, H8, M3, Helium cylinder, switch off vacuum pump and remove heater

12) Follow *procedure - vacuum*

(iii) Helium buoyancy measurement

Helium buoyancy measurement was done to know the buoyancy volume of sample and was generally done only once for a sample. In this non-adsorbing assumption was considered for Helium and measurements were done generally at 294 K in the pressure range of 0 − 26 bar.

1) After activating the sample, the balance chamber was brought down to the experimental temperature by following water from the circulating bath

2) Connect Helium cylinder to H3

3) Open H5, H8, M3

4) Open H3 and close it after getting ~2000 torr in the P3

5) Follow *procedure - vent*

6) Follow *procedure - vacuum*

7) Close H5, H8, M3

8) Follow *procedure - charge pressure* (use H3 in place of H2)

9) Follow *procedure - vent*

10) Follow *procedure - vacuum*

(iv) Adsorption measurement

1) Activate the adsorbent sample

2) Bring down the balance chamber temperature to the experimental value by following water from the circulating bath

3) Connect desired gas cylinder to H2

4) Open H5, H8, M3

5) Open H2 and close it after getting ~2000 torr in the P3

6) Follow *procedure - vent*

7) Follow *procedure - vacuum*

8) Close H5, H8, M3

9) Follow *procedure - charge pressure*

10) Follow *procedure - vent*

11) Follow *procedure – vacuum*

Table A1. Details of activation protocols used for different MOFs.

Adsorbent	**Temperature *(K)***	**Time *(hours)***
Ni/DABCO	453	2
Cu/DABCO	453	2
Zn/DABCO	453	2
Mg/DOBDC	523	5
Mn/DOBDC	523	5
Co/DOBDC	523	5
Ni/DOBDC	523	5
MIL-53(Al) (sample **lp_0**)	493	2
MIL-53(Al) (sample **np_0**)	293	2

APPENDIX: B

Measured Net and Excess Adsorption Isotherm Data on Studied MOFs

Table A2. Adsorption and desorption isotherm data of CO_2 onto MIL-53(Al).

Adsorbent	Gas	Temperature (K)	Adsorption			Desorption		
			P (bar)	N_{net} (mol kg^{-1})	N_{excess} (mol kg^{-1})	P (bar)	N_{net} (mol kg^{-1})	N_{excess} (mol kg^{-1})
lp tuned form of MIL-53(Al) (**Sample lp_0**)	CO_2	293	0.00	0.00	0.00	0.00	0.00	0.00
			0.06	0.15	0.15	0.06	1.23	1.23
			0.15	0.38	0.38	0.15	1.64	1.64
			0.34	1.36	1.37	0.34	1.98	1.99
			0.68	2.26	2.28	0.65	2.30	2.32
			1.01	2.52	2.55	1.00	2.57	2.60
			1.27	2.69	2.72	1.26	2.76	2.79
			1.7	2.88	2.92	2.0	3.94	3.99
			2.7	3.20	3.27	2.7	5.42	5.49
			3.4	3.35	3.44	3.3	6.19	6.28
			4.0	3.46	3.57	4.0	6.78	6.89
			4.7	3.56	3.68	4.6	7.15	7.27
			5.4	4.09	4.23	5.3	7.51	7.65
			5.7	4.73	4.88	5.7	7.64	7.79
			6.0	5.74	5.90	6.0	7.76	7.92
			6.3	6.68	6.85	6.4	7.89	8.06
			6.7	7.47	7.65	6.6	7.96	8.14
			8.1	8.30	8.52	8.0	8.33	8.55
			12.0	8.92	9.25	11.7	8.90	9.22
np tuned form of MIL-53(Al) (**Sample np_0**)	CO_2	293	0.00	0.00	0.00	0.00	0.00	0.00
			0.04	0.73	0.73	0.08	1.32	1.32
			0.17	1.75	1.75	0.13	1.59	1.59
			0.27	1.93	1.94	0.24	1.85	1.84
			0.37	2.07	2.08	0.40	2.07	2.06
			0.55	2.25	2.26	0.73	2.35	2.33
			0.81	2.39	2.41	1.01	2.53	2.50
			1.10	2.53	2.56	1.23	2.68	2.65
			1.31	2.59	2.62	1.7	3.12	3.08
			1.7	2.70	2.74	2.0	3.76	3.71
			2.0	2.77	2.82	2.4	4.52	4.46
			2.4	2.85	2.91	2.7	5.40	5.33
			2.7	2.88	2.95	3.0	5.79	5.71
			3.0	2.93	3.01	3.3	6.29	6.20
			3.4	2.98	3.07	3.6	6.50	6.40
			3.7	3.00	3.10	4.0	6.82	6.71
			4.0	3.02	3.13	4.3	7.02	6.91
			4.3	3.05	3.16	4.6	7.22	7.10
			4.7	3.10	3.22	5.0	7.40	7.27
			5.0	3.14	3.27	5.4	7.59	7.45
			5.3	3.32	3.46	5.6	7.69	7.54
			5.7	3.67	3.82	6.0	7.83	7.67
			6.0	4.10	4.26	6.4	7.98	7.81
			6.3	4.69	4.86	6.7	8.09	7.91
			6.7	5.32	5.50	7.0	8.20	8.01
			7.0	6.11	6.30	7.4	8.30	8.10
			7.3	6.85	7.05	7.7	8.38	8.17
			7.7	7.68	7.89	8.0	8.45	8.23
			8.1	8.09	8.31	8.3	8.51	8.28
			8.3	8.22	8.45	8.7	8.62	8.38
			8.3	8.27	8.50	9.0	8.68	8.43
			8.6	8.36	8.59	9.3	8.74	8.49
			9.1	8.44	8.69	9.6	8.79	8.53
			9.4	8.49	8.75	10.1	8.87	8.59
			9.7	8.54	8.81			
			10.1	8.59	8.87			

Table A3. Adsorption and desorption isotherm data of N_2 onto MIL-53(Al).

Adsorbent	Gas	Temperature (K)	Adsorption			Desorption		
			P (bar)	N_{net} (mol kg^{-1})	N_{excess} (mol kg^{-1})	P (bar)	N_{net} (mol kg^{-1})	N_{excess} (mol kg^{-1})
lp tuned form of MIL-53(Al) (**Sample lp_0**)	N_2	293	0.00	0.00	0.00	0.00	0.00	0.00
			0.06	0.02	0.02	0.19	0.04	0.04
			0.13	0.03	0.03	0.43	0.09	0.10
			0.28	0.06	0.07	1.03	0.20	0.23
			0.41	0.09	0.10	2.0	0.39	0.44
			0.56	0.12	0.13	4.1	0.71	0.82
			0.69	0.14	0.16	8.1	1.22	1.43
			0.89	0.18	0.20	11.9	1.59	1.90
			1.02	0.20	0.23	15.8	1.88	2.29
			2.0	0.39	0.44	19.9	2.12	2.64
			3.0	0.55	0.63	26.3	2.37	3.06
			4.0	0.71	0.81			
			5.1	0.86	0.99			
			6.1	0.99	1.15			
			8.0	1.23	1.44			
			12.0	1.61	1.92			
			16.0	1.90	2.32			
			20.0	2.13	2.65			
			26.3	2.37	3.06			
np tuned form of MIL-53(Al) (**Sample np_0**)	N_2	293	0.00	0.00	0.00	0.00	0.00	0.00
			0.06	0.01	0.01	0.24	0.03	0.04
			0.14	0.00	0.00	1.02	0.17	0.20
			0.28	0.00	0.01	2.0	0.39	0.44
			0.42	0.00	0.01	3.9	0.68	0.78
			0.54	0.01	0.02	8.0	1.18	1.39
			0.68	-0.01	0.01	12.1	1.60	1.91
			0.90	0.02	0.04	15.8	1.87	2.28
			1.03	0.00	0.03	19.8	2.06	2.58
			2.0	0.00	0.05	26.2	2.35	3.03
			3.0	0.02	0.10			
			4.0	0.12	0.22			
			5.0	0.26	0.39			
			6.0	0.46	0.62			
			7.0	0.73	0.91			
			8.0	1.00	1.21			
			12.1	1.59	1.90			
			16.0	1.88	2.30			
			20.0	2.08	2.60			
			26.2	2.35	3.03			

Table A4. Adsorption and desorption isotherm data of CH_4 onto MIL-53(Al).

Adsorbent	Gas	Temperature (K)	Adsorption			Desorption		
			P (bar)	N_{net} (mol kg^{-1})	N_{excess} (mol kg^{-1})	P (bar)	N_{net} (mol kg^{-1})	N_{excess} (mol kg^{-1})
lp tuned form of MIL-53(Al) (**Sample lp_0**)	CH_4	293	0.00	0.00	0.00	0.00	0.00	0.00
			0.15	0.11	0.11	0.33	0.23	0.24
			0.35	0.25	0.26	0.56	0.40	0.41
			0.69	0.49	0.51	1.01	0.67	0.70
			1.03	0.68	0.71	1.34	0.90	0.93
			1.34	0.91	0.94	2.1	1.27	1.32
			2.0	1.25	1.30	3.1	1.77	1.85
			3.0	1.75	1.83	3.9	2.07	2.17
			4.0	2.14	2.24	8.1	3.25	3.46
			8.1	3.26	3.47	11.9	3.88	4.20
			12.1	3.96	4.28	15.6	4.35	4.77
			16.1	4.41	4.84	20.0	4.70	5.24
			20.0	4.71	5.25	26.0	4.97	5.68
			26.0	4.97	5.68			
np tuned form of MIL-53(Al) (**Sample np_0**)	CH_4	293	0.00	0.00	0.00	0.00	0.00	0.00
			0.66	0.02	0.04	0.33	0.20	0.21
			1.02	0.11	0.14	0.59	0.39	0.41
			1.31	0.28	0.31	1.01	0.66	0.69
			2.0	1.13	1.18	1.32	0.86	0.89
			3.1	1.72	1.80	2.0	1.23	1.28
			4.0	2.11	2.21	3.1	1.74	1.82
			8.0	3.22	3.43	4.0	2.14	2.24
			12.0	3.92	4.24	8.1	3.27	3.48
			16.0	4.36	4.79	11.7	3.92	4.23
			20.0	4.70	5.24	15.8	4.40	4.82
			26.0	5.01	5.72	19.9	4.73	5.27
						26.0	5.01	5.72

Table A5. Adsorption and desorption isotherm data of CO onto MIL-53(Al).

Adsorbent	Gas	Temperature (K)	Adsorption			Desorption		
			P (bar)	N_{net} (mol kg^{-1})	N_{excess} (mol kg^{-1})	P (bar)	N_{net} (mol kg^{-1})	N_{excess} (mol kg^{-1})
lp tuned form of MIL-53(Al) (**Sample lp_0**)	CO	293	0.00	0.00	0.00	0.00	0.00	0.00
			0.16	0.05	0.05	0.30	0.12	0.13
			0.33	0.09	0.10	0.65	0.21	0.23
			0.68	0.18	0.20	1.03	0.31	0.34
			1.02	0.26	0.29	2.0	0.54	0.59
			2.0	0.51	0.56	4.1	0.94	1.05
			4.0	0.91	1.01	6.1	1.28	1.44
			6.0	1.24	1.40	7.9	1.54	1.75
			8.0	1.56	1.77	10.1	1.80	2.06
			10.1	1.82	2.08	11.8	1.98	2.29
			12.1	2.00	2.32	16.1	2.33	2.75
			16.1	2.32	2.74	19.9	2.57	3.09
			20.0	2.56	3.08	25.8	2.82	3.50
			25.8	2.82	3.50			
np tuned form of MIL-53(Al) (**Sample np_0**)	CO	293	0.00	0.00	0.00	0.00	0.00	0.00
			0.36	0.00	0.01	0.41	0.13	0.14
			0.85	0.00	0.02	0.71	0.21	0.23
			1.06	0.00	0.03	1.01	0.29	0.32
			2.0	0.04	0.09	2.0	0.53	0.58
			3.0	0.19	0.27	4.0	0.94	1.04
			4.0	0.43	0.53	6.0	1.30	1.46
			5.0	0.82	0.95	8.1	1.61	1.82
			6.2	1.21	1.37	10.0	1.85	2.11
			8.0	1.55	1.76	12.0	2.05	2.36
			10.0	1.80	2.06	15.8	2.38	2.79
			12.0	2.02	2.33	19.6	2.62	3.13
			16.0	2.36	2.78	26.2	2.89	3.58
			20.0	2.63	3.15			
			26.2	2.89	3.58			

Table A6. Adsorption and desorption isotherm data of O_2 onto MIL-53(Al).

Adsorbent	Gas	Temperature (K)	Adsorption			Desorption		
			P (bar)	N_{net} (mol kg^{-1})	N_{excess} (mol kg^{-1})	P (bar)	N_{net} (mol kg^{-1})	N_{excess} (mol kg^{-1})
lp tuned form of MIL-53(Al) (**Sample lp_0**)	O_2	293	0.00	0.00	0.00	0.00	0.00	0.00
			0.14	0.02	0.02	0.38	0.11	0.12
			0.36	0.06	0.07	0.75	0.18	0.20
			0.67	0.09	0.11	1.01	0.22	0.25
			1.02	0.19	0.22	2.09	0.42	0.47
			2.0	0.37	0.42	3.9	0.73	0.83
			4.0	0.69	0.79	6.0	1.05	1.21
			6.1	1.01	1.17	8.0	1.34	1.55
			8.1	1.28	1.49	10.4	1.65	1.92
			10.3	1.55	1.82	12.0	1.85	2.16
			12.1	1.76	2.08	15.8	2.25	2.66
			16.1	2.14	2.56	20.1	2.62	3.15
			20.0	2.46	2.99	26.0	3.00	3.69
			26.0	2.86	3.55			
np tuned form of MIL-53(Al) (**Sample np_0**)	O_2	293	0.00	0.00	0.00	0.00	0.00	0.00
			0.13	0.00	0.00	0.38	0.06	0.07
			0.32	-0.01	0.00	0.75	0.14	0.16
			0.71	-0.01	0.01	1.01	0.18	0.21
			1.03	-0.02	0.01	2.09	0.38	0.43
			2.0	0.00	0.05	3.9	0.69	0.79
			4.0	0.17	0.27	6.0	1.00	1.16
			6.0	0.57	0.73	8.0	1.30	1.51
			8.0	1.11	1.32	10.4	1.61	1.88
			10.5	1.57	1.84	12.0	1.81	2.12
			12.0	1.76	2.07	15.8	2.21	2.62
			15.9	2.16	2.58	20.1	2.58	3.11
			19.9	2.52	3.04	26.0	2.93	3.62
			26.0	2.93	3.62			

Table A7. Adsorption isotherm data of CO_2 onto DOBDC MOFs.

Adsorbent	Gas	At 294 K			At 315 K			At 352 K		
		P (bar)	N_{net} (mol kg^{-1})	N_{excess} (mol kg^{-1})	P (bar)	N_{net} (mol kg^{-1})	N_{excess} (mol kg^{-1})	P (bar)	N_{net} (mol kg^{-1})	N_{excess} (mol kg^{-1})
Mg/DOBDC	CO_2	0.000	0.00	0.00	0.000	0.00	0.00	0.000	0.00	0.00
		0.002	0.64	0.64	0.004	0.34	0.34	0.002	0.04	0.04
		0.006	1.29	1.29	0.006	0.48	0.48	0.004	0.07	0.07
		0.012	2.12	2.12	0.009	0.69	0.69	0.009	0.16	0.16
		0.02	2.69	2.69	0.02	1.03	1.03	0.013	0.22	0.22
		0.04	3.73	3.73	0.03	1.62	1.62	0.03	0.42	0.42
		0.09	4.68	4.68	0.05	2.40	2.40	0.05	0.74	0.74
		0.13	4.99	4.99	0.10	3.21	3.21	0.09	1.17	1.17
		0.19	5.37	5.37	0.14	3.69	3.69	0.14	1.57	1.57
		0.38	6.08	6.09	0.20	4.13	4.13	0.20	2.02	2.02
		0.67	6.84	6.85	0.31	4.65	4.66	0.41	2.98	2.99
		1.04	7.55	7.57	0.67	5.53	5.54	0.64	3.64	3.65
		1.29	7.96	7.99	1.01	6.05	6.07	1.00	4.28	4.30
		2.0	8.93	8.97	1.27	6.38	6.41	1.31	4.68	4.70
		4.0	10.54	10.63	2.1	7.17	7.21	2.09	5.36	5.40
		8.0	11.88	12.06	4.0	8.48	8.56	3.99	6.36	6.43
		12.0	12.41	12.68	8.1	9.99	10.16	7.99	7.67	7.81
		16.0	12.66	13.03	12.0	10.70	10.95	12.1	8.47	8.69
		20.0	12.77	13.25	16.0	11.11	11.45	16.1	8.96	9.26
		25.6	12.82	13.46	20.0	11.35	11.78	20.0	9.30	9.68
		33	12.63	13.53	26.3	11.51	12.10	26.2	9.52	10.02
					33	11.38	12.16	32	9.71	10.34
Mn/DOBDC	CO_2	0.000	0.00	0.00	0.000	0.00	0.00	0.000	0.00	0.00
		0.001	0.02	0.02	0.005	0.06	0.06	0.009	0.04	0.04
		0.004	0.10	0.10	0.011	0.13	0.13	0.03	0.11	0.11
		0.010	0.25	0.25	0.03	0.32	0.32	0.07	0.24	0.24
		0.02	0.52	0.52	0.06	0.68	0.68	0.12	0.43	0.43
		0.04	0.88	0.88	0.11	1.12	1.12	0.19	0.66	0.66
		0.07	1.53	1.53	0.17	1.66	1.66	0.27	0.90	0.90
		0.10	2.12	2.12	0.27	2.28	2.28	0.45	1.41	1.42
		0.19	3.14	3.14	0.45	3.31	3.32	0.67	1.97	1.98
		0.27	3.84	3.84	0.68	4.04	4.05	1.02	2.68	2.69
		0.45	4.83	4.84	1.03	4.89	4.91	1.35	3.13	3.15
		0.66	5.51	5.52	1.37	5.44	5.46	2.0	3.88	3.91
		1.03	6.36	6.38	2.0	6.18	6.21	3.0	4.75	4.79
		2.0	7.79	7.82	3.0	7.06	7.10	4.0	5.29	5.34
		4.0	9.26	9.32	4.0	7.61	7.67	8.0	6.82	6.93
		8.1	10.36	10.49	8.1	9.00	9.12	12.0	7.61	7.77
		12.1	10.76	10.96	11.9	9.57	9.75	16.1	8.08	8.30
		16.0	10.95	11.23	15.9	9.89	10.14	20.1	8.39	8.67
		20.0	11.03	11.39	20.0	10.06	10.38	26.1	8.66	9.03
		26.0	11.03	11.52	26.1	10.13	10.57	32	8.75	9.22
		32	10.78	11.42	31	10.03	10.57			

Adsorbent	Gas	At 294 K			At 315 K			At 352 K		
		P (bar)	N_{net} (mol kg^{-1})	N_{excess} (mol kg^{-1})	P (bar)	N_{net} (mol kg^{-1})	N_{excess} (mol kg^{-1})	P (bar)	N_{net} (mol kg^{-1})	N_{excess} (mol kg^{-1})
Co/DOBDC	CO_2	0.000	0.00	0.00	0.000	0.00	0.00	0.000	0.00	0.00
		0.003	0.10	0.10	0.004	0.06	0.06	0.006	0.03	0.03
		0.007	0.23	0.23	0.009	0.12	0.12	0.011	0.05	0.05
		0.010	0.34	0.34	0.02	0.33	0.33	0.02	0.10	0.10
		0.02	0.58	0.58	0.05	0.69	0.69	0.03	0.14	0.14
		0.03	0.93	0.93	0.11	1.33	1.33	0.06	0.23	0.23
		0.05	1.77	1.77	0.19	2.21	2.21	0.11	0.43	0.43
		0.10	2.73	2.73	0.33	3.19	3.19	0.20	0.74	0.74
		0.17	3.89	3.89	0.66	4.60	4.61	0.35	1.21	1.21
		0.33	5.15	5.15	1.03	5.47	5.48	0.67	2.11	2.12
		0.68	6.31	6.32	1.28	5.86	5.88	1.03	2.96	2.97
		1.04	7.06	7.07	2.0	6.70	6.72	1.28	3.42	3.43
		1.32	7.48	7.50	4.0	8.02	8.07	2.0	4.40	4.42
		2.0	8.37	8.40	8.0	9.22	9.32	4.0	5.84	5.88
		4.0	9.69	9.74	12.0	9.78	9.93	8.0	7.24	7.33
		8.0	10.68	10.79	15.9	10.13	10.33	12.1	7.98	8.11
		12.8	11.11	11.28	20.0	10.29	10.55	16.0	8.42	8.60
		16.0	11.23	11.45	26.1	10.39	10.74	20.0	8.70	8.92
		20.0	11.28	11.57	33	10.36	10.82	26.2	8.95	9.25
		25.8	11.27	11.66				33	9.11	9.50
Ni/DOBDC	CO_2	0.000	0.00	0.00	0.000	0.00	0.00	0.000	0.00	0.00
		0.002	0.13	0.13	0.005	0.11	0.11	0.007	0.06	0.06
		0.004	0.25	0.25	0.009	0.20	0.20	0.02	0.12	0.12
		0.007	0.43	0.43	0.02	0.38	0.38	0.05	0.31	0.31
		0.010	0.62	0.62	0.04	0.78	0.78	0.10	0.55	0.55
		0.013	0.83	0.83	0.12	1.95	1.95	0.20	0.98	0.98
		0.02	1.40	1.40	0.17	2.58	2.58	0.34	1.53	1.53
		0.04	1.98	1.98	0.33	3.61	3.61	0.72	2.66	2.67
		0.06	2.78	2.78	0.70	4.87	4.88	1.05	3.35	3.36
		0.11	3.57	3.57	1.06	5.65	5.66	1.32	3.79	3.80
		0.20	4.56	4.56	1.32	6.01	6.03	2.0	4.70	4.72
		0.34	5.28	5.28	2.1	6.84	6.87	4.0	5.99	6.03
		0.69	6.34	6.35	4.1	8.18	8.23	8.0	7.36	7.45
		1.06	7.12	7.13	8.1	9.55	9.65	12.0	8.19	8.33
		1.28	7.48	7.50	12.0	10.19	10.35	16.0	8.69	8.88
		2.0	8.44	8.47	16.0	10.57	10.78	20.0	9.04	9.28
		4.0	9.88	9.93	20.1	10.77	11.04	26.1	9.43	9.74
		8.0	11.00	11.11	26.0	10.89	11.26			
		12.0	11.43	11.60	32	10.86	11.33			
		16.0	11.65	11.88						
		19.9	11.77	12.07						
		26.0	11.78	12.19						

Table A8. Adsorption isotherm data of CO onto DOBDC MOFs.

Adsorbent	Gas	At 294 K			At 315 K			At 352 K		
		P (bar)	N_{net} (mol kg^{-1})	N_{excess} (mol kg^{-1})	P (bar)	N_{net} (mol kg^{-1})	N_{excess} (mol kg^{-1})	P (bar)	N_{net} (mol kg^{-1})	N_{excess} (mol kg^{-1})
Mg/DOBDC	CO	0.0000	0.00	0.00	0.0000	0.00	0.00	0.0000	0.00	0.00
		0.0028	0.04	0.04	0.0031	0.01	0.01	0.0081	0.03	0.03
		0.0070	0.09	0.09	0.0064	0.03	0.03	0.0130	0.04	0.04
		0.0106	0.14	0.14	0.0104	0.05	0.05	0.04	0.06	0.06
		0.02	0.22	0.22	0.02	0.11	0.11	0.07	0.10	0.10
		0.03	0.35	0.35	0.04	0.19	0.19	0.11	0.15	0.15
		0.06	0.70	0.70	0.06	0.27	0.27	0.21	0.26	0.26
		0.10	1.01	1.01	0.11	0.44	0.44	0.35	0.39	0.40
		0.19	1.61	1.61	0.20	0.76	0.76	0.67	0.68	0.69
		0.68	3.08	3.09	0.32	1.08	1.09	1.05	0.98	1.00
		1.05	3.57	3.59	0.67	1.82	1.83	1.26	1.13	1.15
		1.32	3.83	3.86	1.03	2.32	2.34	2.1	1.61	1.65
		2.1	4.30	4.34	1.32	2.63	2.66	4.1	2.44	2.51
		2.7	4.56	4.62	2.0	3.16	3.20	8.1	3.36	3.50
		4.1	4.95	5.04	4.0	4.03	4.11	12.1	3.93	4.14
		8.1	5.55	5.72	8.1	4.79	4.95	16.2	4.31	4.60
		12.2	5.91	6.17	12.2	5.20	5.44	20.3	4.57	4.93
		16.0	6.14	6.48	16.1	5.47	5.79	26.2	4.83	5.29
		20.0	6.32	6.75	20.2	5.66	6.06	32	4.99	5.56
		26.4	6.50	7.07	26.2	5.85	6.37	41	5.14	5.86
		33	6.59	7.30	33	5.95	6.61	50	5.25	6.13
		41	6.63	7.51	41	6.04	6.86	65	5.27	6.42
		50	6.65	7.73	51	6.05	7.07	86	5.25	6.77
		65	6.53	7.94	64	6.03	7.31			
		86	6.25	8.14	86	5.81	7.54			
Mn/DOBDC	CO	0.0000	0.00	0.00	0.0000	0.00	0.00	0.0000	0.00	0.00
		0.0053	0.03	0.03	0.0054	0.01	0.01	0.0074	0.01	0.01
		0.03	0.17	0.17	0.02	0.04	0.04	0.04	0.03	0.03
		0.07	0.35	0.35	0.07	0.16	0.16	0.12	0.08	0.08
		0.11	0.55	0.55	0.13	0.28	0.28	0.34	0.23	0.23
		0.31	1.25	1.25	0.33	0.67	0.67	0.69	0.44	0.45
		0.65	2.02	2.03	0.68	1.19	1.20	1.03	0.63	0.64
		1.06	2.61	2.63	1.07	1.63	1.65	2.0	1.13	1.16
		2.0	3.43	3.46	2.0	2.45	2.48	4.0	1.88	1.93
		4.0	4.25	4.31	4.0	3.38	3.44	8.0	2.80	2.91
		8.0	4.98	5.11	8.0	4.25	4.37	12.0	3.44	3.60
		12.1	5.37	5.56	12.1	4.71	4.89	16.1	3.83	4.04
		16.0	5.61	5.86	16.2	5.01	5.25	20.0	4.12	4.38
		20.0	5.80	6.12	20.1	5.18	5.48	26.5	4.42	4.77
		26.0	5.96	6.37	26.3	5.36	5.75	32	4.58	5.00
		32	6.05	6.56	33	5.48	5.97	39	4.68	5.19
		43	6.10	6.79	40	5.53	6.12	50	4.85	5.51
		50	6.11	6.92	50	5.59	6.33	67	4.89	5.77
		68	5.99	7.09	70	5.52	6.57	86	4.89	6.02
		87	5.83	7.25	87	5.44	6.74	102	4.77	6.11
		104	5.60	7.32	105	5.25	6.83			

Adsorbent	Gas	At 294 K			At 315 K			At 352 K		
		P (bar)	N_{net} (mol kg^{-1})	N_{excess} (mol kg^{-1})	P (bar)	N_{net} (mol kg^{-1})	N_{excess} (mol kg^{-1})	P (bar)	N_{net} (mol kg^{-1})	N_{excess} (mol kg^{-1})
Co/DOBDC	CO	0.0000	0.00	0.00	0.0000	0.00	0.00	0.0000	0.00	0.00
		0.0002	0.10	0.10	0.0012	0.15	0.15	0.0033	0.08	0.08
		0.0007	0.27	0.27	0.0025	0.26	0.26	0.0086	0.16	0.16
		0.0015	0.53	0.53	0.0037	0.37	0.37	0.0117	0.21	0.21
		0.0023	0.74	0.74	0.0051	0.50	0.50	0.02	0.38	0.38
		0.0035	1.02	1.02	0.0063	0.59	0.59	0.06	0.87	0.87
		0.0045	1.25	1.25	0.0102	0.90	0.90	0.11	1.29	1.29
		0.0073	1.74	1.74	0.02	1.57	1.57	0.20	1.94	1.94
		0.0095	2.06	2.06	0.05	2.59	2.59	0.33	2.56	2.56
		0.02	2.79	2.79	0.11	3.48	3.48	0.69	3.51	3.52
		0.03	3.46	3.46	0.19	4.11	4.11	1.05	4.03	4.04
		0.05	4.14	4.14	0.33	4.66	4.66	1.29	4.27	4.28
		0.10	4.79	4.79	0.69	5.22	5.23	2.0	4.75	4.77
		0.20	5.25	5.25	1.05	5.47	5.48	4.1	5.32	5.36
		0.36	5.55	5.55	1.30	5.57	5.59	8.1	5.71	5.80
		0.70	5.76	5.77	2.0	5.76	5.78	12.1	5.88	6.01
		1.07	5.90	5.91	4.1	5.98	6.03	16.1	6.05	6.22
		1.29	5.91	5.93	8.2	6.24	6.34	20.2	6.15	6.36
		2.0	6.03	6.06	12.1	6.39	6.53	26.3	6.23	6.51
		4.1	6.22	6.27	16.1	6.51	6.70	33	6.28	6.63
		8.1	6.48	6.58	20.1	6.59	6.83	41	6.31	6.74
		12.1	6.67	6.82	26.2	6.70	7.01	51	6.34	6.88
		16.2	6.81	7.02	33	6.76	7.15	72	6.31	7.07
		20.0	6.95	7.20	40	6.79	7.26	93	6.14	7.12
		26.1	7.07	7.40	51	6.79	7.40	116	6.10	7.32
		33	7.16	7.58	72	6.71	7.57			
		42	7.19	7.73	91	6.57	7.66			
		51	7.18	7.84	114	6.35	7.72			
		72	7.06	7.99						
		86	6.91	8.03						
		117	6.54	8.09						
Ni/DOBDC	CO	0.0000	0.00	0.00	0.0000	0.00	0.00	0.0000	0.00	0.00
		0.0002	0.15	0.15	0.0007	0.21	0.21	0.0038	0.14	0.14
		0.0009	0.56	0.56	0.0017	0.40	0.40	0.0121	0.35	0.35
		0.0018	1.02	1.02	0.0050	0.90	0.90	0.02	0.57	0.57
		0.0037	1.62	1.62	0.0098	1.41	1.41	0.04	0.92	0.92
		0.0087	2.48	2.48	0.03	2.29	2.29	0.07	1.29	1.29
		0.03	3.51	3.51	0.05	2.91	2.91	0.10	1.59	1.59
		0.04	3.91	3.91	0.10	3.61	3.61	0.20	2.25	2.25
		0.06	4.24	4.24	0.21	4.19	4.19	0.34	2.82	2.82
		0.11	4.64	4.64	0.34	4.54	4.54	0.68	3.53	3.54
		0.20	4.98	4.98	0.71	4.96	4.97	1.06	3.95	3.96
		0.36	5.28	5.28	1.09	5.19	5.20	1.31	4.18	4.19
		0.68	5.63	5.64	1.33	5.28	5.30	2.1	4.57	4.59
		1.03	5.90	5.91	2.0	5.50	5.52	4.0	5.14	5.18
		1.29	6.07	6.09	4.1	5.85	5.90	8.0	5.60	5.69
		4.0	6.81	6.86	8.0	6.19	6.29	12.0	5.94	6.07
		8.1	7.37	7.48	12.1	6.47	6.62	16.1	6.20	6.38
		12.2	7.77	7.93	16.0	6.67	6.87	20.1	6.41	6.63
		16.1	7.98	8.20	20.0	6.82	7.07	26.1	6.55	6.84
		20.0	8.20	8.47	26.0	7.04	7.36	33	6.69	7.06
		26.1	8.33	8.68	33	7.15	7.56	40	6.77	7.21
		33	8.40	8.84	40	7.25	7.75	51	6.79	7.35
		40	8.41	8.95	51	7.36	8.00	73	6.75	7.56
		51	8.37	9.06	72	7.38	8.29	90	6.62	7.62
		72	8.23	9.22	90	7.32	8.46	111	6.44	7.67
		91	8.01	9.27	110	7.29	8.69			
		113	7.77	9.35						

Table A9. Adsorption isotherm data of CH_4 onto DOBDC MOFs.

Adsorbent	Gas	At 294 K			At 315 K			At 352 K		
		P (bar)	N_{net} (mol kg^{-1})	N_{excess} (mol kg^{-1})	P (bar)	N_{net} (mol kg^{-1})	N_{excess} (mol kg^{-1})	P (bar)	N_{net} (mol kg^{-1})	N_{excess} (mol kg^{-1})
Mg/DOBDC	CH_4	0.00	0.00	0.00	0.00	0.00	0.00	0.00	0.00	0.00
		0.20	0.21	0.21	0.35	0.22	0.23	1.02	0.32	0.34
		0.36	0.38	0.39	0.69	0.42	0.43	1.28	0.41	0.43
		0.68	0.71	0.72	1.02	0.61	0.63	2.0	0.61	0.65
		1.04	1.05	1.07	1.30	0.76	0.79	4.0	1.12	1.19
		1.28	1.26	1.29	2.1	1.16	1.20	8.0	1.98	2.12
		2.1	1.92	1.96	4.1	2.09	2.17	12.1	2.69	2.91
		4.0	3.19	3.28	8.1	3.41	3.57	16.0	3.26	3.55
		8.0	4.77	4.94	12.0	4.26	4.50	20.0	3.68	4.04
		12.0	5.63	5.89	16.0	4.86	5.18	26.0	4.08	4.55
		16.0	6.18	6.53	20.0	5.27	5.68	33	4.47	5.07
		20.1	6.54	6.98	26.0	5.71	6.25	40	4.72	5.46
		26.0	6.86	7.44	33	5.96	6.65	50	4.90	5.83
		33	7.02	7.77	40	6.10	6.94			
		40	7.07	7.99	50	6.16	7.23			
		50	7.03	8.21						
Mn/DOBDC	CH_4	0.00	0.00	0.00	0.00	0.00	0.00	0.00	0.00	0.00
		0.04	0.05	0.05	0.04	0.03	0.03	0.72	0.25	0.26
		0.11	0.13	0.13	0.11	0.08	0.08	1.04	0.36	0.37
		0.34	0.37	0.38	0.33	0.21	0.21	2.0	0.64	0.67
		0.69	0.73	0.74	0.68	0.43	0.44	4.1	1.26	1.31
		1.07	1.10	1.12	1.06	0.65	0.67	8.0	2.14	2.25
		2.0	1.92	1.95	2.1	1.22	1.25	12.1	2.87	3.03
		4.0	3.18	3.24	4.0	2.14	2.20	16.3	3.41	3.63
		8.0	4.62	4.75	8.0	3.44	3.56	20.0	3.84	4.11
		12.0	5.37	5.56	11.9	4.28	4.46	26.1	4.26	4.61
		16.3	5.84	6.11	16.2	4.83	5.07	32	4.57	5.01
		20.0	6.10	6.43	20.1	5.15	5.46	39	4.78	5.31
		26.0	6.35	6.78	26.1	5.49	5.89	50	4.97	5.66
		31	6.43	6.95	32	5.65	6.15	69	4.97	5.95
		40	6.48	7.17	39	5.79	6.40	93	4.79	6.15
		49	6.43	7.29	49	5.85	6.63	115	4.41	6.14
		68	6.05	7.31	69	5.58	6.73			
		92	5.26	7.13	92	5.16	6.78			
		116	4.23	6.94	114	4.59	6.72			

Adsorbent	Gas	At 294 K			At 315 K			At 352 K		
		P (bar)	N_{net} (mol kg^{-1})	N_{excess} (mol kg^{-1})	P (bar)	N_{net} (mol kg^{-1})	N_{excess} (mol kg^{-1})	P (bar)	N_{net} (mol kg^{-1})	N_{excess} (mol kg^{-1})
Co/DOBDC	CH_4	0.00	0.00	0.00	0.00	0.00	0.00	0.00	0.00	0.00
		0.07	0.10	0.10	0.12	0.10	0.10	1.07	0.42	0.43
		0.11	0.16	0.16	0.22	0.18	0.18	1.29	0.51	0.52
		0.22	0.31	0.31	0.34	0.28	0.28	2.0	0.77	0.79
		0.34	0.47	0.47	0.70	0.55	0.56	4.0	1.40	1.44
		0.70	0.93	0.94	1.03	0.81	0.82	8.2	2.44	2.53
		1.06	1.38	1.39	1.29	0.98	1.00	12.0	3.18	3.31
		1.29	1.63	1.65	2.0	1.48	1.50	16.2	3.77	3.94
		2.0	2.41	2.44	4.0	2.59	2.64	20.0	4.19	4.40
		4.0	3.87	3.92	8.1	4.02	4.12	25.3	4.64	4.91
		8.0	5.35	5.45	12.0	4.83	4.97	33	5.02	5.38
		12.0	6.04	6.19	16.1	5.37	5.56	40	5.26	5.70
		16.1	6.51	6.72	20.1	5.73	5.97	51	5.43	6.00
		20.0	6.78	7.04	26.2	6.07	6.39	72	5.50	6.32
		26.0	7.01	7.36	33	6.28	6.69	91	5.33	6.39
		33	7.14	7.59	40	6.39	6.89	113	5.10	6.45
		41	7.18	7.74	51	6.45	7.10			
		51	7.12	7.84	72	6.15	7.11			
		72	6.60	7.68	90	5.81	7.07			
		91	5.99	7.46	115	5.10	6.82			
		116	4.91	7.08						
Ni/DOBDC	CH_4	0.00	0.00	0.00	0.00	0.00	0.00	0.00	0.00	0.00
		0.10	0.13	0.13	0.35	0.27	0.27	1.05	0.40	0.41
		0.20	0.25	0.25	0.70	0.49	0.50	1.30	0.48	0.49
		0.34	0.41	0.41	1.09	0.74	0.75	2.1	0.72	0.74
		0.70	0.80	0.81	1.31	0.86	0.88	4.0	1.28	1.32
		1.07	1.19	1.20	2.0	1.29	1.31	6.1	1.77	1.84
		1.33	1.44	1.46	4.0	2.27	2.32	8.0	2.20	2.29
		2.1	2.11	2.14	6.0	3.04	3.12	12.1	2.93	3.07
		4.0	3.41	3.46	8.1	3.64	3.74	16.0	3.52	3.70
		6.0	4.32	4.40	12.1	4.49	4.64	20.0	3.98	4.21
		8.0	4.96	5.07	16.0	5.05	5.25	26.2	4.51	4.81
		12.0	5.80	5.96	20.0	5.47	5.73	33	4.84	5.22
		16.2	6.32	6.54	26.5	5.91	6.25	40	5.09	5.55
		20.1	6.65	6.93	33	6.20	6.63	51	5.37	5.97
		26.3	7.00	7.37	41	6.38	6.92	72	5.52	6.38
		33	7.17	7.64	51	6.44	7.13	87	5.52	6.58
		40	7.28	7.86	72	6.32	7.33	117	5.37	6.85
		51	7.31	8.07	92	6.00	7.36			
		72	6.87	8.01	117	5.38	7.24			
		92	6.33	7.90						
		118	5.28	7.64						

Table A10. Adsorption isotherm data of N_2 onto DOBDC MOFs.

Adsorbent	Gas	At 294 K			At 315 K			At 352 K		
		P (bar)	N_{net} (mol kg^{-1})	N_{excess} (mol kg^{-1})	P (bar)	N_{net} (mol kg^{-1})	N_{excess} (mol kg^{-1})	P (bar)	N_{net} (mol kg^{-1})	N_{excess} (mol kg^{-1})
Mg/DOBDC	N_2	0.00	0.00	0.00	0.00	0.00	0.00	0.00	0.00	0.00
		0.04	0.04	0.04	0.11	0.06	0.06	1.04	0.20	0.22
		0.10	0.10	0.10	0.22	0.11	0.11	1.29	0.25	0.27
		0.19	0.18	0.18	0.34	0.16	0.17	2.0	0.37	0.41
		0.35	0.32	0.33	0.66	0.31	0.32	4.1	0.71	0.78
		0.67	0.59	0.60	1.03	0.46	0.48	8.1	1.27	1.41
		1.02	0.85	0.87	1.31	0.58	0.61	12.0	1.72	1.93
		1.32	1.05	1.08	2.0	0.85	0.89	16.2	2.10	2.39
		2.0	1.47	1.51	4.1	1.51	1.59	20.1	2.41	2.76
		4.1	2.40	2.49	8.0	2.38	2.54	26.1	2.75	3.21
		8.1	3.46	3.63	12.1	2.99	3.23	32	2.99	3.55
		12.0	4.06	4.31	16.2	3.46	3.78	39	3.24	3.93
		16.2	4.49	4.83	20.1	3.77	4.17	50	3.48	4.36
		20.1	4.77	5.20	26.0	4.13	4.65	72	3.47	4.73
		26.1	5.05	5.61	33	4.38	5.03	94	3.46	5.11
		32	5.22	5.90	39	4.53	5.30	122	3.28	5.41
		39	5.34	6.17	51	4.58	5.59			
		50	5.40	6.47	73	4.57	6.02			
		71	5.23	6.76	94	4.40	6.28			
		93	4.96	6.98	120	4.10	6.50			
		121	4.54	7.19						
Mn/DOBDC	N_2	0.00	0.00	0.00	0.00	0.00	0.00	0.00	0.00	0.00
		0.11	0.05	0.05	0.33	0.09	0.09	1.04	0.15	0.16
		0.32	0.14	0.15	0.66	0.18	0.19	2.0	0.28	0.31
		0.66	0.27	0.28	1.02	0.26	0.28	4.0	0.52	0.57
		1.04	0.43	0.45	2.0	0.49	0.52	8.1	0.94	1.05
		2.0	0.78	0.81	4.0	0.92	0.98	12.0	1.32	1.48
		4.0	1.39	1.45	8.0	1.58	1.70	16.1	1.61	1.82
		8.0	2.26	2.39	12.0	2.10	2.28	20.0	1.87	2.13
		12.0	2.90	3.09	16.0	2.52	2.76	26.2	2.19	2.53
		16.0	3.33	3.58	20.0	2.83	3.13	31	2.41	2.82
		20.0	3.63	3.95	26.0	3.24	3.62	38	2.65	3.15
		25.9	4.00	4.41	32	3.48	3.95	49	2.85	3.49
		32	4.21	4.72	39	3.65	4.23	68	3.06	3.95
		39	4.41	5.03	50	3.83	4.57	90	3.14	4.32
		49	4.53	5.31	70	3.97	5.01	113	3.12	4.59
		69	4.53	5.64	92	3.88	5.25			
		92	4.35	5.84	114	3.74	5.44			
		113	4.15	5.99						

Adsorbent	Gas	At 294 K			At 315 K			At 352 K		
		P (bar)	N_{net} (mol kg^{-1})	N_{excess} (mol kg^{-1})	P (bar)	N_{net} (mol kg^{-1})	N_{excess} (mol kg^{-1})	P (bar)	N_{net} (mol kg^{-1})	N_{excess} (mol kg^{-1})
Co/DOBDC	N_2	0.00	0.00	0.00	0.00	0.00	0.00	0.00	0.00	0.00
		0.07	0.05	0.05	0.35	0.15	0.15	1.06	0.21	0.22
		0.11	0.08	0.08	0.69	0.27	0.28	1.30	0.25	0.26
		0.22	0.17	0.17	1.01	0.40	0.41	2.0	0.37	0.39
		0.36	0.27	0.27	1.28	0.49	0.51	4.0	0.70	0.74
		0.68	0.49	0.50	2.0	0.75	0.77	8.1	1.24	1.33
		1.04	0.72	0.73	4.0	1.34	1.39	12.1	1.71	1.84
		1.31	0.88	0.90	8.0	2.24	2.33	16.1	2.10	2.27
		2.0	1.28	1.31	12.1	2.88	3.02	20.2	2.42	2.63
		4.1	2.18	2.23	16.0	3.34	3.53	26.3	2.81	3.09
		8.0	3.30	3.40	20.0	3.70	3.94	33	3.11	3.46
		12.1	3.99	4.14	26.0	4.08	4.39	40	3.36	3.78
		16.0	4.43	4.63	33	4.38	4.77	51	3.61	4.14
		20.0	4.75	5.00	40	4.59	5.06	72	3.90	4.65
		25.6	5.06	5.38	51	4.73	5.33	94	4.00	4.98
		33	5.29	5.71	72	4.86	5.71	123	3.91	5.19
		42	5.44	5.98	94	4.76	5.88			
		51	5.53	6.18	123	4.55	6.02			
		72	5.49	6.42						
		94	5.31	6.53						
		123	5.02	6.62						
Ni/DOBDC	N_2	0.00	0.00	0.00	0.00	0.00	0.00	0.0	0.00	0.00
		0.68	0.52	0.53	1.03	0.41	0.42	4.1	0.70	0.75
		1.03	0.74	0.75	1.30	0.49	0.51	8.1	1.21	1.30
		1.31	0.89	0.91	2.0	0.73	0.75	12.2	1.62	1.76
		2.1	1.29	1.32	4.0	1.27	1.32	16.1	2.01	2.19
		4.0	2.06	2.11	8.1	2.08	2.18	20.1	2.34	2.56
		8.0	3.05	3.16	12.1	2.65	2.80	26.2	2.65	2.94
		12.2	3.70	3.86	16.0	3.07	3.27	33	2.94	3.30
		16.2	4.10	4.32	20.0	3.41	3.66	40	3.22	3.66
		20.0	4.40	4.67	26.1	3.78	4.10	51	3.51	4.07
		26.2	4.75	5.10	33	4.05	4.46	72	3.88	4.67
		33	4.97	5.41	40	4.28	4.78	91	4.04	5.04
		40	5.13	5.67	51	4.48	5.12	123	4.34	5.69
		51	5.32	6.01	72	4.67	5.57			
		72	5.35	6.33	91	4.68	5.82			
		94	5.31	6.59	122	4.66	6.19			
		122	5.16	6.84						

Table A11. Adsorption isotherm data of C_2H_6 onto DOBDC MOFs.

Adsorbent	Gas	At 294 K			At 315 K			At 352 K		
		P (bar)	N_{net} (mol kg^{-1})	N_{excess} (mol kg^{-1})	P (bar)	N_{net} (mol kg^{-1})	N_{excess} (mol kg^{-1})	P (bar)	N_{net} (mol kg^{-1})	N_{excess} (mol kg^{-1})
Mg/DOBDC	C_2H_6	0.000	0.00	0.00	0.000	0.00	0.00	0.00	0.00	0.00
		0.003	0.04	0.04	0.010	0.07	0.07	0.06	0.15	0.15
		0.007	0.10	0.10	0.02	0.14	0.14	0.11	0.25	0.25
		0.010	0.15	0.15	0.07	0.43	0.43	0.21	0.50	0.50
		0.02	0.22	0.22	0.11	0.74	0.74	0.36	0.85	0.86
		0.03	0.39	0.39	0.21	1.37	1.37	0.70	1.61	1.62
		0.05	0.80	0.80	0.32	2.13	2.14	1.01	2.24	2.26
		0.09	1.33	1.33	0.65	3.68	3.69	1.27	2.70	2.72
		0.18	2.60	2.60	1.01	4.62	4.64	2.0	3.71	3.75
		0.30	3.84	3.85	1.28	5.06	5.09	4.0	4.99	5.06
		0.64	5.40	5.41	2.1	5.84	5.88	8.1	5.98	6.13
		1.04	6.14	6.16	4.2	6.63	6.72	12.1	6.32	6.55
		2.0	6.92	6.96	8.1	7.15	7.32	16.0	6.50	6.81
		4.0	7.46	7.55	12.4	7.36	7.63	20.0	6.59	6.98
		8.0	7.87	8.05	16.2	7.41	7.77	26.2	6.60	7.13
		12.1	7.97	8.26	20.1	7.40	7.86			
		16.0	7.97	8.36	26.0	7.29	7.93			
		20.0	7.90	8.42						
		26.0	7.70	8.45						
Mn/DOBDC	C_2H_6	0.000	0.00	0.00	0.00	0.00	0.00	0.00	0.00	0.000
		0.007	0.10	0.10	0.02	0.20	0.20	0.05	0.16	0.16
		0.011	0.18	0.18	0.05	0.43	0.43	0.10	0.29	0.29
		0.03	0.47	0.47	0.09	0.80	0.80	0.32	0.89	0.89
		0.05	0.83	0.83	0.17	1.46	1.46	0.49	1.35	1.36
		0.09	1.56	1.56	0.28	2.30	2.30	0.68	1.82	1.83
		0.14	2.54	2.54	0.41	3.10	3.11	1.02	2.55	2.56
		0.28	3.92	3.92	0.64	3.94	3.95	1.35	3.09	3.11
		0.45	4.65	4.66	1.01	4.67	4.68	2.0	3.80	3.83
		0.67	5.15	5.16	1.37	5.04	5.06	4.0	4.79	4.84
		1.01	5.56	5.58	2.0	5.45	5.48	8.0	5.48	5.59
		1.39	5.85	5.87	4.1	6.02	6.08	12.0	5.75	5.92
		2.0	6.17	6.20	8.1	6.40	6.53	16.0	5.85	6.08
		4.0	6.58	6.65	12.1	6.54	6.73	20.0	5.90	6.19
		8.1	6.87	7.01	16.0	6.58	6.84	26.0	5.89	6.28
		12.1	6.95	7.16	20.0	6.55	6.89			
		16.0	6.93	7.22	26.0	6.44	6.92			
		20.0	6.85	7.24						
		26.0	6.68	7.24						

Adsorbent	Gas	At 294 K			At 315 K			At 352 K		
		P (bar)	N_{net} (mol kg^{-1})	N_{excess} (mol kg^{-1})	P (bar)	N_{net} (mol kg^{-1})	N_{excess} (mol kg^{-1})	P (bar)	N_{net} (mol kg^{-1})	N_{excess} (mol kg^{-1})
Co/DOBDC	C_2H_6	0.000	0.00	0.00	0.000	0.00	0.00	0.000	0.00	0.00
		0.003	0.07	0.07	0.014	0.14	0.14	0.04	0.25	0.13
		0.009	0.20	0.20	0.02	0.24	0.24	0.07	0.46	0.25
		0.02	0.56	0.56	0.04	0.44	0.44	0.13	0.76	0.46
		0.04	0.90	0.90	0.06	0.65	0.65	0.21	1.24	0.76
		0.06	1.42	1.42	0.12	1.30	1.30	0.34	2.34	1.24
		0.09	2.43	2.43	0.19	2.05	2.05	0.67	3.17	2.35
		0.20	4.17	4.17	0.33	3.24	3.24	1.01	3.64	3.18
		0.35	5.11	5.11	0.66	4.65	4.66	1.27	4.50	3.65
		0.70	5.95	5.96	1.01	5.29	5.30	2.0	4.93	4.52
		1.04	6.31	6.32	1.30	5.60	5.62	2.7	5.42	4.96
		1.33	6.51	6.53	2.0	6.07	6.09	4.0	6.05	5.46
		2.7	6.99	7.02	2.7	6.31	6.34	8.0	6.26	6.14
		4.0	7.19	7.24	4.0	6.59	6.64	12.0	6.37	6.39
		8.0	7.45	7.56	8.0	6.94	7.04	16.0	6.40	6.55
		12.1	7.50	7.67	12.1	7.06	7.21	20.0	6.38	6.63
		16.0	7.47	7.70	16.0	7.08	7.29	26.1		6.70
		20.0	7.38	7.69	20.0	7.07	7.34			
		26.2	7.21	7.66	26.1	6.98	7.36			
Ni/DOBDC	C_2H_6	0.000	0.00	0.00	0.00	0.00	0.00	0.00	0.00	0.00
		0.003	0.06	0.06	0.02	0.20	0.20	0.10	0.32	0.32
		0.009	0.19	0.19	0.04	0.39	0.39	0.19	0.58	0.58
		0.02	0.38	0.38	0.10	0.93	0.93	0.35	1.04	1.04
		0.04	0.84	0.84	0.18	1.57	1.57	0.68	1.84	1.85
		0.07	1.33	1.33	0.31	2.41	2.41	1.03	2.53	2.54
		0.09	1.87	1.87	0.65	3.77	3.78	1.32	2.98	2.99
		0.20	3.27	3.27	1.06	4.55	4.56	2.0	3.73	3.75
		0.34	4.17	4.17	1.28	4.81	4.83	4.1	4.74	4.79
		0.68	5.17	5.18	2.0	5.39	5.42	8.0	5.55	5.64
		1.03	5.67	5.68	4.1	6.08	6.13	12.0	5.87	6.01
		1.30	5.90	5.92	8.0	6.56	6.66	16.0	6.03	6.22
		2.0	6.33	6.36	12.0	6.76	6.92	20.1	6.12	6.37
		4.2	6.87	6.93	16.0	6.82	7.04	26.0	6.25	6.58
		8.0	7.20	7.31	20.1	6.84	7.13			
		12.0	7.30	7.48	26.1	6.79	7.19			
		16.2	7.31	7.56						
		20.0	7.30	7.63						
		26.3	7.19	7.67						

Table A12. Adsorption isotherm data of C_3H_8 onto DOBDC MOFs.

Adsorbent	Gas	At 294 K			At 315 K			At 352 K		
		P (bar)	N_{net} (mol kg^{-1})	N_{excess} (mol kg^{-1})	P (bar)	N_{net} (mol kg^{-1})	N_{excess} (mol kg^{-1})	P (bar)	N_{net} (mol kg^{-1})	N_{excess} (mol kg^{-1})
Mg/DOBDC	C_3H_8	0.0000	0.00	0.00	0.0000	0.00	0.00	0.0000	0.00	0.00
		0.0019	0.25	0.25	0.0041	0.21	0.21	0.0112	0.15	0.15
		0.0034	0.46	0.46	0.0067	0.36	0.36	0.02	0.21	0.21
		0.0055	0.84	0.84	0.0095	0.52	0.52	0.03	0.40	0.40
		0.0083	1.39	1.39	0.0136	0.74	0.74	0.06	0.90	0.90
		0.0115	1.95	1.95	0.02	1.16	1.16	0.11	1.75	1.75
		0.02	3.37	3.37	0.03	1.80	1.80	0.21	2.84	2.84
		0.03	4.17	4.17	0.05	3.06	3.06	0.45	4.05	4.06
		0.07	5.06	5.06	0.12	4.36	4.36	1.07	4.93	4.95
		0.11	5.48	5.48	0.22	5.03	5.03	1.30	5.08	5.10
		0.21	5.87	5.87	0.49	5.57	5.58	2.8	5.55	5.60
		0.45	6.21	6.22	1.08	5.99	6.01	4.1	5.74	5.82
		1.05	6.53	6.55	1.32	6.08	6.11	7.0	5.94	6.07
		1.30	6.59	6.62	2.7	6.33	6.39			
		2.7	6.78	6.84	4.1	6.44	6.53			
		4.0	6.88	6.97	6.7	6.53	6.68			
		7.0	7.00	7.17						
Mn/DOBDC	C_3H_8	0.0000	0.00	0.00	0.0000	0.00	0.00	0.0000	0.00	0.00
		0.0013	0.19	0.19	0.0020	0.13	0.13	0.0041	0.08	0.08
		0.0029	0.53	0.53	0.0040	0.27	0.27	0.0065	0.11	0.11
		0.0043	0.88	0.88	0.0064	0.46	0.46	0.0094	0.17	0.17
		0.0064	1.43	1.43	0.0090	0.68	0.68	0.01	0.28	0.28
		0.0080	1.92	1.92	0.0120	1.06	1.06	0.02	0.41	0.41
		0.0107	2.66	2.66	0.02	1.71	1.71	0.04	0.79	0.79
		0.02	3.58	3.58	0.04	2.89	2.89	0.10	1.86	1.86
		0.05	4.38	4.38	0.11	4.09	4.09	0.19	2.93	2.93
		0.11	4.77	4.77	0.21	4.52	4.52	0.46	3.88	3.89
		0.21	4.99	4.99	0.49	4.88	4.89	1.01	4.42	4.43
		0.47	5.23	5.24	1.01	5.11	5.13	1.31	4.56	4.58
		1.01	5.42	5.44	1.30	5.19	5.21	2.7	4.84	4.88
		1.29	5.49	5.51	2.7	5.37	5.41	4.0	4.96	5.01
		2.7	5.64	5.68	4.0	5.45	5.51	7.0	5.05	5.15
		4.0	5.69	5.76	7.0	5.52	5.63			
		7.0	5.76	5.89						

Adsorbent	Gas	At 294 K			At 315 K			At 352 K		
		P (bar)	N_{net} (mol kg^{-1})	N_{excess} (mol kg^{-1})	P (bar)	N_{net} (mol kg^{-1})	N_{excess} (mol kg^{-1})	P (bar)	N_{net} (mol kg^{-1})	N_{excess} (mol kg^{-1})
Co/DOBDC	C_3H_8	0.0000	0.00	0.00	0.0000	0.00	0.00	0.0000	0.00	0.00
		0.0007	0.19	0.19	0.0024	0.23	0.23	0.0029	0.07	0.07
		0.0015	0.42	0.42	0.0047	0.48	0.48	0.0079	0.19	0.19
		0.0030	1.01	1.01	0.0069	0.76	0.76	0.0115	0.29	0.29
		0.0042	1.56	1.56	0.0102	1.19	1.19	0.02	0.50	0.50
		0.0055	2.23	2.23	0.01	1.73	1.73	0.03	0.94	0.94
		0.0070	2.88	2.88	0.02	2.48	2.48	0.06	1.76	1.76
		0.0093	3.53	3.53	0.05	4.01	4.01	0.10	2.74	2.74
		0.0120	3.96	3.96	0.06	4.40	4.40	0.19	3.69	3.69
		0.02	4.73	4.73	0.11	4.91	4.91	0.47	4.57	4.57
		0.03	5.02	5.02	0.20	5.27	5.27	1.05	5.10	5.11
		0.06	5.42	5.42	0.48	5.64	5.65	1.31	5.21	5.22
		0.11	5.65	5.65	1.02	5.87	5.88	2.7	5.50	5.53
		0.11	5.68	5.68	1.30	5.92	5.94	4.0	5.62	5.66
		0.22	5.87	5.87	2.7	6.07	6.10	7.0	5.71	5.79
		0.23	5.88	5.88	4.0	6.12	6.17			
		0.49	6.06	6.07	7.0	6.16	6.25			
		1.06	6.24	6.25						
		1.29	6.27	6.29						
		2.7	6.41	6.45						
		4.0	6.46	6.51						
		7.0	6.45	6.55						
Ni/DOBDC	C_3H_8	0.0000	0.00	0.00	0.0000	0.00	0.00	0.00	0.00	0.00
		0.0008	0.16	0.16	0.0022	0.20	0.20	0.02	0.38	0.38
		0.0017	0.35	0.35	0.0046	0.42	0.42	0.05	0.87	0.87
		0.0030	0.68	0.68	0.0098	0.92	0.92	0.06	1.25	1.25
		0.0044	1.05	1.05	0.02	1.42	1.42	0.09	1.80	1.80
		0.0064	1.60	1.60	0.03	2.33	2.33	0.19	2.80	2.80
		0.0092	2.28	2.28	0.04	3.05	3.05	0.33	3.43	3.43
		0.0122	2.81	2.81	0.09	3.90	3.90	0.69	4.10	4.11
		0.02	3.50	3.50	0.22	4.62	4.62	1.05	4.42	4.43
		0.03	3.92	3.92	0.35	4.91	4.91	1.31	4.56	4.57
		0.06	4.59	4.59	0.72	5.29	5.30	2.7	4.94	4.97
		0.12	5.01	5.01	1.05	5.47	5.48	4.0	5.12	5.17
		0.21	5.35	5.35	1.30	5.55	5.57	6.7	5.30	5.38
		0.35	5.59	5.59	2.7	5.79	5.82			
		0.71	5.84	5.85	4.0	5.88	5.93			
		1.06	5.98	5.99	6.7	5.95	6.04			
		1.32	6.03	6.05						
		2.7	6.19	6.23						
		4.0	6.26	6.32						
		6.7	6.28	6.38						

Table A13. Adsorption isotherm data of Ar onto DOBDC MOFs.

Adsorbent	Gas	At 294 K			At 315 K			At 352 K		
		P (bar)	N_{net} (mol kg^{-1})	N_{excess} (mol kg^{-1})	P (bar)	N_{net} (mol kg^{-1})	N_{excess} (mol kg^{-1})	P (bar)	N_{net} (mol kg^{-1})	N_{excess} (mol kg^{-1})
Mg/DOBDC	Ar	0.00	0.00	0.00	0.00	0.00	0.00	0.00	0.00	0.00
		0.20	0.05	0.05	1.00	0.16	0.18	0.68	0.06	0.07
		0.32	0.07	0.08	1.27	0.19	0.22	1.01	0.09	0.11
		0.67	0.15	0.16	2.0	0.31	0.35	1.27	0.11	0.13
		1.02	0.23	0.25	4.0	0.59	0.67	2.0	0.17	0.21
		1.28	0.28	0.31	8.0	1.09	1.25	4.0	0.34	0.41
		2.0	0.44	0.48	12.0	1.53	1.77	8.1	0.64	0.78
		4.1	0.85	0.94	16.1	1.94	2.26	12.0	0.92	1.13
		8.0	1.56	1.73	20.0	2.26	2.66	16.1	1.17	1.46
		12.0	2.15	2.41	26.1	2.70	3.22	20.1	1.40	1.76
		16.1	2.68	3.02	32	3.04	3.68	26.1	1.72	2.18
		20.1	3.07	3.50	39	3.33	4.12	32	1.99	2.56
		26.0	3.56	4.12	50	3.63	4.64	39	2.24	2.94
		33	3.99	4.71	50	3.66	4.67	50	2.54	3.44
		40	4.31	5.18	72	3.96	5.44	51	2.51	3.42
		50	4.57	5.67	94	4.01	5.96	72	2.89	4.19
		50	4.59	5.69	113	3.94	6.31	94	3.07	4.77
		72	4.81	6.42				112	3.13	5.17
		94	4.73	6.87						
		115	4.52	7.18						
Mn/DOBDC	Ar	0.00	0.00	0.00	0.00	0.00	0.00	0.00	0.00	0.00
		0.67	0.14	0.15	1.03	0.14	0.16	1.06	0.11	0.12
		1.03	0.21	0.23	2.0	0.28	0.31	2.0	0.18	0.21
		2.0	0.41	0.44	4.0	0.56	0.62	4.0	0.36	0.41
		4.0	0.81	0.87	8.1	1.06	1.18	8.1	0.66	0.77
		8.1	1.47	1.60	12.1	1.50	1.68	12.1	0.95	1.11
		12.0	2.02	2.21	16.0	1.86	2.10	16.0	1.19	1.40
		15.9	2.48	2.73	20.0	2.18	2.48	20.1	1.40	1.67
		20.0	2.88	3.20	26.2	2.61	3.00	26.0	1.72	2.06
		26.1	3.35	3.77	32	2.88	3.36	32	1.98	2.40
		31	3.68	4.18	39	3.17	3.76	39	2.19	2.71
		39	3.97	4.60	50	3.46	4.21	50	2.47	3.14
		50	4.26	5.08	70	3.79	4.86	70	2.86	3.80
		71	4.47	5.65						

Adsorbent	Gas	At 294 K			At 315 K			At 352 K		
		P (bar)	N_{net} (mol kg^{-1})	N_{excess} (mol kg^{-1})	P (bar)	N_{net} (mol kg^{-1})	N_{excess} (mol kg^{-1})	P (bar)	N_{net} (mol kg^{-1})	N_{excess} (mol kg^{-1})
Co/DOBDC	Ar	0.00	0.00	0.00	0.00	0.00	0.00	0.00	0.00	0.00
		0.13	0.04	0.04	0.20	0.04	0.04	1.33	0.15	0.16
		0.21	0.06	0.06	0.36	0.07	0.07	2.0	0.22	0.24
		0.35	0.10	0.10	0.68	0.12	0.13	4.1	0.43	0.47
		0.69	0.18	0.19	1.06	0.19	0.20	8.1	0.77	0.86
		1.05	0.28	0.29	1.29	0.23	0.25	12.0	1.10	1.23
		1.32	0.34	0.36	2.0	0.36	0.38	16.1	1.40	1.57
		2.0	0.52	0.55	4.1	0.69	0.74	20.0	1.67	1.88
		4.0	1.00	1.05	8.0	1.28	1.37	26.0	2.02	2.30
		8.0	1.82	1.92	12.1	1.79	1.93	33	2.38	2.73
		12.0	2.48	2.63	16.0	2.22	2.41	40	2.64	3.06
		16.0	3.01	3.21	20.2	2.61	2.85	50	2.96	3.49
		20.0	3.44	3.70	26.0	3.06	3.37	72	3.40	4.17
		26.0	3.96	4.29	33	3.48	3.87	94	3.66	4.67
		33	4.43	4.86	40	3.83	4.31	109	3.73	4.91
		40	4.71	5.23	51	4.14	4.76			
		51	5.00	5.67	72	4.52	5.40			
		72	5.25	6.21	94	4.63	5.79			
		94	5.23	6.50	109	4.62	5.98			
		111	5.13	6.65						
Ni/DOBDC	Ar	0.00	0.00	0.00	0.00	0.00	0.00	0.00	0.00	0.00
		2.0	0.54	0.57	0.35	0.06	0.06	1.30	0.14	0.15
		4.1	0.99	1.04	0.71	0.12	0.13	2.0	0.20	0.22
		8.0	1.73	1.84	1.06	0.18	0.19	4.1	0.38	0.43
		12.2	2.40	2.56	1.29	0.21	0.23	8.1	0.73	0.82
		16.0	2.90	3.11	2.0	0.35	0.37	12.1	1.05	1.18
		19.3	3.27	3.53	4.1	0.66	0.71	16.0	1.33	1.51
		25.9	3.84	4.19	8.1	1.21	1.31	20.0	1.61	1.83
		33	4.28	4.73	12.1	1.69	1.84	26.5	1.97	2.27
		40	4.62	5.17	16.1	2.13	2.33	33	2.28	2.65
		51	4.99	5.69	20.0	2.48	2.73	40	2.62	3.07
		72	5.33	6.34	26.4	2.98	3.31	51	2.98	3.55
		92	5.43	6.74	33	3.37	3.79	73	3.49	4.31
		101	5.45	6.90	40	3.73	4.24	87	3.75	4.74
					51	4.08	4.73	99	3.92	5.04
					72	4.51	5.44			
					87	4.77	5.90			
					100	4.78	6.09			

Table A14. Adsorption isotherm data of CO_2 onto DABCO MOFs.

Adsorbent	Gas	At 294 K			At 314 K			At 350 K		
		P (bar)	N_{net} (mol kg^{-1})	N_{excess} (mol kg^{-1})	P (bar)	N_{net} (mol kg^{-1})	N_{excess} (mol kg^{-1})	P (bar)	N_{net} (mol kg^{-1})	N_{excess} (mol kg^{-1})
Ni/DABCO	CO_2	0.00	0.00	0.00	0.00	0.00	0.00	0.00	0.00	0.00
		0.14	0.26	0.26	0.34	0.36	0.37	0.34	0.16	0.17
		0.35	0.66	0.67	0.69	0.76	0.78	0.68	0.35	0.36
		0.68	1.36	1.38	1.04	1.19	1.21	1.02	0.53	0.55
		1.00	2.14	2.17	1.32	1.54	1.57	1.32	0.68	0.71
		1.31	2.97	3.00	2.1	2.52	2.57	2.0	1.06	1.10
		2.0	4.86	4.91	2.7	3.33	3.40	2.7	1.42	1.48
		2.7	6.53	6.60	4.0	5.05	5.15	4.0	2.16	2.25
		4.0	8.81	8.91	5.3	6.53	6.66	5.3	2.89	3.01
		5.4	10.11	10.25	8.0	8.44	8.64	8.0	4.25	4.43
		8.0	11.44	11.65	12.0	9.92	10.22	12.0	5.85	6.12
		12.1	12.32	12.65	16.0	10.70	11.11	16.0	6.96	7.32
		16.1	12.72	13.17	20.1	11.12	11.65	20.0	7.71	8.17
		20.1	12.90	13.48	25.9	11.43	12.14	26.0	8.41	9.02
		26.0	13.00	13.79						
Cu/DABCO	CO_2	0.00	0.00	0.00	0.00	0.00	0.00	0.00	0.00	0.00
		0.12	0.16	0.16	0.12	0.09	0.09	0.10	0.03	0.03
		0.34	0.45	0.46	0.27	0.19	0.20	0.27	0.09	0.10
		1.02	1.40	1.43	0.67	0.49	0.51	0.68	0.24	0.25
		1.24	1.74	1.77	1.00	0.74	0.76	1.00	0.35	0.37
		2.6	4.05	4.11	1.28	0.97	1.00	1.22	0.42	0.45
		4.0	5.74	5.84	2.7	2.14	2.20	2.7	0.94	1.00
		5.3	6.85	6.98	4.0	3.26	3.35	4.0	1.41	1.49
		8.0	8.03	8.24	5.3	4.24	4.36	5.4	1.88	1.99
		12.0	8.90	9.22	8.0	5.67	5.86	8.0	2.75	2.92
		16.0	9.31	9.74	12.1	6.86	7.15	12.0	3.84	4.10
		20.0	9.44	10.00	16.0	7.47	7.87	16.0	4.64	4.99
		26.0	9.51	10.27	20.0	7.82	8.33	19.9	5.21	5.65
					26.0	8.11	8.79	26.1	5.75	6.34
Zn/DABCO	CO_2	0.00	0.00	0.00	0.00	0.00	0.00	0.00	0.00	0.00
		0.09	0.16	0.16	0.07	0.07	0.07	0.07	0.03	0.03
		0.23	0.41	0.42	0.07	0.07	0.07	0.20	0.10	0.10
		0.47	0.90	0.91	0.20	0.21	0.21	0.47	0.23	0.24
		0.99	2.07	2.09	0.20	0.21	0.21	1.00	0.49	0.51
		0.99	1.93	1.95	0.47	0.50	0.51	1.6	0.77	0.80
		1.6	3.58	3.62	0.47	0.50	0.51	1.6	0.80	0.83
		1.6	3.48	3.52	1.00	1.09	1.11	2.7	1.33	1.38
		2.6	6.14	6.20	1.01	1.13	1.15	2.7	1.34	1.39
		2.6	6.15	6.21	1.6	1.83	1.86	4.7	2.38	2.47
		4.6	9.06	9.17	1.6	1.90	1.93	4.7	2.37	2.46
		4.6	8.96	9.07	2.7	3.18	3.24	8.0	4.01	4.16
		7.9	10.86	11.05	2.7	3.25	3.31	8.0	3.94	4.09
		8.0	10.92	11.11	4.6	5.67	5.77	13.3	5.95	6.21
		13.3	11.94	12.26	4.7	5.59	5.69	18.7	7.16	7.53
		18.9	12.30	12.78	7.8	8.10	8.27	26.1	8.04	8.58
		26.0	12.40	13.10	8.0	8.14	8.31			
					13.3	9.83	10.13			
					18.7	10.54	10.97			
					25.9	10.95	11.57			

Table A15. Adsorption isotherm data of CO onto DABCO MOFs.

Adsorbent	Gas	At 294 K			At 314 K			At 350 K		
		P (bar)	N_{net} (mol kg^{-1})	N_{excess} (mol kg^{-1})	P (bar)	N_{net} (mol kg^{-1})	N_{excess} (mol kg^{-1})	P (bar)	N_{net} (mol kg^{-1})	N_{excess} (mol kg^{-1})
Ni/DABCO	CO	0.00	0.00	0.00	0.00	0.00	0.00	0.00	0.00	0.00
		0.35	0.08	0.09	1.29	0.21	0.24	2.0	0.19	0.23
		0.68	0.15	0.17	2.0	0.31	0.36	2.7	0.24	0.30
		1.02	0.21	0.24	2.7	0.40	0.46	4.1	0.35	0.44
		1.30	0.28	0.31	4.0	0.58	0.68	5.4	0.45	0.57
		2.0	0.44	0.49	5.4	0.75	0.88	8.0	0.65	0.82
		2.7	0.57	0.64	8.0	1.06	1.25	12.0	0.90	1.16
		4.0	0.82	0.92	12.1	1.47	1.76	16.1	1.12	1.46
		5.4	1.05	1.19	16.0	1.82	2.20	20.1	1.31	1.74
		8.0	1.50	1.70	20.1	2.11	2.59	26.1	1.56	2.12
		12.0	2.04	2.35	26.0	2.49	3.11			
		16.0	2.56	2.97						
		20.0	2.93	3.44						
		26.1	3.38	4.05						
Cu/DABCO	CO	0.00	0.00	0.00	0.00	0.00	0.00	0.00	0.00	0.00
		0.34	0.06	0.07	0.34	0.04	0.05	0.69	0.06	0.07
		0.72	0.11	0.13	0.69	0.08	0.10	1.00	0.08	0.10
		1.03	0.15	0.18	1.01	0.12	0.14	1.27	0.09	0.12
		1.32	0.20	0.23	1.30	0.15	0.18	2.0	0.14	0.18
		2.0	0.29	0.34	2.0	0.22	0.27	2.7	0.17	0.23
		2.7	0.37	0.44	2.7	0.28	0.34	4.0	0.24	0.32
		4.0	0.52	0.62	4.0	0.39	0.48	5.4	0.31	0.42
		5.3	0.66	0.79	5.4	0.49	0.61	8.0	0.42	0.58
		8.0	0.89	1.09	8.0	0.67	0.85	12.0	0.56	0.81
		12.0	1.19	1.49	12.0	0.89	1.17	16.0	0.69	1.02
		16.0	1.38	1.78	16.0	1.06	1.43	20.0	0.79	1.20
		20.0	1.58	2.07	20.0	1.20	1.66	26.1	0.91	1.45
		26.1	1.73	2.38	26.0	1.34	1.94			
Zn/DABCO	CO	0.00	0.00	0.00	0.00	0.00	0.00	0.00	0.00	0.00
		0.20	0.05	0.05	0.20	0.04	0.04	0.21	0.03	0.03
		0.21	0.05	0.05	0.48	0.08	0.09	0.47	0.05	0.06
		0.47	0.11	0.12	1.00	0.17	0.19	0.48	0.05	0.06
		0.48	0.11	0.12	1.00	0.17	0.19	1.00	0.10	0.12
		1.00	0.24	0.26	1.6	0.27	0.30	1.01	0.11	0.13
		1.00	0.25	0.27	1.6	0.28	0.31	1.6	0.17	0.20
		1.6	0.39	0.43	2.7	0.45	0.51	1.6	0.17	0.20
		1.6	0.37	0.41	2.7	0.44	0.50	2.7	0.27	0.32
		2.7	0.62	0.68	4.6	0.76	0.86	2.7	0.27	0.32
		4.7	1.00	1.11	4.7	0.74	0.84	4.7	0.45	0.54
		4.7	1.04	1.15	8.0	1.16	1.33	4.7	0.43	0.52
		8.0	1.62	1.80	13.3	1.78	2.06	8.0	0.70	0.85
		13.3	2.43	2.73	18.7	2.28	2.68	13.2	1.09	1.34
		18.7	3.11	3.53	26.2	2.84	3.39	18.7	1.42	1.77
		26.1	3.83	4.42				26.0	1.82	2.31

Table A16. Adsorption isotherm data of CH_4 onto DABCO MOFs.

Adsorbent	Gas	At 294 K			At 314 K			At 350 K		
		P (bar)	N_{net} (mol kg^{-1})	N_{excess} (mol kg^{-1})	P (bar)	N_{net} (mol kg^{-1})	N_{excess} (mol kg^{-1})	P (bar)	N_{net} (mol kg^{-1})	N_{excess} (mol kg^{-1})
Ni/DABCO	CH_4	0.00	0.00	0.00	0.00	0.00	0.00	0.00	0.00	0.00
		0.38	0.23	0.24	0.14	0.06	0.06	1.07	0.24	0.26
		0.69	0.41	0.43	0.36	0.14	0.15	1.31	0.29	0.32
		1.03	0.60	0.63	0.70	0.27	0.29	2.0	0.43	0.47
		1.30	0.74	0.77	1.02	0.39	0.41	2.7	0.55	0.61
		2.0	1.15	1.20	1.29	0.49	0.52	4.1	0.84	0.93
		2.7	1.50	1.57	2.0	0.76	0.81	5.5	1.09	1.21
		4.0	2.20	2.30	2.7	0.99	1.05	8.0	1.53	1.70
		5.4	2.81	2.95	4.0	1.44	1.54	12.0	2.10	2.36
		8.0	3.89	4.10	5.4	1.87	2.00	16.0	2.59	2.94
		13.2	5.36	5.71	8.0	2.63	2.82	20.0	3.00	3.44
		16.0	5.93	6.35	12.0	3.54	3.83	26.0	3.51	4.08
		20.0	6.53	7.06	16.3	4.30	4.70			
		26.1	7.24	7.94	20.0	4.83	5.32			
					26.0	5.45	6.10			
Cu/DABCO	CH_4	0.00	0.00	0.00	0.00	0.00	0.00	0.00	0.00	0.00
		4.1	1.69	1.79	0.12	0.05	0.05	0.30	0.06	0.07
		5.5	2.19	2.33	0.67	0.22	0.24	0.67	0.14	0.15
		8.1	2.94	3.14	1.05	0.35	0.37	1.00	0.20	0.22
		12.0	3.75	4.05	1.26	0.42	0.45	1.38	0.26	0.29
		16.0	4.28	4.69	2.0	0.61	0.66	2.7	0.46	0.52
		20.0	4.60	5.11	3.0	0.89	0.96	4.0	0.64	0.72
		26.0	4.92	5.59	3.9	1.10	1.19	5.3	0.81	0.92
					5.5	1.46	1.59	8.0	1.11	1.28
					8.3	2.03	2.22	12.1	1.52	1.77
					12.0	2.64	2.92	16.6	1.89	2.24
					16.1	3.17	3.55	20.2	2.15	2.57
					20.0	3.56	4.03	26.2	2.47	3.02
					25.9	3.96	4.58			
Zn/DABCO	CH_4	0.00	0.00	0.00	0.00	0.00	0.00	0.00	0.00	0.00
		0.07	0.04	0.04	0.21	0.08	0.08	0.19	0.04	0.04
		0.09	0.05	0.05	0.48	0.16	0.17	0.45	0.09	0.10
		0.20	0.10	0.10	1.03	0.33	0.35	0.98	0.18	0.20
		0.20	0.10	0.10	1.6	0.54	0.57	1.6	0.29	0.32
		0.47	0.25	0.26	2.7	0.86	0.92	2.7	0.49	0.54
		0.48	0.24	0.25	4.7	1.49	1.59	4.6	0.84	0.93
		1.01	0.50	0.52	7.9	2.41	2.58	8.0	1.38	1.53
		1.01	0.55	0.57	13.3	3.57	3.86	13.3	2.09	2.34
		1.6	0.85	0.89	18.7	4.41	4.82	18.7	2.68	3.04
		1.6	0.80	0.84	26.0	5.20	5.77	25.9	3.30	3.80
		1.6	0.85	0.89						
		1.6	0.80	0.84						
		2.7	1.40	1.46						
		2.7	1.30	1.36						
		4.7	2.19	2.30						
		4.7	2.32	2.43						
		7.9	3.30	3.48						
		8.0	3.43	3.61						
		13.3	5.11	5.42						
		18.6	6.03	6.46						
		26.0	6.72	7.34						

Table A17. Adsorption isotherm data of N_2 onto DABCO MOFs.

Adsorbent	Gas	At 294 K			At 314 K			At 350 K		
		P (bar)	N_{net} (mol kg^{-1})	N_{excess} (mol kg^{-1})	P (bar)	N_{net} (mol kg^{-1})	N_{excess} (mol kg^{-1})	P (bar)	N_{net} (mol kg^{-1})	N_{excess} (mol kg^{-1})
Ni/DABCO	N_2	0.00	0.00	0.00	0.00	0.00	0.00	0.00	0.00	0.00
		1.32	0.37	0.40	1.02	0.14	0.16	1.33	0.09	0.12
		2.1	0.55	0.60	1.28	0.18	0.21	2.2	0.15	0.20
		2.7	0.69	0.76	2.0	0.28	0.33	2.7	0.18	0.24
		4.0	0.98	1.08	2.7	0.36	0.42	4.0	0.27	0.36
		8.1	1.61	1.82	4.0	0.53	0.63	5.4	0.35	0.47
		12.3	2.11	2.42	5.4	0.69	0.82	8.0	0.50	0.67
		16.2	2.59	3.00	8.0	0.97	1.16	12.0	0.70	0.96
		19.8	2.91	3.42	12.0	1.32	1.61	16.1	0.88	1.22
		26.0	3.29	3.96	16.0	1.64	2.02	20.0	1.02	1.45
					20.0	1.89	2.37	26.1	1.22	1.78
					26.1	2.19	2.81			
Cu/DABCO	N_2	0.00	0.00	0.00	0.00	0.00	0.00	0.00	0.00	0.00
		1.05	0.11	0.14	2.7	0.22	0.28	0.35	0.01	0.02
		1.33	0.14	0.17	4.0	0.30	0.39	0.68	0.03	0.04
		2.0	0.21	0.26	5.4	0.38	0.50	1.03	0.04	0.06
		2.7	0.27	0.34	8.0	0.52	0.70	1.32	0.04	0.07
		4.0	0.40	0.50	12.1	0.70	0.98	2.0	0.08	0.12
		5.4	0.53	0.66	16.0	0.86	1.23	2.7	0.09	0.15
		8.0	0.73	0.93	20.0	0.99	1.45	4.0	0.14	0.22
		12.0	1.01	1.31	26.0	1.15	1.75	5.3	0.18	0.29
		15.9	1.26	1.65				8.0	0.26	0.42
		20.0	1.45	1.94				12.0	0.36	0.61
		26.0	1.65	2.29				16.0	0.44	0.77
								20.0	0.52	0.93
								26.0	0.61	1.14
Zn/DABCO	N_2	0.00	0.00	0.00	0.00	0.00	0.00	0.00	0.00	0.00
		0.06	0.02	0.02	0.06	0.01	0.01	0.19	0.02	0.02
		0.18	0.05	0.05	0.20	0.03	0.03	0.44	0.03	0.04
		0.45	0.09	0.10	0.45	0.06	0.07	0.98	0.07	0.09
		1.00	0.18	0.20	0.97	0.12	0.14	1.6	0.11	0.14
		1.6	0.28	0.32	1.6	0.20	0.23	2.6	0.17	0.22
		2.7	0.46	0.52	2.6	0.32	0.37	4.6	0.31	0.40
		4.7	0.78	0.89	4.7	0.54	0.64	8.0	0.52	0.67
		8.0	1.27	1.45	8.0	0.90	1.07	13.5	0.81	1.06
		13.3	1.92	2.22	13.3	1.40	1.68	18.7	1.06	1.41
		18.7	2.46	2.88	18.7	1.81	2.20	25.9	1.30	1.79
		25.8	3.04	3.62	26.1	2.23	2.78			